FABRICATION AND CHARACTERIZATION OF FLEXIBLE PIEZOELECTRIC GENERATOR COMPOSED OF SODIUM POTASSIUM NIOBATE (KNN) BASED CERAMICS AND POLYMERS FOR ENERGY HARVESTING APPLICATIONS

A Thesis Submitted
In Partial Fulfillment of the Requirements
for the Degree of

DOCTOR OF PHILOSOPHY

in APPLIED PHYSICS

by

KOMAL VERMA

(Reg. No.: 2K19/PhDAP/06)

Under the Supervision of

Dr. Richa Sharma
Assistant Professor
Department of Applied Physics
Delhi Technological University
Delhi-110042



Department of Applied Physics

DELHI TECHNOLOGICAL UNIVERSITY

(Formerly Delhi College of Engineering)
Shahbad Daulatpur, Main Bawana Road, Delhi-110042. India
September, 2025

©Delhi Technological University-2025 All rights reserved.

Dedicated to... My Family and My Supervisor

CH *

DELHI TECHNOLOGICAL UNIVERSITY

Formerly Delhi College of Engineering

(Under Delhi Act 6 of 2009, Govt. of NCT of Delhi) Shahbad Daulatpur, Bawana Road, Delhi-110 042

CANDIDATE'S DECLARATION

I Ms. Komal Verma (Reg. No.: 2K19/PhDAP/06) hereby certify that the work which is being presented in the thesis entitled "Fabrication and Characterization of Flexible Piezoelectric Generator composed of Sodium Potassium Niobate (KNN) based Ceramics and Polymers for Energy Harvesting Applications" in partial fulfillment of the requirements for the award of the Degree of Doctor of Philosophy in the discipline of Physics, submitted in the Department of Applied Physics, Delhi Technological University (Formerly Delhi College of Engineering), Delhi is an authentic record of my own work carried out during the period from July 2019 to September 2025 under the supervision of Dr. Richa Sharma, Department of Applied Physics, Delhi Technological University, Delhi.

The matter presented in the thesis has not been submitted by me for the award of any other degree of this or any other Institute.

Komal Verma (Reg. No.: 2K19/PhDAP/06)

This is to certify that the candidate has incorporated all the corrections suggested by the examiners in the thesis and the statement made by the candidate is correct to the best of our knowledge.

Dr. Richa Sharma

Supervisor & Assistant Professor Department of Applied Physics Delhi Technological University Delhi-110 042, India

Signature of the External Examiners

i



DELHI TECHNOLOGICAL UNIVERSITY

Formerly Delhi College of Engineering

(Under Delhi Act 6 of 2009, Govt. of NCT of Delhi) Shahbad Daulatpur, Bawana Road, Delhi-110 042

CERTIFICATE BY THE SUPERVISOR

Certified that <u>Ms. Komal Verma (Reg. No.: 2K19/PhDAP/06</u> has carried out their research work presented in this thesis entitled "<u>Fabrication and Characterization of Flexible Piezoelectric Generator composed of Sodium Potassium Niobate (KNN)</u> <u>based Ceramics and Polymers for Energy Harvesting Applications</u>" for the award of <u>Doctor of Philosophy</u> from Department of Applied Physics, Delhi Technological University, Delhi, under my supervision. The thesis embodies results of original work, and studies are carried out by the candidate herself and the contents of the thesis do not form the basis for the award of any other degree to the candidate or to anybody else from this or any other University/Institution.

Dr. Richa Sharma

Assistant Professor Department of Applied Physics Delhi Technological University Delhi-110 042, India

Prof. Vinod Singh

Head, Department of Applied Physics Delhi Technological University Delhi-110 042, India

ACKNOWLEDGMENTS

First and foremost, I would like to extend my deepest gratitude to God, whose divine presence has been a guiding force throughout my life, providing me with the strength and wisdom to complete this journey. I wish to express my deepest gratitude to my parents and family, who have been the foundation of my emotional, physical, and mental well-being throughout my pursuit of this degree. Words cannot fully capture my indebtedness to them. I am profoundly grateful to all the people who have come into my life, each one leaving an indelible mark and contributing to the realization of this thesis. Here I would like to mention a few personalities and show my gratitude from the bottom of my heart.

The unwavering love, care, support, and blessings of my mother, father, in-laws, my loving husband, brother, sister, brother-in-law Mrs. Sharda, Mr. Narender Singh, Mr. Ravinder Kumar, Mrs. Rajesh Kumari, Mr. Aakash Verma, Mr. Sachin Kumar, Mr. Vishal, Mrs. Preeti, and Mr. Abhinav gave me the strength to undertake this work and see it through to the best of my abilities. Their constant belief in my potential and their encouragement during challenging times fueled my determination. I am forever indebted to their sacrifices, which allowed me to pursue my dreams without hesitation. My deepest gratitude to my niece, nephew, and beloved daughter, Shivanya, Gunjan, Ridhi Verma, Namish Verma, and Yashasvi Verma, whose innocent joy and unspoken support brought light and warmth to my journey. Their presence has been a constant reminder of the simple beauties in life, and their laughter have been a source of motivation during the most challenging moments of this work. I extend my heartfelt thanks to my sister-in-law, Mrs. Babita. I am immensely grateful to my loving partner Mr. Aakash Verma, whose steadfast encouragement has been my anchor, providing unwavering support. His belief in me, particularly during the hard stages of my studies, has been a source of strength and motivation that I deeply cherish.

Above all, I offer my boundless gratitude to **Lord Krishna**, whose constant blessings empowered me to carry out this work successfully.

Gratitude, when sincerely expressed, is a beautiful endeavor, yet no words can truly convey the depth of my appreciation. Over the past six years at Delhi Technological University, particularly in the **Materials Research Laboratory**, I have been fortunate to receive guidance and assistance from many kind souls, to whom I extend my sincere thanks.

At the outset, it is with great honor that I express my profound deep sense of gratitude, indebtedness and respect to my supervisor, **Dr. Richa Sharma** for being very humble, and supportive from the Department of Applied Physics at Delhi Technological University. It has been a privilege to work under such a supportive mentor all the time, and for their invaluable guidance, patience, and encouragement throughout this journey. I am deeply honored to have worked under the guidance of such an excellent, enthusiastic, and distinguished supervisor. Their unwavering encouragement, constant support, meticulous supervision, and constructive criticism have been instrumental in carving another milestone in my academic journey.

I express my sincere thanks to **Prof. Vinod Singh**, Head and DRC Chairman, Department of Applied Physics, DTU, for his timely advice, valuable help, suggestions, and support. I extend my heartfelt gratitude to **Prof. Rinku Sharma**, the Dean (Academic PG) at DTU; and my SRC and DRC committee members for their unwavering support. I also extend my heartfelt appreciation to **Prof. A. S. Rao**, the former Head & DRC Chairman, Department of Applied Physics, for their invaluable assistance and suggestions. Further, I extend a very special thanks to **Prof. Suresh C. Sharma**, the former Dean (Academic PG) at DTU; for his motivation and support. I express my sincere gratitude to my SRC external member, **Prof. Pawan Kumar Kulriya**, **School of Physical Sciences**, Jawaharlal Nehru University (JNU), New Delhi, for his continuous guidance during the journey of this thesis.

I express my special thanks to **Dr. M. Jayasimhadri**, **Dr. Amrish K. Panwar**, **Dr. M.S. Mehata**, **Dr. Bharti Singh** and **Dr. Renuka Bokolia**, Delhi Technological University,

Delhi for providing me research facilities.

I wish to convey my deep gratitude to **Dr. Sahil Goel**, Research Associate, SSPL, DRDO, Delhi and **Dr. Pardeep**, CSIR-NPL, Delhi for their support and continuous guidance during this journey.

Further, I wish to convey my deep gratitude to my esteemed mentor, **Dr. Sandeep**, Assistant Professor, Department of Physics, Hindu College, Sonipat for his invaluable lessons which have been crucial in guiding me to this milestone.

I express my special thanks to my closest friend, **Late Ms. Savita**, whose unwavering support and encouragement inspired me throughout my journey and continue to live on in my memories as a source of strength and motivation.

It is my pleasure to express my sincere thanks to all the faculty members of the Department of Applied Physics for their continuous encouragement and help during my research work. I am also grateful to the technical and non-technical staff for their timely support and cooperation whenever required.

I sincerely thank my present lab-mate Mr. Aman Kumar, Ms. Megha Narwan and Ms. Monika whose support helped me in accomplishing my work. It is my pleasure to thank Mr. Anurag, Mr. Sharad, Mr. Naveen Kumar, Mr. Sunil Kumar, Dr. Vikas Sangwan, Dr. Vishal, Dr. Km. Komal, Dr. Shilpa Rana, Dr. Anchali Jain, Ms. Aneesha and Mr. Gagan for helping me in the lab. I would also like to thank all the other research scholars of the Department of Applied Physics, Delhi Technological University, Delhi for their help and advice.

A journey always lasts with some crucial friends; now it's their turn. I would like to highlight the cheerful company and always supportive role of Dr. Shristy Malik, Ms. Kanika, Dr. Jyoti, Mr. Aditya, Dr. Ankit, Dr. Suman, Dr. Richa, Dr. Priyanka, Mr. Abhishek, Dr. Ramesh, Mr. Praveen, Mr. Jasveer, Ms. Sheetal, Ms. Shivani and Ms. Bhawna. Your companionship made this journey enjoyable and memorable.

At last, I gratefully acknowledge the **Delhi Technological University (DTU**), Delhi for extending all the necessary facilities and providing me **DTU fellowship**. I extend my gratitude to the **DTU Staff** in **Administration**, **Accounts**, **Store & Purchase**, **Central Library** and **Computer Centre** for their help and services.

I am sincerely grateful to the Divine for blessing me with the strength and wisdom to pursue and complete this journey. I also extend my heartfelt thanks to all the wonderful people who have been a part of my life during this endeavor. Their unwavering support,

encouragement, and love have been invaluable, and this accomplishment would not have been possible without them.

May we continue to grow, support, learn, and achieve together.

With deepest gratitude to all!!!

Komal Verma

ABSTRACT

In the recent era, the urgent need for sustainable and renewable energy solutions in day-to-day life has gradually increased due to the global energy crisis, driven by increasing demand and the depletion of conventional fossil fuel reserves. In this context, piezoelectric energy harvesting technology has gained significant attention due to its ability to convert abundantly available mechanical energy into useful electrical energy. The present thesis work reports the development of composite-type flexible piezoelectric generators (PEGs) which can potentially provide power to the self-powered and wearable devices by harvesting the abundantly available mechanical energy into useful electrical energy.

For the construction of the PEG device, pure and Lithium (Li), Tantalum (Ta), and Antimony (Sb) modified Potassium Sodium Niobate (KNaNbO₃) (KNN) have been used as filler materials in the poly (vinylidene fluoride) (PVDF) matrix. Pure KNN has been synthesized by two methods: solid state reaction method and hydrothermal method. On the other hand, Li, Ta, and Sb modified KNN was synthesized by solid state method followed by high energy ball milling.

The phase and structure identification of the prepared filler materials and flexible composite films were done by X-ray Diffraction (XRD), Scanning Electron Microscopy (SEM) and Fourier Transform Infrared Spectroscopy (FTIR). The dielectric and ferroelectric properties of the fabricated flexible composite films were also studied. The filler content in the PVDF matrix has been systematically varied to analyze its effect on the piezoelectric output performance of the constructed PEG device. The obtained results indicated the dependency of the β phase of PVDF, dielectric, piezoelectric and ferroelectric properties of composite films on the filler content in the PVDF matrix. The generated output voltage and current of the fabricated PEG devices were also recorded. The generated instantaneous power by the constructed PEG devices has also been measured by connecting the devices with different resistors showing gradual rise in voltage accompanied by the steadily decreasing current as a function of load resistance.

Furthermore, to increase the content of the β phase of PVDF and enhance the energy harvesting performance of PVDF based PEGs, some conducting fillers: ZnO nanorods

synthesized by Co-precipitation method and Multiwall Carbon Nanotube (MWCNT) purchased from Sigma Aldrich were dispersed in the PVDF matrix along with the ceramic particles. The addition of some conducting fillers in the polymer matrix can enhance the nucleation and improve the formation of β phase of PVDF and also helps in transfer of the generated charges. It is the combined effect of the filler materials and polymer in the PVDF-based composites which enhance the piezoelectric performance of the devices for wider applications.

To further evaluate the performance of the constructed PEG devices in harvesting mechanical energy from human body motions such as finger tapping, wrist movement, elbow bending etc. the device was attached to the human body and generated voltage was recorded. The obtained result indicated that the device is very sensitive to the applied force and can harvest energy from the human body movements. The electrical energy generated by the fabricated PEG devices by harvesting external mechanical vibration have been used to light up light emitting diodes (LEDs) and powering small electronic devices. The present thesis work demonstrated that high-performance flexible PEG device with simple structure and high sensitivity can be developed by using modified KNN ceramics along with some conducting fillers in the PVDF matrix that can be used in self-powered and wearable devices.

Chapter 1 of the thesis begins by systematically addressing the energy crisis and the growing need for energy harvesting, highlighting the existing shortfalls in meeting these demands. It then reviews various energy harvesting techniques, emphasizing particularly on piezoelectric energy harvesting as a promising method, which converts mechanical energy into electrical energy by using piezoelectric generators (PEGs). Owing to their versatility and effectiveness, PEGs have emerged as a focal point of research, since they can harvest energy from human body motions and mechanical vibrations by using piezoelectric effect while also serving as self-powered devices in a wide range of applications. Furthermore, various types of piezoelectric materials, including inorganic, organic, and composite-based materials have been discussed which can be employed for the construction of PEGs. A review of existing literature on piezoelectric generators is conducted to identify research gaps and to establish the primary objectives of the present thesis work.

Chapter 2 elaborates the experimental methods utilized for the synthesis of filler particles in the PVDF matrix and the fabrication of composite films. For the synthesis of the filler materials, solid state method, hydrothermal method and co-precipitation method were used and are discussed in detail in the chapter. Further, for the fabrication of the flexible composite films, drop casting method was employed. In addition, the working principle of various experimental techniques and equipment that were used for the characterization of the prepared samples have also been provided in this chapter to get a comprehensive understanding. To study the phase formation and morphology of the prepared powders and flexible composite films, X-ray Diffraction (XRD), Scanning Electron Microscopy (SEM), Field Emission Scanning Electron Microscopy (FESEM) and Fourier Transform Infrared Spectroscopy (FTIR) were used. Furthermore, dielectric, ferroelectric and piezoelectric properties of the fabricated composite films were also measured using Impedance analyzer, Polarisation vs. Electric field (P-E) loop tracer and Strain measurement system (Butterfly loop), respectively. With the aid of a vibrator shaker and finger tapping, force was applied on the surface of the constructed PEG devices and generated open circuit voltage and short circuit current were measured by using digital storage oscilloscope and an electrometer, respectively. Furthermore, load resistances were also attached to the PEG devices to measure the output power of the manufactured PEG device.

Chapter 3 is divided into two sections. The first section focuses on the fabrication and characterization of piezoelectric generator (PEG) based on flexible composite films composed of Potassium Sodium Niobate (KNN) and Poly (vinylidene fluoride) (PVDF), with varying concentrations of KNN ceramic particles (0 wt.%, 5 wt.%, 10 wt.%, 15 wt.%, and 20 wt.%) in the polymer matrix. In the first section, KNN was synthesized using the solid-state reaction method and used for the construction of PEG. The second section explores the effect of KNN particle size synthesized by hydrothermal method as filler in the PVDF matrix on the piezoelectric output performance of the constructed piezoelectric generator device. The obtained result demonstrates a considerable enhancement in the piezoelectric output performance of a device constructed with KNN synthesized by hydrothermal method over the PEG device constructed using KNN synthesized by solid-state method.

Chapter 4 presents the development of piezoelectric energy harvesters based on PVDF/KNN/ZnO nanocomposite films. Initially, KNN nanoparticles were synthesized using the hydrothermal method, as described in Chapter 3. Zinc oxide (ZnO) nanorods were prepared through co-precipitation method and subsequently integrated into the PVDF polymer matrix along with KNN nanoparticles to enhance the overall piezoelectric performance of the fabricated piezoelectric nanogenerator (PENG). ZnO is well-known for its semiconducting properties and remarkable piezoelectric characteristics, making it an ideal candidate for boosting the energy harvesting efficiency of the constructed PENG device. The synergistic effect of KNN and ZnO within the PVDF matrix is expected to result in superior piezoelectric output, contributing to the development of efficient energy harvesting PENG devices.

Chapter 5 presents the fabrication of a flexible piezoelectric generator (PEG) based on a composite film of (Li, Ta, Sb)-modified (K, Na)NbO₃ (KNNLTS) and poly(vinylidene fluoride) (PVDF). KNNLTS particles were synthesized using the solid-state method and subsequently incorporated into the PVDF polymer to develop PVDF/KNNLTS-based piezoelectric energy harvesters. The integration of KNNLTS into the PVDF matrix significantly enhanced the composite's ferroelectric, piezoelectric, and dielectric properties, leading to improved energy harvesting performance.

Chapter 6 focuses on the development of PVDF/KNNLTS/MWCNT-based piezoelectric energy harvester devices. KNNLTS nanoparticles were synthesized using a high-energy ball milling process, while multi-walled carbon nanotubes (MWCNTs) were procured from Sigma-Aldrich. Both KNNLTS nanoparticles and MWCNTs were incorporated into the PVDF polymer matrix to enhance overall piezoelectric performance of the PENG device. MWCNTs, known for their excellent electrical conductivity, also promote the formation of the electroactive β -phase in PVDF by acting as an effective nucleating agent, thereby enhancing the piezoelectric response of the composite. The combined incorporation of KNNLTS ceramic nanoparticles and MWCNTs into the PVDF matrix significantly improves the overall piezoelectric performance of the piezoelectric nanogenerator (PENG) device, making it a promising candidate for energy harvesting applications.

Chapter 7 provides a conclusion of all findings of the present thesis work. The findings of this research lay the groundwork for further advancements in the field of flexible energy harvesters. Additionally, it outlines the future scope, potential social impact, and the challenges associated with the research.

References also form part along with bibliography at the end of each chapter.

LIST OF RESEARCH PUBLICATIONS INCLUDED IN THESIS

- 1. Komal Verma, Richa Sharma, A flexible piezoelectric generator based on KNN/PVDF composite films: Role of KNN concentration on the piezoelectric performance of generator, Chinese Journal of Physics, 84 (2023) 198 215. [Impact Factor: 5]
- 2. Komal Verma, Richa Sharma, Development of KNNLTS-PVDF-based flexible piezoelectric generator for energy-harvesting application, Bulletin of Materials Science, 47 (2024) 38. [Impact Factor: 2.1]
- 3. Komal Verma, Aman Kumar, Richa Sharma, Development of flexible piezoelectric nanogenerator based on PVDF/KNN/ZnO nanocomposite film for energy harvesting application, Journal of Materials Science: Materials in Electronics, 35 (2024) 1732. [Impact Factor: 2.8]
- 4. Komal Verma, Aman Kumar, Richa Sharma, Fabrication of lead-free PVDF/KNNLTS/MWCNT piezoelectric nanogenerator: Role of MWCNT in the piezoelectric performance of nanogenerator for energy harvesting application, Journal of Electronic and Materials, 53 (11) (2024) 7574-7592. [Impact Factor: 2.5]

LIST OF RESEARCH PUBLICATIONS OTHER THAN THESIS

1. Komal Verma, Sahil Goel, and Richa Sharma, Influence of calcination and sintering temperature on the microstructure, dielectric, ferroelectric and piezoelectric properties of the lead-free KNN ceramics, Journal of Materials Science: Materials in Electronics, 33 (2022) 26067-26085. [Impact Factor: 2.8]

RESEARCH WORK PRESENTED AT CONFERENCES

INTERNATIONAL CONFERENCES:

- K. Verma and R. Sharma, "A Flexible piezoelectric nanogenerator based on KNN/PVDF nanocomposite film for energy harvesting application" in the International Conference on Advanced Functional Materials and Devices for Sustainable Development (AFMD-2025) from 03-05 March, 2025, Atma Ram Sanathan Dharma College, University of Delhi, New Delhi, India. (ORAL TALK) (Received Best Oral Presentation Award)
- 2. <u>K. Verma</u>, "A Two-day Workshop on Structural Analysis (X-Ray Diffraction, Rietveld Refinement, HRTEM & SAED)", organized by Centre for Nanoscience and Nanotechnology, International Research Centre & Advanced Characterization Facility, Sathyabama Centre for Advanced Studies, Sathyabama Institute of Science and Technology, Chennai during February, 24-25, 2025. (ATTENDED)
- 3. <u>K. Verma</u> and R. Sharma, "Design of Flexible PVDF/KNaNbO₃ /NrGO nanogenerator and Understanding the Role of Nanofillers in the Output Voltage Signal" in the International Conference on Recent Advances in Functional Materials (RAFM-2024) held on March 14-16, 2024, at Atma Ram Sanatan Dharma College, University of Delhi, New Delhi-110078, India. (ORAL TALK)
- 4. <u>K. Verma</u> and R. Sharma, "KNN/PVDF composite films-based flexible piezoelectric generator: KNN concentration impact on a generator piezoelectric performance" in International Conference on Environment, Water, Agriculture, Sustainability and Health EWASH-2022: Strategizing A Greener Future, held on 12th -13th January 2023 Hindu College, University of Delhi, India. (ORAL TALK) (Received Best Oral Presentation Award)

- 5. K. Verma and R. Sharma, "Fabrication of lead-free PVDF/KNNLTS/MWCNT piezoelectric nanogenerator: Role of MWCNT in the piezoelectric performance of nanogenerator for energy harvesting application" at International Conference on Atomic, Molecular, Material, Nano and Optical Physics with Applications (ICAMNOP-2023), held during December 20-23, 2023 at Delhi Technological University, New Delhi, India. (POSTER)
- 6. <u>K. Verma</u> and R. Sharma, "Graphene oxide and KNN incorporated PVDF matrix to enhance mechanical energy as a flexible piezoelectric energy harvester" at the International Conference on Advanced Materials for Emerging Technologies (ICAMET-2023), held on May 4-6, 2023, at Netaji Subhash University of Technology, New Delhi, India. (ORAL TALK) (Received Best Oral Presentation Award)

NATIONAL CONFERENCES:

- 1. <u>K. Verma</u> and R. Sharma, "Fabrication of Flexible Piezoelectric Generator based on Li modified Potassium Sodium Niobate Ceramic and PVDF for Energy Harvesting Application" in the National Conference on Physics and Chemistry of Materials (NCPCM2023) held on 16th 18th March, 2023 at Govt. Holkar (Model Autonomous) Science College, Indore. (ORAL TALK)
- <u>K. Verma</u>, One Day National Seminar on "Recent Advancement in Semiconductor Devices and Materials "RASDM-2023" at Department of Applied Physics, Delhi Technological University, New Delhi. (ATTENDED)
- 3. <u>K. Verma</u> and R. Sharma, "Study of Dielectric and Piezoelectric Properties of rare-earth substituted KNN ceramics for Piezoelectric Energy Harvester" in National Webinar on Advances in Physics held on June 25-26, 2020, GJU, Hisar, Haryana. (POSTER)

TABLE OF CONTENTS

Table of Contents	Page No.
CANDIDATE'S DECLARATION	i
CERTIFICATE BY SUPERVISOR	ii
ACKNOWLEDGEMENTS	iii - vi
ABSTRACT	vii - xi
LIST OF RESEARCH PUBLICATIONS	xii
RESEARCH WORK PRESENTED AT CONFERENCES	xiii - xiv
CONTENTS	xv - xxi
LIST OF FIGURES	xxii - xxx
LIST OF TABLES	xxxi-xxxii
LIST OF ABBREVIATIONS	xxxiii
Chapter 1: Introduction	1-42
1.1 Overview	2
1.2 Energy Crisis.	3
1.3 Energy Harvesting and its Need	4
1.3.1 Piezoelectric Energy Harvesting Technology	5
1.3.1.1 Piezoelectric Generators (PEGs)	. 6
1.3.1.2 Piezoelectric Effect.	. 7
1.3.1.3 History of Piezoelectricity	. 7
1.4 Piezoelectric Materials	. 9
1.4.1 Piezoelectric Ceramic Materials	. 9
1.4.2 Piezoelectric Polymer Materials	. 11
1.4.3 Piezoelectric Composites	. 11
1.4.4 Applications of Piezoelectric Materials	. 13
1.5 Literature Review	. 14
1.5.1 Literature review on Ceramic-Based Piezoelectric Generators	for Energy
Harvesting Applications	14

1.5.2 Literature Review on Composite-Based Piezoelectric Generators fo	r
Energy Harvesting Applications	16
1.6 Material Selection	21
Potassium Sodium Niobate (KNN)	21
Poly (vinylidene fluoride) (PVDF) polymer	24
1.6.1 Literature Review on KNN-based PEGs for Energy Harvesting	
Applications	26
1.7 Thesis Problem	29
1.7.1 Thesis Objectives	29
1.7.2 Thesis Layout	30
References	35
Chapter 2: Synthesis and Characterization Techniques	43-64
2.1 Material Synthesis Methods	4 4
2.1.1 Solid-State Reaction Method	44
2.1.2 Hydrothermal Method	45
2.1.3 Co-precipitation Method	46
2.2 Fabrication of Flexible Composite Films: Drop Casting Method	47
2.3 Characterizations	48
2.3.1 Brief Description of Various Characterization Techniques	48
2.3.1.1 X-ray Diffraction (XRD)	48
2.3.1.1.1 X-rays	49
2.3.1.1.2 Bragg's Diffraction	49
2.3.1.2 Fourier Transform Infrared Spectroscopy (FTIR)	51
2.3.1.3 Scanning Electron Microscopy (SEM)	54
2.3.1.4 Field Emission Scanning Electron Microscopy (FESEM)	57
2.3.1.5 Polarisation vs. Electric Field Measurements (<i>P-E</i> Loop)	58
2.3.1.6 Dielectric Measurements	60
2.3.1.7 Displacement vs. Voltage (D. IA Rutterfly Loop	61

	2.3.	1.8 Elec	trica	1 Meas	ure	rei	er	r	n	n	1	;])	3	2	2	e	e	(•	•	•	((((•	(•	•	•	•	•	•	•	•	•	•	•	•	•	•	[1	[1	(1	•	•	•	(1	[r	r	ľ	1	1	l1	IJ	IJ	IJ	ľ	IJ	ľ	l	l	l	l	1	1	1	J	J	u	u	ľ	ι	ι	ι	ι	ι	ι	ι	ι	ι	ι	ι	ι	ι	u	J	J	l	l	IJ	ľ	L.	ľ	ľ	ľ	l	ľ	l	l	l	ľ	ľ	ľ	l	ľ	l	ľ	ľ	l	ľ	ľ	ľ	J
Reference	s	•••••	••••	•••••	•••	••	• •		•	•		•	•	•	•	•			•	•	•	•	•	•	•	•	•	•	•	•	•	•	•	•	•	•	•	•	•	•	•	•	•	•	•	•	•	•	•	•				•	•	•	•	•	•	•	•	•	•	•	•	•					•	•	•	•	•	•	•	•	•	•	•	•	•	•	•	•	•	•	•			•	•	•	•	•	•	•	•	•	•	•	•	•	•	•	•	•	•	•	•	•	•	•	•	•
Chapter	3:	Effect	of	KNN	1	c	C)(((:	•	•	C	c	C	C	(((((((•	•	(•	((((((((((•	((•	((•	•	•	•	•	•																										ſ	ſ			ſ	ſ	[ſ	ſ	ſ	[
		perfor	ma	nce of	f I	K	K	<	_	_	_		<	\	•	•	ŀ	ŀ	ŀ				ŀ	ŀ																ľ]]]]]]]]]]	,												•	•	•	•	•	•	•	•	f	f	f	f	f	f	f	f	f	ſ	ſ	f	f	f	f	f	f	f	f	•	•	•				•	•	•	•	•	•	•	•	•	•	•	•	•	•	•		•	•	•	•	•
		genera	ator	· • • • • • •	• • •		• •	, .	•	•	•		,	•	•	•	•	•	,				•	•	,	,		,									,	,	•	,	•	•	•	•	•	,	,	,	•	•	•	•	•	•	,					,		,	,	•	•	•	•	•	•	•	•	•	•	•	,		,	,	,	•	•	•	,			•	•	•	•	•	•	•	, .		,	,	,	,	,		•	,	,	,	,	,	,	,	,	,		,	,	,	,	•
3.1 Section	n 1		••••	•••••	•••	••	••		•	•	•		•	•	•	•	•		•	•	•	•	•	•	•	•	•	•	•	•	•	•	•	•	•	•	•	•	•	•	•	•	•	•	•	•	•	•	•	•	•			•	•	•	•	•	•	•	•	•	•	•	•	•	•	•			•	•	•	•	•	•	•	•	•	•	•	•	•	•	•	•	•	•	•			•	•	•	•	•	•	•	•	•	•	•	•	•	•	•	•	•	•	•	•	•	•	•	•	
3.1.1 I	ntro	duction	• • • • •	•••••	•••	•••	• •	• •	•	•	•	•	•	•	•		, .	•	•	•	•	•	•	•	•	•	•	•	•	•	•	•	•	•	•	•	•	•		•	•	•			•	•	•	•	•	•	, .	•	•	•	•	•	•	•	•	•	•	•	•						•	•	•	•	•	•	•	•	•	•	•	•	•	•	•	•	•	•	•	•	•	•	,		•	•	•	•	•	•	•	•		•	•	•	•	•	•	•	•	•	•	•	•	•	•	•
3.1.2 N	Mate	rials and	l Me	thods.	· • • •	•••	•	•	• •		•	•	•			•		•	•	•	•	•	•	•	•	•	•	•	•	•	•	•	•	•	•	•	•	•		•	•	•			, ,				, ,	•		•	•	•	•	•	•	•	•		•			•	•	•	•	•	•	•	•	•	•							•	•	•				•		•	•	•	•	,		•	, .	•	•	•																		•
	3.1.	2.1 Synt	hesis	s of K _{0.5}	5N	Vа	a	a(l((ŀ	1	а	г	2	ć		[;	I	1	J	Į	Ţ	Ţ	I	I	Į	I	Į	J	Į	Į	Į	Į	Į	Į	1	1	1	1	1	1	1	1	1	1	1	1	1	1	`	`	•	•	<u> </u>	1	ľ	ľ	ľ	ľ	ľ	ľ	ľ]]]	1	1]	.]	;	5	5	5	5	5	5	5	5	5	5	5	5	5	5	5	5	5	;	.]]	ľ	1	ľ	1	1	1	1	ľ	1	ľ	ľ	ľ	1	1	1	ľ	1	ľ	1	ľ	ľ	1	1	1	
	3.1.	2.2 Fabr	icati	on of K	N	11	N	N	V	J	•	•	1	ľ]]]	Γ.	1	1	1	Į	Ī	Ī	I	I	Į	I	Į	1	Į	Į	Į	Į	Į	Į	1	1	1	1	1	1	1	1	1	1	1	1	1	1	`	`		`	<u> </u>	1	ľ	ľ	ľ	ľ	ľ	ľ	ľ]]]	1	1]]			_		_	_	_	_	_	_	_	_	_	_	_	_		_]]	Ì	1	1	1	1	1	1	ľ	1	Ì	ľ	ľ	1	1	1	ľ	1	ľ	1	ľ	ľ	1	1	1	
	3.1.	2.3 Fabr	icati	on of K	ΚN	VI	N	N	\	V	`	1	ľ	1]]	۲.	ſ	1	1	1	1	J	J	J	J	1	J	1	1	J	J	J	J	J	J	I	I		1	J		V	V	J	J	J	J	J	J	\	\	`	\	1	ľ	ľ	ľ	ľ	l	ľ	l	l]]	J	J				_	_	_	_	_	_	_	_	_	_	_	′	_	_	_		_]	ľ	Ì	1	1	1	1	l	l]	l	l	l	l	l	l	l	l	l	l	l	l	l	l	
		(PEC	ਤੋ)					•					•	•						•		•	•	•	•	•	•	•	•								•	•															•		•			•																																																										
	3.1.	2.4 Char	acte	rization	1S.		• •						•		•	,	,			•	•									•	•	•	•	•	•	•			•		•					•	•	•			į,	5.	;	3	3	S	S	S	S	S	S	S	S	S	S	S	S	S			Į.	ı	1	1	1	1	1	1	1	1	1	1	1	1	1	1	1	1	Į.			S	S	S	S	S	S	S	S	S	S	S	S	S	S	S	S	S	S	S	S	S	S	S	S	
3.1.3 I	Resul	lts and I	Discu	ıssions	S			•	• (•	•	•				•	•	•	•	•	•	•	•	•	•	•	•	•	•	•	•	•	•	•	•	•	•			•										•	•	•	•	•			•						•	•	•	•	•	•	•	•	•	•		, ز	,	, ز	, ز	, ز	١,	١,	١,	١,	,	,	١.	•	•	•	•	•	•									•															•
	3.1.	3.1 Str	uctui	ral and	d]	ľ	ľ	N	N	ľ]																																												1	l	l	l	l	l	l	1	1	1	1	1	1	ŀ	1	1	d	d	ć	Ċ	C	C	Ċ	Ċ	C	C	ć	Ċ	C	C	Ċ	Ć	d	1	1	1	l	1	l	l	l	l	l	1	l	l	1	1	l	l	l	1	l	1	l	l	1	l	l	l	1
		Pov	wder							•			•																								•	•	•		•		•	•	•	•	•	•	•	•					•	•	•	•	•		•												•														•	•				•	•	•	•						•															,
	3.1.	3.2 Stru	ctura	al and	Mi	lic	ic	С	C:)	С	C	(į	į	į	i	i	i	1	1	1	i	i	1	1	1	1	1	1	1	1	1	1	1	1	[[[[:	[:	[:	[:	[:	[:	[:	[:	[:	[[I	1	1	1	/]	/	/	/.	/	/	/	/	/	٧	٧	٧	V	V	•	١	١	\	١	١	N	N	N	N	N	N	N	N	N	N	N	N	١	١	١	١	\	V	/	/	V	/	/	/	/	/	V	/	/	/	/	/	/	/	/	/	/	/	/	/	/	١
		Com	posi	te Film	ıs.	•••		•			•	•	•		•	•	•	•	•				•	•																															; .	;	3	5	3	3	3	3	5	S	S	S	S	S	S	S	S	S	S	S	LS	Ľ	ıs	LS	LS	ľ	ľ	Ę	15	Ľ	Ľ	15	5	S	S	S	S	S	;	5	3	3	3	3	5	3	S	5	5	3	3	3	5	3	5	3	3	5	3	3	3	S
	3.1.	3.3 FTIF	R An	alysis o	of l	P	Pı)	' l	Ί	P))	Ρ	P	F	F	I]]]]]]]]]]]]]]]]]]]						, -	, -	, -					Ē	f	f	f	f	f	f	f	f	f	f	1	1	1	1	1	ij)))))))))))))))))))))	j	1	f	f	f	f	f	f	f	f	1	f	f	f	f	f	f	f	f	f	f	f	f	f	f)
	3.1.	3.4 Die	electi	ric Pro	op	эe	eı	31	:1	ľ	;])	3	e	C	e	(() ())))()())))))))))))))))))))))))))	þ	p	ŗ	ľ	ľ	1	1	1	1]	1])]))))))))))	0	C	C	C	C	C	C	C	0	С	C	C	C	0)))))	1	1	<u>ا</u> ر]]])]]))])]]]])]])]]])]]]])
		Filı	ms		• • •	• • •			•	•	•	•		•	•	•	•	•					•	•																	•		•	•						•	•	•	•				•		•	•	•	•	•	•	•	•	•	•	•	•	•	•				•	•			•	•			•	•	•			•	•	•	•				•	•	•	•	•	•	•	•	•	•	•	•	•	•	•	•	•	•	•	•	•
	3.1																																																																																																																			
	3.1	1.3.6 Pie	zoel	ectric P	Per	rf	fo	fo	Ċ	Ċ	•	Ē	f	f	1	1	•]	•	ſ	r	r	r	r	r	r	r	r	r	r	r	r	r	r	r	r	r	r	r	ľ	r	r	ľ	r	r	r	r	r	r	1	1	:1	;1))	•	3	е	2	е	е	е	е	e	e	e	e	e	e	((•	•	•	•	•))	•	•	•	•	•	,)))	•	•	•	(•	E	2	2	2	е	е	е	e	2	E	e	e	2	2	2	e	2	e	2	е	e	2	2	2	(
	3.1	1.3.7 En	ergy	Harves	stir	in	18	18	g	٤	٤	L	1	1	1	1	ם	r	ľ	ľ	1	1	ľ	ľ	ľ	ľ	1	ľ	1	1	1	1	1	1	1	1	1	1	1	1	1	1	1	1	1	1	1	1	.1	11	i	i	i	i	j	ũ	t	t:	t	t	t	t	t	t	t	t	t	t	t	1	1	1	;1	;1	3	3	3	3	3	5	5	31	3	3	3	S	31	;1	1	1	t	t	Ū	t	t	t	t	t	t	t	t	t	t	t	t	t	t	t	t	t	t	t	t	t	t	1
3.2 Section	n 2	• • • • • • • • •	•••••	•••••	•••	••	• •	• •	•	•		•	•	•	•	•		•	•	•	•	•	•	•	•	•	•	•	•	•	•	•	•	•	•	•	•	•	•	•	•	•	•	•	•	•	•	•	•	•			•	•	•	•	•	•	•	•	•	•	•						•	•	•	•	•	•	•	•	•	•	•	•	•	•	•	•	•	•	•	•	•	•		•	•	•	•	•	•	•	•	•	•	•	•	•	•	•	•	•	•	•	•	•	•	•	•	•
3.2.1 1	[ntro	duction	••••	• • • • • • • •	••••	•••	•	•	• •	•	•	•	•	•		•		•	•	•	•	•	•	•	•	•	•	•	•	•	•	•	•	•	•	•	•	•			•					•	•	•				•	•	•	•	•		•					•	•	•	•	•	•	•	•	•	•	•	•	•		•	•	•			•	•			•	•	•	•	•	•	•	•			, .	, .	, .	•	,	•	•	•	,	,	,	•	,	•	,		•	,	,	,	•
3.2.2 N	Mate	rials an	d M	ethods	•••	••	٠.	٠.		•			•	•		•	•				•	•					•		•	•	•	•	•	•	•	•	•	•	•	•	•	•	•	•	•	•	•	•	•	•	•				•	•	•	•	•	•	•	•	•	•	•	•	•	•					•	•	•	•	•	•	•	•	•	•	•	•	•	•	•	•			•	•	•	•	•				•	•	•	•	•	•	•	•	•	•	•	•	•	•	•	•	•	
3: Effect of KNN performance of generator	Effect of KNN performance of generator	of KNN mance of ator	KNN nce of thods s of K _{0.5} on of K on of K on of K all and M te Films alysis o ric Pro ation vs and KN ectric Po						Na Ni	Na NN N	Na Ni	Na Ni	I H								1	1 i					1 i		1 i	1	1 i	1 i	1 i	1 i	1 i	1 i				1																																																																												
3: Effect of KNN performance of generator	Effect of KNN performance of generator	of KNN mance of ator	thods. s of K _{0.5} on of K on of K on of K all and M te Films alysis o ric Pro ation vs and KN ectric P Harves				I N N N N S	Na Ni	Na Ni	Na NN NI fP pe E N/I erf in	Na Ni	C K	Mi Ni	I N N N N N S II N P P II N P P II	I N N N N S	I N N N N S				· · · · · · · · · · · · · · · · · · ·		· · · · · · · · · · · · · · · · · · ·	· · · · · · · · · · · · · · · · · · ·	· · · · · · · · · · · · · · · · · · ·	· · · · · · · · · · · · · · · · · · ·	· · · · · · · · · · · · · · · · · · ·	· · · · · · · · · · · · · · · · · · ·	· · · · · · · · · · · · · · · · · · ·	· · · · · · · · · · · · · · · · · · ·		· · · · · · · · · · · · · · · · · · ·	· · · · · · · · · · · · · · · · · · ·	· · · · · · · · · · · · · · · · · · ·	· · · · · · · · · · · · · · · · · · ·	· · · · · · · · · · · · · · · · · · ·	· · · · · · · · · · · · · · · · · · ·																																																																																
3: Effect of KNN performance of generator 1	Effect of KNN performance of generator	of KNN mance of ator	kNN nce of thods. s of K _{0.5} on of K on of K rization ussions ral and te Film alysis o ric Pro ation vs and KN ectric P Harves				N N N N N N N N N N N N N N N N N N N	Na Ni	c k	Na NN NI S	c k	Na Ni	Ni N	N N N N N N N N N N N N N N N N N N N	N N N N N N N N N N N N N N N N N N N	N N N N N N N N N N N N N N N N N N N	N N N N N N N N N N N N N N N N N N N	N N N N N N N N N N N N N N N N N N N																																																																																																		

3.2.2.1 Synthesis of KNN Nanoparticles	85
3.2.2.2 Fabrication of PVDF/KNN 15 wt.% Flexible Nanocomposite	
Film.	86
3.2.2.3 Fabrication of PENG Device	86
3.2.2.4 Characterizations	86
3.2.3 Results and Discussions	87
3.2.3.1 Structural and Microstructural Analysis of KNN Nanoparticles	. 87
3.2.3.2 Structural and Morphological Analysis of PVDF/KNN 15 wt.9	6
Nanocomposite Film	88
3.2.3.3 Dielectric Properties of the PVDF/KNN 15 wt.% Nanocomp Film	osite 90
3.2.3.4 Polarisation vs. Electric Field (P-E) Hysteresis Loop of	the
PVDF/KNN 15wt.% Nanocomposite Film	91
3.2.3.5 Piezoelectric Performance of PVDF/KNN 15 wt.% PENG	
Device	92
3.2.3.6 Energy Harvesting Performance of PENG Device	93
3.3 Conclusion	95
References	96
Chapter 4: Study of energy harvesting performance of piezoelec	etric
nanogenerator based on three phase PVDF/KNN/ZnO nanocompo	site
films	-128
4.1 Introduction	102
4.2 Experimental Details	105
4.2.1 Synthesis of KNN Nanoparticles	105
4.2.2 Synthesis of ZnO Nanoparticles	105
4.2.3 Fabrication of PVDF/KNN/ZnO Flexible Nanocomposite Films.	106
4.2.4 Fabrication of PENG Device	107
4.2.5 Characterizations	108

4.3 Results and Discussions	109
4.3.1 Structural and Microstructural Analysis of KNN Nanoparticles.	109
4.3.2 Structural and Microstructural Analysis of ZnO Nanorods	109
4.3.3 Structural Analysis of the Nanocomposite Films	110
4.3.3.1 XRD Analysis of the PVDF/KNN/ZnO Flexible Nanoco	omposite
Films	110
4.3.3.2 FTIR Analysis of the PVDF/KNN/ZnO Flexible Nanoco	omposite
Films	111
4.3.3.3 Surface Morphology Studies of PVDF/KNN/ZnO	Flexible
Nanocomposite Films	113
4.3.4 Polarisation vs. Electric Field (<i>P-E</i>) Hysteresis Loops of the Nanoco	omposite
Films	113
4.3.5 Dielectric Properties of the PVDF/KNN/ZnO Nanocomposite	
Films	115
4.3.6 Piezoelectric Performance of PVDF/KNN/ZnO PENG Devices.	117
4.3.6.1 Energy Harvesting Performance of PENG Device	124
4.4 Conclusion	124
References	126
Chapter 5: Effect of Li, Ta and Sb doping on the output perform	ance of
KNN/PVDF based flexible piezoelectric generator	29-149
5.1 Introduction	129
5.2 Materials and Experimental Details	132
5.2.1 Materials.	132
5.2.2 Synthesis of KNNLTS Ceramic Powder	132
5.2.3 Fabrication of PVDF/KNNLTS Flexible Composite Films	132
5.2.4 Fabrication of PVDF/KNNLTS based Piezoelectric Generator (PEG).	133
5.2.5 Characterizations	134
5.3 Results and Discussions	134

5.3.1 Structural Analysis	134
5.3.1.1 Structural Analysis of KNNLTS Ceramic Powder	134
5.3.1.2 Structural Analysis of Pure PVDF Film and PVDF/KNNLTS	Flexible
Composite Film	135
5.3.2 Surface Morphology Studies of KNNLTS Ceramic Powder, Pur	e PVDF
Film and PVDF/KNNLTS Composite Film	136
5.3.3 FTIR Analysis of the Pure PVDF Film and PVDF/KNNLTS Compo	site
Film	137
5.3.4 Dielectric properties of Pure PVDF Film and PVDF/KNNLTS	Flexible
Composite Film	138
5.3.5 Polarisation vs. Electric Field (P-E) hysteresis Loops of Pure PVD	F Film
and PVDF/KNNLTS Flexible Composite Film	139
5.3.6 Piezoelectric Performance of PEG Device	140
5.3.7 Energy Harvesting Performance of PEG Device	145
5.4 Conclusion	146
References	147
Chapter 6: Effect of KNNLTS concentration and conductiv	e filler
(MWCNT) in realizing high perform	mance
PVDF/KNNLTS/MWCNT flexible piezo	electric
nanogenerator for powering electronics devices. 1	50-173
6.1 Introduction	150
6.2 Experimental Section	152
6.2.1 Materials	152
6.2.2 Synthesis of KNNLTS Nanoparticles	152
6.2.3 Development of Nanocomposite Films based on	
PVDF/KNNLTS/MWCNTs	153
6.2.4 Fabrication of Piezoelectric Nanogenerator using	
the PVDF/KNNLTS/MWCNT Nanocomposite Films	155

6.2.5 Characterizations.	155
6.3 Results and Discussions	156
6.3.1 Structural and Microstructural Analysis of KNNLTS Nanoparticles.	156
6.3.2 Structural Analysis of the Nanocomposite Films	157
6.3.2.1 XRD analysis of the PVDF/KNNLTS/MWCNTs	
Flexible Nanocomposite Films	157
6.3.3 FTIR Analysis of PVDF/KNNLTS/MWCNTs Nanocomposites	
Films	158
6.3.4 Surface Morphology Studies of PVDF/KNNLTS/MWCNTs Nanoco	omposite
Films	160
6.3.5 Dielectric Properties of PVDF/KNNLTS/MWCNTs Nanoc	omposite
Films	161
6.3.6 Piezoelectric Performance of PVDF/KNNLTS/MWCNTs	PENG
Device	163
6.3.7 Energy Harvesting Performance of PENG Device	170
6.4 Conclusion	171
References	172
Chapter 7: Conclusion, Future Scope, and Social Impact	174-179
7.1 Conclusion	174
7.2 Future Scope	178
7.3 Social Impact	179

LIST OF FIGURES

Figure No.	Figure Captions	Page No
1.1	(a) Direct piezoelectric effect and (b) Inverse piezoelectric effect.	7
1.2	Applications of piezoelectric materials as an energy harvester.	14
1.3	Orthorhombic crystal structure of Potassium Sodium Niobate (KNN) ceramic.	22
1.4	Structures of α , β and γ phases of polyvinylidene fluoride (PVDF).	26
2.1	Schematic presentation of hydrothermal autoclave used in hydrothermal method.	46
2.2	Schematic illustration of drop casting technique showing the synthesis of composite film.	48
2.3	Schematic representation of the diffraction of X-rays obeying Bragg's law.	50
2.4	High resolution X-ray Diffractometer (Rigaku- Ultima IV).	51
2.5	Schematic of Michelson Interferometer.	53
2.6	Schematic showing Fourier Transform Infrared Spectroscopy (FTIR).	53
2.7	Fourier Transform Infrared Spectroscopy (FTIR) by Perkin Elmer FTIR Spectrum-II Instrument.	54
2.8	Schematic showing the components of a Scanning Electron Microscopy (SEM).	56
2.9	Scanning Electron Microscopy (SEM) by JEOL (JSM-6610LV).	57
2.10	Field Emission Scanning Electron Microscopy (FESEM) by Gemini SEM 500, Zeiss.	58
2.11	Polarisation vs. Electric field (<i>P-E</i>) Loop Ferroelectric Test System (MARINE: 20PF 1KHz 0.1N)	59

2.12	Impedance Analyzer (Model: KEYSIGHT E4990A), Sample Holder	61
	and PID Temperature Controller Unit.	
2.13	(a) Dynamic Shaker (Micron MEV-0025), (b) Digital Storage Oscilloscope (Tektronix MDO 500), (c) Keithley Digital Multimeter (DMM7510) and (d) Electrometer (Keysight B2902B).	62
3.1	Schematic representation of KNN/PVDF flexible composite film fabrication process and the digital photographs of the prepared flexible composite films with different weight percentages of KNN ceramic particles in PVDF matrix.	69
3.2	(a) Schematic diagram of the fabricated PEG device and (b) digital photograph of the prepared PEG devices.	70
3.3	XRD pattern of calcined KNN ceramic powder.	71
3.4	(a) SEM image of the calcined KNN ceramic powder and (b) Histogram showing the distribution of KNN particles.	72
3.5	(a) X-ray Diffraction patterns produced with different content of KNN ceramic powder in PVDF matrix and (b) higher magnified view of Figure 3.5 (a).	73
3.6	SEM surface micrographs of KNN/PVDF composite films with different content of KNN ceramic powder in PVDF matrix (a-d) on $10~\mu m$ scale and (e-h) on $40~\mu m$ scale.	73
3.7	(a) FTIR spectra of pure PVDF film and composite films with different content of KNN ceramics in the PVDF matrix and (b) Magnified view of the Figure 3.7(a) and (c) Variation of absorption intensities at 763 cm ⁻¹ and 836 cm ⁻¹ as a function of KNN ceramic powder concentration in PVDF matrix.	75
3.8	Variation of Dielectric constant (ε_r) with frequency of pure PVDF film and KNN/PVDF composite films.	76

3.9	(a) P - E hysteresis loop of different composite films, (b) Variation of remnant polarization (P_r) and (c) maximum polarization (P_{max}) with	78
	content of KNN ceramic powder in the PVDF matrix.	
3.10	Working Mechanism of PEG device.	79
3.11	(a-e) Open-circuit voltage generated using KNN/PVDF PEG device with different content of KNN ceramic powder in PVDF matrix and (f) Variation of open-circuit voltage as a function of KNN ceramic content in the PVDF matrix.	80
3.12	(a-e) Short-circuit current generated using KNN/PVDF PEG devices with different content of KNN ceramic powder in PVDF matrix and (f) Variation of short-circuit current as a function of KNN ceramic content in the PVDF matrix.	81
3.13	Variation of Maximum Open-Circuit Voltage with number of cumulative taps for 15 wt.% KNN/PVDF PEG device.	81
3.14	Displacement vs. Voltage (<i>D-V</i>) butterfly curve of the flexible composite film containing 15 wt.% KNN in the PVDF.	82
3.15	The generated open-circuit voltage when PEG device containing 15 wt.% KNN ceramic powder in the PVDF matrix (a) elbow curving and (b) bended by finger.	83
3.16	Synthesis of KNN nanoparticles by hydrothermal method.	86
3.17	XRD pattern of the calcined KNN nanoparticles synthesized by hydrothermal method.	87
3.18	(a) FESEM image of the calcined KNN nanoparticles and (b) Histogram showing the distribution of particle size.	88
3.19	X-ray Diffraction pattern of PVDF/KNN 15 wt.% nanocomposite film.	88
3.20	FTIR spectra of PVDF/KNN 15 wt.% nanocomposite film.	89
3.21	SEM image of DVDE/KNN 15 wt % nanocomposite film	90

3.22	Variation of Dielectric constant with frequency of PVDF/KNN 15	91
	wt.% nanocomposite film.	
3.23	<i>P-E</i> hysteresis loop analysis of PVDF/KNN 15 wt.% nanocomposite film.	91
3.24	The generated (a) open circuit piezoelectric output voltage and (b) short circuit current of the PENG PVDF/KNN 15 wt.%.	92
3.25	(a) Variation of voltage and current measured with external load resistances and (b) power density measured with external resistances of PVDF/KNN 15 wt.% film-based PENG device.	93
3.26	The generated voltage with PENG fabricated with PVDF/KNN 15 wt.% nanocomposite film by (a) finger tapping, (b) thumb pressing, (c) fist beating, (d) finger bending, (e) elbow bending and (f) showing glowing LED.	95
4.1	Synthesis of ZnO nanoparticles by Co-precipitation method.	105
4.2	Schematic representation of the preparation of PVDF/KNN/ZnO flexible nanocomposite films.	107
4.3	(a) Schematic diagram of the fabricated PENG device and (b) Photograph of the prepared PENG device.	108
4.4	XRD plot of calcined ZnO nanorods.	109
4.5	(a) FESEM image of calcined ZnO nanorods and (b) Histogram showing the distribution of diameter of ZnO nanorods.	110
4.6	X-ray Diffraction patterns of the flexible nanocomposite films produced with different content of KNN and ZnO in the PVDF matrix.	111
4.7	(a) FTIR spectra of pure PVDF film and nanocomposite films (b) Enlarged view of the FTIR spectra in the range 700 cm ⁻¹ to 870 cm ⁻¹ of Figure 4.7 (a), and (c) Variation of β - phase content as a function of KNN and ZnO nanoparticles concentration in the PVDF matrix.	112

4.8	FESEM surface micrographs of (a) Pure PVDF, (b)	113
	PVDF/KNN/0%ZnO, (c) PVDF/KNN/0.45%ZnO, (d) PVDF/KNN/1%ZnO, (e) PVDF/KNN/7.5%ZnO and (f) PVDF/KNN/15%ZnO.	
4.9	P - E Hysteresis Loops of (a) pure PVDF, (b) PVDF/KNN/0%ZnO, (c) PVDF/KNN/0.45%ZnO, (d) PVDF/KNN/1%ZnO, (e) PVDF/KNN/7.5%ZnO, (f) PVDF/KNN/15%ZnO (g) and (h) Variation of P_r and P_s as a function of KNN/ZnO concentration in PVDF matrix.	114
4.10	Dielectric constant (ε_r) of pure PVDF, PVDF/KNN/0%ZnO, PVDF/KNN/0.45%ZnO, PVDF/KNN/1.5%ZnO, and PVDF/KNN/15%ZnO flexible nanocomposite films.	116
4.11	The generated open circuit piezoelectric plots of the PENG device (a) pure PVDF, (b) PVDF/KNN/0%ZnO, (c) PVDF/KNN/0.45%ZnO, (d) PVDF/KNN/1%ZnO, (e) PVDF/KNN/7.5%ZnO and (f) PVDF/KNN/15%ZnO.	118
4.12	Variation of peak-to-peak open circuit voltage of the PENG devices as a function of KNN and ZnO nanoparticles concentration in the PVDF matrix.	139
4.13	The generated short circuit current plots of the PENG device (a) pure PVDF, (b) PVDF/KNN/0%ZnO, (c) PVDF/KNN/0.45%ZnO, (d) PVDF/KNN/1%ZnO, PVDF/KNN/7.5%ZnO and (f) PVDF/KNN/15%ZnO.	120
4.14	Variation of peak-to-peak short circuit current of the PENG device as a function of KNN and ZnO nanoparticles concentration in the PVDF matrix.	121

4.15	(a) Plot of current density with type of sample, (b) Output voltage and	122
	current measured with external resistance, (c) Power density	
	measured with external resistance for PVDF/KNN/0.45%ZnO film-	
	based PENG and (d) Displacement vs. Voltage (D-V) butterfly curve	
	for PVDF/KNN/0.45%ZnO film-based PENG.	
4.16	The generated voltage with PENG fabricated with	125
	PVDF/KNN/0.45%ZnO nanocomposite film by (a) pen tapping, (b)	
	elbow bending, (c) finger moving, (d) wrist stretching, (e) circuit with	
	full wave bridge rectifier for glowing LEDs, (f) showing glowing	
	LED and (g) power a digital wrist watch.	
5.1	(a) Schematic representation of fabrication process of	133
	PVDF/KNNLTS flexible composite film and (b) Schematic diagram	
	of the fabricated PEG device.	
5.2	(a) XRD pattern of calcined KNNLTS ceramic powder and (b)	135
	enlarged XRD pattern in the 2θ range of 44.5° – 47° .	
5.3	X-ray Diffraction pattern of (a) PVDF film and (b) PVDF/KNNLTS	136
	15 wt.% flexible composite film.	
5.4	SEM image of KNNLTS calcined ceramic powder.	137
5.5	SEM surface micrographs of (a) Pure PVDF film and (b) PVDF/	137
5. 5	KNNLTS 15 wt.% composite film.	157
. (•	120
5.6	FTIR spectra of (a) PVDF film and (b) PVDF/KNNLTS 15 wt.% composite film.	138
	•	120
5.7	Dielectric constant (ε_r) of (a) PVDF, and (b) PVDF/KNNLTS 15	139
	wt.% composite film as a function of frequency.	
5.8	Polarisation vs. Electric field (<i>P-E</i>) ferroelectric hysteresis loop for	140
	(a) PVDF film and (b) PVDF/KNNLTS 15 wt.% composite film at	
	room temperature.	
5.9	Working Mechanism of PEG device.	141

5.10	Open-circuit voltage generated using (a) PVDF and (b) PVDF/KNNLTS 15 wt.% PEG devices.	142
5.11	Short-circuit current generated using (a) PVDF and (b) PVDF/KNNLTS 15 wt.% PEG devices.	142
5.12	Variation in (a) Voltage and (b) Current by varying the load resistance from $10M\Omega$ to $100M\Omega$ for PVDF/KNNLTS 15 wt.% PEG device.	143
5.13	Displacement vs. Voltage (<i>D-V</i>) butterfly curve for PVDF/KNNLTS 15 wt.% composite film.	145
5.14	The generated open-circuit voltage using PEG device containing 15 wt.% KNNLTS ceramic particles in the PVDF matrix for (a) fist beating, (b) elbow bending, (c) quenching, and fist opening and (d) Glowing LEDs.	146
6.1	Synthesis of KNNLTS nanoparticles via solid-state reaction method followed by high energy ball mill.	153
6.2	Synthesis of PVDF/KNNLTS/MWCNTs flexible nanocomposite films.	154
6.3	(a) Schematic diagram of the fabricated PENG device and (b) Digital photograph of piezoelectric nanogenerator.	155
6.4	XRD pattern of calcined KNNLTS nanoparticles.	157
6.5	SEM image of calcined KNNLTS nanoparticles (a) 100 nm scale & (b) 1µm scale.	157
6.6	X-ray Diffraction patterns of the flexible nanocomposite films produced with pure PVDF and different content of KNNLTS nanoparticles and MWCNT in the PVDF matrix.	158
6.7	FTIR spectra of the pure PVDF film and flexible nanocomposite films with different content of KNNLTS nanoparticles and MWCNT in the PVDF matrix.	160

6.8	PVDF/0%KNNLTS/MWCNT, (c) PVDF/10%KNNLTS/MWCNT,	161
	(d) PVDF/15%KNNLTS/MWCNT, (e)	
	PVDF/20%KNNLTS/MWCNT and (f) PVDF/25%KNNLTS/MWCNT.	
6.9	Variation of Dielectric constant (ε_r) as a function of frequency of PVDF/KNNLTS/MWCNTs nanocomposite films.	163
6.10	The generated open circuit piezoelectric output voltage plots of the PENG (a) Pure PVDF, (b) PVDF/0%KNNLTS/MWCNT, (c) PVDF/10%KNNLTS/MWCNT, (d) PVDF/15%KNNLTS/MWCNT, (e) PVDF/20%KNNLTS/MWCNT and (f) PVDF/25%KNNLTS/MWCNT.	164
6.11	The generated short circuit current plots of the PENG (a) Pure PVDF, (b) PVDF/0%KNNLTS/MWCNT, (c) PVDF/10%KNNLTS/MWCNT, (d) PVDF/15%KNNLTS/MWCNT, (e) PVDF/20%KNNLTS/MWCNT and (f) PVDF/25%KNNLTS/MWCNT.	165
6.12	Variation of peak-to-peak (a) open circuit voltage (b) short circuit current and (c) current density of the PENG device as a function of KNNLTS and MWCNT nanoparticles concentration in the PVDF matrix.	166
6.13	(a) Variation of generated output voltage and current with varying external resistance and (b) Variation of power density with external resistance of PVDF/20%KNNLTS/MWCNT film-based PENG device.	167
6.14	Stability test of PVDF/20%KNNLTS/MWCNT film-based PENG under 2000 cycles.	169
6.15	Displacement vs. Voltage (<i>D-V</i>) butterfly curve for PVDF/20%KNNLTS/MWCNT film-based PENG device.	169

- (a) Electrical circuit used for powering LEDs (b) Lighting LEDS (c)
 Pictorial representation of the devices digital thermometer and (d)
 digital wrist watch derived by PVDF/20%KNNLTS/MWCNT based
 PENG device.
- 6.17 The output voltage generated by PVDF/20%KNNLTS/MWCNT 171 film-based PENG by (a) finger tapping, (b) thumb pressing, (c) fist beating, (d) elbow beating, (e) elbow bending, and (f) wrist stretching.

LIST OF TABLES

Гable No.	Table Captions	Page No
1.1	A brief comparison of the various properties of lead-free piezoelectric materials.	10
1.2	Comparison of piezoelectric performance of various piezoelectric generators using different fillers in polymer matrix.	20
1.3	Various properties of the pure and modified KNN ceramics.	24
1.4	Comparison of piezoelectric performance of various KNN based piezoelectric generators.	25
3.1	Details of weight percentages of KNN and PVDF in the fabricated flexible composite films.	69
3.2	Comparison of the piezoelectric performance between PVDF/KNN PEG fabricated in the present work and various generators reported in the literature.	
4.1	Details of weight percentages of KNN, ZnO and PVDF in the fabricated flexible nanocomposite films.	106
4.2	Comparison of the piezoelectric performance between PVDF/KNN/ZnO PENG fabricated in the present work and various nanogenerators reported in the literature.	
5.1	Comparison of the piezoelectric performance of the PEG device developed in present work with other reported PEG devices.	143
6.1	Details of the weight (gm) of PVDF, KNNLTS and MWCNT & volume (ml) of the DMF used in the fabricated flexible nanocomposite films.	
6.2	Dielectric properties of pure PVDF and different nanocomposite films.	162

6.3 Comparison of the piezoelectric performance between 167 PVDF/KNNLTS/MWCNT PENG nanogenerator fabricated in the present work and various nanogenerators reported in the literature.

LIST OF ABBREVIATIONS

Acronyms Meaning

PEG Piezoelectric energy generator

BaTiO₃ Barium titanate

PZT Lead zirconate titanate

KNN Potassium sodium niobate

PVDF Polyvinylidene fluoride

PDMS Polydimethylsiloxane

PTFE Polytetrafluoroethylene

PET Polyethylene terephthalate

TPU Thermoplastic polyurethane

PLZT Lead lanthanum zirconate titanate

PMN-PT Lead magnesium niobate-lead titanate

LiNbO₃ Lithium niobate

LiTaO₃ Lithium tantalate

KNbO₃ Potassium niobate

NaNbO₃ Sodium niobate

DMF N, N-dimethyl formamide

V_{oc} Open circuit voltage

I_{sc} Short circuit current

wt.% Weight percentage

Chapter 1

Introduction

Chapter 1

Introduction



This chapter begins by systematically addressing the energy crisis and the growing need for energy harvesting, highlighting the existing shortfalls in meeting these demands. It then reviews various energy harvesting techniques, emphasizing particularly on piezoelectric energy harvesting as a promising method, which converts

mechanical energy into electrical energy by using piezoelectric generators (PEGs). Owing to their versatility and effectiveness, PEGs have emerged as a focal point of research, since they can harvest energy from human body motions and mechanical vibrations by using piezoelectric effect while also serving as self-powered devices in a wide range of applications. Furthermore, various types of piezoelectric materials, including inorganic, organic and composite-based materials have been discussed which can be employed for the construction of PEGs. A review of existing literature on piezoelectric generators is conducted to identify research gaps and to establish the primary objectives of the present thesis work.

1.1 Overview

Energy harvesting is increasingly vital in today's world due to growing demand for sustainable and renewable energy sources. Energy harvesting, also known as energy scavenging, is the process of capturing and converting ambient energy from external sources such as solar, thermal, wind and mechanical vibrations into usable electrical energy that would otherwise get wasted [1-4]. Furthermore, as traditional energy resources like fossil fuels become scarcer and their environmental impacts are more severe, alternative solutions are necessary to ensure sustainable energy production, reduce greenhouse gas emission and meet the growing global energy demand with minimal environmental impact. This not only reduces dependency on conventional power grids but also enables the development of self-powered systems, particularly in remote or inaccessible locations where frequent battery replacement is impractical.

Among various energy harvesting technologies, piezoelectric energy harvesting has gained significant attention of the scientific community due to its ability to convert abundantly available mechanical energy in the surrounding into useful electrical energy using piezoelectric generators (PEGs), making them ideal for powering low-energy devices such as wireless sensors, portable electronics and medical implants [5-7]. For constructing PEGs both organic and inorganic piezoelectric materials have been used [8-11, 3]. However, the inherent defects of the ceramic materials such as brittleness, low toughness and high temperature fabrication processes, have led to the efforts for the development of composite - based flexible piezoelectric generators

composed of piezoelectric materials as fillers and polymer as the flexible matrix. These types of devices have shown outstanding piezoelectric response in wearable and flexible applications enabling innovative solutions for energy harvesting, self-powered sensors, health monitoring systems and smart textiles, thanks to their lightweight, biocompatibility and mechanical adaptability [12-15].

Various studies on piezoelectric energy harvesting technologies have primarily been reviewed to identify the research gaps that guide the major objectives of the present thesis. Within this framework, the thesis introduces innovative strategies for harnessing mechanical energy through the piezoelectric effect, with a strong emphasis on understanding the underlying mechanisms and fabricating devices capable of enhancing harvesting efficiency.

Building on existing research, this thesis aims to develop high-performance flexible PEGs using PVDF-based composites. The study incorporates pure and Li, Ta and Sb-modified KNN ceramics as fillers in the PVDF matrix to enhance piezoelectric properties of the composites. Additionally, ZnO nanorods and MWCNT have also been added as fillers along with KNN ceramic in the PVDF matrix which is expected to significantly improves β -phase formation in PVDF, thereby increasing energy harvesting performance of PEGs. The fabricated PEG devices successfully converted mechanical energy from biomechanical motions, such as finger tapping and elbow bending, into usable electrical power, demonstrating their ability to drive LEDs and small electronic devices. These findings highlight the potential of PEGs based on KNN-PVDF composites for applications in flexible, self-powered and wearable electronic systems.

Overall, the thesis work aims to establish a practical, durable and cost-effective approach that also ensures environmental sustainability, thereby contributing to the advancement of next-generation energy harvesting solutions.

1.2 Energy Crisis

An energy crisis occurs when there is a significant shortage or disruption in the supply of energy resources, leading to economic, social and environmental challenges. There are various factors by which energy can be influenced that disrupts the balance between energy supply and demand. The rising global population and industrialization have led to increased energy consumption without corresponding increase in supply or improvement in efficiency. The energy crisis is not driven by a single factor but rather a combination of geopolitical, economic, environmental and technologies issues. Addressing this crisis requires a comprehensive approach, including investment in renewable energy, improving energy efficiency, modernizing infrastructure and promoting international cooperation.

1.3 Energy Harvesting and its Need

Energy harvesting, also known as energy scavenging, is the process of capturing and converting ambient energy from external sources that would otherwise be wasted into usable-electrical energy. This energy can be harvested from various sources such as thermal (heat), wind (airflow), solar (sunlight), mechanical (vibrations), etc. It is increasingly vital in today's world due to growing demand for sustainable and renewable energy sources. As traditional energy resources like fossil fuels become scarcer and their environmental impact is more severe, alternative solutions are necessary to power the small and low power devices which are integral to modern technology. Addressing the reduction of carbon footprints, global warming and climate change, governments and environmental protection agencies worldwide are promoting the adoption of sustainable practices and eco-friendly technologies across various industries. Furthermore, this not only reduces dependency on conventional power grids but also enables the development of self-powered systems, particularly in remote or inaccessible locations where frequent battery replacement is impractical.

In our environment, various energy sources are present, including fuel energy, nuclear energy, wind energy, hydropower, solar energy and others. These sources are broadly categorized into two groups: renewable and non-renewable energy. Renewable energy sources, such as solar power, hydropower, wind, geothermal energy and biofuels, are those that naturally replenish and are sustainable over time. On the other hand, non-renewable energy sources, like fossil fuels (oil, coal, natural gas) are finite and can be depleted, as they take millions of years to form and are not quickly replenished once used. Thus, energy harvesting is key to advancing the Internet of Things (IoT), enabling the deployment of sensor networks and smart devices that can operate

autonomously, thereby supporting a more efficient and connected world. Despite its potential, energy harvesting faces several challenges, including the efficiency of energy conversion and the amount of power that can be generated. The energy available from ambient sources is often low and can fluctuate, making it difficult to maintain a stable power supply. The goal of energy harvesting is to convert these otherwise unusable forms of energy into electrical energy that can power devices, particularly those that require minimal amounts of energy, such as sensors, wireless devices and portable electronics.

Advances in materials science, such as the development of novel thermoelectric, piezoelectric and pyroelectric materials, have significantly enhanced the efficiency and applicability of energy harvesting technologies. Among these, Piezoelectric energy harvesting technology which utilizes piezoelectric materials has emerged as a promising field of energy harvesting. Piezoelectric materials generate electrical energy in response to mechanical stress or vibrations.

1.3.1 Piezoelectric Energy Harvesting Technology

Piezoelectric energy harvesting technology, mechanical energy, such as vibrations or pressure is converted, into useful electrical energy using piezoelectric materials. They enable self-powered operation of low-power electronic systems in various environments. This technology is valuable for harvesting energy from ambient mechanical sources such as vibrations, pressure changes and movements. It is particularly effective in environments with consistent mechanical vibrations, such as machinery, bridges and roads. Recent research has also explored integrating piezoelectric materials into wearable devices to harvest energy from human motions.

The ongoing advancements in materials and the growing demand for sustainable, maintenance-free power solutions in dynamic environments further enhance its appeal. This is particularly valuable in remote or hard-to-reach locations, where changing batteries is impractical. The growing interest in smart infrastructure is another significant demand driver, as piezoelectric systems can be integrated into buildings, bridges and roads to monitor structural health continuously. As technology continues to evolve, piezoelectric energy harvesting is expected to play a crucial role in the development of smart, energy-efficient systems across multiple industries.

1.3.1.1 Piezoelectric Generators (PEGs)

Piezoelectric generator is a broad term used for any device that produce electrical energy from mechanical stress or deformation through piezoelectric effect. While, piezoelectric nanogenerator (PENG) refers to the device which uses nanostructures such as nanoparticles, nanotubes, nanorods etc. to achieve higher efficiency, flexibility and applications in wearable energy harvesting. They are commonly used for powering small-scale electronic devices in self-sustaining systems. In recent years, a wide range of piezoelectric generators have been developed utilizing various piezoelectric ceramic materials due to their excellent electromechanical properties. Despite their high piezoelectric performance, these ceramic materials possess inherent drawbacks such as brittleness, low mechanical flexibility, poor fracture toughness and the necessity for high-temperature processing during fabrication. These limitations significantly hinder their application in emerging fields that demand flexibility, stretchability and mechanical robustness, such as wearable electronics and soft robotics.

To overcome these challenges, research has increasingly focused on the development of composite-based flexible piezoelectric generators. These devices are typically fabricated by embedding piezoelectric ceramic fillers—such as Barium Titanate (BaTiO₃), Lead Zirconate Titanate (PZT), or Potassium Sodium Niobate (KNN)—into a flexible polymer matrix like polyvinylidene fluoride (PVDF), polydimethylsiloxane (PDMS), or thermoplastic polyurethane (TPU). This combination allows for the retention of the piezoelectric properties of the ceramic fillers while simultaneously imparting flexibility, processability and durability from the polymer matrix. Such composite-based PEGs have demonstrated excellent performance in flexible and wearable technologies. Their advantages include lightweight nature, biocompatibility, enhanced mechanical adaptability and the ability to conform to curved or moving surfaces. As a result, these devices have opened new opportunities for sustainable and self-powered systems, including energy harvesting from human motions, real-time health monitoring, interactive textiles and smart wearable sensors. This evolution marks a significant step toward integrating advanced materials into next-generation electronic and energy devices.

1.3.1.2 Piezoelectric Effect

Piezoelectricity can be categorized into two ways i.e. direct and inverse piezoelectric effect and are depicted in Figure 1.1. In direct piezoelectric effect, electric charge is generated when the material is mechanically stressed. When pressure, tension, or shear stress is applied on a piezoelectric material, its internal structure undergoes a shift, resulting in the separation of positive and negative charge centers. This separation leads to the formation of an electric dipole moment, which generates an electric charge on the material's surface. On the other hand, in inverse piezoelectric effect, strain is induced into the material due to the application of the external electric field.

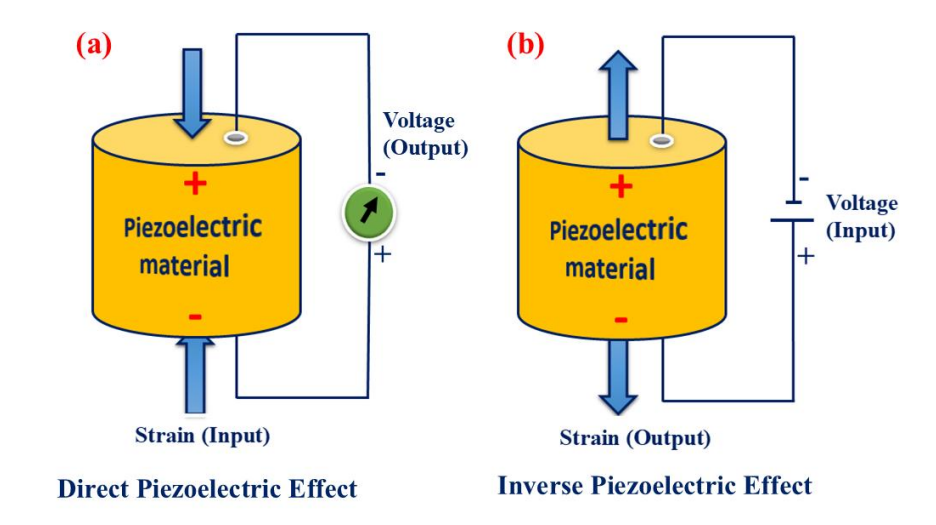


Figure 1.1 (a) Direct piezoelectric effect and (b) Inverse piezoelectric effect.

When an external electric field is applied to a piezoelectric material, the dipoles within the material align with the field, causing the material to stretch or compress. This deformation can be controlled by varying the strength and direction of the electric field. These effects are crucial in various applications, including sensors, actuators, energy harvesters, medical devices etc. Different types of piezoelectric materials such as single crystals, ceramics, polymers and the composite materials have been studied so far.

1.3.1.3 History of Piezoelectricity

Piezoelectricity, derived from the Greek word "Piezein" meaning "to press", is a phenomenon where certain materials generate an electric charge when mechanically stressed. The phenomenon of piezoelectricity was first discovered by the French physicists Pierre and Jacques Curie in 1880. They observed that certain crystals, such as quartz, topaz, tourmaline, cane sugar and Rochelle salt, generated an electric charge when subjected to mechanical stress. This effect was termed "direct piezoelectricity". However, in 1881, Gabriel Lippmann, a French physicist, provided a theoretical foundation for the piezoelectric effect based on thermodynamics. He mathematically proved the existence of the inverse piezoelectric effect, which the Curie brothers subsequently verified. Piezoelectricity is defined as the phenomenon involving the coupling between mechanical and electrical behaviour. In 1910, Woldemar Voigt published a textbook on crystal physics that describes the piezoelectric behaviour of 20 natural crystals in detail with their piezoelectric constants using various tensor analysis.

In the early 20th century, piezoelectricity was used in sonar technology, particularly during World War I. Paul Langevin and his team developed the first practical application by using quartz to create ultrasonic waves for detecting submarines. World War II saw a significant advancement in piezoelectric materials, particularly with the development of barium titanate (BaTiO₃) in the year 1945, a ceramic material exhibiting strong piezoelectric properties. This period marked the transition from natural crystals to synthetic materials, which were easier to synthesize and manipulate. After the war, piezoelectric materials have become an integral part in various industries, from consumer electronics (e.g., phonographs, microphones) to medical devices (e.g., ultrasound imaging).

The latter half of the 20th century saw the development of new piezoelectric materials, including lead zirconate titanate (PZT), which offered superior piezoelectric properties and became widely used in various applications. Research in the 1960s and 1970s focused on developing polymers like polyvinylidene fluoride (PVDF), which exhibited piezoelectric properties in a flexible, lightweight form. Today, piezoelectric materials are ubiquitous in modern technology. The rise of nanotechnology has also opened new avenues for piezoelectric materials applications, such as nanoscale sensors and energy-harvesting devices.

1.4 Piezoelectric Materials

Piezoelectric materials possess the unique ability to produce an electric charge when subjected to mechanical stress. These materials are generally categorized into two main types: naturally occurring and man-made. Examples of natural piezoelectric materials include quartz (SiO₂), Rochelle salt (potassium sodium tartrate), topaz, tourmaline and certain organic substances such as silk, rubber, bone, hair, wood and enamel. Among these, quartz is widely recognized as one of the most prominent natural piezoelectric materials. It has a trigonal crystal structure and is commonly used in watches, clocks and various sensing devices. Man-made piezoelectric materials, on the other hand, can indeed be broadly classified into three major classes i.e., inorganic materials, organic materials and composites. In the next sections, these have been discussed in detail.

1.4.1 Piezoelectric Ceramic Materials

Inorganic piezoelectric materials are known for their high piezoelectric coefficients and often used in applications requiring high performance, stability and durability. There are variety of inorganic piezoelectric materials including lead zirconate titanate (PZT), barium titanate (BaTiO₃), cadmium sulphide (CdS), bismuth ferrite (BiFeO₃), lead lanthanum zirconate titanate (PLZT), lead magnesium niobate-lead titanate (PMN-PT), lithium niobate (LiNbO₃), lithium tantalate (LiTaO₃), potassium niobate (KNbO₃), sodium niobate (NaNbO₃), potassium sodium niobate (KNN)and many more. PZT is one of the most commonly used piezoelectric materials due to its excellent piezoelectric properties and high dielectric constant. It exhibits a high piezoelectric coefficient ($d_{33} \approx 500-600 \text{ pC/N}$), making it highly efficient in converting mechanical energy into electrical energy. However, PZT contains lead, which raises significant environmental and health concerns. Regulatory frameworks like the EU's RoHS directive have restricted the use of hazardous substances, including lead, prompting a global push for eco-friendly alternatives. In this context, lead-free ceramics such as Potassium Sodium Niobate (KNN) have gained prominence for offering promising piezoelectric performance without the environmental drawbacks associated with lead-based materials. BaTiO₃ is another lead-free piezoelectric ceramic that demonstrates promising piezoelectric performance along with enhanced environmental compatibility, making it a sustainable alternative to traditional leadbased materials. In Table 1.1, various properties of different lead-free piezoelectric materials are summarized.

Table 1.1 A brief comparison of the various properties of lead-free piezoelectric materials.

S. No.	Piezoelectric Material	Synthesis Method	E _c (kV/cm)	P_r (μ C/cm ²)	<i>T_c</i> (°C)	<i>d</i> ₃₃ (pC/N)	Ref.
1.	K _{0.5} Na _{0.5} NbO ₃	Solid- state	4.57	25.5	409	117	[16]
2.	0.95BaTiO ₃ - 0.05Bi(Zn _{2/3} Nb _{1/3})O ₃	Solid- state	8	5	120	22.7	[17]
3.	Bi _{0.5} Na _{0.35} K _{0.1} Li _{0.05} Ti O ₃	Solid- state	24	31		300	[18]
4.	0.98NaNbO₃- 0.02BiErKZrO₃	Solid- state	2.91	4.93	420	156	[19]
5.	K _{0.5} Na _{0.5} NbO ₃ - K ₄ CuNb ₈ O ₂₃	Solid- state	40	13.3		102	[20]
6.	0.79(Bi _{0.5} Na _{0.5} TiO ₃)_ 0.14(Bi _{0.5} K _{0.5} TiO ₃)_ 0.07BaTiO ₃ :0.25 mol % MnO ₂	Solid- state	23.2	24.3	251	150	[21]
7.	(Ba _{0.85} Ca _{0.15}) (Zr _{0.1} Ti _{0.9})O ₃	Solid- state	1.23	10.45	90	585	[22]
8.	0.94(K _{0.5} Na _{0.5}) NbO ₃ -0.06 Ba(Zr _{0.05} Ti _{0.95})O ₃	Solid- state	1.08	18.8	318	234	[23]
9.	0.7BiFeO ₃ - 0.3BaTiO ₃	Solid- state	20.7	26	530	134	[24]
10.	0.7BiFeO ₃ -0.3SrTiO ₃	Solid- state	85	50	422	69	[25]

1.4.2 Piezoelectric Polymer Materials

Organic piezoelectric materials, have attracted considerable interest due to their flexibility, lightweight, cost-effective production and scalability. Organic piezoelectric materials are especially attractive in applications like wearable electronics, sensors and energy harvesting devices because of their mechanical flexibility, biocompatibility and ease of processing. Unlike brittle ceramic materials, piezoelectric polymers can be bent, stretched and deformed without breaking, making them ideal for use in flexible and wearable devices. These materials are typically much lighter than their ceramic counterparts. The first discovery of piezoelectricity in a polymer was made by Kawai in 1969 [26]. Kawai's research showed that when PVDF was stretched and polarized, it exhibited a piezoelectric effect, a property previously not associated with polymers. This ground breaking work opened the door to further research into the piezoelectric properties of polymers, leading to the development of other piezoelectric polymers and copolymers.

There are different polymer-based piezoelectric materials which include poly (vinylidene fluoride) (PVDF) and its copolymers, such as poly (vinylidene fluoride-trifluoro ethylene) (PVDF-TrFE) and poly (vinylidene fluoride-hexafluoropropylene) (PVDF-HFP), along with polylactic acid (PLA), polyurethane (PU) and polyimide (PI). Among these, PVDF is one of the most widely studied piezoelectric polymers. Furthermore, Poly (L-lactic acid) (PLLA) is a biodegradable and biocompatible polymer with piezoelectric properties, often used in medical applications [27]. Piezoelectric polymers can be processed at lower temperatures using standard polymer processing techniques, such as extrusion, injection moulding and film casting. This ease of processing makes it possible to produce large-area and complex-shaped piezoelectric devices at a lower cost.

1.4.3 Piezoelectric Composites

Piezoelectric composites are materials that combine the unique properties of piezoelectric materials with the mechanical flexibility and durability of polymers. Piezoelectric polymer composites were first developed by Kawai in 1969 [26]. Kawai's work laid the foundation for the development of polymer-based piezoelectric composites, marking a key milestone in piezoelectric materials research. Common

piezoelectric materials embedded in a polymer matrix like polyvinylidene fluoride (PVDF) include lead zirconate titanate (PZT), barium titanate (BaTiO₃) and potassium sodium niobate (KNN), etc.

For instance, Wankhade *et al.* reported the development of a nanohybrid of PVDF and lead zirconate titanate (PZT) prepared via the solution route for energy harvesting applications. The incorporation of PZT enhanced the β-phase content of PVDF, thereby improving its piezoelectric response of the device. A device fabricated from this nanohybrid successfully converted mechanical energy from human motions into electrical energy, generating a maximum output voltage of 55 V and a power density of 36 μWcm⁻², demonstrating its potential for powering low-power electronic devices [28]. PVDF polymer has a significantly higher voltage constant—about ten times greater than that of PZT—it suffers from a much lower piezoelectric charge constant and dielectric constant compared to PZT [29, 30]. On the other hand, PZT possesses high charge and dielectric constants, which are crucial for efficient piezoelectric performance. By combining these two materials, their individual limitations can be effectively mitigated, creating a composite that leverages the strengths of both.

BaTiO₃ is a well-known piezoelectric material that is often combined with PVDF to create composite films for energy harvesting applications. A device fabricated using this composite generated an output voltage and current of 8.22 V and 3.36 μ A, respectively, demonstrating its potential for mechanical energy conversion [31]. Similarly, another study reported the construction of a nanogenerator using BaTiO₃ nanoparticles embedded in a PVDF-HFP matrix, which achieved a remarkable output of approximately 75 V and 15 μ A under a lower applied pressure of 0.23 MPa [32]. These findings highlight the effectiveness of BaTiO₃/PVDF-based composites in enhancing piezoelectric performance through optimized material design. Potassium Sodium Niobate (KNN) has also been explored as a filler in PVDF-based electrospun fibrous web nanogenerators, achieving a high output voltage of approximately 21 V and an output current of around 22 μ A. The enhanced performance is attributed to the improved interaction between the PVDF chains and KNN nanorods [33], facilitated by the surface modification of the nanofiller. This strong interfacial bonding effectively

promotes polarization and charge transfer, contributing to the superior piezoelectric response of the nanogenerator.

Based on this, our thesis work is focussed on the development of a piezoelectric nanogenerator using ceramic materials as fillers and polymers as the matrix. This approach aims to enhance energy harvesting performance of the PEGs through composite design.

1.4.4 Applications of Piezoelectric Materials

Recent advancements in material science and the increasing demand for energyefficient and intelligent technologies have expanded the applications of piezoelectric materials. These materials, capable of generating electrical charge under mechanical stress or undergoing deformation in response to an electric field, are widely utilized across various fields, including energy harvesting and medical devices. Among their most promising applications is energy harvesting, where mechanical energy from ambient sources such as vibrations, motions and pressure is converted into electrical energy. Piezoelectric materials, especially in the form of flexible composites, are being integrated into various structures to harness energy from ambient mechanical sources. In wearable technology, they are integrated into smart clothing, shoes and fitness trackers to harvest energy from human motions, powering low-energy devices like sensors and health monitors. In infrastructure and industrial applications, they capture vibrations from machinery, buildings and bridges to power remote structural health monitoring systems. Roadways and sidewalks embedded with piezoelectric materials generate energy from traffic, which can be used for powering streetlights or stored for later use.

In the medical field, piezoelectric materials play a crucial role in diagnostic and therapeutic devices. They are key components in ultrasound transducers, implantable sensors and pacemakers, where they aid in real-time imaging, physiological monitoring and precise stimulation of biological tissues. Industries such as automotive, aerospace rely on piezoelectric sensors for pressure, force and acceleration measurements, enhancing performance and safety. Acoustic sensors are used in hearing aids, microphones and noise-cancelling devices, while actuators enable precise inkjet printing and microfluidic control. In consumer electronics, piezoelectric buzzers,

speakers and haptic feedback systems improve user experience in smartphones, gaming and virtual reality applications.

The continuous development of flexible and biocompatible piezoelectric materials is driving innovations in energy harvesting, healthcare and smart infrastructure, paving the way for sustainable and advanced technological applications. Figure 1.2 shows the various ways of harvesting energy using the piezoelectric materials.



Figure 1.2 Applications of piezoelectric materials as an energy harvester.

1.5 Literature Review

1.5.1 Literature review on Ceramic-Based Piezoelectric Generators for Energy Harvesting Applications

Ceramic-based piezoelectric materials are widely studied for energy harvesting due to their good piezoelectric performance, durability and high energy conversion efficiency. Their crystalline structure and mechanical strength make them ideal for applications such as powering sensors and small devices, particularly in remote areas. Lead zirconate titanate (PZT) is the most extensively researched piezoelectric ceramic material due to its superior piezoelectric and dielectric properties and has been widely used for the construction of PEGs. A. Hussain *et al.* reported the development of a piezoelectric energy harvesting device based on Y-doped PMN-PT ceramics [34].

Their device demonstrated improved performance, generating an output voltage of approximately 60 V under periodic mechanical tapping conditions (2.0 kgf at 5 Hz), indicating its suitability for powering various self-sustaining electronic systems. Despite its widespread use, the presence of lead in PZT based ceramic raises environmental and health concerns, motivating research into lead-free piezoelectric alternatives. Zhai *et al.* reported the development of a piezoelectric energy harvester based on textured CuO-doped KNN-LS ceramics. The incorporation of CuO and texturing significantly enhanced the material's energy harvesting capability. The fabricated cantilever-type device achieved an open-circuit voltage of 19 V and a power density of 3 µW/mm³ under an applied acceleration of 1 m/s², demonstrating its strong potential for efficient energy harvesting applications [35].

Furthermore, Shekhar et al. fabricated an energy harvester utilizing Praseodymium (Pr)-modified lead-free BCZT ceramics [36]. Their device achieved an open-circuit voltage of around 5.1 V and a power density of 1.213 mW/cm² under finger-tapping excitation. In addition, when subjected to machine tapping over 10,000 cycles, the output voltage increased to approximately 9 V, demonstrating good durability and stable performance. In another study, Camargo et al. integrated a BNKT ceramic sample onto a steel beam mounted on an electrodynamic shaker [37]. Their setup revealed the practical potential of BNKT ceramics for mechanical energy harvesting, achieving a peak output voltage of around 19.9 V and a corresponding power density of 3.36 mW/cm². Liu *et al*. developed CuO doped BCZT piezoelectric energy harvester which demonstrated significant potential in energy harvesting applications. At 0.50 mol% CuO-doped BCZT PEG achieved peak-to-peak voltage of 14.1 V and a current of 28.2 µA with power generation of 1.8 µW/mm³ [38]. Zhang et al. reported the development of a vibrational energy harvester based on NBT-KBT-BT ceramics. The cantilever-type device exhibited a high open-circuit voltage of approximately 12.2 V and a power density of 0.37 µW/mm³. This study highlights the potential of such ceramics as a promising platform for designing high-performance mechanical energy harvesting systems [39]. However, brittleness and lack of flexibility of ceramics limit their use in applications requiring material deformation, such as wearable or flexible devices, where cracking or failure can occur under bending or strain.

1.5.2 Literature Review on Composite-Based Piezoelectric Generators for Energy Harvesting Applications

Composite based piezoelectric materials have attracted considerable attention because they are flexible, lightweight and easy to process. This makes them useful in wearable devices, sensors and other self-powered systems. Typically, these materials consist of a polymer matrix such as polyvinylidene fluoride (PVDF) with inorganic fillers like lead zirconate titanate (PZT), barium titanate (BaTiO₃), potassium sodium niobate (KNN), zinc oxide (ZnO), etc. The spatial distribution and structural integration of fillers within the polymer matrix play a crucial role in determining the composite's mechanical, electrical and piezoelectric performance. The addition of piezoelectric ceramic fillers significantly improves the dielectric, ferroelectric and piezoelectric responses of the polymer, thereby increasing energy harvesting performance of the PEGs devices. Given their ability to convert mechanical vibrations into electrical energy, these composites serve as a promising alternative to traditional rigid ceramics, especially in environments where flexibility is essential.

Paradiso et al. were among the first to explore wearable energy harvesting by integrating piezoelectric materials into footwear [40]. They used PZT strips and PVDF foils in shoe soles to generate electricity from walking, successfully powering lowenergy devices and highlighting the potential of piezoelectric materials in wearable applications. Li et al. fabricated a flexible piezoelectric nanocomposite by incorporating hydrothermally synthesized PMN-PT nanorods into a PVDF matrix. The resulting film achieved a peak output voltage of 10.3 V and a current of 0.046 µA approximately 13 times higher than that of pure PVDF [41]. When compared to PMN-PT/PDMS composites, the PMN-PT/PVDF configuration exhibited superior performance [42]. Siddiqui et al. developed a flexible piezoelectric nanogenerator using BaTiO₃ nanoparticles embedded in PVDF-TrFE via spin coating [43]. At 40 wt.% BaTiO₃, the device generated output voltage and current of approximately 9.8 V and 0.69 µA, respectively with a power density of 13.5 µW/cm² under repeated bending. The device also demonstrated practical energy harvesting from body movements, producing voltages of 7.5 V by index finger joint, 4.3 V by wrist bending and 1.5 V by elbow bending.

In another study, Zhao *et al.* fabricated a nanogenerator with 70 wt.% BaTiO₃ in PVDF using a scalable solvent evaporation method [44]. The device showed uniform particle dispersion and produced an output voltage and current of up to 35 V and 0.6 μA, respectively under 1 MPa and 150 V and 1.5 μA under 10 MPa. Aluri *et al.* studied the piezoelectric performance of a hybrid nanogenerator made by incorporating barium titanate zirconate (BTZO) into a PVDF polymer matrix [45]. Their results showed that the BTZO/PVDF nanogenerator generated a higher output voltage of 11.5 V, which was significantly greater than the 7.99 V produced by the BTO/PVDF nanogenerator, indicating improved energy harvesting efficiency with BTZO.

Baek *et al.* achieved outstanding performance from a piezoelectric nanogenerator by incorporating BaTiO₃ nanoparticles (NPs) and nanowires (NWs) into a PDMS matrix [46]. The PENG generated a maximum open-circuit voltage (V_{oc}) of approximately 60 V, a short-circuit current (I_{sc}) of 1.1 μ A and an instantaneous power output of 40 μ W. Furthermore, the device demonstrated excellent durability, maintaining stable performance for up to 3000 bending and unbending cycles, highlighting its reliability for energy harvesting applications. Lin *et al.* fabricated a flexible piezoelectric nanogenerator using a nanocomposite consisting of 3 wt.% BaTiO₃ nanotubes embedded in a PDMS matrix [47]. The BaTiO₃ nanotubes were synthesized through a hydrothermal process, ensuring high aspect ratios and effective stress transfer. Under an applied pressure of 1 MPa, the PENG produced an output voltage of 5.5 V and a current of 350 nA, successfully powering a commercial LCD. The incorporation of PDMS provided the device with excellent flexibility and long-term stability.

Barium Calcium Zirconate Titanate (BCZT) is another promising lead-free piezoelectric material with a high piezoelectric coefficient, similar to that of traditional PZT [48]. Patra *et al.* developed flexible and biocompatible nanocomposites by adding BCZT powder into PVDF using tape casting and hot pressing [49]. Nanogenerators with 60 wt.% PVP-modified BCZT/PVDF produced a peak voltage of 23 V, which was higher than the 14 V from unmodified composites. This improved output was enough to light up 55 LEDs without an external capacitor, showing strong potential for wearable and implantable devices.

Zinc Oxide (ZnO) is another effective nanofiller that has shown promising results when incorporated into the PVDF matrix. Thakur *et al.* reported that adding 0.85 vol% ZnO nanoparticles increased the β -phase content of PVDF to around 84%, which enhances its piezoelectric properties [50]. Additionally, Juan Yi *et al.* developed electrospun PVDF films containing Y-doped ZnO and studied the effect of filler content on piezoelectric performance [51]. The device with 15 wt.% ZnO generated output voltages of approximately 20 V during walking and about 35 V during running, demonstrating its potential for wearable energy harvesting. Li *et al.* developed a PVDF/ZnO nanogenerator by hydrothermally growing ZnO nanowires on a spin-coated PVDF film. The resulting hybrid device produced an output voltage of approximately 2 V higher than that of pure PVDF [52].

Jung *et al.* fabricated a flexible piezoelectric nanogenerator (PENG) using a NaNbO₃ nanowire (NW)/PDMS composite [53]. The device demonstrated an output voltage of 3.2 V and a current of 72 nA under a 0.23% compressive strain, attributed to the high d_{33} coefficient of the perovskite NaNbO₃ NWs, which enhanced its piezoelectric response. Ren *et al.* developed a flexible piezoelectric nanogenerator (PENG) based on a bismuth ferrite (BiFeO₃) nanoparticle (NPs)/PDMS nanocomposite, utilizing various BiFeO₃ concentrations ranging from 10 to 40 wt.% [54]. The PENG with 40 wt.% BiFeO₃ achieved an output voltage (V_{oc}) of approximately 3 V and a short-circuit current (I_{sc}) of 0.25 μ A under repeated hand pressing. Similarly, Abinnas *et al.* fabricated a PENG using a bismuth titanate (BiTiO₃)/PDMS nanocomposite [55], which generated an output voltage of 8 V when subjected to finger tapping, following poling at 5 kV for 3 hours.

In recent advancements, nanomaterials such as carbon-based additives (like graphene and its reduced form (rGO), CNTs, MWCNTsand carbon nanofillers) and metallic nanoparticles (silver and gold) have also been used as filler into the polymer matrix to further enhance the functional properties of these composites. Incorporating CNTs into PVDF enhances its electrical conductivity and facilitates charge mobility, while also promoting the formation of the piezoelectric β -phase, thereby improving energy harvesting performance [56]. Levi *et al.* used the solvent casting method to fabricate PVDF and its copolymer-based nanocomposites with various types of CNTs. Their

results showed an increased β -phase content in PVDF/CNT composites compared to pure PVDF, with a corresponding rise in piezoelectric coefficient from ~20 pC/N in pure PVDF-TrFE to ~25 pC/N in the CNT-based composites [57].

The inclusion of nanomaterials like multiwalled carbon nanotubes (MWCNTs) not only enhances mechanical strength but also contributes to improved dielectric properties and overall energy output. Park et al. designed a nanocomposite-based generator by combining piezoelectric barium titanate (BaTiO₃) nanoparticles with carbon-based materials, including carbon nanotubes and reduced graphene oxide [58]. These nanomaterials were dispersed in a polydimethylsiloxane (PDMS) matrix and then spin-coated onto a metal-coated plastic substrate. The resulting device generated an output voltage of 3.2 V and a current of 0.3 µA when subjected to a mechanical strain of 0.33%, demonstrating its effectiveness for energy harvesting applications. Similarly, Shi et al. synthesized PVDF nanofibers reinforced with 15 wt.% BaTiO₃ and 0.15 wt.% graphene nanosheets, achieving up to 11 V and 4.1 µW output under 2 Hz loading [59]. The device maintained stable performance over 1800 bending cycles and could generate up to 12 V from finger tapping, sufficient to power 15 LEDs and a digital watch. Sun et al. studied a flexible nanogenerator composed of zinc oxide nanoparticles (ZnO-NPs) and MWCNTs embedded in a PDMS matrix for energy harvesting applications [60]. Their results showed that the nanogenerator produced a significantly higher output, delivering 7.5 V and 18.75 µW per cycle, highlighting its enhanced performance.

Furthermore, Graphene has emerged as a promising conductive filler due to its large surface area, high aspect ratio and excellent thermal, mechanical and electrical properties [61-63]. Alamusi *et al.* demonstrated that incorporating reduced graphene oxide (rGO) into PVDF enhanced its piezoelectric performance, with a peak output voltage of 3.28 V achieved at 0.05 wt.% rGO loading [64]. Higher rGO content (0.2 wt.%) slightly reduced the output, as excessive filler content hindered β -phase formation of the PVDF. Further studies using PVDF-TrFE/rGO composites showed that 0.1 wt.% rGO yielded a maximum output of 2.4 V and 0.8 μ A under a 2 N force, with 3.2 μ W power at 1.8 M Ω load resistance [65]. Abolhasani *et al.* fabricated PVDF/graphene nanofiber-based nanogenerators via electrospinning, finding that 0.1

wt.% graphene enhanced β -phase content the most [66]. Under 0.2 MPa pressure and 1 Hz frequency, the device produced output voltage and current of 7.9 V and 4.5 μ A, respectively - nearly double the output of pure PVDF nanofibers. The stored energy was sufficient to power an LED for over 30 seconds. Table 1.2 shows the comparison of piezoelectric performance of various piezoelectric generators using different fillers in the polymer matrix.

Table 1.2 Comparison of piezoelectric performance of various piezoelectric generators using different fillers in the polymer matrix.

S. No.	Filler material in the polymer matrix	Polymer used	Film Synthesis Method	V _{oc} (V)	<i>I_{sc}</i> (μA)	Power (μW)/ Power density (μW/cm²)	Ref.
1.	ZnO nanoparticles	PVDF	Drop- casting	1.81	0.57	0.21	[67]
2.	PZT particles	PVDF	Electro- spinning	0.184		30.69	[68]
3.	ZnO microrods	PVDF	Supersonic spraying	15.2	32	12.5	[69]
4.	BaTi _{0.95} Zr _{0.05} O ₃	PVDF	Solution casting	26	0.028	22.5	[70]
5.	PMN-PT/rGO	PVDF- TrFE	Drop casting	30	30		[71]
6.	ZnO nanofibers	PVDF	electrospin ning	0.079	0.170	0.091	[72]
7.	Na _{0.5} Bi _{0.5} TiO ₃ - BaFe ₁₁ Co _{0.5} Ti _{0.} ₅ O ₁₉	PVDF	Solution casting	23.5	0.21	0.336	[73]
8.	PDA@BaTiO ₃ nanoparticles & CNT	PVDF	Drop- casting	4.4	0.66		[74]

9.	ZnO nanoparticles & MWCNT	PVDF	Drop- casting	22		21.41	[75]
10.	Pt nanoparticles	PVDF	Electro- spinning	30	6	22	[76]
11.	CNT	PVDF	Electro- spinning	1.89	0.011		[77]
12.	BaTiO ₃ Nanowires	PDMS	Spin coating	60	1.1	40	[46]
13.	BaTiO ₃ /ZrO ₂	PVDF- HFP	Electro- spinning	6.3	0.67	3.09	[78]
14.	NaNbO ₃ NPs	PDMS	Spin coating	3.2	0.072	0.0006	[53]
15.	BCZT/MWCN Ts	PDMS	Spin coating	39.7	1.9	9.85	[79]
16.	KNN nanoparticles	PDMS	Solution casting	14.49	2.10	0.75	[80]
17.	KNN nanorods & CNT	PVDF	Electrospin ning	23.24	9.0	52.29	[81]

1.6 Material Selection

Potassium Sodium Niobate (KNN)

Potassium Sodium Niobate (KNN) is a prominent lead-free piezoelectric material belonging to the perovskite family with the chemical formula $(K_xNa_{1-x})NbO_3$. Its perovskite crystal structure, represented as ABO₃, consists of alkali metal ions (K^+/Na^+) occupying the A-site, while the niobium ion (Nb^{5+}) resides at the B-site, surrounded by oxygen ions (O^{2-}) in an octahedral configuration. KNN is a solid solution of ferroelectric potassium niobate $(KNbO_3)$ and antiferroelectric sodium niobate $(NaNbO_3)$, exhibiting piezoelectric coefficients ranging from 100 to 300 pC/N, a high Curie temperature of 420 °Cand a remnant polarization of 33 μ C/cm² [82]. At

its morphotropic phase boundary (MPB), where the composition is K_{0.5}Na_{0.5}NbO₃, KNN achieves peak piezoelectric performance, demonstrating stability across various compositions. Figure 1.3 shows the orthorhombic crystal structure of KNN ceramic. The orthorhombic phase of KNN provides structural distortion and spontaneous polarization, which are essential for achieving good piezoelectric performance [83].

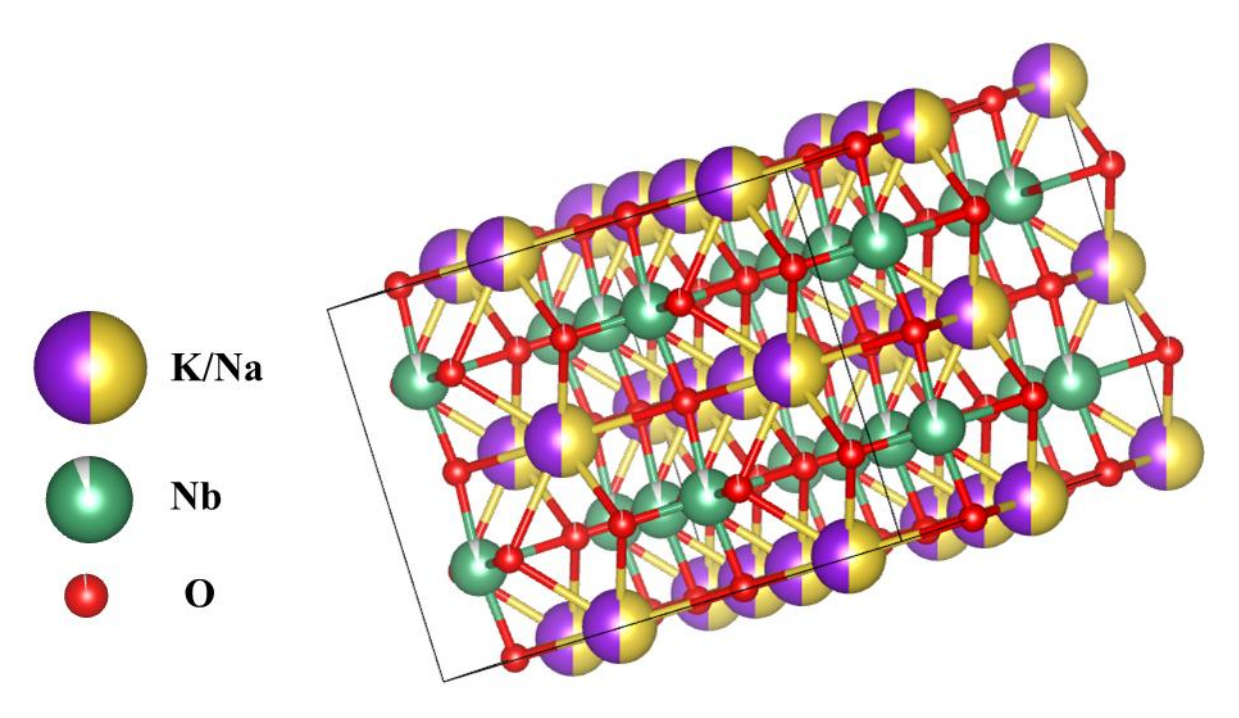


Figure 1.3 Orthorhombic crystal structure of Potassium Sodium Niobate (KNN) ceramic.

Different techniques are available for synthesizing KNN ceramic powder such as solid-state, hydrothermal, sol-gel, combustion, etc. Among these, the solid-state route is most widely employed due to its simplicity and scalability, while wet-chemical methods such as sol-gel and hydrothermal techniques offer better control over particle size, morphology and compositional homogeneity.

Piezoelectric output performance of the PEG devices is significantly dependent on the dielectric, piezoelectric and ferroelectric properties of the materials used for their construction [84]. Literature reports suggest that compositional modifications such as doping or forming solid solutions with suitable perovskite oxides serves as an effective approach to enhance the dielectric, piezoelectric and ferroelectric properties of ceramic materials. For instance, Hao *et al.* synthesized KNN-LT ceramic using the

hydrothermal method and reported a piezoelectric constant of 187 pC/N, a remnant polarization of 19.85 μC/cm² and a Curie temperature of 461.8 °C [85]. Furthermore, Lin *et al.* investigated the structural and electrical properties of KNN-LS piezoelectric ceramics prepared via the conventional solid-state method. They reported that the incorporation of lithium and antimony into the KNN matrix resulted in a piezoelectric constant of approximately 212 pC/N, a remnant polarization of 15 μC/cm², a coercive field of 1.74 kV/cm, which were considerably higher compared to those of unsubstituted KNN [86]. Wang *et al.* investigated the structural and piezoelectric properties of Li-modified KNN lead-free ceramics and observed the coexistence of orthorhombic and tetragonal phases. They reported an enhanced piezoelectric constant of 280 pC/N along with a high Curie temperature of 475 °C, both of which are higher than those of pure KNN [87].

Satio and co-workers successfully developed textured doped KNN using a reactive templated grain growth method [88]. This innovative approach led to a significant enhancement in the material's piezoelectric properties, achieving a piezoelectric constant of 416 pC/N for $(K_{0.44}Na_{0.52}Li_{0.04})(Nb_{0.86}Ta_{0.10}Sb_{0.04})O_3$ composition. This represents a considerable improvement over traditionally synthesized KNN. Furthermore, Gao et al. obtained a remarkably strong piezoelectricity in KNN based ceramics doped with Li, Ta and Sb with chemical composition $(K_{0.45}Na_{0.55})_{0.98}L_{i0.02}(Nb_{0.77}Ta_{0.18}Sb_{0.05})$ O₃ ceramic $(d_{33} = 413 \text{ pC/N})$ which were synthesized by conventional solid – state reaction method [89]. These findings suggest that by tailoring the synthesis process and adding dopants, KNN's piezoelectric and dielectric properties can be substantially improved, making it a more viable candidate for the construction of PEGs for energy harvesting applications. Table 1.3 summarises the various properties of the pure and modified KNN ceramics. From here it can be analyzed that KNN is a leading candidate in the ongoing search for lead-free piezoelectric materials, offering a promising combination of good piezoelectric properties, environmental safety and thermal stability.

Table 1.3 Various properties of the pure and modified KNN ceramics.

S. No.	Pure/Doped Ceramic	Synthesis Method	\mathcal{E}_r	<i>T_c</i> (°C)	d33 (pC/N)	Ref.
1.	K _{0.5} Na _{0.5} NbO ₃	Solid-state	1015	411	80	[90]
2.	0.94(K _{0.5} Na _{0.5} NbO ₃) + 0.06BaTiO ₃	Solid-state	1100	314	193	[91]
3.	K _{0.5} Na _{0.5} NbO ₃ (ZnO ₂ +SnO ₂)	Solid-state	503	420	124	[92]
4.	0.9825(K _{0.5} Na _{0.5})NbO ₃ -0.0175BiScO ₃	Solid-state	1150	351	253	[93]
5.	0.98(K _{0.5} Na _{0.5})NbO ₃ - 0.02(Bi _{0.5} K _{0.5})TiO ₃	Solid-state	1260	376	251	[94]
6.	(Na _{0.475} K _{0.525}) (Nb _{0.92} Sb _{0.08}) O ₃ + 1mol% MnO ₂	Solid-state	850	300	204	[95]
7.	0.98(K _{0.5} Na _{0.5})NbO ₃ - 0.02(Bi _{0.5} Na _{0.5})TiO ₃	Solid-state	900	375	195	[96]
8.	(Na _{0.535} K _{0.485}) _{0.926} Li _{0.074} (Nb _{0.942} Ta _{0.058}) O ₃	Solid-state	650	445	276	[97]
9.	0.94(K _{0.5} Na _{0.5} Nb) O ₃ – 0.06LiSbO ₃	Solid-state	1372	385	286	[86]
10.	(Na _{0.52} K _{0.41}) (Nb _{0.77} Sb _{0.16}) O ₃ - 0.07LiTaO ₃	Solid-state	2500	230	400	[98]

Poly (vinylidene fluoride) (PVDF) Polymer

Polyvinylidene fluoride (PVDF) is a chemically resistant and thermally stable semicrystalline fluoropolymer widely used in various applications due to its excellent piezoelectric and ferroelectric properties. Initially developed by Solvay in 1969 through the radical polymerization of vinylidene fluoride (CH₂=CF₂), PVDF gained attention for its high durability and ability to perform in harsh environments. Its structure, consisting of repeating –CH₂–CF₂– units, provides mechanical strength from the carbon backbone and chemical resistance from the strong carbon-fluorine bonds.

PVDF is commercially available under various brand names such as Kynar (Arkema), Solef (Solvay)and Hylar (Solvay)and is widely used in industries such as construction, electronics, and chemical processing. It also has a high melting point of around 177°C and is transparent in thin films, which makes it suitable for optoelectronic applications. PVDF can be copolymerized with other fluorinated monomers to tailor its properties. For instance, PVDF-TrFE (polyvinylidene fluoride–trifluoroethylene) offers enhanced ferroelectric and piezoelectric properties due to its more ordered crystalline structure, while PVDF-HFP (polyvinylidene fluoride–hexafluoropropylene) provides improved flexibility and is often used in membranes and battery separators. Other copolymers like PVDF-TFE (polyvinylidene fluoride–tetrafluoroethylene) and PVDF-CTFE (polyvinylidene fluoride–chlorotrifluoroethylene) improve chemical resistance and flexibility for specialized applications [99].

PVDF can crystallize into several different phases, including α , β , γ , δ and ε , based on the molecular chain arrangement. The α -phase is the most thermodynamically stable at room temperature and adopts a TGTG' conformation, which is non-polar and exhibits weak piezoelectric behavior. In contrast, the β -phase, with its all-trans (TTTT) chain conformation, is highly polar and exhibits the strongest piezoelectric properties, making it the most desirable phase for applications such as sensors, actuators and energy harvesting devices. The α -phase can be transformed into the β -phase through various methods such as mechanical stretching, electric poling, the incorporation of fillers or additives and by using electrospinning techniques [100].

The γ -phase adopts a mixed trans-gauche conformation, offering moderate polarity and piezoelectricity. Additionally, the β and γ phases can be promoted by using polar solvents such as N,N-dimethylformamide (DMF), N,N-dimethylacetamide (DMAc)and dimethyl sulfoxide (DMSO) during film processing. These solvents interact with PVDF chains to encourage the formation of polar crystalline phases over the non-polar α -phase, resulting in improved piezoelectric performance in the final

material. The schematic depictions of the α -phase, β -phase and γ phase of PVDF are presented in Figure 1.4.

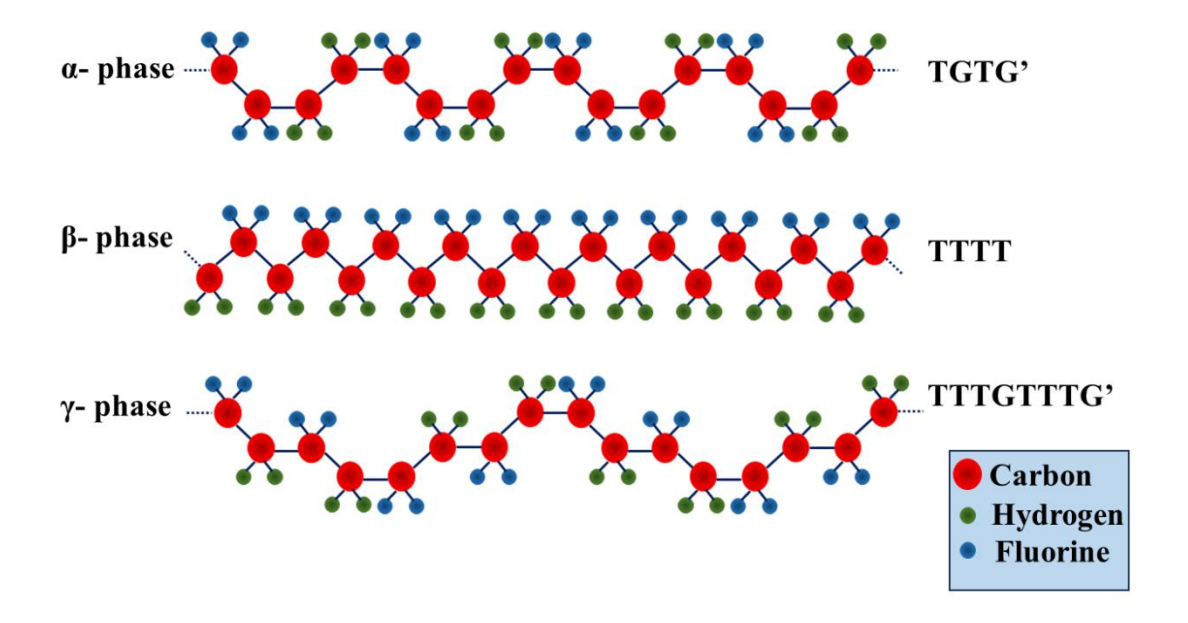


Figure 1.4 Structures of α , β and γ phases of polyvinylidene fluoride (PVDF).

1.6.1 Literature Review on KNN-based PEGs for Energy Harvesting Applications

Over the years, KNN based ceramics have been incorporated in the PVDF matrix to optimize the PVDF based piezoelectric energy harvester devices for higher sensitivity and larger piezoelectric output and thus laying a foundation to enhance the technological aspects of PVDF [101, 102]. Bairagi *et al.* fabricated the PVDF/KNN nanorods based nanogenerator and studied the effect of KNN concentration in the PVDF matrix on the device performance and obtained 3.4 V open circuit voltage for nanogenerator containing 10 wt. % KNN nanorods [103]. The high piezoelectric performance of the prepared device was attributed to the significant enhancement in the fraction of the β phase of the PVDF and its improved piezoelectricity which was strengthened by the addition of KNN nanorods.

For instance, Bairagi *et al.* developed silane modified KNN incorporated PVDF electrospun fibrous web based nanogenerator. They found remarkably high output voltage of \sim 21 V and output current of \sim 22 μ A which was attributed to deagglomeration of the nano fillers and better interaction between PVDF chains and KNN nanorods resulting from the surface modification of the nano filler material

[102]. In another study, A. M. Abdullah *et al.* fabricated the KNN- based piezotriboelectric hybrid energy films by incorporating the KNN particles in a PVDF polymer matrix and investigated the piezoelectric response of the synthesized energy film under the varying concentrations of KNN in the energy film and varying tapping frequency [104]. The maximum output voltage and current observed are 35.3 V and $15.8 \, \mu A$, respectively.

Wang *et al.* fabricated fully rollable nanogenerator using nominal composition of 0.915(Na_{0.5}K_{0.5})(Nb_{0.94}Sb_{0.06})O₃ - 0.045LiTaO₃-0.04BaZrO₃ (NKNS-LT-BZ) as a filler material in the PVDF polymer matrix [105]. The fabricated device generated a short-circuit current of 2.6 μA and an open-circuit voltage of 18 V on application of periodical agitation at a compressive force of 50 N and 1 Hz. Ichangi *et al.* fabricated a flexible nanogenerator based on electrospun Li and Ta-modified KNN nanofibers yielding a high output voltage of 5.6 V which is about 9 times higher than for the Mndoped KNN nanofibers (previously reported by Ichangi). In addition, a high-output power of 9.7 μW was achieved with nanogenerator composed of 5 wt.% Liand 10 wt.% Ta modified KNN nanofibers [106]. This work highlights the potential of KNN nanofibers as an effective material for capturing ambient vibrations to power self-sustaining sensors and wearable electronic devices.

Furthermore, PEGs performance can further be enhanced by effectively incorporating conductive fillers alongside piezoelectric ceramic fillers into the PVDF matrix. This dual addition not only increases the β -phase content due to the nucleation effect but also enhances the composite's conductivity, facilitating electron transport during piezoelectric operation. Wang and colleagues, for instance, fabricated a composite-type PENG by employing Ag particles, CNT and ($K_{0.4425}Na_{0.52}Li_{0.0375}$) ($Nb_{0.86}Ta_{0.06}Sb_{0.08}$) O₃ (KNNLTS) nanoparticles in the (poly dimethyl siloxane) PDMS matrix and reported a piezoelectric output voltage and a short-circuit current of 282 V and 32.2 mA, respectively [107]. Furthermore, Abdullah *et al.* fabricated a piezoelectric/triboelectric hybrid nanogenerator using composite film made by incorporating the KNN particles and MWCNT in the PVDF matrix and reported a very high values of open-circuit voltage and short-circuit current of 54.1 V and ~29.4 μ A, respectively [108]. Cheng *et al.* fabricated a nanogenerator using lithium-doped

potassium sodium niobate (KNLN) ceramic nanoparticles combined with conductive copper (Cu) nanorods as fillers, employing a spin casting technique [109]. The device achieved a peak output of 12 V and 1.2 μ A, demonstrating strong performance along with excellent stability and durability over repeated operation cycles. Bairagi *et al.* reported a PENG based on PVDF as polymer matrix and KNN, CNT as fillers and they obtained a maximum output voltage of 23.24 V and current of 18 μ A. whereas in the absence of CNT, the output voltage and current was ~ 17.5 V and ~ 0.522 μ A, respectively [110]. Table 1.4 depicts the comparison of piezoelectric performance of various KNN based piezoelectric generators.

Table 1.4 Comparison of piezoelectric performance of various KNN based piezoelectric generators.

S. No.	Filler material in the polymer matrix	Polymer used	Film Synthesis Method	V _{oc} (V)	<i>I_{sc}</i> (μ A)	Power Density (μW/cm²)	Ref.
1.	KNN nano blocks	PVDF	Hot- Injection	2.1	0.042	3.26	[111]
2.	KNN- BiScO ₃ ceramic particles	Polymide	Drop- casting	4	0.24		[112]
3.	KNN nanorods	PVDF	Drop- casting	3.4	0.100	0.025	[113]
4.	KNN nanorods & ZnO nanorods	PVDF	electrospi nning	25	1.81	11.31	[114]
5.	KNN nanorods	PVDF	Twin screw melt mixing	3.7	0.326		[103]

6.	KNN nanofibers	PVDF	Twin screw melt mixing	17.5	0.522		[115]
7.	KNN-ZS nanofiber	PVDF	Electrospi nning	25	2.11		[116]
8.	KNN nanorods & CNT	PVDF	Electro- spinning	23.2	9	52.29	[110]
9.	KNN particles & MWCNT	PVDF	Drop- casting	35.3	15.8		[117]
10.	NKNS-LT- BZ	PVDF	Electrospi nning	18	2.6		[105]

1.7 Thesis Problem

The main goal of the present thesis is to enhance the output efficiency of PVDF-based piezoelectric generators by using pure and modified KNN in different concentrations as filler material in the PVDF matrix. In addition, the study explores the incorporation of conductive fillers into the PVDF matrix alongside KNN particles to form composite films with improved functional properties. A substantial part of the work focuses on demonstrating how these material modifications can lead to higher output power, thereby broadening the potential applications and practical utility of piezoelectric generators.

1.7.1 Thesis Objectives

The research objectives of the present thesis work are as follows:

1. To synthesize bulk and nanoparticles of pure Potassium Sodium Niobate (KNaNbO₃) (KNN) and Lithium (Li), Tantalum (Ta) and Antimony (Sb) modified KNN.

- 2. To fabricate flexible composite films of KNN/PVDF and KNNLTS/PVDF with varying content of ceramic particles in PVDF matrix.
- 3. To investigate the structural, microstructural and electrical properties of the fabricated flexible composite films.
- 4. To construct the PEG devices using the flexible composite films and measure its piezoelectric output performance.
- 5. To study the effect of dispersing conducting fillers: ZnO and MWCNT in the PVDF matrix along with the ceramic particles in composite films on the piezoelectric output performance of PEG devices.
- 6. To investigate and utilize the potential of constructed PEG devices for energy harvesting applications.

1.7.2 Thesis Layout

The thesis consists of 7 parts. Each part is self-explanatory keeping in mind the objectives of the research work.

Chapter 1. Introduction

The first chapter of the thesis begins by addressing the growing global energy demand and the continued reliance on fossil fuels, highlighting the need for sustainable alternatives. This leads to a discussion on the increasing research interest in renewable and green technologies as viable solutions. The necessity of energy harvesting is then emphasized, followed by an overview of various energy harvesting techniques, including thermal, solar and piezoelectric approaches, etc. Among these, piezoelectric energy harvesting in which mechanical energy is converted into useful electric energy using piezoelectric generators (PEGs) is explored in detail, focusing on its working principle and advantages. To construct PEG, piezoelectric materials are required thus, in the present chapter various organic, inorganic and composite piezoelectric materials along with their different properties and their suitability for energy harvesting applications have been discussed in detail. A comprehensive literature review is also presented, summarizing various research studies related to energy harvesting advancements particularly, the composite-based flexible piezoelectric generator for energy harvesting applications.

Chapter 2. Synthesis and Characterization Techniques

This chapter elaborates the experimental methods utilized for the synthesis of filler particles in the PVDF matrix and the fabrication of composite films. For the synthesis of the filler materials, solid state method, hydrothermal method and co-precipitation method were used and are discussed in detail in the chapter. Further, for the fabrication of the flexible composite films, drop casting method was employed. In addition, the working principle of various experimental techniques and equipment that were used for the characterization of the prepared samples have also been provided in this chapter to get a comprehensive understanding. To study the phase formation and morphology of the prepared powders and flexible composite films, X-ray Diffraction (XRD), Scanning Electron Microscopy (SEM), Field Emission Scanning Electron Microscopy (FESEM) and Fourier Transform Infrared Spectroscopy (FTIR) were used. Furthermore, dielectric, ferroelectric and piezoelectric properties of the fabricated composite films were also measured using Impedance analyser, Polarisation vs. Electric field (P-E) loop tracer and Strain measurement system (Butterfly loop), respectively. With the aid of a vibrator shaker and finger tapping, force was applied on the surface of the constructed PEG devices and generated open circuit voltage and short circuit current were measured by using digital storage oscilloscope and an electrometer, respectively. Furthermore, load resistances were also attached to the PEG devices to measure the output power of the manufactured PEG device.

Chapter 3. Effect of KNN concentration and size on the output performance of KNN/PVDF based flexible piezoelectric generator

This chapter was divided in two sections in which comparison of the piezoelectric performance of the PEG devices constructed with KNN synthesized by solid state method and hydrothermal method was done in detail. In Section 1, PEG devices based on Potassium Sodium Niobate/Poly (vinylidene fluoride) (KNN/PVDF) flexible composite films with various percentages of KNN ceramic particles (0 wt.%, 5 wt.%, 10 wt.%, 15 wt.% and 20 wt.%) in the PVDF matrix were constructed. Among the different percentages of KNN, 15 wt.% KNN particles @ PVDF composite film demonstrated the highest values of β phase content of PVDF, dielectric constant (ε_r), remnant polarisation (P_r) and spontaneous polarisation (P_s). When force was applied

on the surface of the fabricated PEG device, measured values of maximum open-circuit voltage and short-circuit current were 11.2~V and $0.3~\mu A$, respectively for the device prepared with 15~wt.% KNN in the PVDF matrix.

Further, in Section 2, KNN nanoparticles were synthesized via hydrothermal method and used as filler in the PVDF matrix for fabricating PENG device. Based on the result obtained in the first section, concentration of KNN was fixed to 15 wt.% in the PVDF matrix and different properties of the prepared composite film were investigated. PVDF/KNN 15 wt.% nanocomposite film showed promising results. The nanocomposite film displayed improved β phase content of PVDF, dielectric, ferroelectric and piezoelectric performance in comparison to the film fabricated with KNN synthesized by solid state reaction method for same filler concentration. The output voltage, output current and power density generated by the nanogenerator were 20.2 V, 2.01 μ A and 8.71 μ W/cm², respectively. Finally, its practical applicability was demonstrated by harvesting energy from human body motion. Overall, the PENG constructed with KNN synthesized by hydrothermal method outperformed PEG constructed with KNN synthesized by solid state method.

Chapter 4. Study of energy harvesting performance of piezoelectric nanogenerator based on three phase PVDF/KNN/ZnO nanocomposite films

In this chapter, we report Potassium Sodium Niobate (KNN) and /Zinc Oxide (ZnO) incorporated Poly (vinylidene fluoride) (PVDF) polymer-based flexible piezoelectric nanogenerator (PENG) were constructed and the effect of KNN and ZnO concentrations on the various properties and piezoelectric performance of the PENG device was investigated. The FTIR result showed that PVDF/14.55%KNN/0.45%ZnO nanocomposite film possesses the highest content of electroactive (β) phase (~59.81%). Furthermore, dielectric and ferroelectric properties of the prepared nanocomposite films were also measured. The maximum values of open circuit voltage, short circuit current and power density were 39.5 V, 8.75 μ A and 22.26 μ W/cm² (with 10 M Ω load resistance), respectively obtained for the PENG fabricated with PVDF/14.55%KNN/0.45%ZnO nanocomposite film. The maximum and average values of inverse piezoelectric charge coefficient were found to be $d_{33}^*_{max} \sim 83.82$ pm/V and $d_{33}^*_{avg} \sim 32.22$ pm/V, respectively for the same nanocomposite film. The

synergistic effect of KNN and ZnO nanoparticles in PVDF polymer matrix considerably improves the resultant piezoelectric performance of the nanogenerator, enabling it to glow four red light-emitting diodes (LEDs) and power a digital wrist watch. Moreover, the developed nanogenerator was also able to generate output voltages of 3.08 V, 1.72 V, 1.46 V and 660 mV for pen tapping, elbow bending, finger moving and wrist stretching, respectively. Finally, it can be concluded that the versatile, durable and flexible PENG based on PVDF/KNN/ZnO nanocomposite film has the potential for future applications in energy harvesting and portable self-powered electronic devices.

Chapter 5. Effect of Li, Ta and Sb doping on the output performance of KNN/PVDF based flexible piezoelectric generator

In this chapter, flexible PEGs based on (Li, Ta, Sb) modified (K, Na) NbO₃ (KNNLTS)/poly (vinylidene fluoride) (PVDF) flexible composite film and pure PVDF film were fabricated. The concentration of KNNLTS was fixed to 15 wt.% in the PVDF matrix. For the PVDF/ KNNLTS 15 wt.% composite film, the dielectric constant (ε_r) was measured as 33.56 at 1 KHz and 29.92 at 10 KHz. Additionally, the remnant polarisation (P_r) and maximum polarisation (P_s) were recorded as 0.32 μ C/cm² and 3.70 µC/cm², respectively for the composite film. These values were significantly higher compared to pure PVDF film. The maximum value of inverse piezoelectric charge coefficient (d_{33}^*) for the same composite film were measured as ~ 24 pm/V. Furthermore, the maximum generated peak to peak open circuit voltage and shortcircuit current for the PVDF/KNNLTS 15 wt.% composite film-based generator were 36.58 V and 5.04 µA, respectively which were higher than the voltage and current obtained using pure PVDF film-based generator. The performance of the PEG was also tested under different human body motions. The output voltages for fist beating, elbow bending, quenching and fist opening were 5.48 V, 4.12 Vand 1.72 V, respectively. The fabricated PEG demonstrated practical applicability by successfully lighting 11 LEDs. The present chapter demonstrated that high performance PEG can be developed by modifying KNN ceramics by suitable dopants.

Chapter 6. Effect of KNNLTS concentration and conductive fillers (MWCNT) in realizing high performance PVDF/KNNLTS/MWCNT flexible piezoelectric nanogenerator for powering electronics devices

In this chapter, Polyvinylidene fluoride/ potassium sodium niobate doped with lithium, tantalum, and antimony/ multiwall carbon nanotube (PVDF/KNNLTS/MWCNT) based flexible nanocomposite films have been synthesized by drop casting method and then used for the construction of PENG devices. It was observed that KNNLTS incorporated with MWCNT in the PVDF matrix showed improved structural, dielectric and piezoelectric performance. The maximum values of piezoelectric output voltage, output current and power density were measured to be 87.2 V, 20.3 µA and of 145.48 µW/cm², respectively for the PENG device constructed with nanocomposite film containing 20 wt.% KNNLTS and MWCNT in the PVDF matrix. In addition, the PENG device was utilized to test the ability to harness energy from human body motions. The output voltages for finger tapping, thumb pressing, fist beating, elbow beating, elbow bending and wrist stretching were 11.4 V, 27.2 V, 24.8 V, 34 V, 37 Vand 55.2 V, respectively. The fabricated PENG demonstrated practical applicability, by powering a digital thermometer, digital wrist watch and successfully lighted 18 LEDs. The present chapter demonstrated that high performance PENG can be developed by employing modified KNN together with conductive filler in the PVDF matrix which has the potential to be used in self-powered wearable and portable electronic gadgets.

Chapter 7. Conclusion, Future Scope and Social Impact

This chapter provides a summary of all findings of the present thesis work. This chapter also includes the future scope of the research work and challenges. In future work, PENG, TENG and hybrid nanogenerator can be fabricated using modified KNN and some conducting nanomaterials (rGO, ZnO, 2D materials, etc.) as fillers in the polymer matrix for use in flexible and wearable electronics, self-powered sensors and energy harvesting applications. The increasing energy crisis highlights the need for sustainable alternatives, as traditional energy sources like fossil fuels significantly impact the environment through carbon emissions and resource depletion. In contrast, piezoelectric energy harvesters offer a renewable, eco-friendly and green energy

solution, generating power without harming the environment. With applications in self-powered devices, wearable electronics and smart infrastructure, these energy harvesters contribute to a cleaner and more sustainable future.

References

- [1] F. Tasnim, S.A. Iqbal, A.R. Chowdhury, Renewable Energy, 109, (2017), 434–439
- [2] A.M. Abdullah, A.R. Chowdhury, Y. Yang, H. Vasquez, H.J. Moore, J.G. Parsons, K. Lozano, J.J. Gutierrez, K.S. Martirosyan, M.J. Uddin, Journal of Molecular Liquids, 297, (2020), 111982
- [3] X. Chen, X. Li, J. Shao, N. An, H. Tian, C. Wang, T. Han, L. Wang, B. Lu, Small, 13 (23), (2017), 1604245
- [4] A.R. Chowdhury, A.M. Abdullah, I. Hussain, J. Lopez, D. Cantu, S.K. Gupta, Y. Mao, S. Danti, M.J. Uddin, Nano Energy, 61, (2019), 327–336
- [5] Z. Lou, L. Li, L. Wang, G. Shen, Small, 13, (2017), 1701791
- [6] P. Bai, G. Zhu, Z.-H. Lin, Q. Jing, J. Chen, G. Zhang, J. Ma, Z.L. Wang, ACS Nano, 7, (2013), 3713–3719
- [7] L. Jin, J. Tao, R. Bao, L. Sun, C. Pan, Scientific Reports, 7, (2017), 1–6
- [8] A. Boochani, G. Rasoolian, F. Kafi, A. Aminian, S.M. Elahi, Chinese Journal of Physics, 59, (2019), 357-371
- [9] F. Zamanpour, L. Shooshtari, M. Gholami, R. Mohammadpour, P. Sasanpour, N. Taghavinia, Nano Energy, 103, (2022), 107796
- [10] L. Paralı, M. Koç, E. Akça, Ceramics International, 49, (2023), 18388–18396
- [11] H. M. A. Yaseen, S. Park, Journal of Alloys and Compounds, 952, (2023), 169940
- [12] X. Xue, P. Deng, S. Yuan, Y. Nie, B. He, L. Xing, Y. Zhang, Energy and Environmental Science, 6, (2013), 2615
- [13] C. Chang, V. H. Tran, J. Wang, Y. K. Fuh, L. Lin, Nano Letters, 10, (2010), 726–731

- [14] S. Cha, S. M. Kim, H. Kim, J. Ku, J. I. Sohn, Y. J. Park, B. G. Song, M. H. Jung, E. K. Lee, B. L. Choi, J. J. Park, Z. L. Wang, J. M. Kim, K. Kim, Nano Letters, 11, (2011), 5142–5147
- [15] X. Xue, P. Deng, B. He, Y. Nie, L. Xing, Y. Zhang, Z. L. Wang, Advanced Energy Materials, 4 (5), (2013)
- [16] D. Zhang and Z. Zhang, Ferroelectrics, 466, (2014), 8-13
- [17] A. Paterson, H. T. Wong, Z. Liu, W. Ren, Z.-G. Ye, Ceramics International, 41, (2015), 57
- [18] W.K. Tam, K.W. Kwok, J.T. Zeng, H.L.W. Chan, Journal of Physics D: Applied Physics, 41, (2008), 045402
- [19] P. Elaiyaraja, N. Karunagaran, M. Muralidharan, Journal of Alloys and Compounds, 1026, (2025), 180456
- [20] E. Akca, H. Yilmaz, Ceramics International, 41, (2015), 3659-3667
- [21] H. Zheng, E. Sun, K. Li, H. Luo, J. Fan, Y. Yang, B. Yang, R. Zhang, W. Cao, Journal of the European Ceramic Society, 44, (2024), 4622-4630
- [22] X. Wang, Y. Huan, Y. Zhu, P. Zhang, W. Yang, P. Li, T. Wei, L. Li, X. Wang, Journal of Advanced Ceramics, 11 (1), (2022), 184-195
- [23] D. Lin, K. W. Kwok, H.L.W. Chan, Materials Chemistry and Physics, 109, (2008), 455-458
- [24] Y. Wei, X. Wang, J. Zhu, X. Wang, J. Jia, Journal of American Ceramic Society, (2013), 1-6
- [25] M. Makarovic, A. Bencan, J. Walker, B. Malic, T. Rojac, Journal of the European Ceramic Society, 39 (13), (2019), 3693-3702
- [26] H. Kawai, Japanese Journal of Applied Physics, 8, (1969), 975–976
- [27] A. Farahani, A.Z.- Hanzaki, H.R. Abedi, L. Tayebi, E. Mostafavi, Journal of Functional Biomaterials, 12 (4), (2021), 71
- [28] S.H. Wankhade, S. Tiwari, A. Gaur, P. Maiti, Energy Reports, 6, (2020), 358-364
- [29] P. Sampathkumar, P. Gowdhaman, S. Sundaram, V. Annamalai, Nano Vision, 3 (3), (2013), 223-230

- [30] S. Crossley, R. A. Whiter, S. Kar-Narayan, Material Science and Technology, 30, (2014), 1613
- [31] M. Kumar, N.D. Kulkarni, P. Kumari, Materials Research Bulletin, 174, (2024), 112739
- [32] S.H. Shin, Y.H. Kim, H.L. Min, J.Y. Jung, J. Nah, ACS Nano, 8 (3), (2014), 2766–2773
- [33] S. Bairagi, S.W. Ali, Energy, 198, (2020), 117385
- [34] A. Hussain, N. Sinha, S. Goel, A. J. Joseph, B. Kumar, Journal of Alloys and Compounds, 790, (2019), 274-287
- [35] Y. Zhai, X. Qi, G. Tian, J. Wang, F. Yu, Z. Gai, J. Du, W. Su, S. Guo, L. Zheng, Journal of European Ceramic Society, 45, 2025, 116984
- [36] J. Kaarthik, C. Kaushiga, G. Sradha, N. Ram, S. G. Reddy, K.C. Sekhar, A. Venkateswarlu, Journal of Alloys and Compounds, 943, (2023), 169069
- [37] J. Camargo, S. Osinaga, M. Febbo, S.P. Machado, F. Rubio-Marcos, L. Ramajo, M. Castro, Journal of Materials Science: Materials in Electronics, 32, (2021), 19117-19125
- [38] Y. Liu, Y. Chang, S. Yang, F. Li, Y. Sun, J. Wu, B. Yang, W. Cao, Ceramics International, 45, (2019), 10518-10524
- [39] Y. Zhang, X. Liu, G. Wang, Y. Li, S. Zhang, D. Wang, H. Sun, Journal of Alloys and Compounds, 825, (2020), 154020
- [40] J. Kymissis, C. Kendall, J. Paradiso, N. Gershenfeld, IEEE Xplore, (1998), 132-139
- [41] C. Li, W. Luo, X. Liu, D. Xu, K. He, Nanomaterials, 6 (4), (2016), 67
- [42] S. Xu, Y. Yeh, G. Poirier, M.C. McAlpine, R.A. Register, N. Yao, Nano Letters, 13 (6)
- (2013), 2393-2398
- [43] S. Siddiqui, D.I. Kim, T.D. Le, M.T. Nguyen, S. Muhammad, W.S. Yoon, N.E. Lee,

Nano Energy, 15, (2015)

- [44] Y. Zhao, Q. Liao, G. Zhang, Z. Zhang, Q. Liang, X. Liao, Y. Zhang, Nano Energy, 11, (2015), 719-727
- [45] N. R. Alluri, B. Saravanakumar, S. J. Kim, ACS Applied Materials & Interfaces, 7, (2015), 9831-9840
- [46] C. Baek, J. H. Yun, H. S. Wang, J. E. Wang, H. Park, K.-I. Park, D. K. Kim, Applied Surface Science, 429, (2018), 164
- [47] Z.-H. Lin, Y. Yang, J. M. Wu, Y. Liu, F. Zhang, Z. L. Wang, Journal of Physical Chemistry Letters, 3, (2012), 3599
- [48] W. Liu, X. Ren, Physical Review Letters, 103 (25), (2009), 257602
- [49] A. Patra, A. Pal, S. Sen, Ceramics International, 44, (2018), 11196–11203
- [50] P. Thakur, A. Kool, N. A. Hoque, B. Bagchi, F. Khatun, P. Biswas, D. Brahma,S. Roy, S. Banerjee, S. Das, Nano Energy, 44, (2018), 456-467
- [51] J. Yi, Y. Song, Z. Cao, C. Li, C. Xiong, Composites Science and Technology, 215, (2021), 109011
- [52] L. Z, Z. X, L. G, Physical Chemistry Chemical Physics, 16 (12), (2014), 5475–5479
- [53] J. H. Jung, M. Lee, J.-I. Hong, Y. Ding, C.-Y. Chen, L.-J. Chou, Z. L. Wang, ACS Nano, 5, (2011), 10041
- [54] X. Ren, H. Fan, Y. Zhao, Z. Liu, ACS Applied Materials & Interfaces, 8, (2016), 26190
- [55] N. Abinnas, P. Baskaran, S. Harish, R. S. Ganesh, M. Navaneethan, K. D. Nisha, S. Ponnusamy, C. Muthamizhchelvan, H. Ikeda, Y. Hayakawa, Applied Surface Science, 418, (2017), 362
- [56] N. Levi, R. Czerw, S. Xing, P. Iyer, D.L. Carroll, Nano Letters, 4 (7), (2004), 1267–1271
- [57] C. Yang, J.H. Kim, J.H. Kim, J. Kim, H.S. Kim, Sensors and Actuators A: Physical, 154 (1), (2009), 117–122
- [58] K. II Park, M. Lee, Y. Liu, S. Moon, G. T. Hwang, G. Zhu, J. E. Kim, S. O. Kim,
- D. K. Kim, Z. L. Wang, K. J. Lee, Advanced Materials, 24, (2012), 2999-3004
- [59] K. Shi, B. Sun, X. Huang, P. Jiang, Nano Energy, 52, (2018), 153-162

- [60] H. Sun, H. Tian, Y. Yang, D. Xie, Y. C. Zhang, X. Liu, S. Ma, H. M. Zhao, T. L. Ren, Nanoscale, 5, (2013), 6117-6123
- [61] A.K. Geim, Science, 324 (5934), (2009), 1530–1534
- [62] A.K. Geim, K.S. Novoselov, Nature Materials, 6, (2007), 183–191
- [63] Y. Zhu, S. Murali, W. Cai, X. Li, J.W. Suk, J.R. Potts, R.S. Ruoff, Advanced Materials, 22 (35), (2010), 3906-3924
- [64] Alamusi, J. Xue, L. Wu, N. Hu, J. Qiu, C. Chang, S. Atobe, H. Fukunaga, T. Watanabe, Y. Liu, Nanoscale, 4 (22), (2012), 7250–7255
- [65] R.M. Habibur, U. Yaqoob, S. Muhammad, A.S.M.I. Uddin, H.C. Kim, Materials Chemistry and Physics, 215, (2018), 46–55
- [66] M.M. Abolhasani, K. Shirvanimoghaddam, M. Naebe, Composites Science and Technology, 138, (2017), 49–56
- [67] H.H. Singh, S. Singh, N. Khare, Polymer for Advanced Technologies, 29, (2017), 143-150
- [68] N. Chamankar, R. Khajavi, A. A. Yousefi, A. Rashidi, F. Golestanifard, Ceramics International, 46, (2020), 19669-19681
- [69] D. P. Ojha, B. Joshi, E. Samuel, A. Khadka, A. Aldalbahi, G. Periyasami, D. Choi, S. An, Sam S. Yoon, International Journal of Energy Research, 1, (2023), 3074782
- [70] P. Elorika, S. Anwar, S. Anwar, Composites Part A: Applied Science and Manufacturing, 199, (2025), 109219
- [71] S. Das, M. Mallik, K. Parida, N. Bej, J. Baral, Applied Surface Science Advances,23, (2024), 100626
- [72] M. Kim, YS. Wu, E.C. Kan, J. Fan, Polymers, 10, (2018), 10070745
- [73] K. Jyotsna, S. Phanjoubam, Sensors & Actuators: A. Physical, 394, (2025), 116885
- [74] A. S. M. I. Uddin, D. Lee, C. Cho, B. Kim, Coatings, 12, (2022), 77
- [75] S. Pratihar, A. Patra, A. Sasmal, S. K. Medda, S. Sen, Soft Matter, 17, (2021), 8483
- [76] S. K. Ghosh, D. Mandal, Nano Energy, 53, (2018), 245-257

- [77] C.-M. Wu, M.-H. Chou, W.-Y. Zeng, Nanomaterials, 8(6), (2018), 420
- [78] J. C, L. Praba, S. Kuppusamy, M. R, T. R, J.W. Jung, P. Deivasigamani, S. Rajesh, Materials Today Communications, 41, (2024), 110904
- [79] N. Buatip, D. Munthala, P. Amonpattaratkit, P. Pakawanit, X. Hu, W. Jongpint,
 P. Janphuang, C. Wan, C. Bowen, S. Pojprapai, Materials Research Bulletin, 173,
 (2024), 112686
- [80] B. Sharma, R. Gupta, A. Sharma, A. Chowdhuri, M. Tomar, Materials Today Communication, 44, (2025), 112140
- [81] N. Sezer, M. Koç, A comprehensive review on the state-of-the-art of piezoelectric energy harvesting, Nano Energy, 80, (2021), 105567
- [82] D. Hongliang, Z. Li, F. Tang, S. Qu, Z. Pei, W. Zhou, Materials Science and Engineering B, 131 (1), (2006), 83-87
- [83] B. Malic, J. Koruza, J. Hrescak, J. Bernard, K. Wang, J.G. Fisher, A. Bencan, Materials, 8 (12), (2015), 8117-8146
- [84] T. Vijayakanth, S. Shankar, G.F.-Zuta, S.R.-Lazar, S. Gilead, E. Gazit, Royal Society of Chemistry, 52, (2023), 6191-6220
- [85] H. Hao, G. Tan, H. Ren, A. Xia, P. Xiong, Ceramics International, 40 (7), (2014), 9485-9491
- [86] D. M. Lin, K. W. Kwok, K. H. Lamand H. L. W. Chan, Journal of Applied Physics, 101 (7), (2007), 074111
- [87] K. Wang, J.-F. Liand N. Liu, Applied Physics Letters, 93 (9), (2008), 092904
- [88] Y. Saito, H. Takao, T. Tani, T. Nonoyama, K. Takatori, T. Homma, Nature, 423, (2004), 84
- [89] Y. Gao, J. Zhang, Y. Qing, Y. Tan, Z. Zhang, X. Hao, Journal of American Ceramic Society, 94, (2011), 2968
- [90] H. Uršič, A. Benčan, M. Škarabot, M. Godecand M. Kosec, Journal of Applied Physics, 107, (2010)
- [91] D. Lin, K.W. Kwok, H.L.W. Chan, Journal of Applied Physics, 102, (2007), 074113

- [92] Z. Li, G. Xu, Y. Li, A. Sun, L. Jiang, P. Cui, Physica B: Condensed. Matter, 405, (2010), 296-299
- [93] H. Du, W. Zhou, F. Luo, D. Zhu, S. Qu, Y. Li, Z. Pei, Journal of Applied Physics, 104 (3), (2008), 034104
- [94] H. Du, W. Zhou, F. Luo, D. Zhu, S. Qu, Y. Li, Z. Pei, Journal of Physics D: Applied Physics, 41, (2008), 115413
- [95] D. M. Lin, K. W. Kwok, H. Y. Tianand H. W. L. W. Chan, Journal of American Ceramic Society, 90 (5), (2007), 1458–62
- [96] R. Zuo, X. Fang, C. Ye, Applied Physics Letters, 90, (2007), 092904
- [97] Z.-Y. Shen, Y. Zhen, K. Wang, J.-F. Li, Journal of American Ceramic Society, 92 (8), (2009), 1748–52
- [98] R. Z. Zuo, J. Fuand D. Y. Lv, Journal of American Ceramic Society, 92 (1), (2009), 283–285
- [99] N. Ahbab, S. Naz, T-B. Xu, S. Zhang, Micromachines, 16 (4), (2025), 386
- [100] L. Li, M. Zhang, M. Rong, W. Ruaan, RSC Advances, 4 (8), (2014), 3938-3943
- [101] L. Jin, S. Ma, W. Deng, C. Yan, T. Yang, X. Chu, Nano Energy, 50, (2018), 632
- [102] S. Bairagi, S.W. Ali, Energy, 198, (2020), 117385
- [103] S. Bairagi, S. W. Ali, European Polymer Journal, 116, (2019), 554 561
- [104] Y. Shiratori, A. Magrez, W. Fischer, C. Pithan, R. Waser, The Journal of Physical Chemistry C, 111, (2007), 18493–18502
- [105] C. Zhang, Y. Fan, H. Li, Y. Li, L. Zhang, S. Cao, ACS Nano, 12, (2018), 4803
- [106] A. Ichangi, V-V. Shvartsman, D-C. Lupascu, K. Le, M. Grosch, A.K.S- Verma, C. Bohr, A. Verma, T. Fischer, S. Mathur, Journal of European Ceramic Society, 15 (41), (2021), 7662-7669
- [107] Y. Huan, T. Wei, Z. Wang, H. Shen, X. Lin, S. Huang, X. Wang, Journal of Materiomics, 6, (2020), 355
- [108] N. Sezer, M. Koç, Nano Energy 80, (2021), 105567
- [109] C.K. Jeong, K. Park, J. Ryu, G.T. Hwang, K.J. Lee, Advanced Functional Materials, 24, (18), (2014), 10

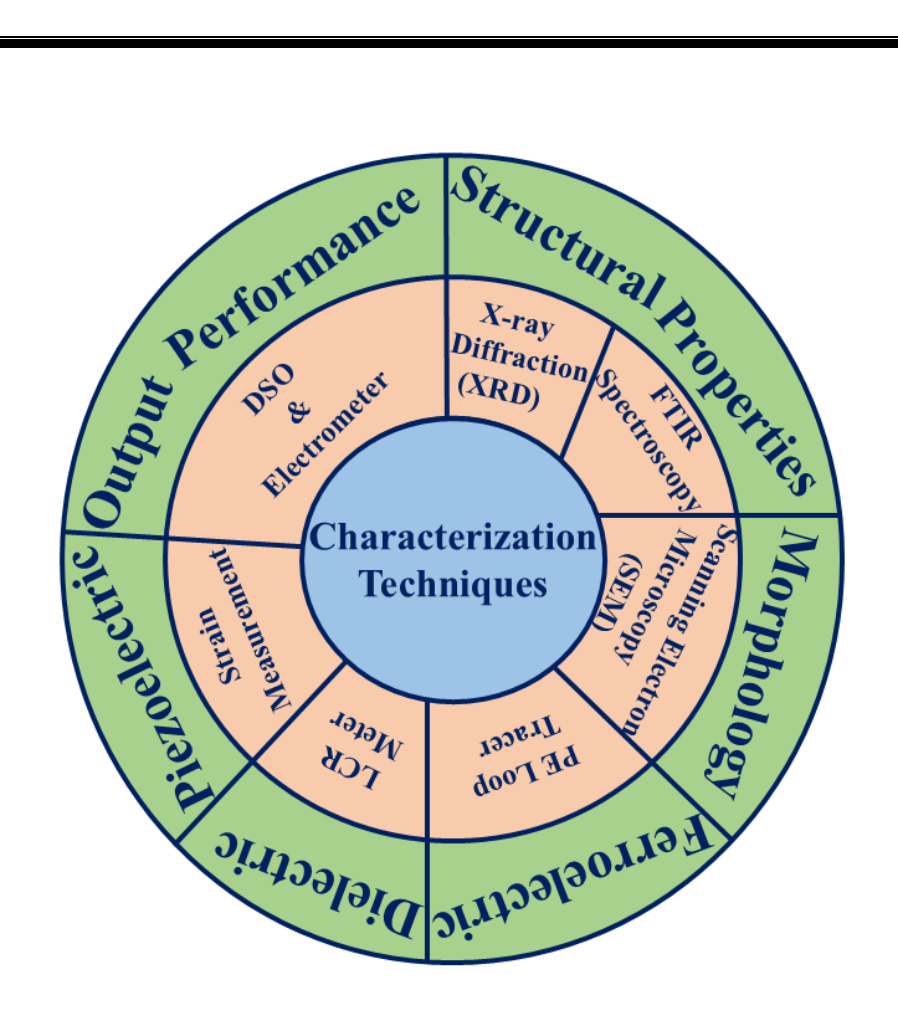
- [110] S. Bairagi, S.W. Ali, Soft Matter, 16, (2020), 4876–4886
- [111] K.S Nair, H. Varghese, A. Chandran, U.N.S. Hareesh, A. Chouprik, M. Spiridonov, Material Today Communication, 31, (2022), 103291
- [112] D.Y. Hyeon, G.J. Lee, S. H. Lee, J.J. Park, S. Kim, M. Lee, Composites B: Engineering, 234, (2022), 109671
- [113] S. Bairagi, S.W. Ali, Organic Electronics, 78, (2020), 105547
- [114] S. Bairagi, S.W. Ali, International Journal of Energy Research, (2020), 1-19
- [115] S. Bairagi, S. W. Ali, Energy Technologies, 7, (2019), 1900538
- [116] S. Banerjee, S. Bairagi, S.W. Ali, Energy, 244, (2022), 123102
- [117] A. M. Abdullah, M. U. K. Sadaf, F. Tasnim, H. Vasquez, K. Lozano, M. J. Uddin, Nano Energy, 86, (2021), 106133

Chapter 2

Synthesis and Characterization
Techniques

Chapter 2

Synthesis and Characterization Techniques



The present chapter elaborates the experimental methods utilized for the synthesis of filler particles in the PVDF matrix and the fabrication of composite films. For the synthesis of the filler materials, solid state method, hydrothermal method and coprecipitation method were used and are discussed in detail in the chapter. Further, for the fabrication of the flexible composite films, drop casting method was employed. In addition, the working principle of various experimental techniques and equipment that were used for the characterization of the prepared samples have also been provided in this chapter to get a comprehensive understanding. To study the phase formation and

morphology of the prepared powders and flexible films, X-ray Diffraction (XRD), Scanning Electron Microscopy (SEM), Field Emission Scanning Electron Microscopy (FESEM) and Fourier Transform Infrared Spectroscopy (FTIR) were used. Furthermore, dielectric, ferroelectric and piezoelectric properties of the fabricated composite films were also measured using Impedance analyser, Polarisation vs. Electric field (*P-E*) loop tracer and Strain measurement system (Butterfly loop), respectively. With the aid of a vibrator shaker and finger tapping, force was applied on the surface of the constructed PEG devices and generated open circuit voltage and short circuit current were measured by using digital storage oscilloscope and an electrometer, respectively. Furthermore, load resistances were also attached to the PEG devices to measure the output power of the manufactured PEG device.

2.1 Material Synthesis Methods

For the synthesis of potassium sodium niobate (KNN), lithium, tantalum and antimony doped potassium sodium niobate (KNNLTS) and zinc oxide (ZnO) powders, solid state reaction method, hydrothermal method and co-precipitation method have been used. In the following subsections, the underlying principle of these methods along with various processing steps involved are discussed in detail.

2.1.1 Solid-State Reaction Method

The solid-state reaction method is one of the most widely used techniques for the synthesis of polycrystalline solids. In this method, the starting precursors, typically in powder form, undergo direct reaction through diffusion at high temperatures [1]. The experimental procedure for the preparation of the materials was carried out in the following steps.

(i) Weighing

High purity raw materials were used as the starting precursors and accurately weighed according to the stoichiometric ratio of the desired compound.

(ii) Mixing

After weighing, the starting precursors were mixed using ball milling with zirconia balls in a suitable liquid medium. The liquid medium was carefully chosen to ensure that no reaction occurred with the raw materials. In the present work, ethanol and isopropanol were employed as liquid media. Following homogeneous mixing, the slurry was dried in an oven at an appropriate temperature, depending on the liquid medium used.

(iii) Calcination

Calcination is a process in which thoroughly mixed precursors are heated at high temperatures, leading to partial or complete phase formation of the compound through diffusion [2]. The calcination temperature varies depending on the material and for oxides, it is typically performed at elevated temperatures that must be optimized to achieve desirable properties. During this process, unwanted gases, moisture and residual organic matter are also eliminated. Calcination is generally carried out in a furnace.

2.1.2 Hydrothermal Method

For synthesis of nanoparticles, hydrothermal method is a useful technique as this method allows for precise control over the size, shape and crystalline phase of the particles, contributing to high-purity and uniformity in materials. This technique operates at relatively low energy consumption during synthesis compared to other methods like solid-state reactions. The hydrothermal word consists of two important terminologies; "hydro" which signifies water and "thermal" which denotes heat. In 1845, the first report of crystal formation by using hydrothermal technique was published by Karl Emil von Schafhautl. The synthesis of nanoparticles is carried out through chemical reactions within a stainless-steel autoclave, which is internally lined with Teflon. The setup of the hydrothermal autoclave designed to carry out this process is illustrated in Figure 2.1.

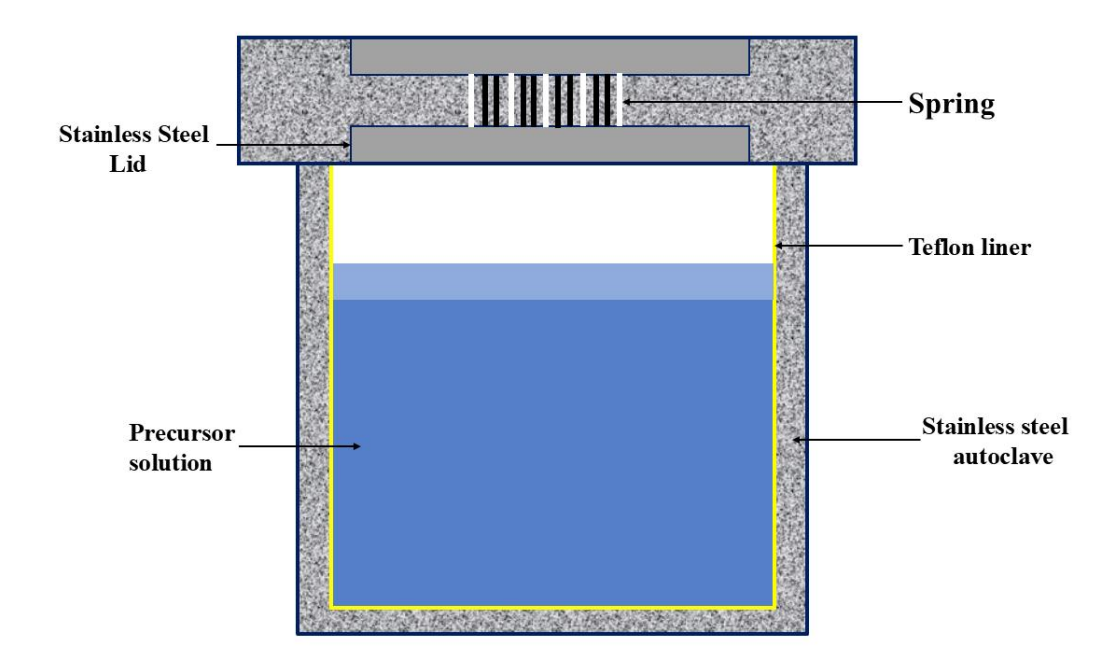


Figure 2.1 Schematic presentation of hydrothermal autoclave used in hydrothermal method.

The autoclave is sealed and loaded with reagents dissolved in water, subjected to specific temperature and pressure conditions. The Teflon liner is filled precisely with aqueous reagents to provide the pressure needed to produce nanoparticles with required morphology and properties. In a high-temperature oven, the optimum combination of temperature, pressure, and reaction time can give a significant yield of well-crystallized nanoparticles [3].

2.1.3 Co-precipitation Method

The co-precipitation method is a widely used synthesis technique for preparing nanomaterials, particularly metal oxides and composite materials, due to its simplicity, cost-effectiveness, use of cheap chemicals and mild reaction conditions and ability to produce homogeneous products. In this process, desired metal ions (nitrates/chlorides/acetates) were used as starting precursors without any further purification. The required stoichiometric amounts of the precursors were dissolved in deionized water under constant magnetic stirring to obtain a clear and homogeneous solution.

A precipitating agent, typically sodium hydroxide (NaOH) or ammonium hydroxide (NH₄OH), was prepared in a separate beaker. The base solution was added dropwise

into the previously prepared precursor solution under vigorous stirring using a magnetic stirrer to carefully raise the pH of the solution and induce the precipitate formation. Further, in the solution, metal ions undergo nucleation and then aggregate to form nanoparticles.

The resulting precipitate was separated by centrifugation (or filtration), followed by repeated washing with solvent (deionized water or ethanol) until the filtrate became neutral (pH ~7), ensuring the removal of residual ions and byproducts. The washed precipitate was then dried in a hot air oven to remove the solvent. Finally, the dried precipitate was subjected to a heating process called calcination at an optimized temperature (typically 400–800 °C depending on the desired material system) for several hours to obtain the final material product.

2.2 Fabrication of Flexible Composite Films: Drop Casting Method

In the present work, the drop-casting method was employed to fabricate flexible composite films. Drop-casting is a widely adopted method for the synthesis of composite films onto a substrate due to its simplicity and cost-effectiveness. Initially, the solutes were thoroughly mixed in appropriate solvents at a fixed concentration using a magnetic stirrer. The desired film characteristics can be achieved by adjusting the solute concentration in the solution. The specific volume of the prepared solution is then drawn into a micropipette and carefully dropped onto a flat substrate, such as glass, as illustrated in Figure 2.2. By controlling the volume of the solution and the deposition rate, a uniform film is formed on the substrate. Finally, the substrate is dried in a temperature-controlled oven to complete the synthesis process of the film. Further, the drop-casting method allows researchers to rapidly investigate how variations in solute concentration, choice of solvent, and deposition conditions influence the properties of the resulting films. However, it is important to note that this technique may result in variations in film thickness, which can be affected by factors such as the solvent evaporation rate and the surface characteristics of the substrate. These variations can, in turn, impact the overall properties of the fabricated films.

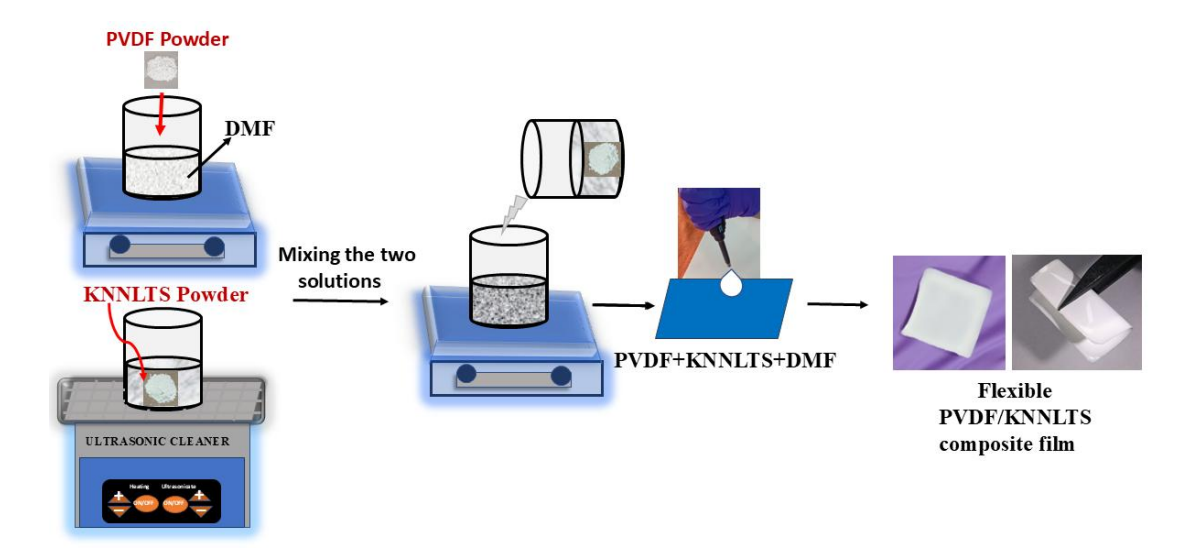


Figure 2.2 Schematic illustration of drop casting technique showing the synthesis of composite film.

2.3 Characterizations

2.3.1 Brief Description of Various Characterization Techniques

A variety of characterization techniques are utilized to characterize the prepared filler materials and composite films. The phase formation is analysed using X-ray Diffraction (XRD) and Fourier Transform Infrared Spectroscopy (FTIR) followed by morphological analyses using Scanning Electron Microscopy (SEM) and Field Emission Scanning Electron Microscopy (FESEM).

2.3.1.1 X-ray Diffraction (XRD)

XRD technique is one of the most widely non-destructive techniques used to investigate crystallographic properties such as phase formation, determination of crystallite size, crystal texture, cell parameters, deformation stress, energy density, quantification of sample crystallinity. A century has elapsed since 1916 - 1917, when the pioneering work of Debye, Scherrer and Hull introduced the first X-ray diffraction experiments [4]. In the early years of the birth of Powder X-ray Diffraction (PXRD), several pioneers discovered key concepts in the field. The upcoming sections will cover the basic fundamentals of X-rays, powder diffraction, and the specific diffractometer used for the sample characterization.

2.3.1.1.1 X-rays

X-rays are high-energy electromagnetic waves characterized by wavelengths ranging from 0.1 Å to 100 Å. For X-ray crystallography, the wavelength of X-ray lies in the range from ~ 0.5 Å to 2.5 Å as it is comparable to the interatomic spacing in crystals.

2.3.1.1.2 Bragg's Diffraction

When X-rays interact with matter, the interaction can be either coherent or incoherent, involving elastic or inelastic scattering. To analyse the crystal structure of a synthesized material, coherent elastic scattering of X-rays is employed. When X-rays interact with the electron clouds of atoms, they produce spherical wavefronts that propagate in all directions [5]. The distribution of these scattered wave amplitudes is influenced by the phase differences between waves scattered from various atoms, resulting in either constructive or destructive interference.

In 1913, pioneers W.H. Bragg and W.L. Bragg discovered that crystalline materials produce distinctive reflection patterns when exposed to X-rays. In these materials, for specific wavelengths and incidence angles, intense reflections known as Bragg peaks are observed. W.L. Bragg proposed that crystals are composed of parallel planes separated by a distance 'd,' referred to as the interplanar spacing. To achieve sharp and intense peaks, constructive interference must occur among the reflections from successive parallel planes.

Figure 2.3 illustrates the two X-rays reflected from adjacent crystal planes, where the angle of incidence equals the angle of reflection. These reflected rays are separated by a path difference of $2d \sin \theta$, where θ represents the angle of incidence (equivalent to half the deviation angle of the incident X-ray). According to Bragg's condition, constructive interference takes place when the path difference is an integer multiple of the X-ray wavelength, which is described by the following equation:

$$2d\sin\theta = n\lambda \tag{2.1}$$

where, n denotes the order of constructive Bragg reflection.

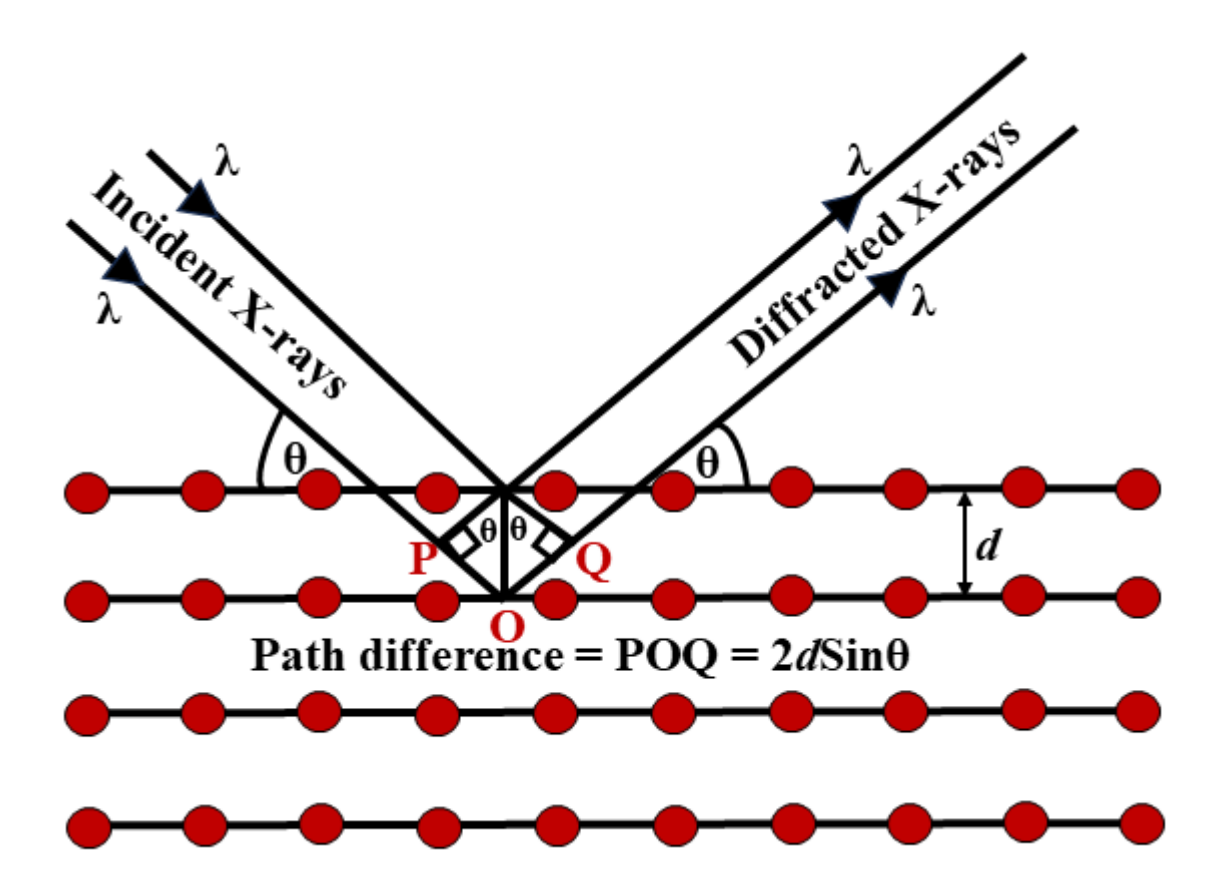


Figure 2.3 Schematic representation of the diffraction of X-rays obeying Bragg's law.

All the XRD patterns of powders and films in the present thesis work are recorded using Cu- $K\alpha$ radiation on high-resolution X-ray diffractometer (Rigaku- Ultima IV see Figure 2.4) of wavelength ($\lambda = 1.5408 \text{ Å}$) at room temperature, with a step size of 0.02° and scan speed of 2° per minute.



Figure 2.4 High resolution X-ray Diffractometer (Rigaku- Ultima IV).

2.3.1.2 Fourier Transform Infrared Spectroscopy (FTIR)

Fourier Transform Infrared Spectroscopy (FTIR) serves as a vital tool for investigating the vibrational behavior of functional groups in organic and semi-organic compounds. The analysis is performed by subjecting the compounds to electromagnetic spectrum in the range of 400 cm⁻¹ to 4000 cm⁻¹. As the molecules absorb infrared light, there is change in the energy levels of the molecule's vibration and this absorption manifests in two modes: stretching and bending. The energy absorbed enables the adjustment in these energy levels. This method is especially useful for identifying organic molecules that contain strong dipoles and polar bonds, such as NH, OH, and CH [6-8].

A major advantage of FTIR spectroscopy is its fast-scanning capability compared to other dispersive methods, along with its ability to analyze solids, liquids and gases.

This technique is based on the molecular bonds in the sample's component, whose nature is determined by the constituent atoms. When the sample is irradiated with infrared light (IR), its molecules absorb energy and transition to higher energy levels (excited state). As they relax back to their original (de-excited) states, they emit radiation corresponding to the energy difference between excited state and de-excited state. The incident light contains multiple wavelengths, and each material absorbs specific IR wavelength, resulting in a distinct spectral fingerprint [9]. The resonant frequencies depend on factors such as atomic masses, vibronic coupling and molecule potential energy surfaces. As a result, there is a relationship between the bond types and their corresponding vibrational frequencies. For example, simple diatomic molecules exhibit a single stretching vibration, while more complex molecules contain multiple bonds that stretch and conjugate vibrations. These interactions produce specific infrared absorption frequencies linked to certain chemical groups. Because each functional group possesses a characteristic vibrational energy, IR spectroscopy offers a distinctive spectral fingerprint that enables their identification.

By measuring the wavelengths absorbed by the sample, FTIR spectroscopy can determine the identity of materials and their bonding characteristics. The resulting spectrum usually shows either "transmittance" or "absorption" of infrared light along the y-axis, while the x-axis represents the wavenumber. The number and position of peaks vary according to the chemical nature of the sample. By carefully analyzing and comparing these peaks with established IR spectra for different bonds and substances, the functional groups present in the sample can be accurately identified.

FTIR spectroscopy is based on the Michelson interferometer, as shown in Figure 2.5. The various steps involved in the FTIR are illustrated in Figure 2.6. In this arrangement, infrared radiation emitted from the source passes through a collimator before reaching a beam splitter. The splitter divides the incoming beam into two, with each part reflected toward mirrors-one of mirrors moves all the time. This motion creates a path difference between the two beams, modulating the wavelengths in the incident beam at different frequencies. After suffering reflection from the mirrors, the beams recombine, producing a complex interferogram.

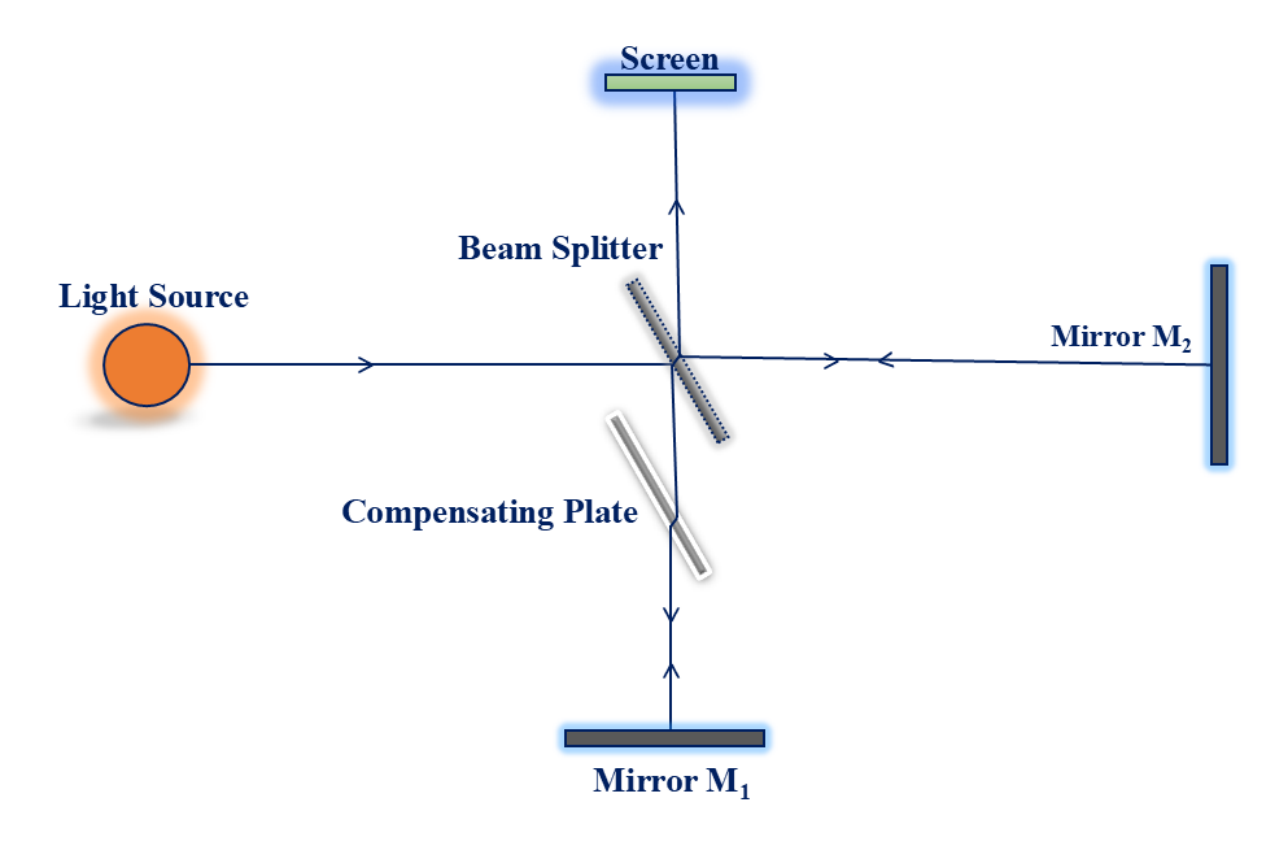


Figure 2.5 Schematic of Michelson Interferometer.

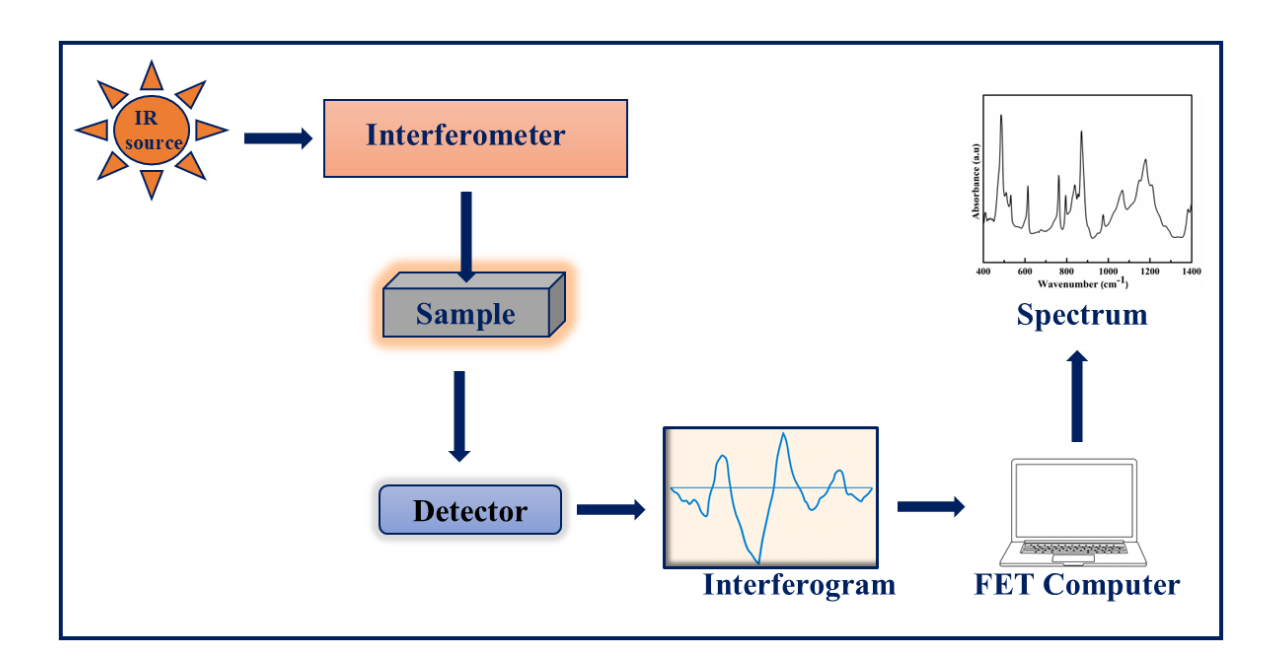


Figure 2.6 Schematic showing Fourier Transform Infrared Spectroscopy (FTIR).

The sample is subsequently exposed to the resulting interferogram. As mentioned before, various transmitted light wavelengths from the incident spectrum are selectively absorbed by the sample. The intensity of various transmitted light wavelengths is measured using a detector. The incoming signal is analysed and transformed into interpretable data using the "Fourier transform" method. Several functional groups within the examined sample may be identified with the help of the final graph created by applying the Fourier transform technique. In the present thesis work, Perkin Elmer FTIR spectrum-II instrument (see Figure 2.7) was used for FTIR analysis of prepared films.



Figure 2.7 Fourier Transform Infrared Spectroscopy (FTIR) by Perkin Elmer FTIR spectrum-II instrument.

2.3.1.3 Scanning Electron Microscopy (SEM)

Scanning electron microscopy (SEM) is a powerful technique widely employed to investigate the surface morphology, microstructure, and chemical composition of the materials. It offers detailed insights into surface morphology, crystal orientation, phase distribution, crystal structure and compositional variations within the material. In addition, SEM is also extensively used to identify and analyze surface fractures.

Figure 2.8 illustrates a visual depiction of basic SEM components. In SEM, electromagnetic lenses are utilized to focus a beam of electrons onto the specimen. The sample under investigation may consist of materials such as ceramics, metals, metal oxides, or biological specimens. The interaction between the electron beam and the specimen surface produces signals that are recorded, to generate an image. As the electron beam interacts with the material, it leads to the deflection in different types of electrons.

Preparation of a sample for SEM analysis typically involves dispersing powder samples, applying composite films, or arranging pellets onto conductive carbon tape, followed by coating them with a thin layer of conductive metals such as platinum (Pt) or gold (Au) [10]. This coating prevents the accumulation of incident electrons on specific regions of the sample. As a result, the electron beam can be systematically directed across the specimen, ensuring effective interaction with the sample. During this interaction, electrons are scattered from the surface, producing both secondary electrons and backscattered electrons (BSE). These emitted electrons, particularly secondary electrons released from the few surface layers with energies below 50 eV, provide valuable information regarding the surface morphology of the sample.

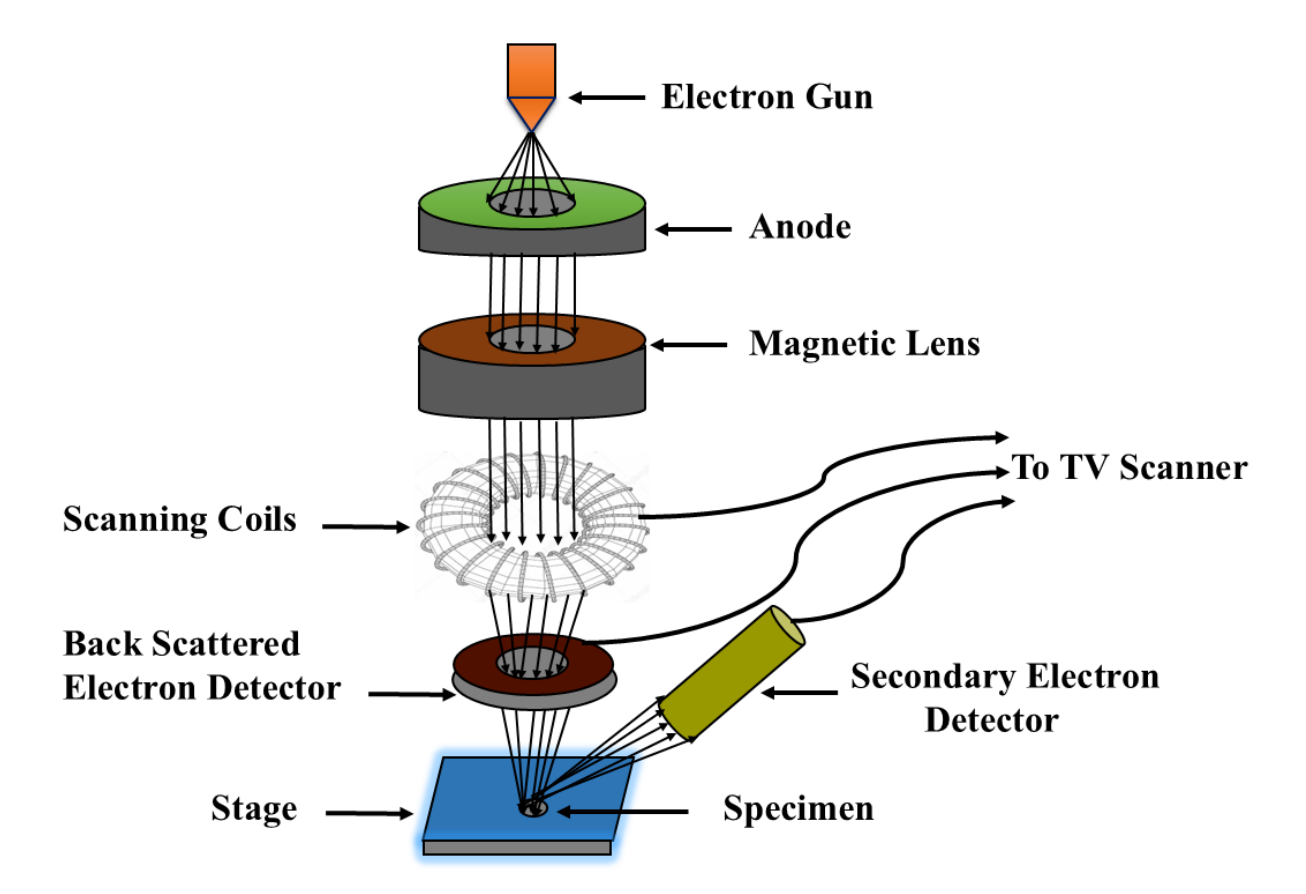


Figure 2.8 Schematic showing the components of a Scanning Electron Microscopy (SEM).

In contrast, BSE have energies exceeding 50 eV, undergo elastic scattering from the surface, and can penetrate deeper into the specimen as compared to secondary electrons [11]. More backscattered electrons are yielded by elements with higher atomic numbers than by those with lower atomic numbers. This difference is demonstrated by the appearance of brighter patches in SEM images. As a result, variations in the surface chemical composition can be detected through the contrast within images produced using backscattered electrons. The density of backscattered electrons is reflected by the interplay between bright and dark areas in these regions while the intensity of the signal is correlated with the concentration of secondary electrons [12]. In the present thesis work, the surface morphology of the synthesized samples was examined through scanning electron microscopy on a JEOL instrument (Model: JSM-6610LV) which is depicted in Figure 2.9.



Figure 2.9 Scanning Electron Microscopy (SEM) by JEOL (JSM-6610LV).

2.3.1.4 Field Emission Scanning Electron Microscopy (FESEM)

The Field Emission Scanning Electron Microscopy (FESEM) approach is a powerful tool which gives information such as surface topography and material's composition [13-18]. In this microscope, a highly energetic electron beam is used to irradiate the sample surface, with its wavelength expressed as:

$$\lambda = \frac{h}{p} = \frac{h}{mv} = \frac{h}{\sqrt{2meV}} \tag{2.2}$$

where, h stands for Planck's constant, while m, v, and e denote the mass of an electron, velocity and charge on the electron, respectively and V is the applied voltage. Thus, by changing the applied voltage, the wavelength of the electrons can be changed and therefore, a resolution on the order of nanometres (nm) may be achieved. In FESEM, a high electric field is applied to eject electrons, which are subsequently accelerated by using a potential gradient. Using a condenser (electromagnetic) lens, the beam of electrons is focused on the sample. The bombardment of these electrons on the surface of the sample results in various processes, which includes the ejection of backscattered electrons, secondary electrons, X-rays and Auger electrons. The FESEM detector picks

up the secondary electrons and then uses them to construct the image of the sample on the screen.

In the present work, a Gemini SEM 500 Zeiss FESEM (see Figure 2.10) was used to examine the samples. Prior to scanning, the samples were coated with a thin layer of gold using a Quorum gold sputter coater to reduce charging effects.



Figure 2.10 Field Emission Scanning Electron Microscopy (FESEM) by Gemini SEM 500, Zeiss.

2.3.1.5 Polarisation vs. Electric Field (*P-E*) Loop Measurements

Ferroelectricity is exhibited by a subclass of piezoelectric materials that possess spontaneous electric polarisation, which can be reversed under an applied electric field. The phenomenon of ferroelectricity was first discovered by Prof. J. Valasek in 1921. Ferroelectrically active materials contain specific regions of uniform polarisation,

referred to as ferroelectric domains. A ferroelectric material may consist of multiple domains, which are separated by interfaces known as domain walls.

The ferroelectric behavior of the prepared samples was examined by recording the Polarisation vs. Electric field (P-E) hysteresis loop at room temperature. In ferroelectrically active materials, the variation of polarisation with an applied electric field is nonlinear and forms a closed loop, known as the P-E hysteresis loop. Even after the removal of the external field, a certain amount of residual polarisation remains. During measurement, the applied electric field is gradually increased to induce polarisation in the sample and then decreased to examine the depolarisation process. The shape and size of the loop yield key information about ferroelectric parameters such as remnant polarisation, coercive field, and spontaneous polarisation.

In the present work, the *P-E* hysteresis loops of the composite films were measured using a *P-E* loop tracer manufactured by Marine India Instrument (Model:20PE 1kHz 0.1N) (see Figure 2.11).

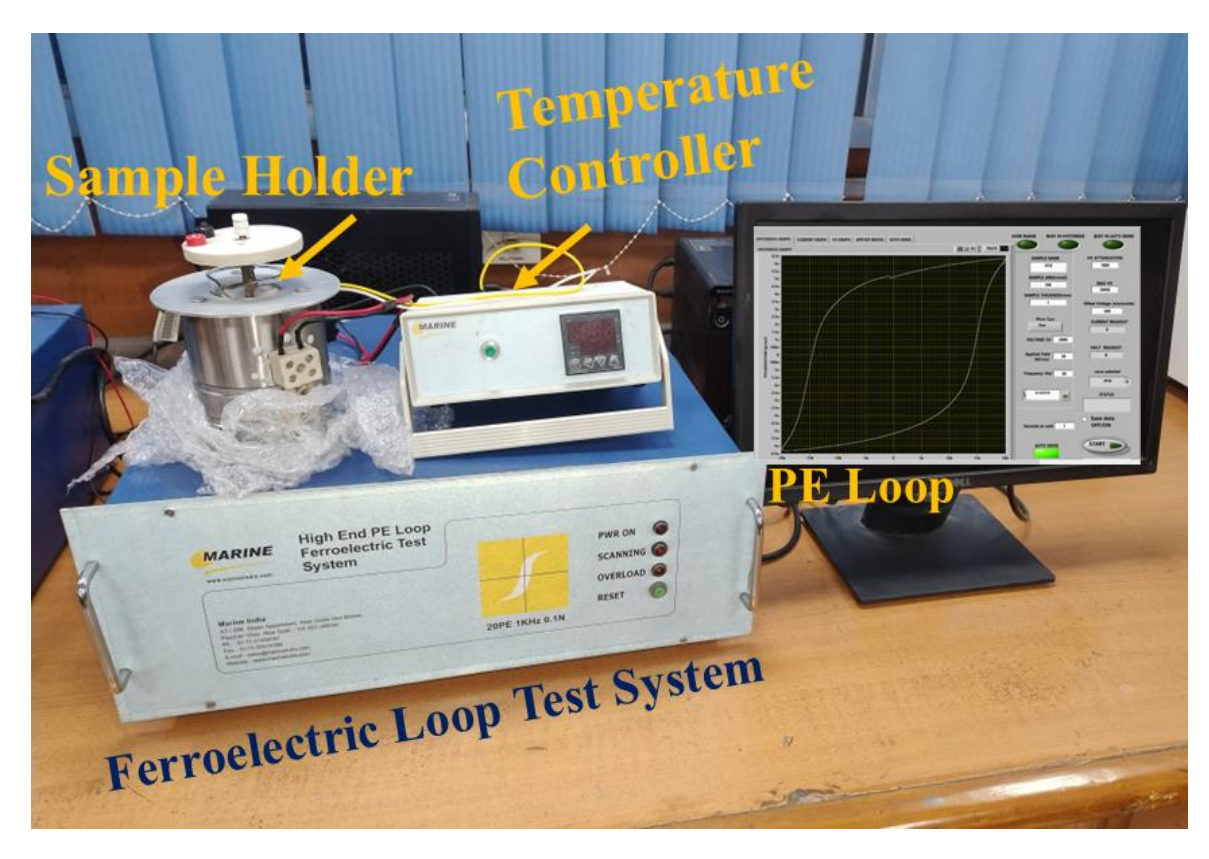


Figure 2.11 Polarisation vs. Electric field (*P-E*) hysteresis loop Ferroelectric Test System (MARINE: 20PE 1KHz 0.1N).

2.3.1.6 Dielectric Measurement

The term "dielectric" was first introduced by William Whewell. The dielectric property of material refers to its ability to store electrical energy and is defined as the ratio of the capacitance of a capacitor containing the material to that of the same capacitor in vacuum, expressed as:

$$\varepsilon' = \frac{c}{c_o} \tag{2.3}$$

where, where ε' is the dielectric constant, C is the capacitance of the dielectric material and C_o is the capacitance in vacuum.

A parallel plate capacitor consists of two parallel conducting plates separated by a distance (d). When a parallel plate capacitor is sandwiched between its two plates using vacuum, its capacitance C_o is shown as [19]:

$$C_o = \frac{\varepsilon_o A}{d} \tag{2.4}$$

where, ε_o (= 8.854 x 10⁻¹² F/m) is the permittivity of free space, A is the area of the plates of capacitor.

On combining equation 2.3 and 2.4,

$$\varepsilon' = \frac{CA}{\varepsilon_0 d} \tag{2.5}$$

For an alternating electric field, dielectric constant is given by [20]

$$\varepsilon^* = \varepsilon' - \varepsilon'' \tag{2.6}$$

where, (ε') is real component of dielectric constant and (ε'') is an imaginary component of dielectric constant.

Dielectric loss ($tan \delta$), also known as the dissipation factor, is calculated as the ratio of the imaginary part to the real part of the complex permittivity, as expressed by:

$$tan \delta = \frac{\varepsilon''}{\varepsilon'} \tag{2.7}$$

In the present work, the dielectric constant of the prepared samples was measured using an Impedance Analyzer (Model: KEYSIGHT E4990A). Instrument consists of a

sample holder, PID temperature controller unit, Vacuum chamber, and Impedance Analyzer as shown in Figure 2.12.

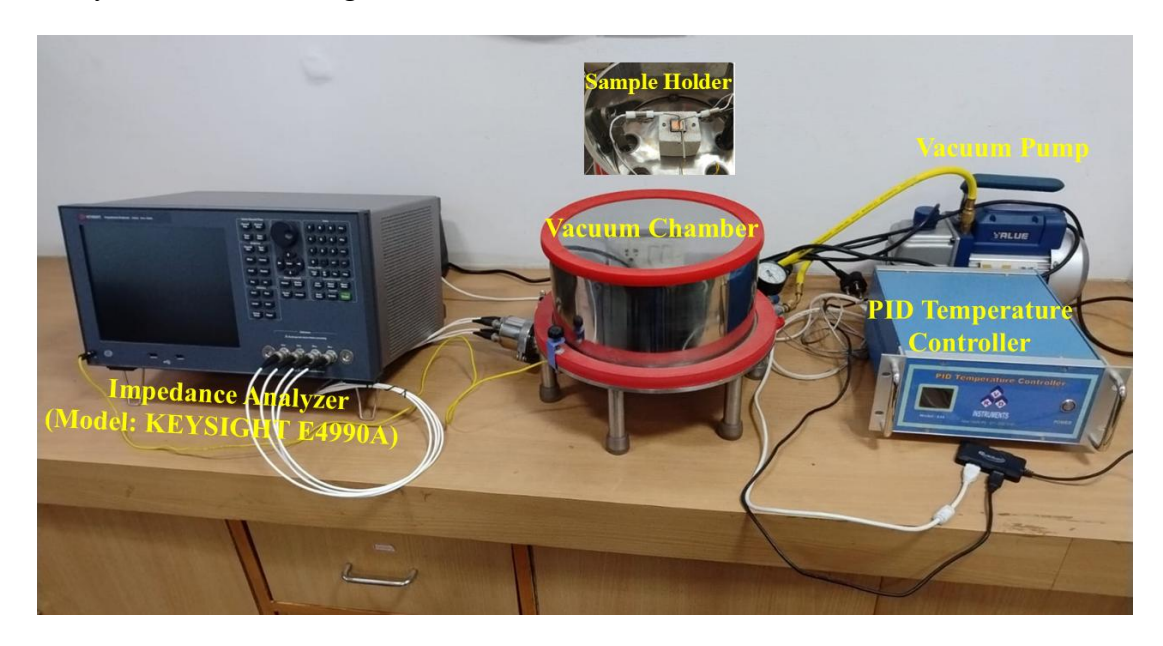


Figure 2.12 Impedance Analyzer (Model: KEYSIGHT E4990A), Sample Holder and PID Temperature Controller Unit.

2.3.1.7 Displacement vs. Voltage (D-V) Butterfly Loop

The Displacement vs. Voltage (D-V) Butterfly Loop is a characteristic feature of ferroelectric materials, illustrating the inverse piezoelectric effect i.e. when an external electric field is applied, the sample undergoes mechanical strain, leading to a displacement response that exhibits a butterfly-shaped curve. The phenomenon is also employed to calculate the effective inverse piezoelectric charge coefficient (d_{33}^*) by evaluating the slope of the D-V (butterfly) curve of the sample [21-26], which is as follows:

$$d_{33}^{*} = \frac{(D - D_0)}{(V - V_0)} \tag{2.8}$$

where, D denotes the displacement (measured in μ m) caused by the applied voltage V (in Volts). V_o and D_o correspond to the voltage and displacement values, respectively at the intersection point of the D-V loop, which are subtracted from each (D, V) data point to correct for any shift in the origin. In the present work, D-V butterfly loop of the composite films was recorded using the Strain Measurement System of Radiant

Precision LCII Ferroelectric tester (Model No. P-HVi210KSC) and the obtained data was then used to calculate d_{33}^* .

2.3.1.8 Electrical Measurements

For the electrical measurement of the constructed piezoelectric generator devices, electrodes were attached on both the sides of the fabricated composite films to provide electrical contacts. A dynamic shaker (Micron MEV-0025) (refer to Figure 2.13 (a)) was employed to apply the mechanical stress on the surface of the constructed PEG device for measuring the energy harvesting performance. A digital storage oscilloscope (Tektronix MDO 500) (see Figure 2.13 (b)) was used for measuring the generated output voltage. A Keithley digital multimeter (DMM7510) (see Figure 2.13 (c)) and electrometer (Keysight B2902B) (see Figure 2.13 (d)) were used to measure the generated output current.

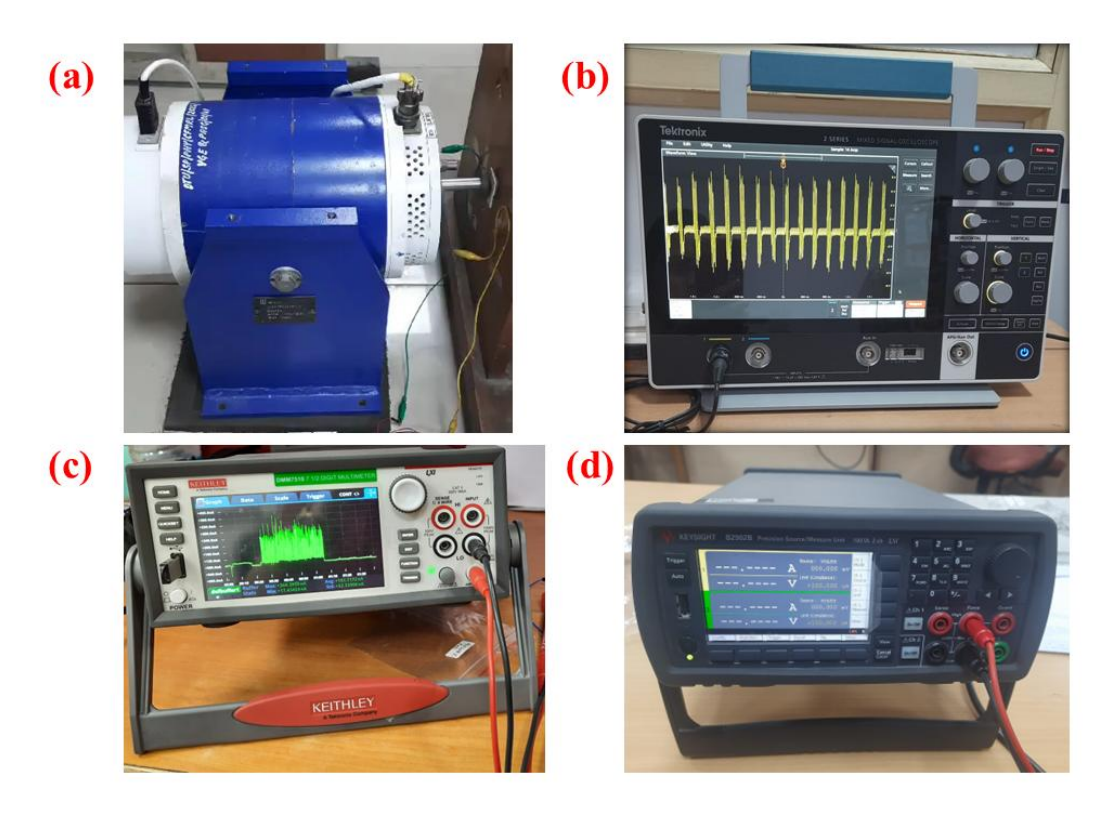


Figure 2.13 (a) Dynamic Shaker (Micron MEV-0025), (b) Digital Storage Oscilloscope (Tektronix MDO 500), (c) Keithley Digital Multimeter (DMM7510) and (d) Electrometer (Keysight B2902B)

References

- [1] Y. Matsuo, H. Sasaki, Journal of American Ceramic Society, 48, (1965), 289
- [2] Y. Xu, Elsevier Science Pub. Co. New York, 1991, USA
- [3] J. Li, Q. Wu, J. Wu, Synthesis of Nanoparticles via Solvothermal and Hydrothermal Methods, 12, (2016)
- [4] M. Etter, R.E. Dinnebier, Zeitschrift Für Anorganische und Allgemeine Chemie, 640 (15), (2014), 3015-3028
- [5] B. Cullity, S. Stock, Addison-Wesley Publishing Company Inc., (2001)
- [6] W.M. Doyle, Process Control Qual, 2, (1992), 11-41
- [7] E. Knözinger, Wiley Online Library, (1986)
- [8] G.C. Schatz, R.P. Van Duyne, J.M. Chalmers, P.R. Griffiths, Handbook of vibrational spectroscopy, New York: Wiley, 1, (2002), 759
- [9] D. Titus, E.J.J. Samuel, S.M. Roopan, Elsevier, (2019), 303-319
- [10] A. Mohammed, A. Abdullah, 7-9
- [11] W. Zhou, R. Apkarian, Z.L. Wang, D. Joy, Fundamentals of scanning electron microscopy (SEM), Scanning Microscopy for Nanotechnology: Techniques and Applications, (2007), 1-40
- [12] B.J. Inkson, Elsevier, (2016), 17-43
- [13] J. Kuo, Springer Science & Business Media, (2007)
- [14] A. Tiwari, R.A. Gerhardt, M. Szutkowska, Advanced Ceramic Materials, John Wiley & Sons, Inc., Hoboken, NJ, USA, (2016)
- [15] M.K. Basher, R. Mishan, S. Biswas, M. Khalid Hossain, M.A.R. Akand, M.A. Matin, AIP Advanced, 9, (2019), 075118
- [16] P. J. Goodhew, J. Humphreys, R. Beanland, Third Edition, CRC Press, (2000)
- [17] C. E. Lyman, Springer Science & Business Media, (1990)
- [18] J. Goldstein, D. E. Newbury, D. C. Joy, C. E. Lyman, Third Edition, Springer US, (2013)
- [19] R.J.D. Tilley, John Wiley and Sons Ltd., England, (2004)
- [20] K.C. Kao, Elsevier Academic Press, (2004)

- [21] H. Yadav, N. Sinha, S. Goel, and B. Kumar, Journal of Alloys and Compounds, 689, (2016), 333
- [22] S. Goel, N. Sinha, A. Hussain, A. J. Joseph, and B. Kumar, Ionics (Kiel), 86, (2018),

142907

- [23] S. Goel, N. Sinha, and B. Kumar, Physics E Low-Dimensional System Nanostructures, 105, (2019), 29
- [24] S. Goel, N. Sinha, H. Yadav, A. J. Joseph, and B. Kumar, Physics E Low-Dimensional System Nanostructures, 91, (2017), 72
- [25] S. Goel, N. Sinha, H. Yadav, S. Godara, A. J. Joseph, and B. Kumar, Materials Chemistry and Physics, 202, (2017), 56
- [26] N. Sinha, S. Goel, A. J. Joseph, H. Yadav, K. Batra, M. K. Gupta, and B. Kumar, Ceramics International, 44, (2018), 8582

Chapter 3

Effect of KNN concentration and size on the output performance of KNN/PVDF based flexible piezoelectric generator

Chapter 3 Effect of KNN concentration and size on the output performance of KNN/PVDF based flexible piezoelectric generator

This chapter is divided into two sections. The first section focuses on the fabrication and characterization of piezoelectric generator (PEG) based on flexible composite films composed of Potassium Sodium Niobate (KNN) and Poly (vinylidene fluoride) (PVDF), with varying concentrations of KNN ceramic particles (0 wt.%, 5 wt.%, 10 wt.%, 15 wt.%, and 20 wt.%) in the polymer matrix. In the first section, KNN was synthesized using the solid-state reaction method and used for the construction of PEG. The second section explores the effect of KNN particle size synthesized by hydrothermal method as filler in the PVDF matrix on the piezoelectric output performance of the constructed piezoelectric generator device. The obtained result demonstrates a considerable enhancement in the piezoelectric output performance of a device constructed with KNN synthesized by hydrothermal method over the PEG device constructed using KNN synthesized by solid-state method.

3.1 Section 1

3.1.1 Introduction

Piezoelectric generators (PEGs) utilize piezoelectric materials to convert mechanical energy from the surrounding environment into electrical energy. The efficiency of this energy conversion is closely linked to the piezoelectric coefficient of the material - materials with higher value of piezoelectric coefficient generally yield greater energy output. Therefore, selecting materials with elevated charge constants is crucial for optimizing the performance of piezoelectric generators. Commonly explored lead-free piezoelectric materials include Barium Titanate (BT), Potassium Sodium Niobate (KNN), Zinc Oxide (ZnO), Bismuth Sodium Titanate (BNT), and Bismuth Potassium Titanate (BKT), etc [1–4].

A. Hussain *et al.* reported the development of a piezoelectric energy harvesting device based on Y-doped PMN-PT ceramics [5]. Their device demonstrated improved performance, generating an output voltage of approximately 60 V under periodic mechanical tapping conditions (2.0 kgf at 5 Hz), indicating its suitability for powering various self-sustaining electronic systems. Similarly, Shekhar *et al.* fabricated an

energy harvester utilizing Praseodymium (Pr)-modified lead-free BCZT ceramics [6]. Their device achieved an open-circuit voltage of around 5.1 V and a power density of 1.213 mW/cm² under finger-tapping excitation. Furthermore, when subjected to machine tapping over 10,000 cycles, the output voltage increased to approximately 9 V, demonstrating good durability and stable performance. In another study, Camargo et al. integrated a Bismuth Sodium Potassium Titanate (BNKT) ceramic sample onto a steel beam mounted on an electrodynamic shaker [7]. Their setup revealed the practical potential of BNKT ceramics for mechanical energy harvesting, achieving a peak output voltage of around 19.9 V and a corresponding power density of 3.36 mW/cm². However, the inherent defects of these ceramic materials such as brittleness, low toughness and high temperature fabrication process have led to the efforts for the development of composite based flexible PEGs composed of piezoelectric materials as filler and polymer as the flexible matrix [8]. In this way, the resulting composites are expected to have both: excellent piezoelectric properties of the piezoelectric material and mechanical flexibility of the polymer [9-11]. These types of devices have shown outstanding piezoelectric performance in wearable applications enabling innovative solutions for energy harvesting.

Li *et al.* fabricated a flexible piezoelectric nanocomposite by incorporating hydrothermally synthesized PMN-PT nanorods into a PVDF matrix. The resulting film achieved a peak output voltage of 10.3 V and a current of 0.046 μA—approximately 13 times higher than that of pure PVDF [12]. Siddiqui *et al.* developed a flexible piezoelectric nanogenerator using BaTiO₃ nanoparticles embedded in PVDF-TrFE via spin coating [13]. At 40 wt.% BaTiO₃, the device generated approximately 9.8 V and 0.69 μA, with a power density of 13.5 μW/cm² under repeated bending. The device also demonstrated practical energy harvesting from body movements, producing voltages of 7.5 V by index finger joint, 4.3 V by wrist bending, and 1.5 V by elbow bending. In another study, Zhao *et al.* fabricated a nanogenerator with 70 wt.% BaTiO₃ in PVDF using a scalable solvent evaporation method [14]. The device showed uniform particle dispersion and produced up to 35 V and 0.6 μA under 1 MPa, and 150 V and 1.5 μA under 10 MPa. Baek *et al.* achieved outstanding performance from a piezoelectric nanogenerator (PENG) by incorporating BaTiO₃ nanoparticles (NPs) and nanowires (NWs) into a PDMS matrix without the need for dispersion agents [15]. The PENG

generated a maximum open-circuit voltage (V_{oc}) of approximately 60 V, a short-circuit current (I_{sc}) of 1.1 μ A, and an instantaneous power output of 40 μ W. Furthermore, the device demonstrated excellent durability, maintaining stable performance for up to 3000 bending and unbending cycles, highlighting its reliability for energy harvesting applications. Additionally, Juan Yi *et al.* developed electrospun PVDF films containing Y-doped ZnO and studied the effect of filler content on piezoelectric performance [16]. The device with 15 wt.% doped ZnO generated output voltages of approximately 20 V during walking and about 35 V during running, demonstrating its potential for wearable energy harvesting. Li *et al.* developed a PVDF/ZnO nanogenerator by hydrothermally growing ZnO nanowires on a spin-coated PVDF film. The resulting hybrid device produced an output voltage and output current density of approximately 3.2 V and 0.6 μ Acm⁻², respectively higher than that of pure PVDF [17].

Among the various polymers used to fabricate flexible piezoelectric generators, PVDF and its copolymers have proven to be the excellent candidates for the construction of generators owing to their high mechanical flexibility, ease of synthesise, and good biocompatibility [18, 19]. PVDF has several crystallographic phases, such as α , β , γ , δ and ε phases which are related to different chain conformations. Among these, β phase with all TTT (the chain configuration) is most important due to its high piezoelectric sensitivity that can enhance the energy conversion efficiency [20-23].

In view of this, in the present work we report a piezoelectric energy harvester which is constructed by employing PVDF as polymer matrix and K_{0.5}Na_{0.5}NbO₃ (KNN) ceramic particles as filler in the PVDF matrix. KNN stands out due to its high piezoelectric coefficient, high Curie temperature, substantial remnant polarisation, strong dielectric response and environmentally friendly, lead-free composition [24] and have been used for the construction of PEGs [25]. The fabricated KNN/PVDF flexible composite films which were used to prepare the PEG device were characterised using different characterisation tools such as X- Ray diffraction (XRD), Scanning electron microscopy (SEM), and Fourier transform infrared spectroscopy (FTIR). The piezoelectric performance of the device was examined using a finger tapping method on the surface of the PEG device. Further, the influence of KNN ceramic concentration on the piezoelectric performance of the device was also investigated. The open-circuit voltage

and short-circuit current measured for the device were 11.2 V and $0.3 \mu\text{A}$, respectively. The flexibility, wearability, and low cost of the fabricated devices in the present work demonstrated their potential in energy harvesting applications.

3.1.2 Materials and Methods

3.1.2.1 Synthesis of K_{0.5}Na_{0.5}NbO₃ Ceramic Powder

For the synthesis of KNN ceramic powder, a solid-state reaction method was used. Potassium carbonate (K₂CO₃), sodium carbonate (Na₂CO₃) and niobium oxide (Nb₂O₅) purchased from Alfa Aesar were used as raw materials. These raw materials were mixed in the stoichiometric ratio in propanol for 10 hours to prepare a homogeneous mixture followed by drying in the oven at 60 °C for 24 hours. The dried mixture was then calcined in the furnace at 1050 °C for 4 hours in air. Afterward, the obtained calcined powder was grinded again for further use in films.

3.1.2.2 Fabrication of KNN-PVDF Flexible Composite Films

Polyvinylidene fluoride (PVDF) and N, N-Dimethylformamide (DMF) were purchased from Alfa Aesar. PVDF powder was dissolved in DMF by stirring with a magnetic stirrer at 50 °C for 1 hour to prepare a uniform transparent solution. Simultaneously, calcined KNN particles with 0 wt.%, 5 wt.%, 10 wt.%, 15 wt.% and 20 wt.% were separately added in DMF as listed in Table 3.1 and ultrasonicated for 30 minutes at room temperature. Then the prepared KNN solutions with different weight percentages were mixed with PVDF solution by stirring with a magnetic stirrer at 50 °C for 4 hours followed by ultrasonication for 10 minutes to minimize particle agglomeration. The prepared homogeneous solution was then drop cast onto the clean glass substrate and then dried in the oven at 90 °C for 1 hour to form flexible KNN/PVDF composite films. After the drying process, a flexible KNN/PVDF film was obtained on the glass substrate. Finally, the film was peeled off easily from the glass substrate. The complete synthesis process of composite films was done in an air ambient. Figure 3.1 shows the schematic representation of the fabrication process of KNN/PVDF composite films and digital photographs of the prepared composite films with different weight percentages of KNN ceramic powder in PVDF. The prepared flexible composite films are labelled as per the information given in Table 3.1.

Table 3.1 Details of weight percentages of KNN and PVDF in the fabricated flexible composite films.

S. No.	Sample ID	Amount (gm)		
		PVDF	KNN	
1.	0% KNN	1	0	
2.	5% KNN	0.05	0.05	
3.	10% KNN	0.90	0.10	
4.	15% KNN	0.85	0.15	
5.	20% KNN	0.80	0.20	

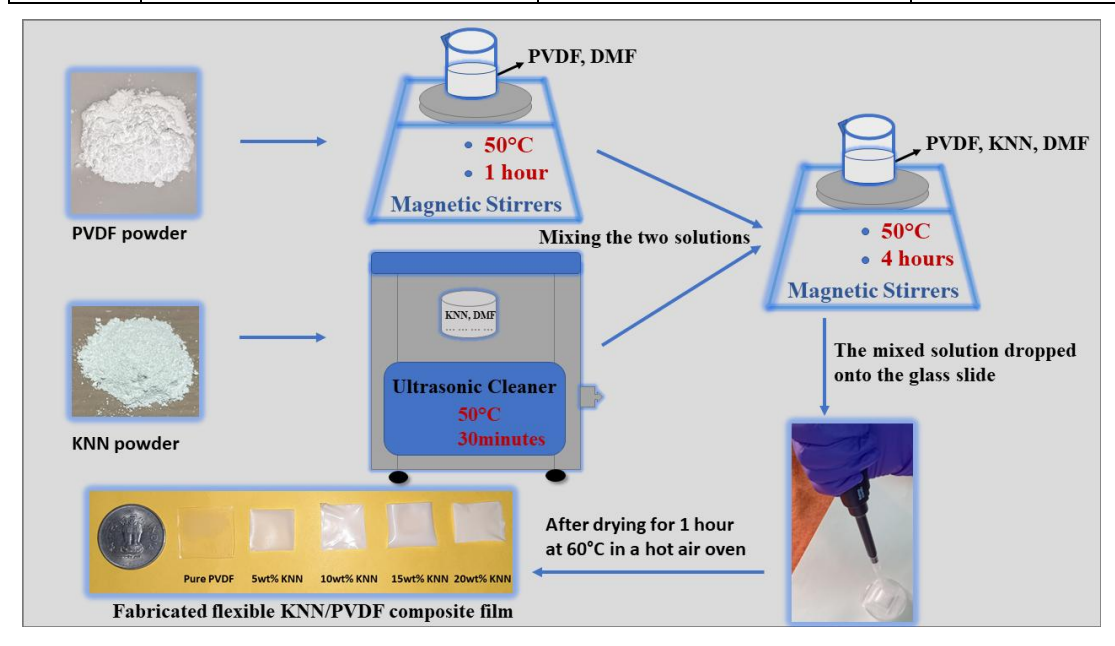


Figure 3.1 Schematic representation of KNN/PVDF flexible composite film fabrication process and the digital photographs of the prepared flexible composite films with different weight percentages of KNN ceramic particles in PVDF matrix.

3.1.2.3 Fabrication of KNN/PVDF based Piezoelectric Generator (PEG)

To construct the PEG, prepared flexible KNN/PVDF composite films were cut into small pieces of 1.5×1.5 cm² and aluminium tape was attached on both the sides of the

films to make top and bottom electrodes. After that, copper wires were attached to the aluminium tape using the silver paste to measure the output signals on application of pressure when connected to the external circuit. Figure 3.2 (a) and (b) show the schematic diagram of the fabricated PEG device and digital photograph of the prepared PEG devices, respectively.

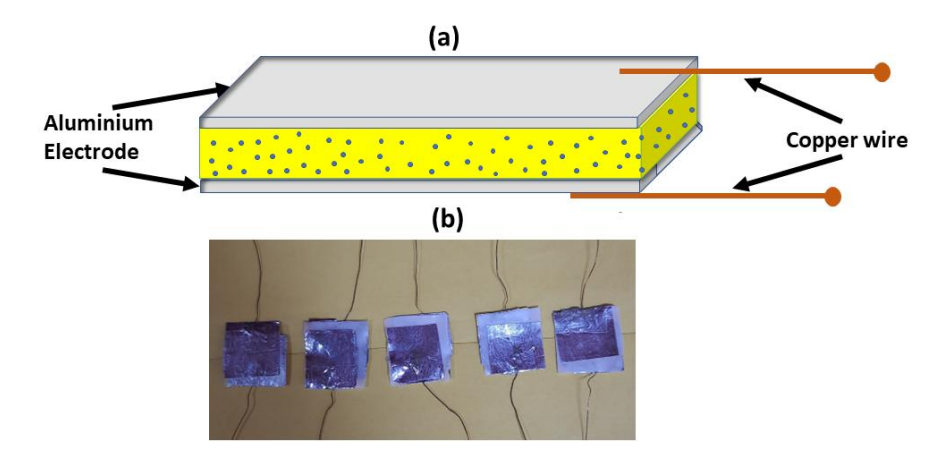


Figure 3.2 (a) Schematic diagram of the fabricated PEG device and (b) digital photograph of the prepared PEG devices.

3.1.2.4 Characterizations

X-ray Diffraction (XRD; Rigaku, Ultima- IV) with Cu- $K\alpha$ radiation source (1.54 Å) was used to analyse the crystalline structure of the prepared KNN powder and composite films. The morphology of the calcined KNN powder and KNN/PVDF composite films was observed with scanning electron microscopy (SEM) (NOVA SEM). To analyse the formation of β phase in the KNN/PVDF composite films, Fourier Transform Infrared (FTIR) spectroscopy was done (Perkin Elmer FTIR spectrum-II). The dielectric measurement as a function of frequency was carried out using a KEYSIGHT Impedance Analyzer E4990A. Further, the generated output voltages and currents of the fabricated PEG devices were recorded by using digital storage oscilloscope (Tektronix, MDO500) and the digital multimeter (Keithley DMM7510), respectively. Inverse Piezoelectric coefficient (d_{33}^*) value of the composite film was measured using the Radiant Precision LCII Ferroelectric tester (Model No. P-HVi210KSC). Finally, to demonstrate the practical applicability of the fabricated PEG

device, it was attached to the elbow, and finger to harvest energy from human body movements.

3.1.3 Results and Discussions

3.1.3.1 Structural and Microstructural Analysis of KNN Ceramic Powder

The crystal structure of the prepared KNN powder was analysed by XRD and the corresponding plot was shown in Figure 3.3. All the peaks in the XRD plot show a pure perovskite structure with the absence of any impurity peaks, indicating that KNN powder was successfully synthesised by the solid-state reaction method. The XRD pattern can be indexed to perovskite KNN according to the standard JCPDS card no. 98-024-7572 of KNN ceramic with orthorhombic structure having space group Amm2. Moreover, the peak splitting around $\sim 45.2^{\circ}$ with higher intensity of (022) peak in comparison to (200) peak further confirmed the formation of orthorhombic phase [26, 27].

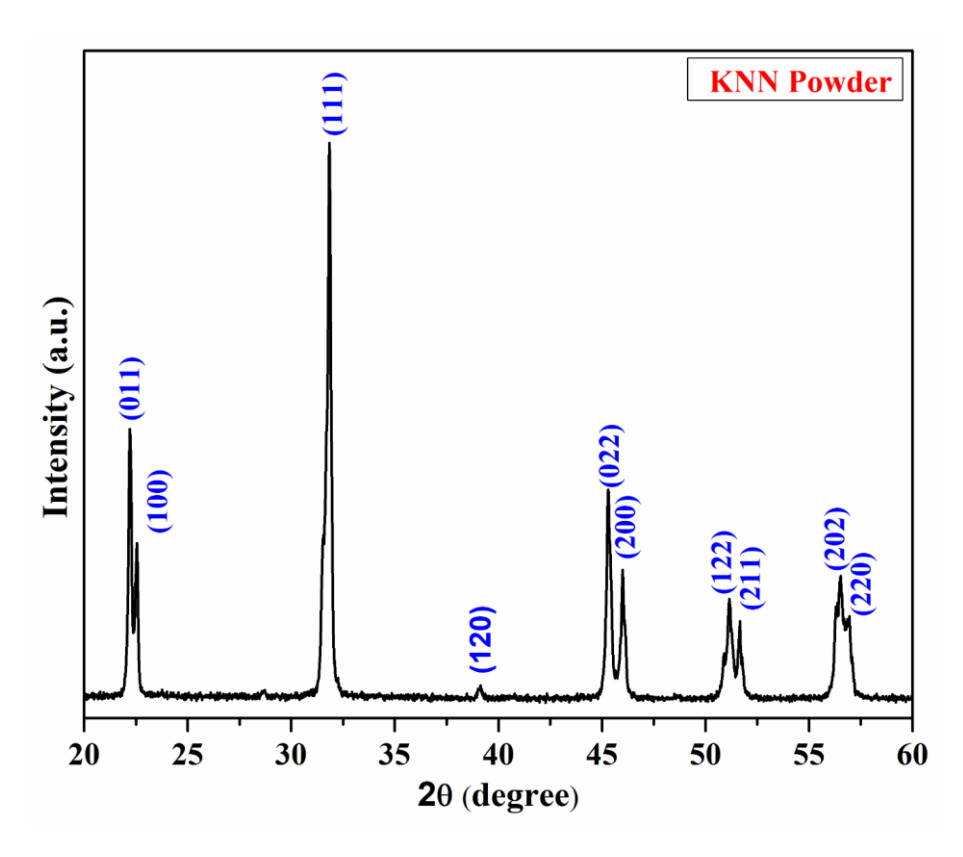


Figure 3.3 XRD pattern of calcined KNN ceramic powder.

Further, the morphology of the synthesized KNN ceramic powder was analysed by SEM and the corresponding image was shown in Figure 3.4 (a). It is observed from the

SEM image that KNN ceramic particles exhibit cubic morphology. Figure 3.4 (b) represents the histogram of particles showing their distribution with respect to frequency. The average particle size of the prepared KNN ceramic powder was 1.32 µm which was calculated using Image J software.

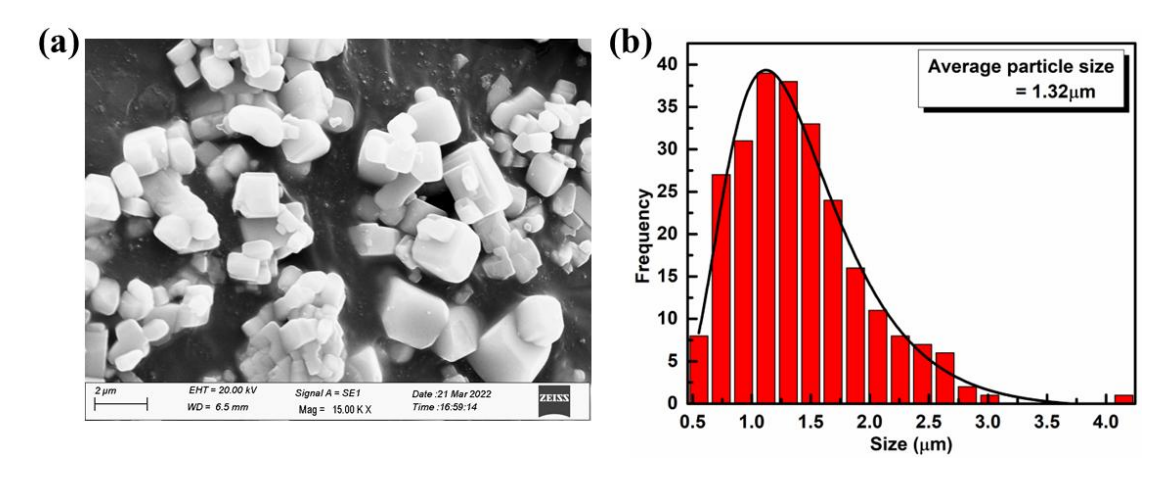


Figure 3.4 (a) SEM image of the calcined KNN ceramic powder and (b) Histogram showing the distribution of KNN particles.

3.1.3.2 Structural and Microstructural Analysis of Pure and KNN/PVDF Composite Films

XRD analysis of pure PVDF film and KNN/PVDF flexible composite films were done to get the crystallographic information and corresponding plots are shown in Figure 3.5. The presence of peak around ~20.1° in all the prepared films corresponds to the polar β -crystalline phase of PVDF polymer whereas a broad and small diffraction peak at ~18.2° can be assigned to the non-polar α -phase of PVDF [28, 25]. In addition, the stronger intensity of the diffraction peak corresponding to β -phase in comparison to the α -phase (see Figure 3.5 (b)) indicates the predominance of the β -phase over the α -phase of PVDF in all the prepared films. Further, it is clearly evident from the XRD plots that the intensity of the diffraction peaks corresponding to the KNN particles increases and the intensity of diffraction peaks corresponding to the PVDF decreases with increase in KNN particles concentration in the PVDF matrix.

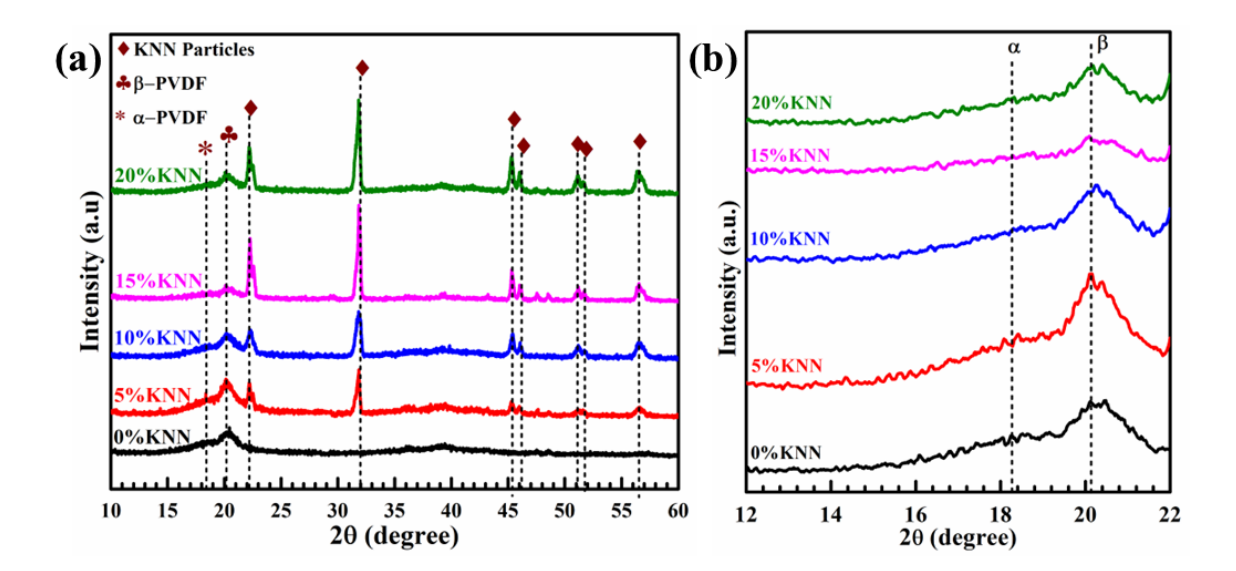


Figure 3.5 (a) X-ray Diffraction patterns produced with different content of KNN ceramic powder in PVDF matrix and (b) higher magnified view of Figure 3.5 (a).

The morphology of the surface of the prepared pure and KNN/PVDF flexible composite films were analysed using SEM and corresponding images are presented in Figure 3.6. In all the KNN/PVDF composite films, uniform dispersion and presence of KNN ceramic particles in the PVDF matrix was clearly evident from Figure 3.6. Besides, surface pores in the 20% KNN sample can also be observed in the Figure 3.6 (d) which contains 20 wt.% of KNN ceramic in the PVDF matrix.

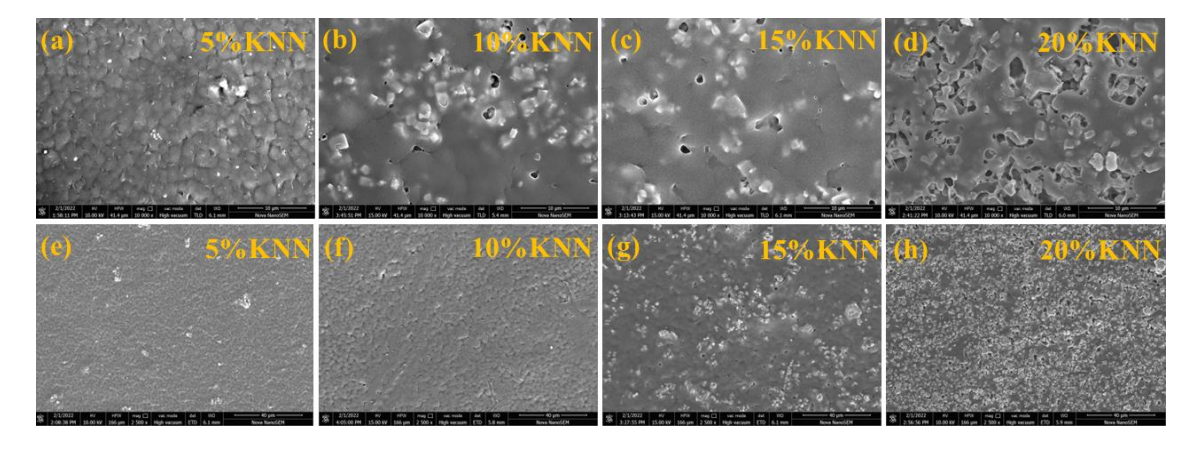


Figure 3.6 SEM surface micrographs of KNN/PVDF composite films with different content of KNN ceramic powder in PVDF matrix (a-d) on 10 μ m scale and (e-h) on 40 μ m scale.

3.1.3.3 FTIR Analysis of Pure and KNN/PVDF Composite Films

The FTIR analysis of the pure and composite films was also done to understand the effect of KNN ceramic particles on the crystal structure of PVDF. The FTIR spectra of pure PVDF film and KNN/PVDF composite films were recorded in the range 500 – 1500 cm⁻¹ at room temperature and are presented in Figure 3.7 (a). From the FTIR spectra it can be seen that α and β phases are present in all the prepared films. The peaks which correspond to α and β phases are marked in the Figure 3.7 (a). The obtained FTIR data was in agreement with the XRD data representing the existence of β phase of PVDF in all the prepared pure PVDF film and KNN/PVDF composite films. The absorption bands at 531, 614, 763 and 1401 cm⁻¹ are assigned as the characteristic peaks of the α phase of PVDF [29-32]. On the other hand, the absorption bands at 509, 600, 836, 876, 1071, 1168 and 1232 cm⁻¹ are assigned as the characteristic peaks of β phase of the PVDF [29-32, 33].

Furthermore, in comparison to the pure PVDF film, the absorption peaks which corresponds to the β phase of the PVDF were intensified in all the KNN/PVDF composite films, indicating that an enhanced β phase crystallization of PVDF was achieved with the incorporation of KNN ceramic powder in the PVDF. The β phase of PVDF is very important as it contributes to the piezoelectric performance of the generator device. Furthermore, in Figure 3.7 (c), absorption intensity of the peaks at 763 cm⁻¹ and 836 cm⁻¹ which corresponds to α phase and β phase, respectively of PVDF was plotted as a function of KNN ceramic content in PVDF matrix. It is clearly evident from the plot that there is an increase in absorption intensity of the band corresponding to β phase with increase in KNN concentration up to 15 wt.% after that it decreases. For this sample (15 % KNN), lowest absorption intensity of the band corresponding to α phase of PVDF was obtained. Further, β -phase fraction was calculated by Beer-Lambert law and the value of β -phase content for 15 wt.% composite film was ~ 52.5 which is higher than the pure PVDF film (~ 46.3) [34]. The observed increase in the β phase of PVDF in the composite films with the addition of KNN ceramic might have a strong influence on the energy harvesting performance of the prepared composite films.

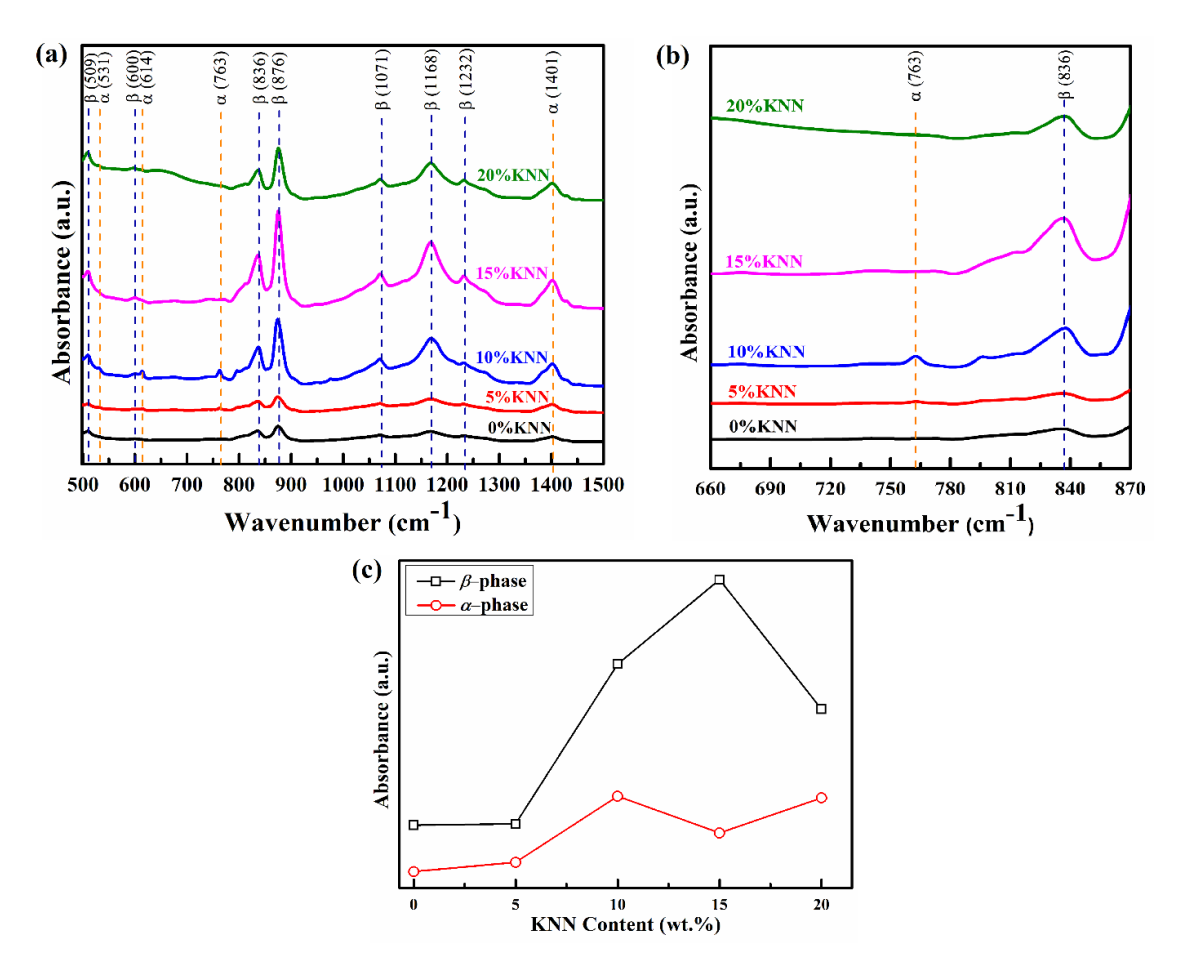


Figure 3.7 (a) FTIR spectra of pure PVDF film and composite films with different content of KNN ceramics in the PVDF matrix and (b) Magnified view of the Figure 3.7(a) and (c) Variation of absorption intensities at 763 cm⁻¹ and 836 cm⁻¹ as a function of KNN ceramic powder concentration in PVDF matrix.

3.1.3.4 Dielectric Properties of Pure and KNN/PVDF Composite Films

The dielectric constant (ε_r) of both pure PVDF and KNN/PVDF composite films were measured by using an Impedance Analyzer over the frequency range of 100 Hz to 1 MHz at room temperature and the corresponding plot is shown in Figure 3.8. It can be seen from the plots that for all the prepared pure PVDF film and KNN/PVDF composite films, dielectric constant is decreasing with increase in the frequency. Different polarisation mechanisms involved are dipolar, ionic, interfacial, and electronic polarisations. When frequency is low, different polarisations respond easily, but with increase in frequency, different polarisation mechanisms cease. This results in the

decrease of net polarisation of the material, which then leads to decrease of dielectric constant [35-37].

Generally, dielectric behaviour is influenced by the presence of the β -phase content in PVDF and the interfacial polarisation caused by the incorporation of KNN ceramic particles into the polymer matrix [38]. The dielectric constant (ε_r) found to increase with increasing KNN percentage to 15 wt.%, after which it began to decline with further increasing the KNN percentage in the PVDF matrix. The composite film containing 15 wt.% KNN exhibited the highest dielectric constant value of 16.87 at 1 kHz in contrast to pure PVDF film, which has a value of 4.41 at 1 kHz.

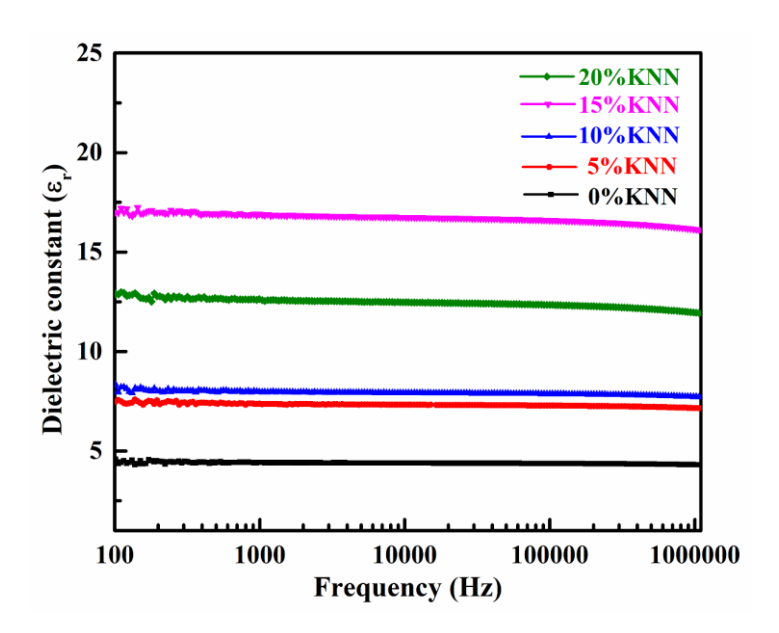


Figure 3.8 Variation of Dielectric constant (ε_r) with frequency of pure PVDF film and KNN/PVDF composite films.

For the composite films, the dielectric constant is dependent on different factors. Firstly, KNN-based ceramics possess significantly higher dielectric permittivity as compared to that of pure PVDF, which contributes to the overall improvement in dielectric constant as the KNN content increases within the PVDF matrix [39-43]. Another contributing factor is the presence of the electroactive β -phase in the PVDF polymer, which combined with the interfacial polarisation between KNN particles and the polymer matrix, further enhances dielectric performance. For composite films, the interface has a prime contribution to the dielectric properties. The accumulation of charges at the interfaces promotes interfacial polarisation between the KNN ceramic

particles and the PVDF matrix and increases with increase in KNN percentage. However, when the KNN content reaches to 20 wt.%, interfacial polarisation effect is reduced attributed to comparatively lower interaction between the KNN ceramic particles and the PVDF matrix. This reduction is because of the agglomeration of KNN particles at a higher percentage in the PVDF matrix [44].

3.1.3.5 Polarisation vs. Electric Field (*P-E*) Hysteresis Loop of the Pure PVDF and KNN/PVDF Composite Films

Polarisation vs. Electric Field (P-E) hysteresis loop analysis has been recorded to inspect the ferroelectric properties of the pure PVDF film and KNN/PVDF composite films and the plot is presented in Figure 3.9 (a). In PVDF polymer, ferroelectric properties are primarily influenced by its polar electroactive phase (β -phase), which plays a crucial role in piezoelectric energy harvesting performance of the constructed device. From Figure 3.9 (a), it can be observed that polarisation increases progressively with increase in applied external electric field which is attributed to better alignment of the dipoles at higher values of applied electric field.

Figure 3.9 (b) and (c) present the variation of remnant polarisation (P_r) and maximum polarisation (P_{max}) for pure PVDF film and KNN/PVDF composite films as a function of KNN ceramic particles content in the PVDF matrix. It is reported in the literature that remnant polarisation (P_r) is mainly dependent on molecular dipole orientation in the polymer matrix [45]. It can be seen from the Figure 3.9 (b) and (c) that both, P_r and P_{max} initially increase with increase in KNN particles content up to 15 wt.% in the PVDF matrix. Thereafter, P_r and P_{max} values decrease for the 20 wt.% KNN. The P_r and P_{max} values are 0.0037 μ C/cm² and 0.040 μ C/cm², respectively for the 15 wt.% KNN incorporated into the PVDF matrix. This is attributed to the higher number of particles assisting towards better realignment of the dipoles. As a result, it is also expected to observe the maximum output voltage for 15 wt.% KNN based composite films since it has higher remnant polarisation value. The decline in P_r and P_{max} values is observed for the 20 wt.% KNN in the PVDF matrix. The possible reason for the observed decrease in P_r and P_{max} might be attributed to the creation of defects in composite films at higher content of KNN particles because of agglomeration and incompatibility between KNN particles and PVDF matrix [46].

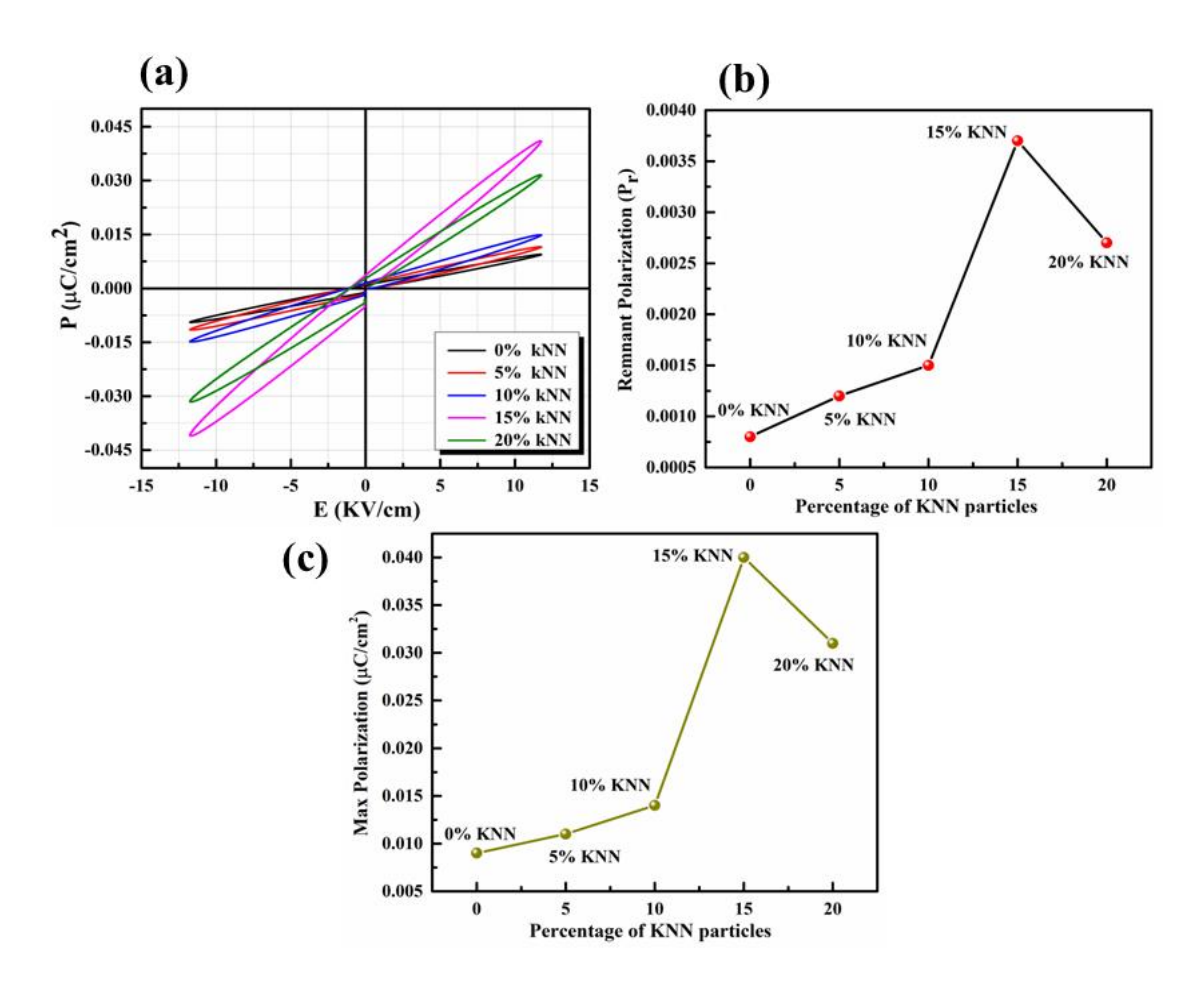


Figure 3.9 (a) P-E hysteresis loop of different composite films, (b) Variation of remnant polarisation (P_r) and (c) maximum polarisation (P_{max}) with content of KNN ceramic powder in the PVDF matrix.

3.1.3.6 Piezoelectric Performance of PEG Devices

The working mechanism of the fabricated piezoelectric generator device is represented in Figure 3.10. On the application of a perpendicular force on the device, electric dipoles align themselves in a single direction which results in the generation of potential difference across both the electrodes. As a result of this, current flows from top to bottom through an outer circuit as depicted in Figure 3.10 (a). Further, when applied force on the device is released then electric dipoles reverses and as a result current flows from the bottom to top electrode as depicted in Figure 3.10 (b). The output signals of the prepared PEG device were measured by finger tapping on the surface of the device. The circuit was constructed by connecting the PEG with a full-wave-bridge rectifier with an oscilloscope for measuring open-circuit voltage and with a digital multimeter

for measuring the short-circuit current. On application of pressure on the surface of the device, there is a development of potential difference across the generator and then this generated output voltage was measured using the digital storage oscilloscope.

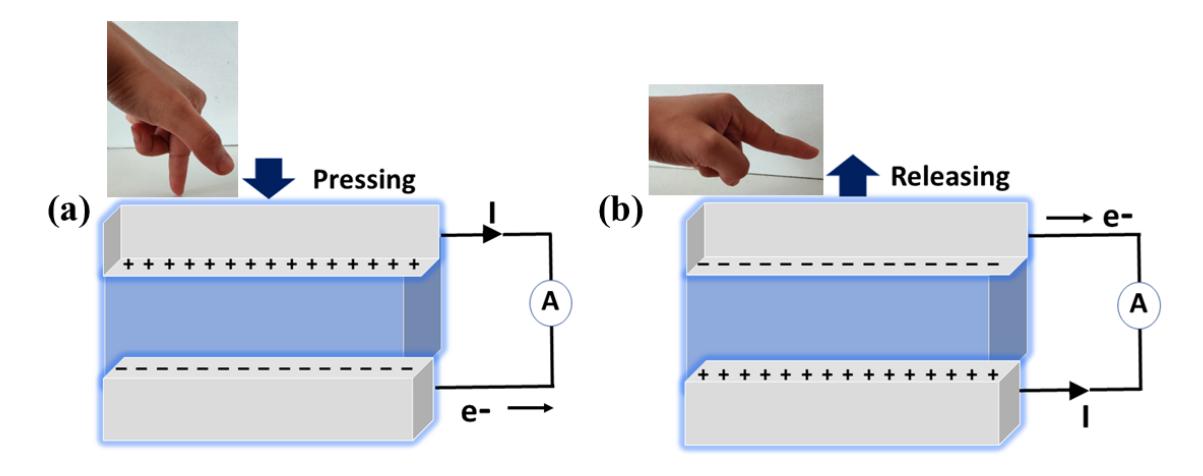


Figure 3.10 Working Mechanism of PEG device.

Figure 3.11 shows the plots of the open circuit voltage generated by the prepared devices with varying concentrations of KNN ceramic powder in the PVDF matrix. Figure 3.11 (f) shows the variation of open-circuit voltage as a function of KNN ceramic particles concentration in the PVDF matrix. It can be seen from the plot that open-circuit voltage first increases with increase in KNN content in the PVDF matrix up to 15 wt.% and after that it decreases with further increasing the KNN concentration to 20 wt.% in the PVDF matrix. The highest open-circuit voltage was 11.2 V for the sample containing 15 wt.% KNN particles. For pure PVDF, 5%KNN, 10%KNN and 20%KNN based piezoelectric generators the generated open-circuit voltages reach 2.8 V, 4.0 V, 5.2 V and 4.2 V, respectively. The observed decrease in the output voltage with the concentration of KNN ceramic particles in the PVDF matrix may be attributed to the fact that more than 15 wt.% KNN fillers are acting in the PVDF matrix in such a way that the nucleation of the β -phase of PVDF is restricted and chances of formation of defects into the polymer matrix are increasing [46].

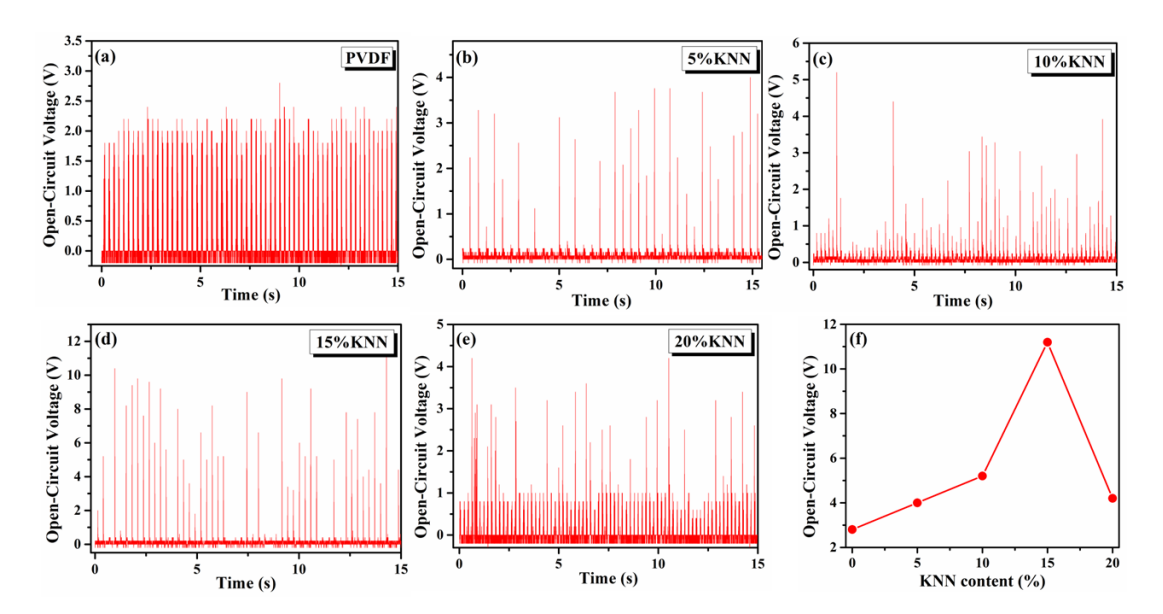


Figure 3.11 (a-e) Open-circuit voltage generated using KNN/PVDF PEG device with different content of KNN ceramic powder in PVDF matrix and (f) Variation of open-circuit voltage as a function of KNN ceramic content in the PVDF matrix.

The short circuit current of the prepared PEG devices was also measured by finger tapping method and corresponding plots are shown in Figure 3.12. The value of short circuit current was 81.5 nA, 102 nA, 202.5 nA, 303.4 nA and 209.7 nA for the sample containing 0 wt.%, 5 wt.%, 10 wt.%, 15 wt.% and 20 wt.% KNN ceramic powder, respectively in the PVDF matrix, respectively. Figure 3.12 (f) shows the variation of open-circuit voltage as a function of KNN ceramic particles concentration in the PVDF matrix. The maximum value of the short-circuit current was obtained for the PEG device containing 15 wt.% KNN in the PVDF matrix. Furthermore, for testing the mechanical sustainability and durability of the fabricated 15 wt.% KNN/PVDF piezoelectric generator, a continuous force was applied and released for 1000 tapings. Despite some fluctuations, the measured output voltage was very stable during 1000 tapings as shown in Figure 3.13.

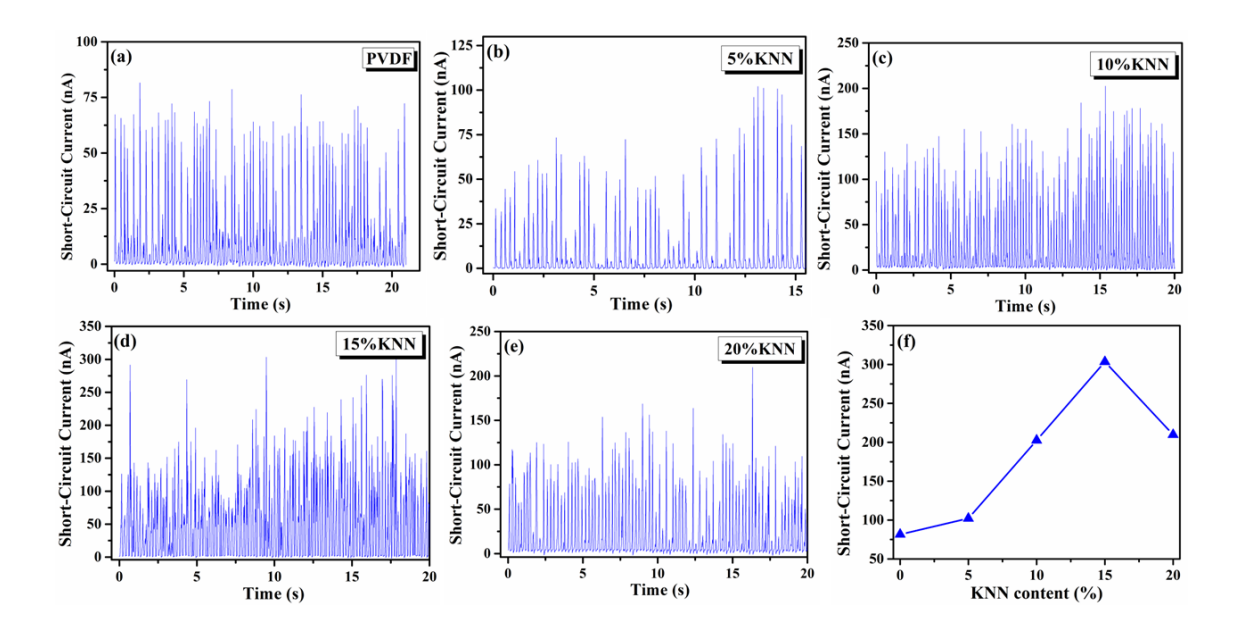


Figure 3.12 (a-e) Short-circuit current generated using KNN/PVDF PEG devices with different content of KNN ceramic powder in PVDF matrix and (f) Variation of short-circuit current as a function of KNN ceramic content in the PVDF matrix.

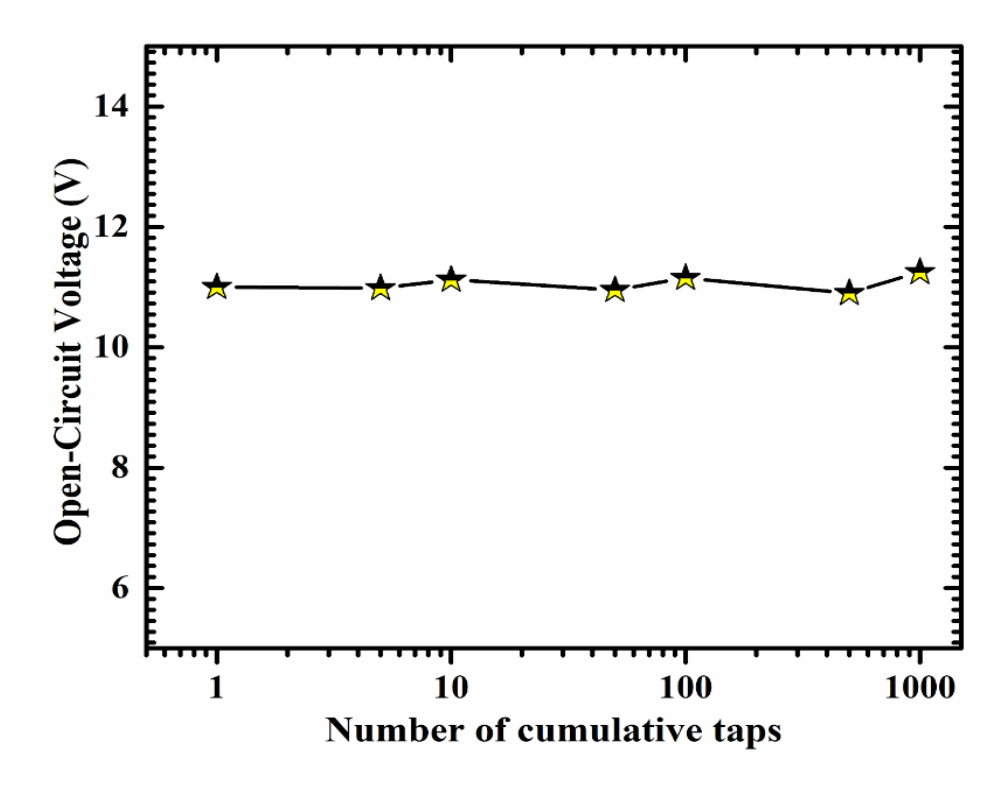


Figure 3.13 Variation of Maximum Open-Circuit Voltage with number of cumulative taps for 15 wt.% KNN/PVDF PEG device.

In addition, the room temperature Displacement vs. Voltage (D-V) butterfly loop for the 15 wt.% KNN/PVDF flexible composite film has been recorded and the corresponding plot is shown in Figure 3.14. From the butterfly loop, the maximum and average value of inverse piezoelectric charge coefficient (d_{33}^*) for 15 wt.% KNN/PVDF composite film was found to be 16 pm/V and 8.86 pm/V, respectively.

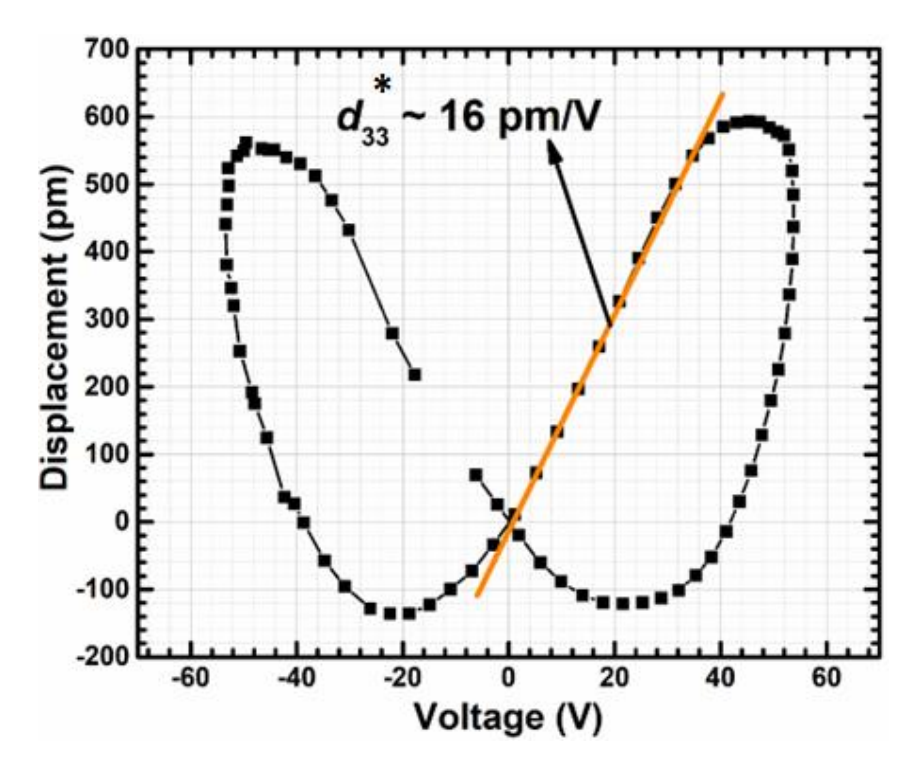


Figure 3.14 Displacement vs. Voltage (*D-V*) butterfly curve of the flexible composite film containing 15 wt.% KNN in the PVDF.

3.1.3.7 Energy Harvesting Performance of PEG Device

Furthermore, mechanical energy is abundantly available in the surrounding environment and most of it gets wasted in our daily life. In the present work, the utilization of the fabricated PEG device prepared with 15 wt.% of KNN ceramic powder in the PVDF matrix for harvesting the human body motions such as elbow curving and finger bending was demonstrated. As shown in Figure 3.15 (a) and (b), the generated output voltages reached to 0.7 V and 0.64 V for elbow curving and finger bending, respectively showing the ability of proposed piezoelectric generator in the present work in harvesting various mechanical energy in our day-to-day life.

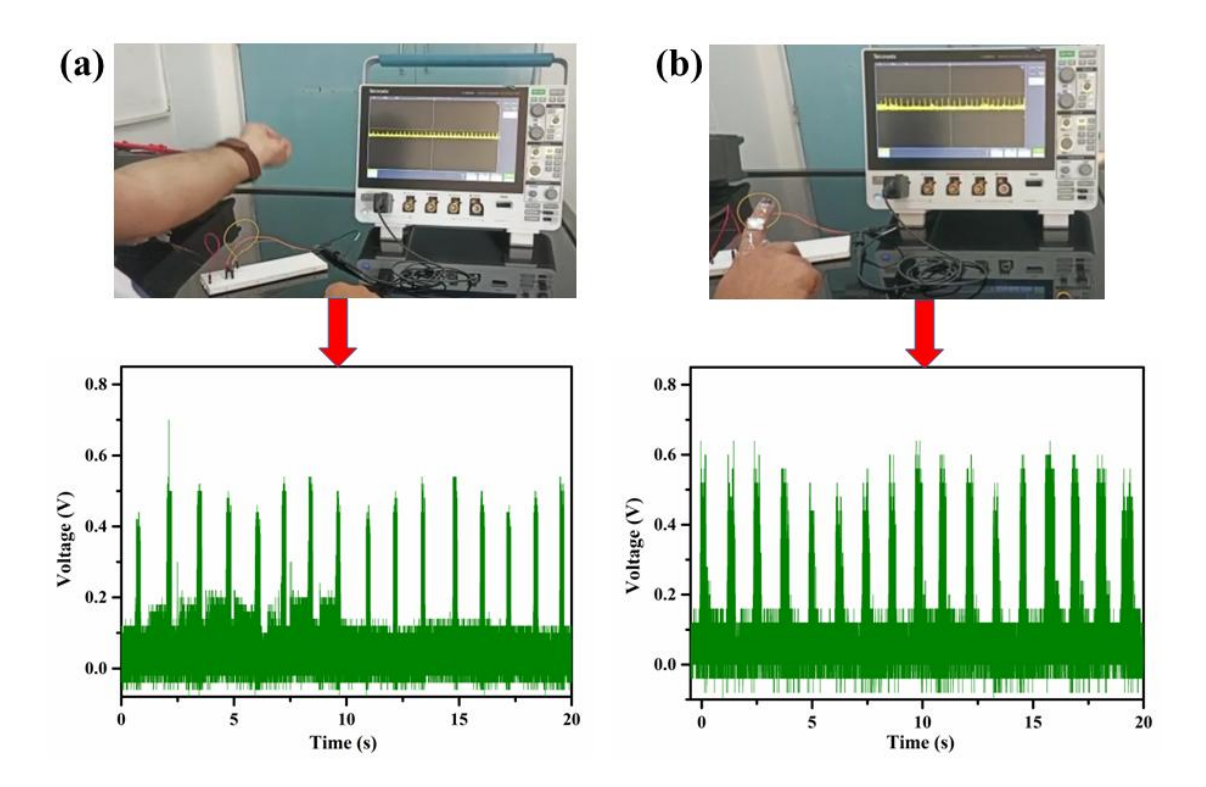


Figure 3.15 The generated open-circuit voltage when PEG device containing 15 wt.% KNN ceramic powder in the PVDF matrix (a) elbow curving and (b) bended by finger.

3.2 Section 2

3.2.1 Introduction

As discussed in the first section, KNN was synthesized by solid state method and then used for the fabrication of PEG devices. In this Section 2, nanoparticles of KNN were synthesized by hydrothermal route and then employed for the construction of PENG device. Furthermore, the piezoelectric performance of the PENG fabricated with KNN synthesized by hydrothermal method was compared with the PEG fabricated with KNN synthesized using solid state route. It is reported in the literature that the type, shape, size, and content of filler in the polymer matrix plays a significant role in determining the overall properties of the composites [47]. Moreover, there are reports that the incorporation of nanofillers generally enhances composite performance by improving the thermal, electrical, and mechanical properties [48]. A key advantage of nanofillers lies in their high surface area, which promotes stronger interactions between the filler and the polymer matrix. Consequently, there are growing research efforts towards the development and utilization of nanocomposites in diverse applications [49]. Previous

studies have also demonstrated that improvements in the dielectric and ferroelectric properties of a PENG device directly contribute to enhancing its overall piezoelectric performance [50, 51].

Additionally, it is reported in the literature that the size of filler particles within the PVDF polymer matrix has a significant effect on the nucleation of the β -phase which is crucial for obtaining better piezoelectric performance of the PVDF based PENG devices. For instance, Eun et al. incorporated multi-walled carbon nanotubes (MWCNTs) into the PVDF matrix and investigated their influence on the mechanical and piezoelectric properties of PVDF nanofibers. The nanofibers with 0.008 wt.% MWCNTs demonstrated an excellent tensile strength while, FTIR analysis confirmed that the β -phase content increased with higher MWCNT loading, thereby leading to improved piezoelectric properties of the nanofibers [52]. Paik et al. introduced Ag nanoparticles into the P(VDF-TrFE), and examined the effect of Ag nanoparticles concentration on the electrical behavior of the nanocomposite films. They found that both the remnant polarisation and the direct piezoelectric coefficient increased significantly, reaching values of 12.14 µC/cm², and 20.23 pC/N, respectively, at an Ag concentration of 0.005 vol. % compared to the pure PVDF film. The enhancement was attributed to the presence of Ag nanoparticles in facilitating dipole alignment within the P(VDF-TrFE) matrix under an external electric field, thereby strengthening the overall polarisation of the film [53].

Ponraj *et al.* developed PENG devices using nano and micron- sized crystallites of KNN as the fillers in the PVDF matrix and studied the effect on various properties of the composites. They observed that device fabricated with nanosized KNN exhibited superior dielectric performance compared to those containing micron-sized KNN. It is also observed that the peak intensity corresponding to the β phase of PVDF is found to improve with increase in volume fraction of nano crystallites of KNN as compared to micron-sized crystallites of KNN in the PVDF matrix [54]. Furthermore, Hari *et al.* fabricated ZnO/PVDF nanocomposite film and they demonstrated that the incorporation of ZnO nanoparticles into the PVDF matrix led to an increase surface roughness of the nanocomposite film. This is attributed to the increase in the effective

surface area because of the addition of nanoparticles, which in turn is expected to demonstrate more significant piezoelectric effect [55].

In view of this, in this section of the chapter, KNN nanoparticles have been synthesized by hydrothermal method. Hydrothermal method is considered as a good method for synthesizing nanoparticles with low cost, controlled size, high purity, and better crystallinity [56]. Based on the result obtained in the first section, concentration of KNN nanoparticles was fixed to 15 wt.% in the PVDF matrix to prepare the flexible nanocomposite film and different properties of the film were investigated. The piezoelectric output performance of the developed piezoelectric nanogenerator was also measured by applying a force on the device surface using a dynamic shaker unit. In addition, the practical applicability of the fabricated PENG devices was demonstrated by harnessing energy from the human body motion.

3.2.2 Materials and Methods

3.2.2.1 Synthesis of KNN Nanoparticles

The hydrothermal method has been used to synthesize KNN nanoparticles as illustrated in Figure 3.16. For the synthesis of KNN nanoparticles, 0.006 mol of Niobium Oxide (Nb₂O₅, Alfa Aesar, 99.5% metal basis) was mixed into a solution containing KOH (Thermo Fischer Scientific India Pvt. Ltd. AR, 92%) and NaOH (Avantor Performance Material India Limited, AR, 96%) with a K: Na molar ratio of 1:5 by continuous stirring using a magnetic stirrer for 2 hours. Then, the properly mixed solution was poured into a 200 ml Hydrothermal autoclave and kept in a hot air oven at 230 °C for 18 hours. Thereafter, the precipitates from the autoclave were collected and washed multiple times with deionized water and ethanol to get rid of the residual alkali followed by drying in the oven at 80 °C for 10 hours. The obtained dried powder was then calcined at 700 °C for 4 hours in the furnace to obtain the KNN nanoparticles.

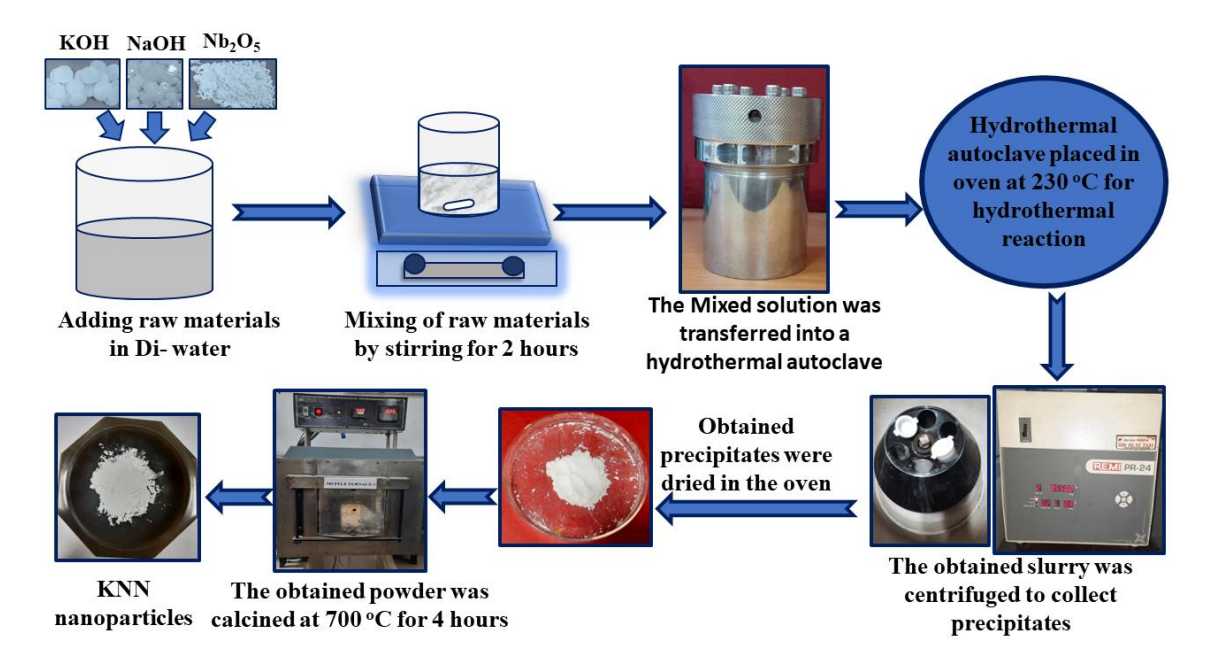


Figure 3.16 Synthesis of KNN nanoparticles by hydrothermal method.

3.2.2.2 Fabrication of PVDF/KNN 15 wt.% Flexible Nanocomposite Film

For the fabrication of PVDF/KNN flexible nanocomposite film, PVDF is dissolved in DMF by using a magnetic stirrer at 50 °C for 1 hour until a uniform transparent solution is obtained. Then KNN nanoparticles are added into the DMF and ultrasonicated for 30 minutes at room temperature. Finally, the prepared solution is mixed by a magnetic stirrer at 50 °C for 4 hours. The obtained uniform solutions are dropped onto the glass slide and kept in the oven for drying at 90 °C. After this process, a flexible PVDF/KNN 15 wt.% nanocomposite film was peeled off from the glass slide.

3.2.2.3 Fabrication of PENG Device

The PVDF/KNN 15 wt.% nanocomposite film have been cut into small pieces of 2×2 cm². Then conductive aluminium tape has been attached on both sides of nanocomposite films. Then copper wires were attached to the aluminium tape using the silver paste to measure the output signals on application of pressure when connected to the external circuit.

3.2.2.4 Characterizations

The structural analysis of the KNN nanoparticles and PVDF/KNN 15 wt.% nanocomposite film was analysed by XRD and FTIR. The morphology of synthesized

KNN nanoparticles was studied using FESEM and PVDF/KNN 15 wt.% nanocomposite film was studied using SEM. Ferroelectric behavior and dielectric properties of the prepared nanocomposite film were also studied. Electrical output performance of the fabricated PENG was tested under mechanical force using an electrodynamic shaker (Micron MEV-0025), with measurements recorded via a digital storage oscilloscope (Tektronix MDO500) and an electrometer (Keysight B2902B). Finally, practical applicability was demonstrated by harvesting energy from various human body movements.

3.2.3 Results and Discussions

3.2.3.1 Structural and Microstructural Analysis of KNN Nanoparticles

The crystal structure and morphology of the synthesized KNN nanoparticles are investigated by XRD and FESEM as presented in Figure 3.17 and Figure 3.18, respectively. The XRD pattern shown in Figure 3.17 reveals that a pure perovskite phase with orthorhombic structure without the presence of any secondary phase has been successfully synthesized using the hydrothermal method. The FESEM micrograph presented in Figure 3.18 (a) shows that synthesized KNN consists of regular cubic nanoparticles. The average particle size of the KNN nanoparticles is estimated to be ~303 nm as illustrated in Figure 3.18 (b).

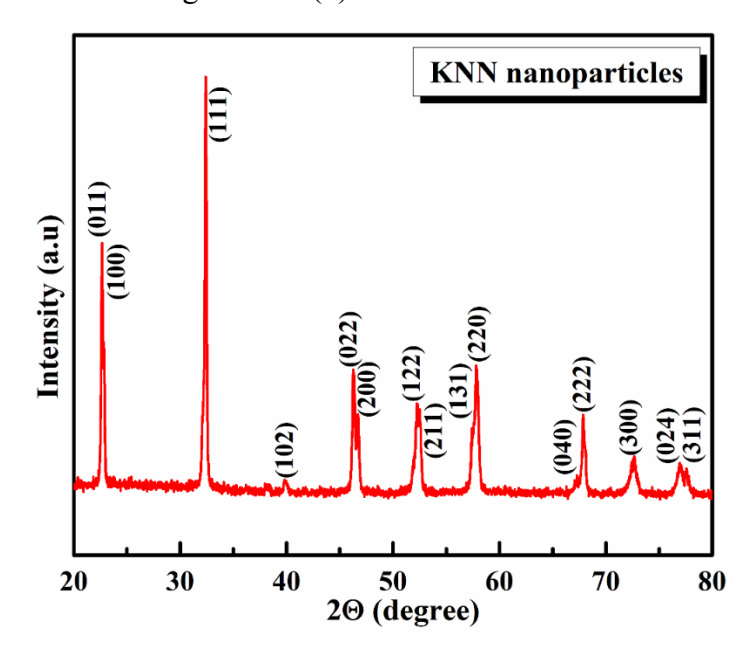


Figure 3.17 XRD pattern of the calcined KNN nanoparticles synthesized by hydrothermal method.

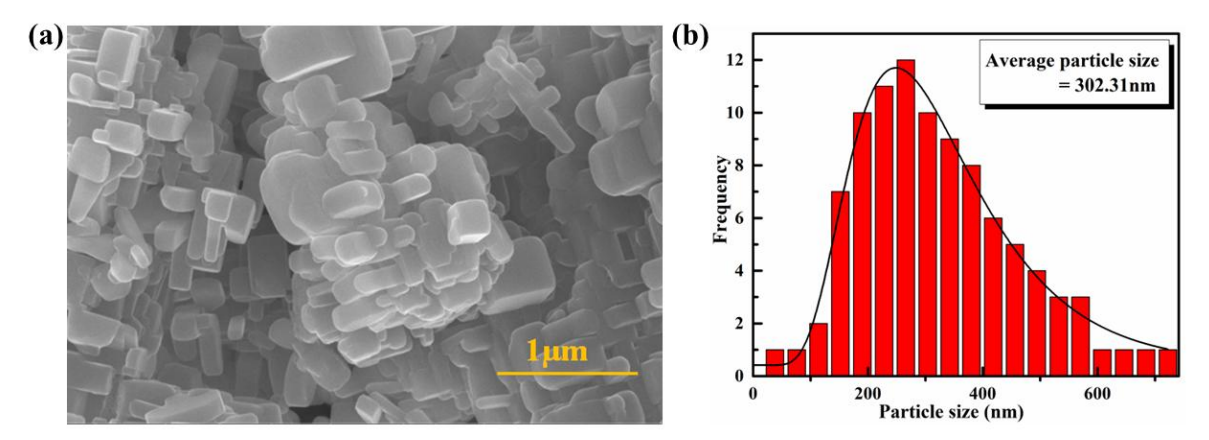


Figure 3.18 (a) FESEM image of the calcined KNN nanoparticles and (b) Histogram showing the distribution of particle size.

3.2.3.2 Structural and Morphological Analysis of PVDF/KNN 15 wt.% Nanocomposite Film

To get the crystallographic information of the prepared PVDF/KNN 15 wt.% nanocomposite film, XRD analysis was performed and the corresponding plot is shown in Figure 3.19. The peaks marked by (*, \clubsuit) and \blacklozenge , corresponds to the PVDF and KNN, respectively. The peaks at 18° and 20° correspond to the non-polar α -phase and polar β -phase of the PVDF, respectively. Further, stronger intensity of the β -phase peak compared to the α -phase suggests that β -phase predominates over the α -phase.

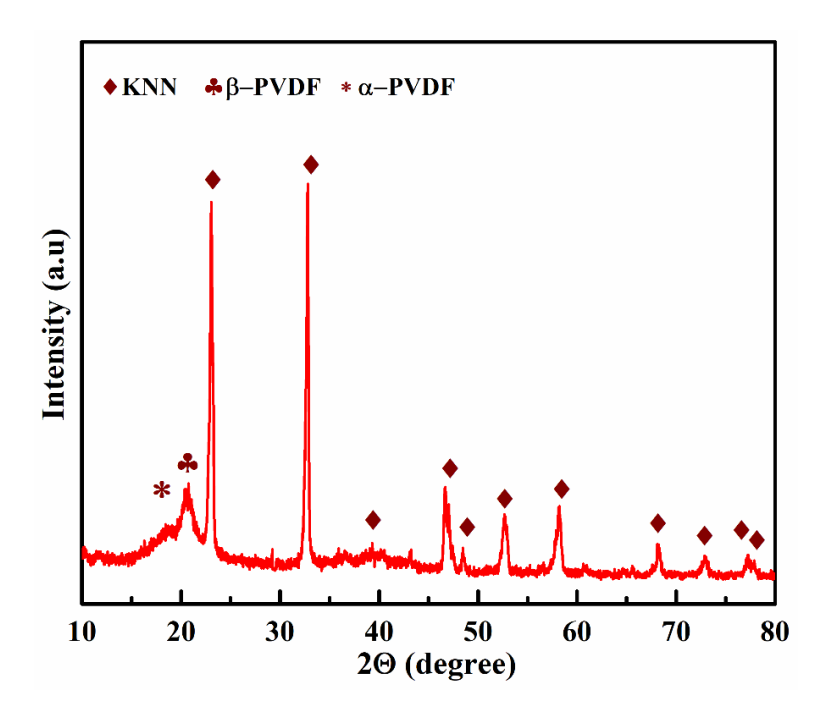


Figure 3.19 X-ray Diffraction pattern of PVDF/KNN 15 wt.% nanocomposite film.

FTIR absorbance spectra of PVDF/KNN 15 wt.% nanocomposite film has been recorded in the range 500-1500 cm⁻¹ as shown in Figure 3.20. The presence of α and β phases of the PVDF in the prepared nanocomposite film can be identified by the presence of peaks at 766 cm⁻¹ and 840 cm⁻¹, respectively. All the peaks corresponding to α and β phases of the PVDF are marked in the plot shown in Figure 3.20 [57-60]. The content of the β -phase ($F(\beta)$) in the prepared flexible film has been calculated using Beer- Lambert law [34] given below:

$$F(\beta) = \frac{A_{\beta}}{\binom{K_{\beta}}{K_{\alpha}} A_{\alpha} + A_{\beta}}$$
(3.1)

where $K_{\alpha} = 6.1 \text{ x } 10^4 \text{ cm}^2 \text{mol}^{-1}$ and $K_{\beta} = 7.7 \text{ x } 10^4 \text{ cm}^2 \text{mol}^{-1}$ are the absorption coefficient at 840 cm⁻¹ and 766 cm⁻¹, respectively; A_{α} and A_{β} , are the absorbance intensities at 766 cm⁻¹ and 840 cm⁻¹, respectively [61]. Further β -phase fraction for nanocomposite film was ~ 58.5 , which is higher than obtained for the film fabricated using solid state synthesized KNN particles.

The morphology of prepared PVDF/KNN 15 wt.% nanocomposite film was analysed using SEM and the corresponding image is shown in Figure 3.21. SEM image shows that the KNN NPs are distributed uniformly into the PVDF matrix.

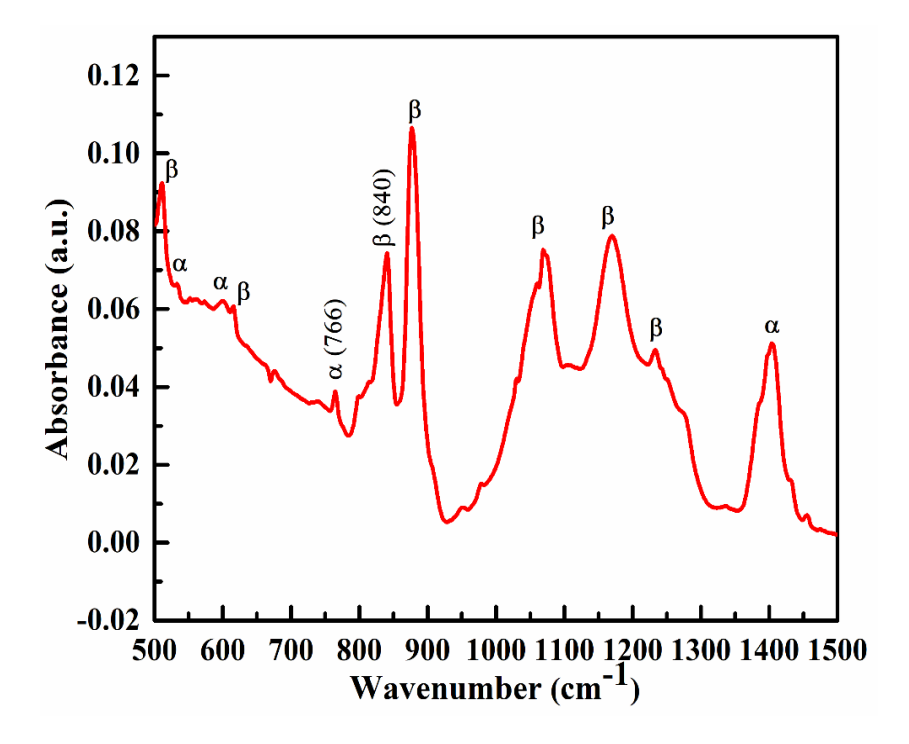


Figure 3.20 FTIR spectra of PVDF/KNN 15 wt.% nanocomposite film.

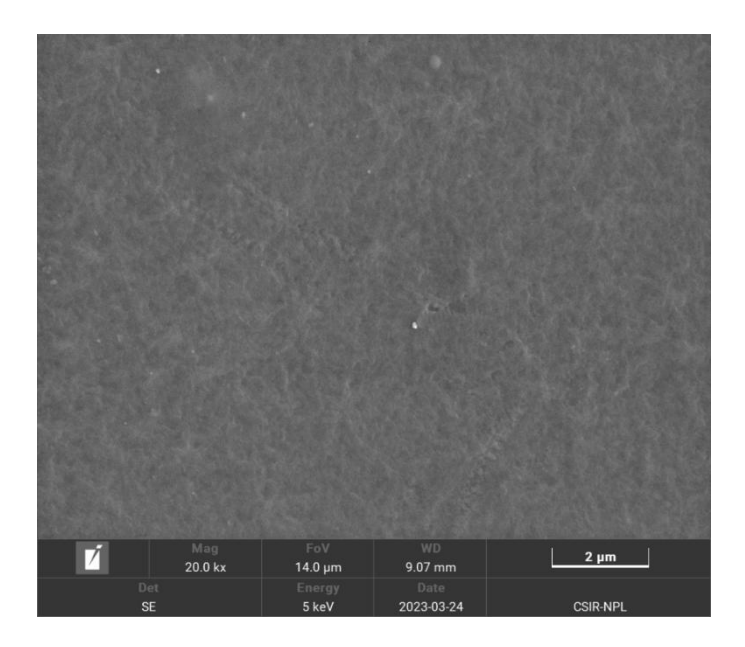


Figure 3.21 SEM image of PVDF/KNN 15 wt.% nanocomposite film.

3.2.3.3 Dielectric Properties of the PVDF/KNN 15 wt.% Nanocomposite Film

For studying the electrical properties of the prepared PVDF/KNN 15 wt.% flexible nanocomposite film, dielectric constant (ε_r) was measured at room temperature as a function of frequency in the range from 100 Hz to 1 MHz and the corresponding plot is illustrated in Figure 3.22. The dielectric constant of the PVDF/KNN 15 wt.% flexible nanocomposite film decreases with increase in the frequency. For PVDF/KNN 15 wt.% nanocomposite film, ε_r value is found to be 36.54 at 1 KHz which is significantly higher in comparison to the value of dielectric constant obtained for the composite film prepared using KNN synthesized by solid state route. The obtained higher value of ε_r for PVDF/KNN 15 wt.% nanocomposite film is mainly ascribed to an increase in dipole-dipole interaction between PVDF matrix and the KNN nanoparticles at the interface and also because of ion-dipole interaction between the surface of nanoparticles and the PVDF polymer [62, 63, 54]. In addition, PVDF/KNN 15 wt.% nanocomposite film has higher β -phase content of PVDF which further enhances the dielectric constant of the nanocomposite film [38]. The obtained high value of dielectric constant will lead to enhanced piezoelectric constant and improved piezoelectric performance of the prepared nanocomposite film [50, 51].

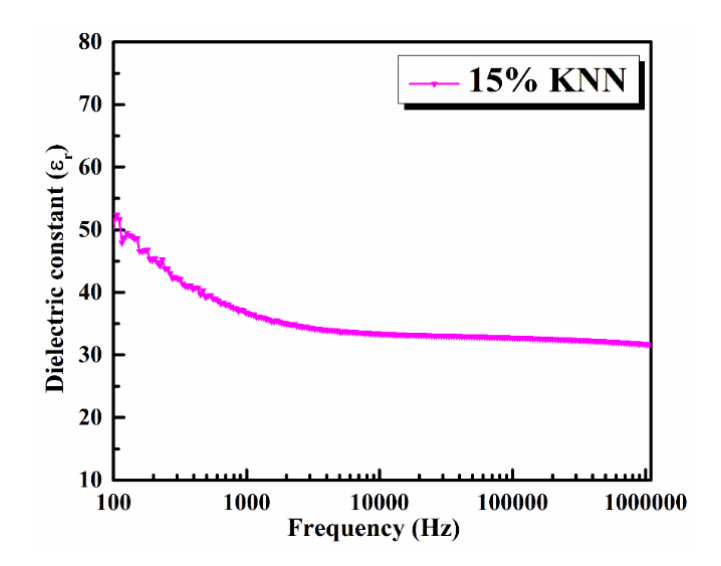


Figure 3.22 Variation of Dielectric constant with frequency of PVDF/KNN 15 wt.% nanocomposite film.

3.2.3.4 Polarisation vs. Electric Field (*P-E*) Hysteresis Loop of the PVDF/KNN 15 wt.% Nanocomposite Film

The room temperature Polarisation vs. Electric Field (P-E) hysteresis plot of the prepared PVDF/KNN 15 wt.% flexible nanocomposite film is presented in Figure 3.23. The prepared film shows a non-saturated hysteresis loop. The observed values of remnant polarisation ($P_r = 0.251 \,\mu\text{C/cm}^2$) and maximum polarisation ($P_s = 2.506 \,\mu\text{C/cm}^2$) for the PVDF/KNN 15 wt.% nanocomposite film is higher in comparison to the P_r and P_s values obtained for the composite film prepared using KNN synthesized by solid state route.

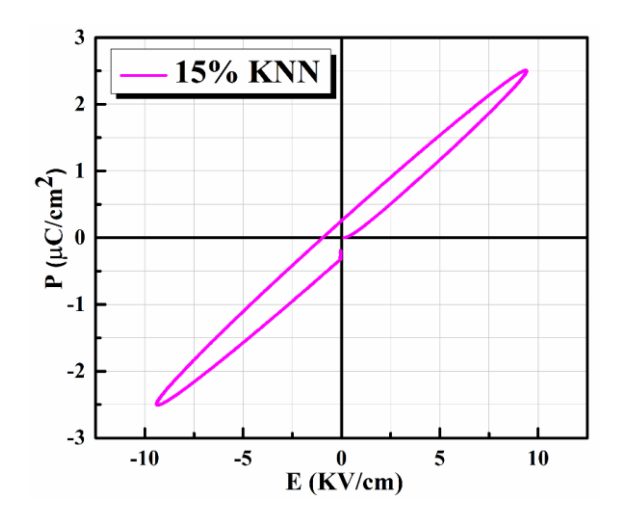


Figure 3.23 *P-E* hysteresis loop analysis of PVDF/KNN 15 wt.% nanocomposite film.

3.2.3.5 Piezoelectric Performance of PVDF/KNN 15 wt.% PENG Device

To test the piezoelectric performance of the fabricated PENG device, mechanical force was applied on the surface of the PENG device by finger tapping. Figure 3.24 depicts the peak-to-peak open-circuit voltage and peak-to-peak short-circuit current of the fabricated PENG device. The values of peak-to-peak open circuit output voltage and peak-to-peak short circuit current obtained for PVDF/KNN 15 wt.% nanocomposite film are 20.2 V and $\sim 2.01~\mu A$, respectively. These obtained values of voltage and current are significantly higher in comparison to the values obtained in the Section 1 of the chapter for the film fabricated using KNN particles synthesized by solid state route. The obtained better performance of the PENG device in comparison to the PEG fabricated in Section 1 of this chapter is mainly attributed to its higher β phase content and enhanced dielectric and ferroelectric properties [50].

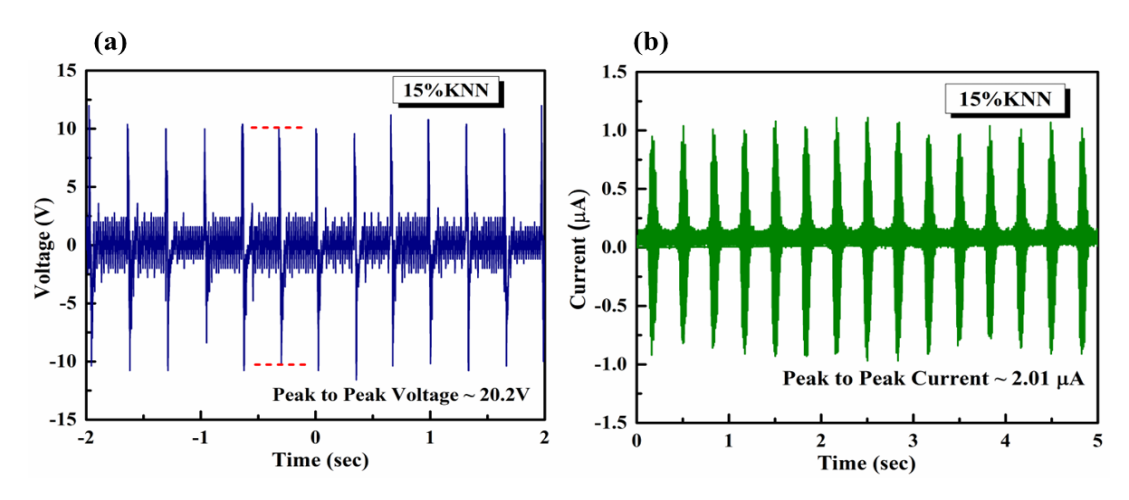


Figure 3.24 The generated (a) open circuit piezoelectric output voltage and (b) short circuit current of the PENG PVDF/KNN 15 wt.%.

With the help of external resistance, the power output of the PENG was measured by varying the load resistance in the range 10^1 to 10^3 M Ω and the corresponding plots are presented in Figure 3.25. Figure 3.25 (a) shows the output voltage and current for varying external loads. Ohm's law (V=IR), states that as the resistance rises, the voltage rises, and the current falls. The point where the voltage and current meet at 100 M Ω , is known as the optimum point. It has been found that the power is expected to be maximum at this optimum resistance. The variation of output power density as a function of variable external resistance is shown in Figure 3.25 (b). At an external

resistance of 100 M Ω (Optimum point), the maximum power density measured was \sim 8.71 μ W/cm 2 . The comparison of the generated output voltage and current by the device fabricated in the present work with the values reported by the other researchers is summarized in Table 3.2.

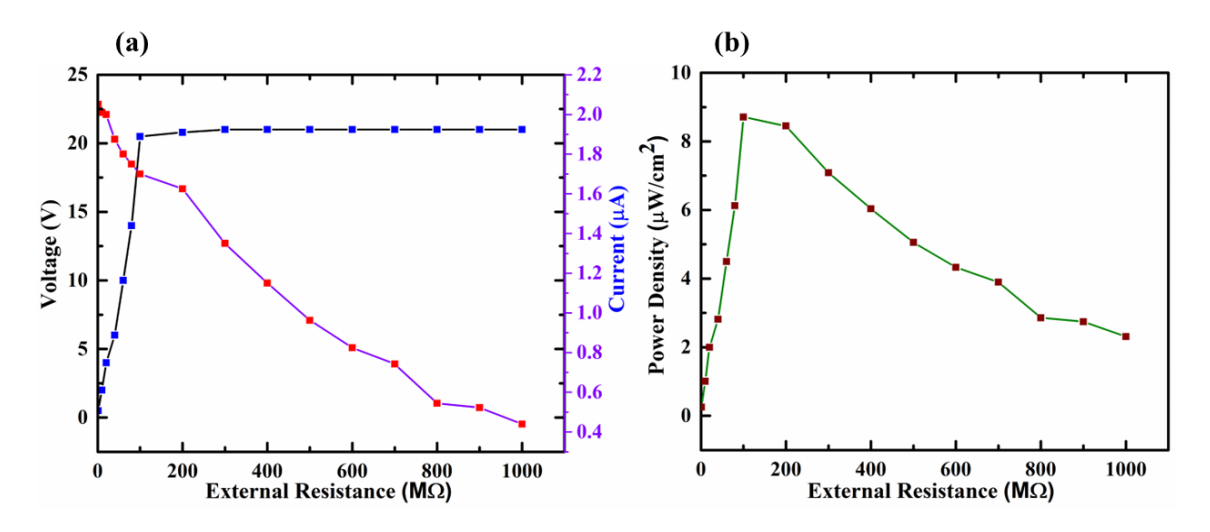


Figure 3.25 (a) Variation of voltage and current measured with external load resistances and (b) power density measured with external resistances of PVDF/KNN 15 wt.% film-based PENG device.

3.2.3.6 Energy Harvesting Performance of PENG Device

Further, to explore the ability of the fabricated PENG device with PVDF/KNN 15 wt.% nanocomposite film in harvesting mechanical energy which is otherwise wasted in our real-life, the device has been attached on the finger, thumb, and elbow of the hand. The generated output voltages for finger tapping, thumb pressing, fist beating, finger bending, and elbow bending were 6.8 V, 11.23 V, 3.08 V, 1.32 V, and 2.28 V, respectively. The corresponding output voltage plots are represented in Figure 3.26 (a-e). This generated output voltage and current using PVDF/KNN 15 wt.% PENG was enough to light up six red light emitting diodes (LEDs) as shown in Figure 3.26 (f), respectively. This shows that the fabricated PENG device is capable of harvesting mechanical energy in our daily life.

Table 3.2 Comparison of the piezoelectric performance between PVDF/KNN PEG fabricated in the present work and various generators reported in the literature.

S. No.	Piezoelectric Filler	Polymer used	V _{oc} (V)	<i>I_{sc}</i> (μA)	Power Density	Ref.
1.	KNN nanorods	PVDF	3.7	0.326		[64]
2.	(K,Na)NbO ₃ -based ceramic	Polyimide	4	0.24		[46]
3.	KNN nanoblocks	PVDF	2.1	0.042	32.67 mW/m ²	[65]
4.	BCZT-CuY/rGO	PDMS	1.36	0.035		[66]
5.	KNN nanostructure materials	PVDF	1.9			[67]
6.	(Ba _{0.85} Ca _{0.15})(Ti _{0.9} Zr _{0.1})O ₃ -0.2 mol%Y nanofibers	PDMS	3.0	0.085		[68]
7.	PbZr _{0.52} Ti _{0.48} O ₃ (PZT) particles	Polysiloxane	8	0.4		[69]
8.	BaTiO ₃ Nanoparticles	PVDF	6.7	2.4		[70]
9.	KNN Nanorods	PVDF	3.4	0.1		[25]
10.	KNN Ceramic Particles	PVDF	11.2	0.3		Present Work (Section 1)

11.	KNN Nanoparticles	PVDF	20.2	2.01	8.71 μW/cm ²	Present Work (Section 2)
-----	----------------------	------	------	------	----------------------------	--------------------------

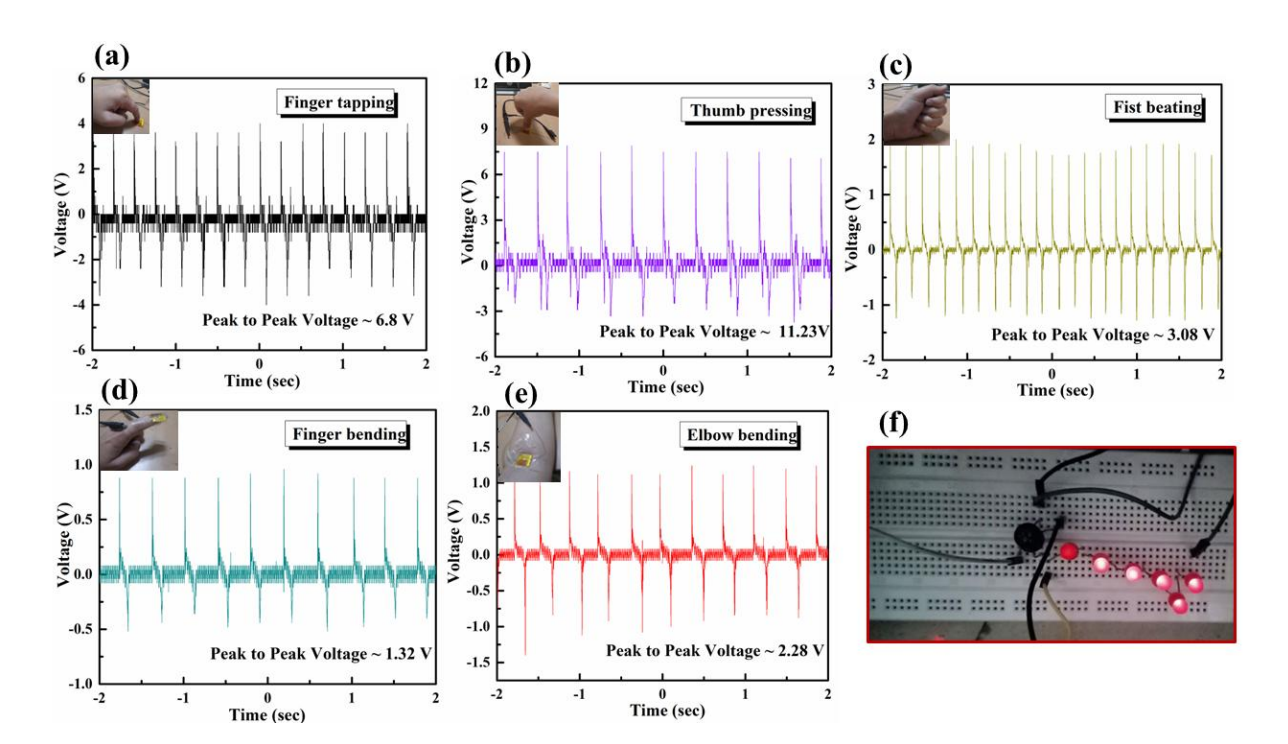


Figure 3.26 The generated voltage with PENG fabricated with PVDF/KNN 15 wt.% nanocomposite film by (a) finger tapping, (b) thumb pressing, (c) fist beating, (d) finger bending, (e) elbow bending and (f) showing glowing LED.

3.3 Conclusion

This chapter was divided in two sections in which comparison of the piezoelectric performance of the PEG devices constructed with KNN synthesized by solid state method and hydrothermal method was done in detail. In the first section of this chapter, PEG devices based on Potassium Sodium Niobate/Poly (vinylidene fluoride) (KNN/PVDF) flexible composite films with various percentages of KNN ceramic particles (0 wt.%, 5 wt.%, 10 wt.%, 15 wt.% and 20 wt.%) in the PVDF matrix were constructed. Among the different percentages of KNN, 15 wt.% KNN particles @ PVDF composite film demonstrated the highest values of β -phase

content of PVDF, dielectric constant (ε_r), remnant polarisation (P_r), and spontaneous polarisation (P_s). When force was applied on the surface of the fabricated PEG device, measured values of maximum open-circuit voltage and short-circuit current were 11.2 V and 0.3 μ A, respectively for the device prepared with 15 wt.% KNN in the PVDF matrix.

Further, in the second section of this chapter, KNN nanoparticles were synthesized via hydrothermal method and used as filler in the PVDF matrix for fabricating PENG device. Based on the result obtained in the first section, concentration of KNN was fixed to 15 wt.% in the PVDF matrix and different properties of the prepared composite film were investigated. PVDF/KNN 15 wt.% nanocomposite film showed promising results. The nanocomposite film displayed improved β -phase content of PVDF, dielectric, ferroelectric and piezoelectric performance in comparison to the film fabricated with KNN synthesized by solid state reaction method for same filler concentration. The output voltage, output current and power density generated by the nanogenerator were 20.2 V, 2.01 μ A and 8.71 μ W/cm², respectively. Finally, its practical applicability was demonstrated by harvesting energy from human body motion. Overall, the PENG constructed with KNN synthesized by hydrothermal method outperformed PEG constructed with KNN synthesized by solid state method.

References

- [1] H. Takahashi, Y. Numamoto, J. Tani, S. Tsurekawa, Japanese Journal of Applied Physics, 45, (2006), 7405–7408
- [2] L. Liu, H. Fan, L. Fang, X. Chen, H. Dammak, M. P. Thi, Materials Chemistry and Physics, 117, (2009), 138–141
- [3] A. Boochani, G. Rasoolian, F. Kafi, A. Aminian, S.M. Elahi, Chinese Journal of Physics, 59, (2019), 357-371
- [4] Y. Hiruma, R. Aoyagi, H. Nagata, T. Takenaka, Japanese Journal of Applied Physics, 44, (2005), 5040–5044

- [5] A. Hussain, N. Sinha, S. Goel, A. J. Joseph, B. Kumar, Journal of Alloys and Compounds, 790, (2019), 274-287
- [6] J. Kaarthik, C. Kaushiga, G. Sradha, N. Ram, S. G. Reddy, K.C. Sekhar, A. Venkateswarlu, Journal of Alloys and Compounds, 943, (2023), 169069
- [7] J. Camargo, S. Osinaga, M. Febbo, S.P. Machado, F. Rubio-Marcos, L. Ramajo, M. Castro, Journal of Material Sciences: Material in Electronics, 32, (2021), 19117-19125
- [8] M. Habib, I. Lantgios, K. Hornbostel, Journal of Physics D: Applied Physics, 55, (2022), 423002
- [9] Y. Huan, T. Wei, Z. Wang, H. Shen, X. Lin, S. Huang, Journal of Materiomics, 6, (2020), 355
- [10] K.O. Iwuozor, T.A. Jimoh, H.T. Ojo, E.C. Emenike, J. Emeghai, A.G. Adeniyi, Surfaces and Surfaces, 70, (2025), 106855
- [11] Y. Wua, F. Maa, J. Qua, Y. Luo, C. Lv, Q. Guo, Applied Surface Science, 469, (2019), 283
- [12] C. Li, W. Luo, X. Liu, D. Xu, K. He, Nanomaterials, 6 (4), (2016), 67
- [13] S. Siddiqui, D.I. Kim, T.D. Le, M.T. Nguyen, S. Muhammad, W.S. Yoon, N.E. Lee,

Nano Energy, 15, (2015)

- [14] Y. Zhao, Q. Liao, G. Zhang, Z. Zhang, Q. Liang, X. Liao, Y. Zhang, Nano Energy, 11, (2015), 719-727
- [15] C. Baek, J. H. Yun, H. S. Wang, J. E. Wang, H. Park, K.-I. Park, D. K. Kim, Applied Surface Science, 429, (2018), 164
- [16] J. Yi, Y. Song, Z. Cao, C. Li, C. Xiong, Composites Science and Technology, 215, (2021), 109011
- [17] Z. Li, X. Zhang, G. Li, Royal Society of Chemistry, 16, (2014), 5475
- [18] M. Sharma, V. Srinivas, G. Madras, S. Bose, RSC Advances, 6, (2016), 6251–6258
- [19] Y. Qi, N.T. Jafferis, K. Lyons, C.M. Lee, H. Ahmad, M.C. McAlpine, Nano Letters, 10, (2010), 524–528

- [20] X. Xue, P. Deng, S. Yuan, Y. Nie, B. He, L. Xing, Y. Zhang, Energy and Environment Science, 6, (2013), 2615
- [21] C. Chang, V. H. Tran, J. Wang, Y. K. Fuh, L. Lin, Nano Letters, 10, (2010), 726–731
- [22] S. Cha, S. M. Kim, H. Kim, J. Ku, J. I. Sohn, Y. J. Park, B. G. Song, M. H. Jung,E. K. Lee, B. L. Choi, J. J. Park, Z. L. Wang, J. M. Kim, K. Kim, Nano Letters, 11,(2011), 5142–5147
- [23] X. Xue, P. Deng, B. He, Y. Nie, L. Xing, Y. Zhang, Z. L. Wang, Advanced Energy Materials, 4 (5), (2013)
- [24] S. Bairagi, S.W. Ali, European Polymer Journal, 116, (2019), 554-561
- [25] S. Bairagi, S.W. Ali, Organic Electronics, 78, (2020), 105547
- [26] H. Du, Z. Li, F. Tang, S. Qu, Z. Pei, W. Zhou, Materials Science and Engineering B, 131, (2006), 83-87
- [27] C. Jiten, R. Gaur, R. Laishram, K.C. Singh, Ceramics International, 42, (2016), 14135-14140
- [28] A. K. Zak, W. C. Gan, W. H. Abd. Majid, M. Darroudi, T.S. Velayutham, Ceramics International, 37, (2011), 1653 1660
- [29] S. Badatya, D.K. Bharti, A.K. Srivastava, M.K. Gupta, Journal of Alloys and Compounds, 863, (2021), 158406
- [30] D. Guo, K. Cai, P. Deng, G. Si, L. Sun, F. Chen, H. Ning, L. Jin, J. Ma, Journal of Materiomics, 6, (2020), 563-572
- [31] T. Prabhakaran, J. Hemalatha, Materials Chemistry and Physics, 137 (3), (2013), 781-787
- [32] A. C. Lopes, C. M. Costa, C. J. Tavares, I. C. Neves, S.L. Mendez, Journal of Physical Chemistry C, 115, (2011),18076–18082
- [33] N. Abzan, M. Kharaziha, S. Labbaf, Materials and Designs, 167, (2019), 107636
- [34] P. Martins, A.C. Lopes, S. Lanceros-Mendez, Progress in Polymer Science, 39(4), (2014), 683-706
- [35] M. Chandrasekhar, P. Kumar, Ceramics International, 41, (2015), 5574

- [36] C.V. Chanmal, J.P. Jog, Express Polymer Letters, 2, (2008), 294-301
- [37] W. Wu, X. Huang, S. Li, Journal of Physical Chemistry C, 116, (2012), 24887-24895
- [38] M. Sharma, G. Madras, S. Bose, Physical Chemistry Chemical Physics, 16, (2014), 14792-14799
- [39] A. Rahman, M. Jiang, G. Rao, S. Lee, M-H. Kim, M. Habib, J.U. Rahman, Ceramics International, 48 (14), (2022), 20251-20259
- [40] L. Wu, C. Li, F. Jiang, T. Wei, Ceramics International, 49 (13), (2023), 22015-22021
- [41] Z. Liu, A. Zhang, J. Lu, B. Xie, B. Liang, Y. Mao, H. Fan, Journal of Alloys and Compounds, 817, (2020), 152798
- [42] B. Adak, I. Chinya, S. Sen, RSC Advances, 6, (2016), 105137-105145
- [43] A. Sasmal, S. Sen, P. Sujatha Devi, Physical Chemistry Chemical Physics, 21, (2019), 5974-5988
- [44] S. Bairagi, S.W. Ali, Journal of Materials Science, 54, (2019), 11462-11484
- [45] T. Furukawa, M. Date, E. Fukada, Journal of Applied Physics, 51, (1980), 1135–1141
- [46] D.Y. Hyeon, G.J. Lee, S.H. Lee, J.J. Park, S. Kim, M. Lee, K.I. Park, Composites Part B 234, (2022), 109671
- [47] R. Kumar, S. Chellemuthu, Materials and Technology, 57 (2), (2023), 141-148
- [48] T. Raja, Y. Devarajan, N. Kailiappan, Discover Applied Sciences, 6 (566), (2024)
- [49] S. Banerjee, S. Bairagi, S.W. Ali, Ceramics International, 47, (2021), 16402-16421
- [50] V. Jella, S. Ippili, J-H. Eom, J. Choi, S-G. Yoon, Nano Energy, 53, (2018), 46-56
- [51] C. Shi, J. Ma, J. Wu, X. Wang, F. Miao, Y. Huang, K. Chen, W. Wu, B. Wu, Journal of Alloys and Compounds, 846, (2020)
- [52] J.H. Eun, S.M. Sung, M.S. Kim, B.K. Choi, J.S. Lee, Materials & Design, 206, (2021), 109785
- [53] H. Paik, Y-Y. Choi, S. Hong, K. No, Scientific Reports in Nature, 5, (2015),13209

- [54] B. Ponraj, R. Bhimireddi, K.B.R. Varma, Journal of Advanced Ceramics, 5 (4), (2016), 308-320
- [55] M.A. Hari, L. Rajan, C.K. Subash, S. Varghese, Materials Today Proceedings, 46, (2021), 5781-5784
- [56] C-W. Ahn, C-S. Park, R. Dittmer, S-H. Hong, S. Priya, Journal of Materials Science, 45 (2010), 3961-3965
- [57] P. K. Sarkar, S, Maji, G. S. Kumar, K. C. Sahoo, D. Mandalb, S. Acharya, RSC Advances, 6, (2016), 910-917
- [58] H. T. T. Nong, A. N. Nguyen, J. Solard, A. Gomez, S. Mercone, Applied Science, 12, (2022), 1589
- [59] J. Y. Yin, C. Boaretti, A. Lorenzetti, A. Martucci, M. Roso, M. Modesti, Nano materials, 12, (2022), 962
- [60] Y. Hou, Y. Deng, Y. Wang, H. L. Gao, RSC Advances, 5, (2015), 72090–72098
- [61] R. K. Singh, S. W. Lye, J. Miao, Polymers, 214, (2021), 123366
- [62] A. Jain, K.J. Prashanth, A.K. Sharma, Polymer Engineering Sciences, 55, (2015), 1589–1616
- [63] E. Kar, N. Bose, S. Das, Physical Chemistry Chemical Physics, 17, (2015), 22784–22798
- [64] S. Xu, Y.W. Yeh, G. Poirier, M.C. McAlpine, R.A. Register, N. Yao, Nano Letters, 13, (2013), 2393–2398
- [65] K.S. Nair, H. Varghese, A. Chandran, U.N.S. Hareesh, A. Chouprik, M. Spiridonov, K.P. Surendran, Materials Today Communications, 31, (2022), 103291
- [66] Y. Wu, F. Ma, J. Qu, T. Qi, Materials Letters, 231, (2018), 20–23
- [67] A. Teka, S. Bairagi, Md. Shahadat, M. Joshi, S.Z. Ahammad, S.W. Ali, Polymer for Advanced Technologies, 29, (2018), 1-8
- [68] Y. Wua, F. Maa, J. Qua, Y. Luo, C. Lv, Q. Guo, T. Qi, Applied Surface Science, 469, (2019), 283–291

Chapter 3: Effect of KNN concentration and size on the output performance of KNN/PVDF based flexible piezoelectric generator

[69] S. Qian, L. Qin, J. He, X. Niu, J. Qian, J. Mu, W. Geng, X. Hou, X. Chou, Materials Letters, 236, (2019), 96–100

[70] P. Hu, L. Yan, C. Zhao, Y. Zhang, J. Niu, Composites Science Technology, 168, (2018), 327–335

Chapter 4

Study of energy harvesting performance of piezoelectric nanogenerator based on three phase PVDF/KNN/ZnO nanocomposite films

Chapter 4 Study of energy harvesting performance of piezoelectric nanogenerator based on three phase PVDF/KNN/ZnO nanocomposite films

This chapter presents the development of piezoelectric energy harvesters based on PVDF/KNN/ZnO nanocomposite films. Initially, KNN nanoparticles were synthesized using the hydrothermal method, as described in Chapter 3. Zinc oxide (ZnO) nanorods were prepared through co-precipitation method and subsequently integrated into the PVDF polymer matrix along with KNN nanoparticles to enhance the overall piezoelectric performance of the fabricated piezoelectric nanogenerator (PENG). ZnO is well-known for its semiconducting properties and remarkable piezoelectric characteristics, making it an ideal candidate for boosting the energy harvesting efficiency of the constructed PENG device. The synergistic effect of KNN and ZnO within the PVDF matrix is expected to result in superior piezoelectric output, contributing to the development of efficient energy harvesting PENG devices.

4.1 Introduction

In recent years, the development of flexible and efficient piezoelectric nanogenerators (PENGs) has gained significant attention for powering wearable and self-sustaining electronic devices. PVDF is a well-known piezoelectric polymer because of its low density, high flexibility, ease of synthesis, good biocompatibility, and mechanical properties suitable for energy harvesting applications [1, 2]. Increasing the β phase content of PVDF is crucial because it is the most electroactive phase responsible for its piezoelectric performance. One simple and effective way to increase the content of the β phase of PVDF and improve the energy conversion efficiency of the PVDF-based PENGs is by dispersing fillers or additives in various concentrations in the PVDF matrix. The positive effects of the addition of additives in the PVDF polymer matrix are mainly attributed to the following aspects: 1) The addition of nanofillers can serve as nucleation and crystallization sites and improve the formation of β phase, crystal orientation, and consequently, the piezoelectric response [3]; 2) The addition of piezoelectric filler material in the PVDF composite can improve the piezoelectric properties [1]; 3) The addition of some conducting fillers in the polymer matrix can enhance the nucleation and also helps in transfer of the generated charges [4]. It is the

Chapter 4: Study of energy harvesting performance of piezoelectric nanogenerator based on three phase PVDF/KNN/ZnO nanocomposite films

combined effect of the filler materials and polymers in the PVDF-based composites that enhance the piezoelectric performance of the devices for wider applications. Presently, the fillers that have been incorporated in the PVDF matrix are lead-based perovskite ceramics [5], lead-free piezoelectric ceramics [6, 7], carbon-based additives [4, 8], metal oxides [9, 10] and other materials [11, 12].

Literature reports suggest that the incorporation of semiconducting nanofillers into the PVDF matrix not only boosts the piezoelectric output but also enhances the dielectric properties and surface roughness, all of which contribute to improved performance of the nanogenerator. A notable example of such a semiconducting nanofiller is Zinc Oxide (ZnO), that has been used extensively in the recent past for enhancing the piezoelectric performance of composites-based PENG devices due to its good piezoelectric coefficient, good biocompatibility, ease of synthesis and eco-friendly nature [13, 14]. Takhur et al. observed a significant increase in the β -phase content up to 84%—with the addition of just 0.85 vol% ZnO nanoparticles to the PVDF polymer, thereby demonstrating its effectiveness in enhancing piezoelectric properties [15]. Ma et al. reported that a single hybrid PVDF/ZnO nanofiber generated an output voltage which is 300 % more than that of a single PVDF nanofiber [16]. Juan Yi et al. fabricated PVDF/Y-doped ZnO electrospun films and investigated the piezoelectric output performance as a function of Y-doped ZnO content in the PVDF [17]. The fabricated device with 15 wt.% ZnO generated output voltages of ~20 V and ~35 V when walking and running, respectively. In another study by Li et al., ZnO nanorods incorporated PVDF electrospun nanocomposite-based PENG has been developed and they achieved ~ 85 V output signal with ZnO nanorods as 30 % filler concentration in the PVDF matrix [13].

Furthermore, in the recent years, two or more fillers have also been added together in the PVDF matrix to further enhance the piezoelectric response of the nanogenerator by synergistically improving the dielectric properties, piezoelectric properties, β -phase content, mechanical strength, and charge transfer efficiency [18]. Lin *et al.* developed a piezoelectric film based on MWCNT–BaTiO₃/PVDF composites. They demonstrated that incorporating MWCNTs into the BaTiO₃/PVDF composite increased the open-circuit voltage of the flexible PENG to 11.4 V, achieving an optimal

Chapter 4: Study of energy harvesting performance of piezoelectric nanogenerator based on three phase PVDF/KNN/ZnO nanocomposite films

power of 8.67 W and an optimal power density of 1.16 W/cm^2 , which was sufficient to simultaneously light up eight LEDs [19]. Sabry *et al.* developed a PENG using a BaTiO₃/ZnO/PVDF nanocomposite, where the incorporation of BaTiO₃ and ZnO into the PVDF matrix enhanced the β -phase content and significantly boosted the output voltage to 12 V under an applied force of 1.5 N, demonstrating its potential for self-powered and wearable electronic applications [20]. Shi *et al.* prepared electrospun PVDF nanofibers by adding different amounts of BaTiO₃ and graphene nanosheets. The best performance was observed with 0.15 wt.% graphene nanosheets and 15 wt.% BT nanoparticles, producing an output voltage of about 11 V and electric power of 4.1 μ W. Graphene nanosheets helped to increase β -phase formation, strengthened the fibers, and formed a conductive network, all of which enhanced charge transfer and overall output [21]. Samadi *et al.* have reported the piezoelectric performance of the Fe₃O₄-GO/PVDF electrospun web based piezoelectric nanogenerator and they have reported the output voltage of 1.75 V [22].

Based on the above literature, in the present work, PENG has been fabricated by using KNN nanoparticles and ZnO nanorods together as fillers in the PVDF matrix to explore the synergistic effect of KNN and ZnO on the piezoelectric performance of the KNN/ZnO/PVDF based piezoelectric nanogenerator. In the present research work, six sets of nanocomposite film of PVDF, PVDF/KNN, PVDF/ZnO, and PVDF/KNN/ZnO with varying concentrations of KNN and ZnO in the PVDF matrix have been fabricated by drop cast method. ZnO will act as a nucleating/conducting nanofiller in the prepared nanocomposite film. The PVDF/KNN/ZnO based PENGs demonstrated superior energy harvesting response and higher content of β phase in PVDF. The ferroelectric properties of the prepared nanocomposite films were also studied. The maximum values of open circuit voltage, short circuit current and power density were 39.5 V, 8.75 μ A and 22.26 μ W/cm² for the PVDF/KNN/ZnO-based PENGs when subjected to force using the dynamic shaker.

4.2 Experimental Details

4.2.1 Synthesis of KNN Nanoparticles

KNN nanoparticles were synthesized using the hydrothermal method, with the detailed synthesis process already discussed in Section 2 of Chapter 3.

4.2.2 Synthesis of ZnO Nanoparticles

The co-precipitation method has been used for the synthesis of ZnO nanoparticles, as presented in Figure 4.1. ZnCl₂ (Thermo Fischer Scientific India Pvt. Ltd., 96%) was dissolved in 50 ml of deionized water and stirred for 30 minutes at 40 °C to make a precursor solution. After that, NaOH (Thermo Fischer Scientific India Pvt. Ltd., 92%) solution was prepared with deionized water and then added to the ZnCl₂ solution dropwise while being continuously stirred to keep the reactant's PH level at 12. The resulting precipitates were washed with ethanol and deionized water multiple times and then dried for 6 hours at 80 °C in the oven. The resulting powder was then calcined at 500 °C for 2 hours in a muffle furnace to obtain the ZnO nanoparticles.

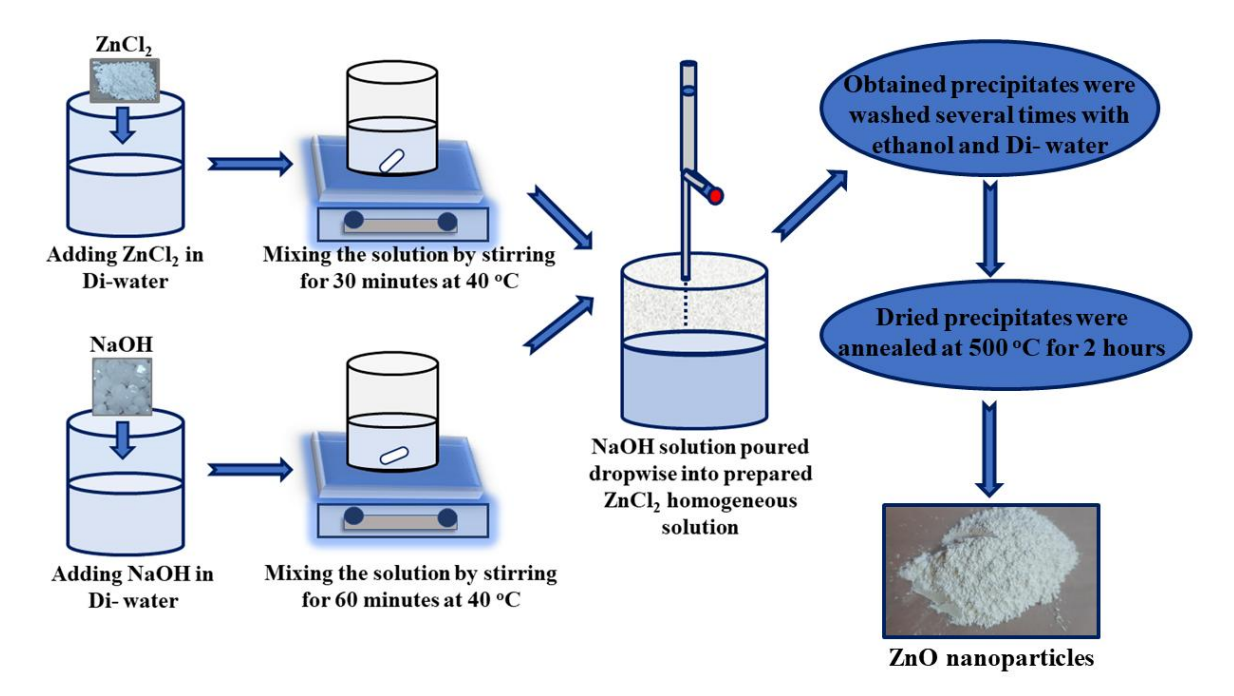


Figure 4.1 Synthesis of ZnO nanoparticles by Co-precipitation method.

4.2.3 Fabrication of PVDF/KNN/ZnO Flexible Nanocomposite Films

For the fabrication of PVDF/KNN/ZnO flexible nanocomposite films, Polyvinylidene fluoride (PVDF, Alfa Aesar) was dissolved in N, N-Dimethylformamide (DMF, Fisher Scientific) by using a magnetic stirrer at 50 °C until a uniform transparent solution was obtained. Then KNN and ZnO nanoparticles were added into the DMF in varying wt. % as listed in Table 4.1 and ultrasonicated for 40 minutes at room temperature. Finally, the two solutions were mixed by a magnetic stirrer for 5 hours. The obtained uniform solutions with varying KNN/ZnO ratios were dropped onto the glass slide and kept in the oven for drying at 80 °C. After this process, a flexible PVDF/KNN/ZnO nanocomposite film was peeled off from the glass slide. For comparative study, films of pure PVDF, PVDF/KNN and PVDF/ZnO were also prepared using a similar method. The detailed schematic representation of the synthesis process of flexible nanocomposite films is shown in Figure 4.2.

Table 4.1 Details of weight percentages of KNN, ZnO and PVDF in the fabricated flexible nanocomposite films.

S. No.	Sample ID	Amount (wt. %)				
		PVDF	KNN	ZnO		
1.	Pure PVDF	100	0	0		
2.	PVDF/KNN/0%ZnO	85	15	0		
3.	PVDF/KNN/0.45%ZnO	85	14.55	0.45		
4.	PVDF/KNN/1%ZnO	85	14	1		
5.	PVDF/KNN/7.5%ZnO	85	7.5	7.5		
6.	PVDF/KNN/15%ZnO	85	0	15		

Chapter 4: Study of energy harvesting performance of piezoelectric nanogenerator based on three phase PVDF/KNN/ZnO nanocomposite films

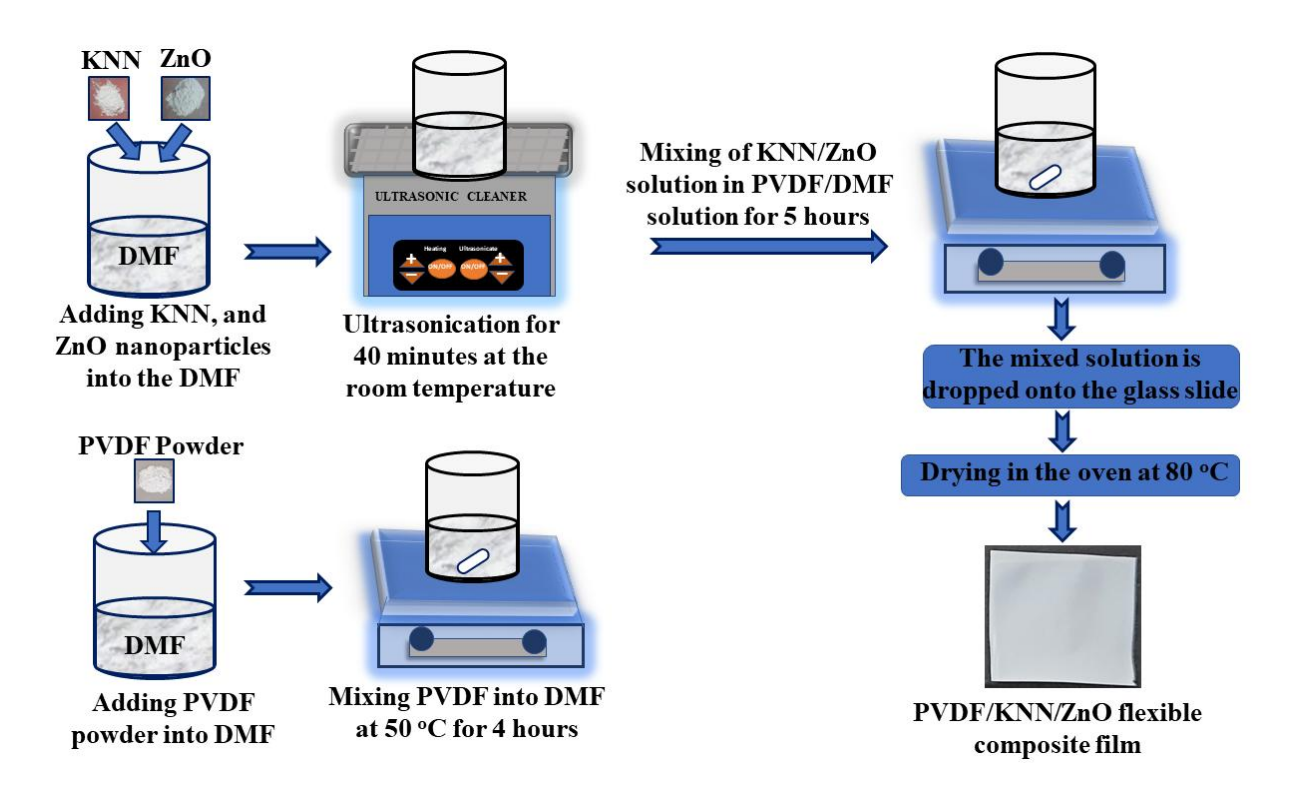


Figure 4.2 Schematic representation of the preparation of PVDF/KNN/ZnO flexible nanocomposite films.

4.2.4 Fabrication of PENG Device

A lightweight, flexible and cost-effective piezoelectric nanogenerator was fabricated by cutting the nanocomposite films into 2×2 cm² and then attaching aluminium tape on both sides of the nanocomposite films to make the electrodes. Then copper strip was attached to the aluminium tape followed by wrapping the complete device in the Kapton tape to pack and fix the nanocomposite film. The schematic representation of the fabricated PENG and the digital photograph of the prepared PENG device are presented in Figure 4.3.

Chapter 4: Study of energy harvesting performance of piezoelectric nanogenerator based on three phase PVDF/KNN/ZnO nanocomposite films

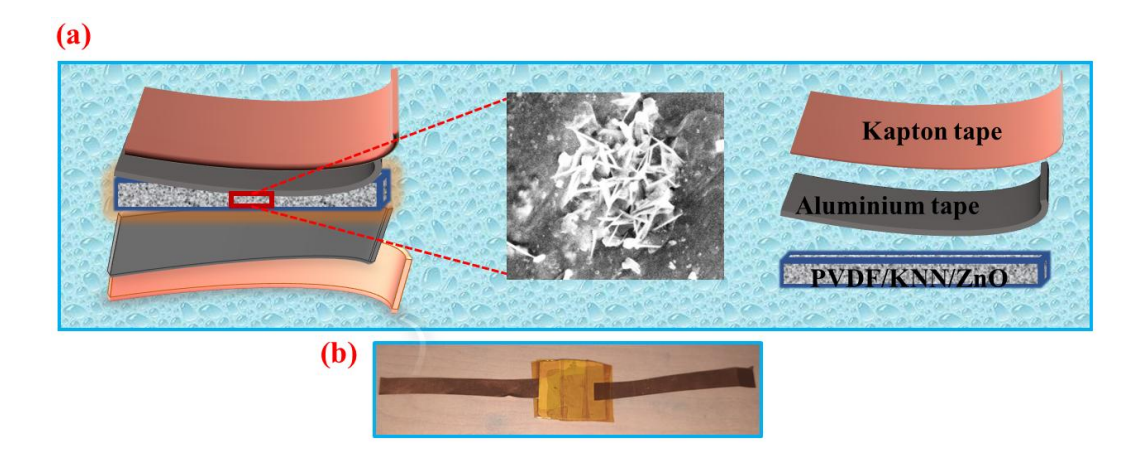


Figure 4.3 (a) Schematic diagram of the fabricated PENG device and (b) Photograph of the prepared PENG device.

4.2.5 Characterizations

To analyse the crystalline structure of the prepared KNN nanoparticles, ZnO nanoparticles, and nanocomposite films, X-ray Diffraction (XRD; Rigaku, Ultima-IV) with Cu-Kα radiation source (1.54 Å) was used. Field Emission Scanning Electron Microscopy (FE-SEM) (MIRA3LMH, TESCAN instrument) was used for the morphological study of KNN nanoparticles, ZnO nanoparticles, and prepared nanocomposite films. Fourier Transform Infrared Spectroscopy (FTIR) (Perkin Elmer FTIR spectrum-II) was used to analyse the formation of the β phase in the nanocomposite films. The polarisation hysteresis loops of the prepared nanocomposite films were recorded at room temperature using the P-E loop tracer. Furthermore, the dielectric measurement as a function of frequency was carried out using a KEYSIGHT Impedance Analyzer E4990A (20Hz- 10MHz). All the electrical measurements of the fabricated PENG devices on application of force on the surface of the devices using an electrodynamic shaker (Micron 0020) were done by using a digital storage oscilloscope (DSO; Tektronix, MDO500) and the electrometer (Keysight B2902B). Inverse piezoelectric coefficient (d_{33}^*) value of the nanocomposite film was measured using the Strain Measurement System of Radiant Precision LCII Ferroelectric tester (Model No. P-HVi210KSC). The power output of the nanocomposite-based PENG device was also determined by varying the external load resistances. Finally, to demonstrate the practical applicability of the fabricated PENG device, it was attached to the elbow, finger, and wrist to harvest energy from human body movements.

4.3 Results and Discussions

4.3.1 Structural and Microstructural Analysis of KNN Nanoparticles

The crystal structure and morphology of the synthesized KNN nanoparticles used in this chapter have already been discussed in Section 2 of Chapter 3.

4.3.2 Structural and Microstructural Analysis of ZnO Nanorods

The XRD pattern of the synthesized ZnO nanoparticles is presented in Figure 4.4. From the XRD pattern it can be seen that observed diffraction peaks for ZnO nanoparticles correspond to hexagonal wurtzite structure.

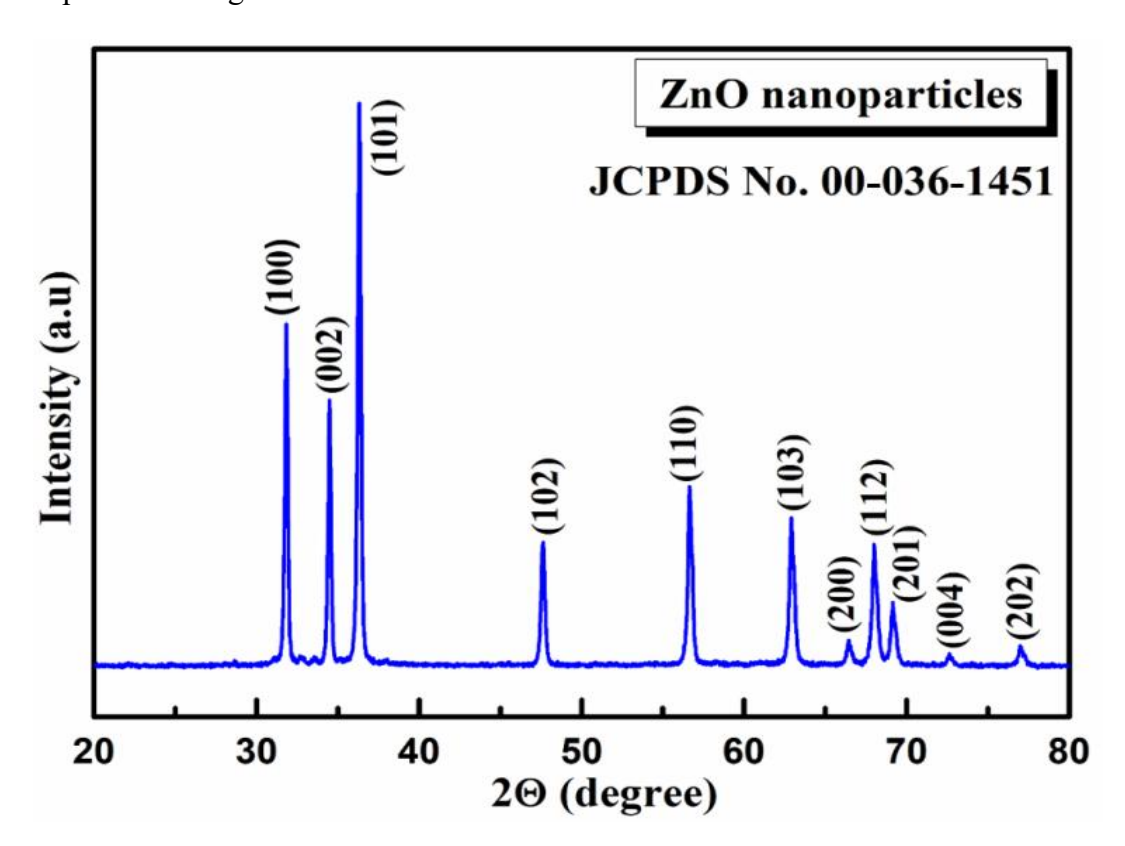


Figure 4.4 XRD plot of calcined ZnO nanorods.

Furthermore, the morphology and the particle size of the synthesized ZnO nanorods are investigated using FESEM and are presented in Figure 4.5 (a) and (b), respectively. The FESEM image of the ZnO nanoparticles, shown in Figure 4.5 (a) reveals the formation of nanorods with a hexagonal shaped cross-section. Figure 4.5 (b) presents the histogram of nanorods diameters, showing their distribution with respect to frequency.

The average diameter of the ZnO nanorods was determined to be approximately ~183 nm, using the Image J software.

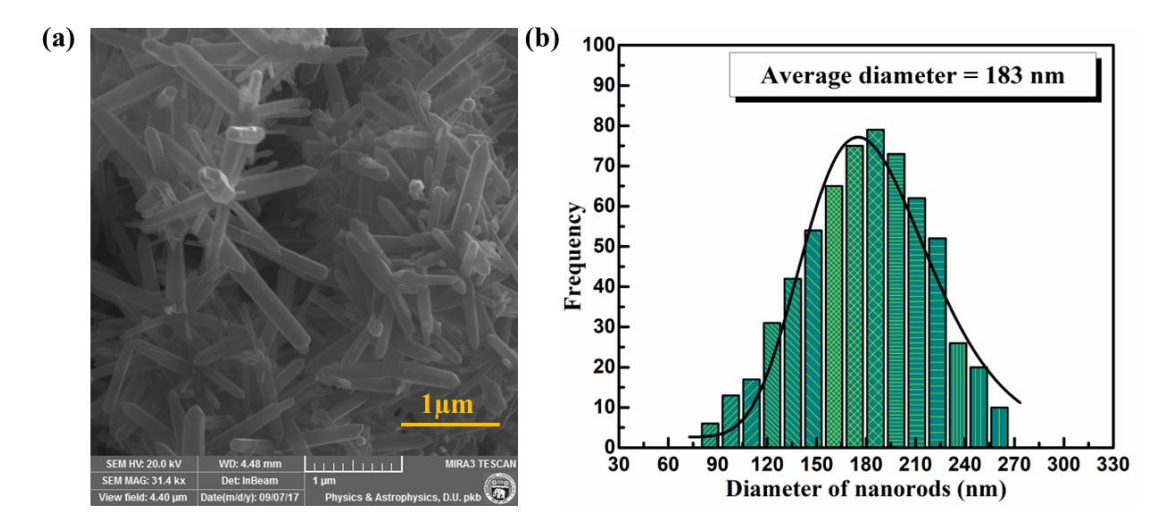


Figure 4.5 (a) FESEM image of calcined ZnO nanorods and (b) Histogram showing the distribution of diameter of ZnO nanorods.

4.3.3 Structural Analysis of the Nanocomposite Films

4.3.3.1 XRD Analysis of the PVDF/KNN/ZnO Flexible Nanocomposite Films

To analyse the structure of the prepared nanocomposite films, XRD analysis is done and the corresponding plot is depicted in Figure 4.6. The peaks which correspond to α and β phases of the PVDF are obtained at 18.6° and 20.2°, respectively in all the prepared films. The intensity of the diffraction peak corresponding to β phase is higher in comparison to α phase, indicating that β phase dominates over α phase in all the prepared nanocomposite films. In addition to this, other peaks that can be seen in the XRD plot are attributed to ZnO and KNN nanoparticles. In the XRD plot presented in Figure 4.6, the signs " \bullet " and " \bullet " are used to mark the diffraction peaks corresponding to those of KNN and ZnO nanoparticles, respectively.

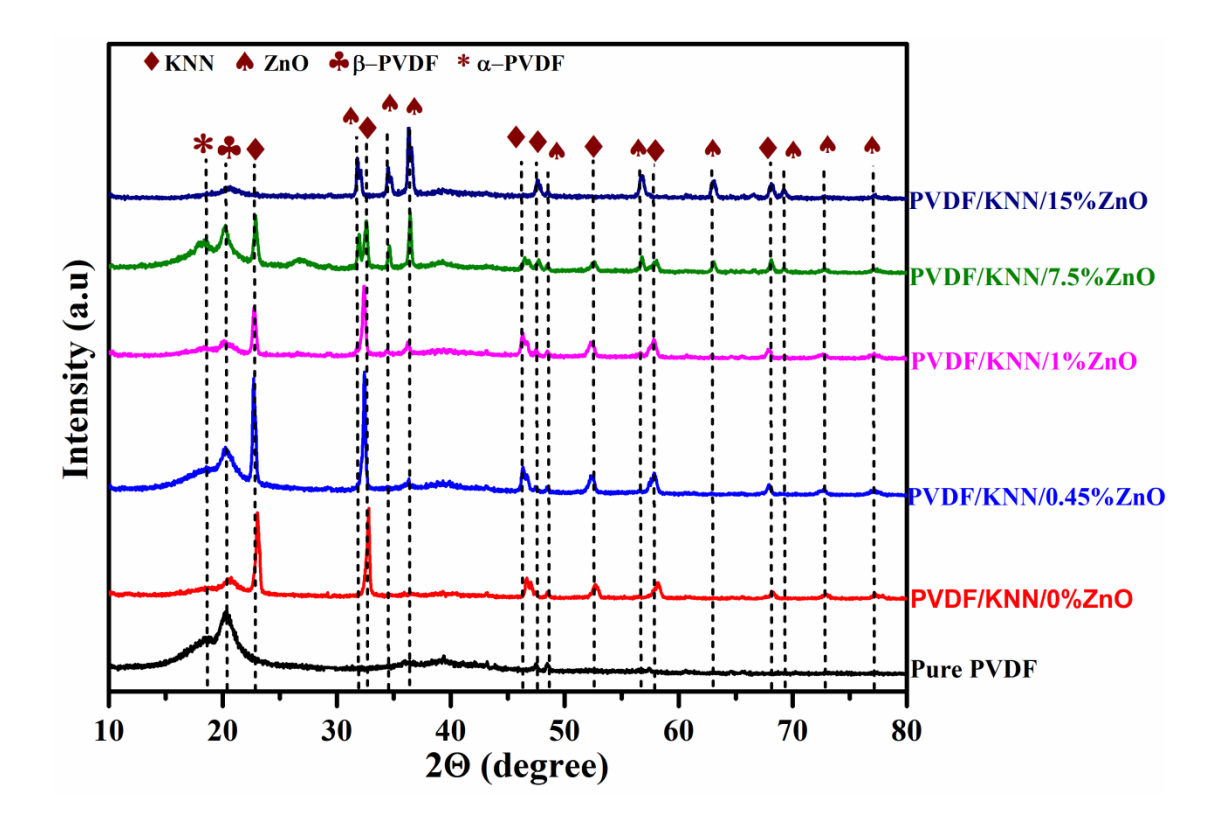


Figure 4.6 X-ray Diffraction patterns of the flexible nanocomposite films produced with different content of KNN and ZnO in the PVDF matrix.

4.3.3.2 FTIR Analysis of the PVDF/KNN/ZnO Flexible Nanocomposite Films

The FTIR plot of the prepared nanocomposite films is presented in Figure 4.7. The presence of α and β phases of the PVDF in the prepared nanocomposite films can be identified by the presence of peaks at 766 cm⁻¹ and 840 cm⁻¹, respectively. All the peaks corresponding to α and β phases of the PVDF are marked in the plot shown in Figure 4.7 (a) [23-26]. The content of the β phase in the prepared flexible films have been calculated using the Beer-Lambert Law [27] given below:

$$F(\beta) = \frac{A_{\beta}}{\binom{K_{\beta}}{K_{\alpha}} A_{\alpha} + A_{\beta}} \tag{4.1}$$

where $K_{\alpha} = 6.1 \text{ x } 10^4 \text{ cm}^2 \text{mol}^{-1}$ and $K_{\beta} = 7.7 \text{ x } 10^4 \text{ cm}^2 \text{mol}^{-1}$ are the absorption coefficient at 840 cm⁻¹ and 766 cm⁻¹, respectively; A_{α} and A_{β} , are the absorbance intensities at 766 cm⁻¹ and 840 cm⁻¹, respectively [28]. The variation of the β phase content in the films as a function of KNN and ZnO concentration is illustrated in Figure 4.7 (c). It can be seen that with the introduction of KNN and ZnO nanoparticles, there is an enhancement

in the β phase fraction in the nanocomposite films in comparison to the pure PVDF film. Furthermore, the highest β phase content is obtained for the nanocomposite film containing 0.45% ZnO nanorods in the PVDF matrix with further increasing the amount of ZnO nanorods above 0.45%, the fraction of β phase has decreased in the nanocomposite films. Therefore, it is expected that the device fabricated with PVDF/KNN/0.45%ZnO nanocomposite film will demonstrate superior piezoelectric performance in comparison to the other nanocomposite films as discussed in the next sections of the paper. Furthermore, the obtained FTIR results are in agreement with the XRD result confirming the presence of the β phase in the prepared nanocomposite films. Based on XRD and FTIR analysis, it is suggested that the crystallinity of the PVDF has been improved with the simultaneous addition of KNN nanoparticles and ZnO nanorods in the PVDF matrix.

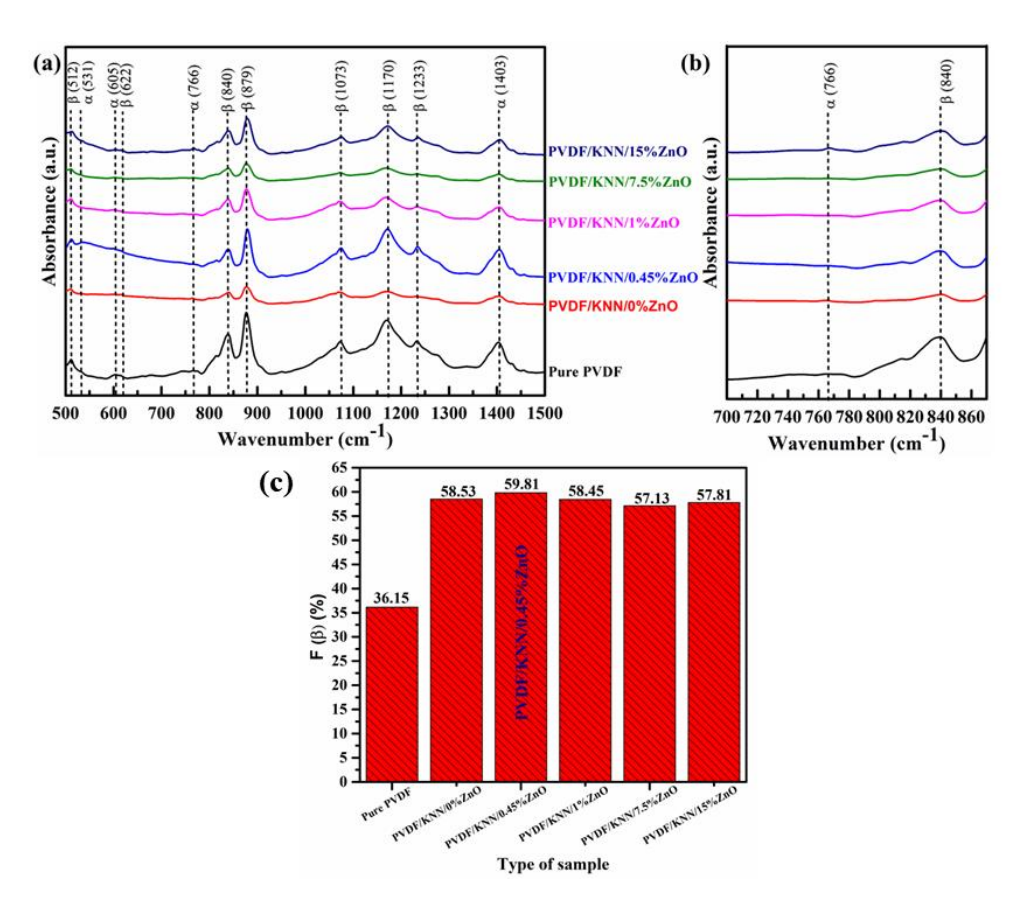


Figure 4.7 (a) FTIR spectra of pure PVDF film and nanocomposite films (b) Enlarged view of the FTIR spectra in the range 700 cm⁻¹ to 870 cm⁻¹ of Figure 4.7 (a), and (c) Variation of β - phase content as a function of KNN and ZnO nanoparticles concentration in the PVDF matrix.

4.3.3.3 Surface Morphology Studies of PVDF/KNN/ZnO Flexible Nanocomposite Films

The surface morphology of fabricated pure PVDF and nanocomposite films are examined using FESEM and corresponding images are presented in Figure 4.8. The pure PVDF film has a smooth surface (Figure 4.8 (a)). It can be seen from Figure 4.8 (b) – (f) that KNN and ZnO nanoparticles are distributed uniformly in the PVDF polymer. Slight roughness on the surface of the nanocomposite films can be seen in the films when both KNN and ZnO nanoparticles are added together in the PVDF polymer.

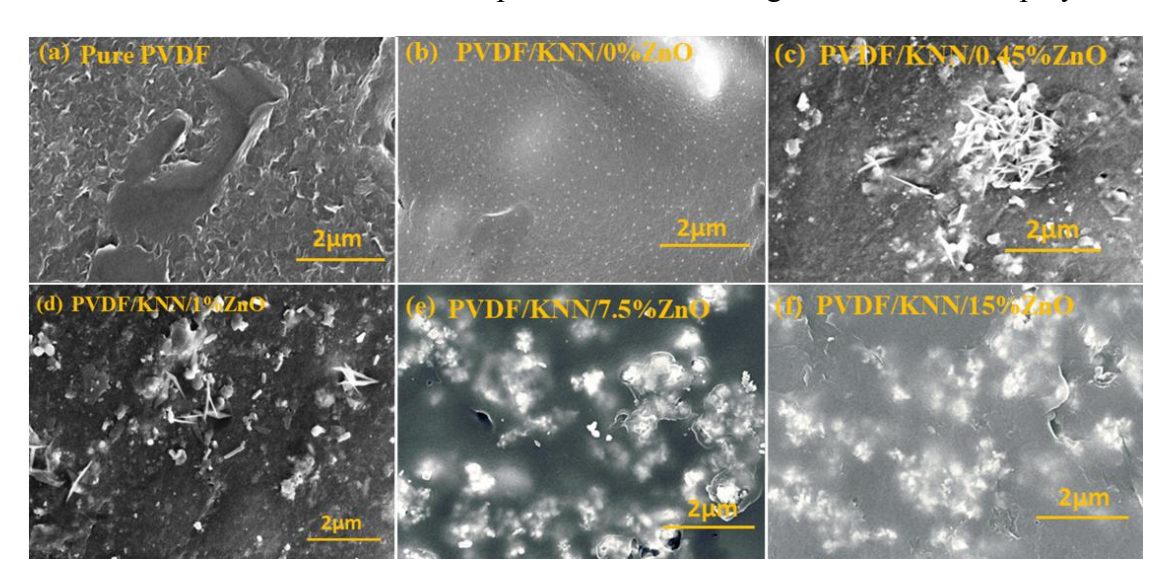


Figure 4.8 FESEM surface micrographs of (a) Pure PVDF, (b) PVDF/KNN/0%ZnO, (c) PVDF/KNN/0.45%ZnO, (d) PVDF/KNN/1%ZnO, (e) PVDF/KNN/7.5%ZnO and (f) PVDF/KNN/15%ZnO.

4.3.4 Polarisation vs. Electric Field (*P-E*) Hysteresis Loops of the Nanocomposite Films

The room temperature P-E hysteresis plots of the prepared PVDF/KNN/ZnO flexible nanocomposite films are presented in Figure 4.9 (a) - (f). For all the prepared films, non-saturated hysteresis loops have been observed. It can be seen from the hysteresis loops that films containing KNN and ZnO nanoparticles demonstrated enhanced ferroelectric behaviour in comparison to the pure PVDF film. Furthermore, the variation of the remnant polarization (P_r) and maximum polarisation (P_s) are also given in Figure 4.9 (g) and (h), respectively. With the increase in the concentration of ZnO

nanoparticles in the nanocomposite films, there is a decrease in both P_r and P_s values. In particular, the maximum values of P_r and P_s obtained are 2.87 μ C/cm² and 32.83 μ C/cm² respectively, for the sample containing the 14.55 wt.% KNN and 0.45 wt.% ZnO in the nanocomposite film. This may be attributed to the larger polarizability of KNN in comparison to ZnO and PVDF [7]. The observed increase in P_r will also increase the piezoelectric behaviour of the nanocomposite films [2].

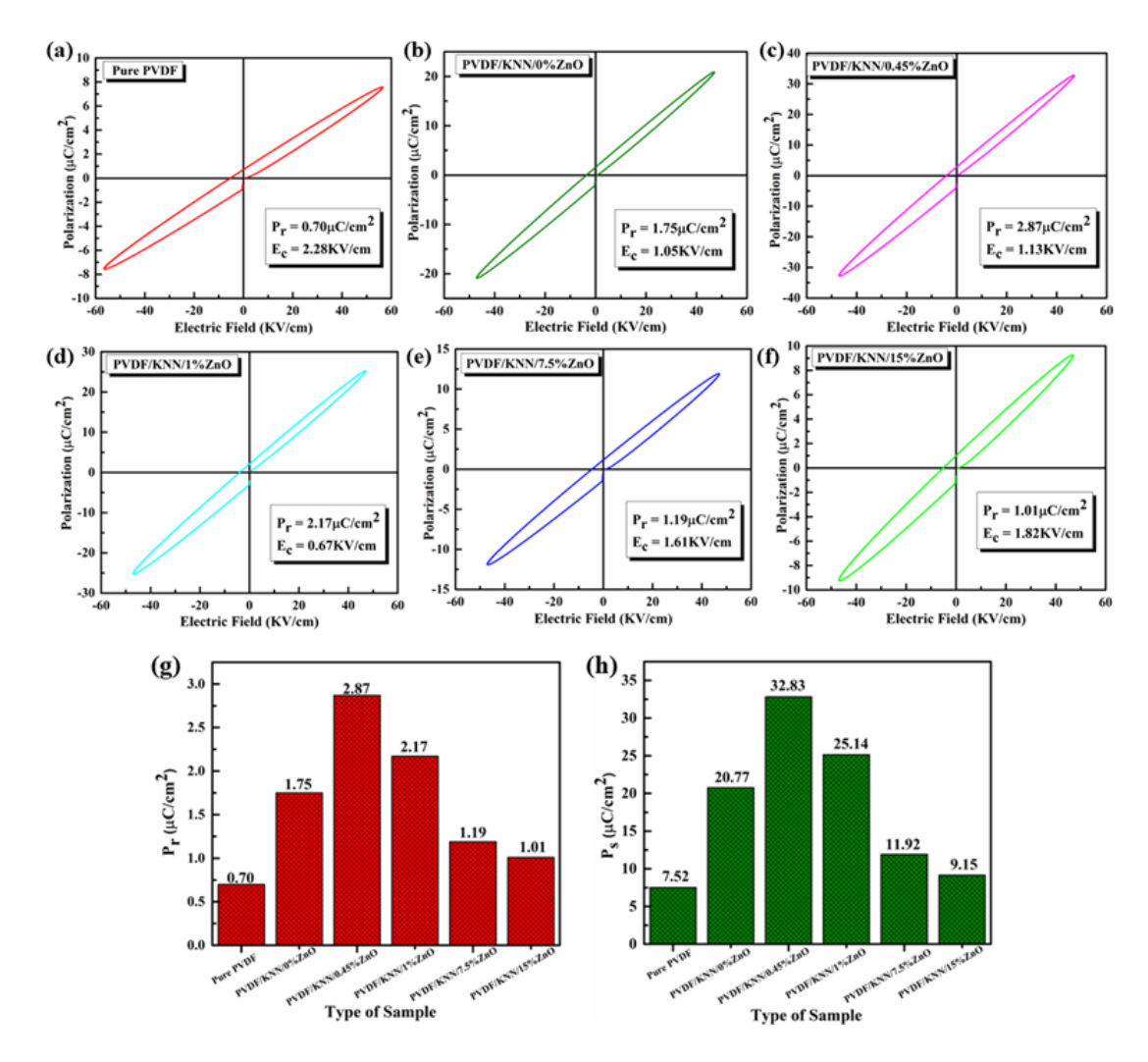


Figure 4.9 P-E Hysteresis Loops of (a) pure PVDF, (b) PVDF/KNN/0%ZnO, (c) PVDF/KNN/0.45%ZnO, (d) PVDF/KNN/1%ZnO, (e) PVDF/KNN/7.5%ZnO, (f) PVDF/KNN/15%ZnO (g) and (h) Variation of P_r and P_s as a function of KNN/ZnO concentration in PVDF matrix.

4.3.5 Dielectric Properties of the PVDF/KNN/ZnO Nanocomposite Films

For studying the dielectric properties of the prepared flexible nanocomposite films, dielectric constant (ε_r) of nanocomposite films was measured as a function of frequency in the range from 100 Hz to 1 MHz at room temperature and the corresponding plot is presented in Figure 4.10. For all the films, the dielectric constant decreases with increase in frequency which is attributed to decrease in polarisation with increase in frequency in all the pure and nanocomposite films. The polarisation is the sum of dipolar, ionic, interfacial and electronic polarisations. When frequency is low, different polarisations respond easily, but with increase in frequency, different polarisation mechanisms cease. This results in the decrease of net polarisation of the material, which then leads to decrease of dielectric constant [29]. Further, the dielectric constant is found to increase first when the content of ZnO is 0.45 wt.% in the PVDF matrix and then it decreases continuously with further increasing the content of ZnO up to 15 wt.%. The values of dielectric constant at 1 KHz are 0.85, 18.11, 43.30, 33.15, 31.25, and 29.48 for pure PVDF film, PVDF/KNN/0%ZnO, PVDF/KNN/0.45%ZnO, PVDF/KNN/1%ZnO, PVDF/KNN/7.5%ZnO, and PVDF/KNN/15%ZnO, respectively.

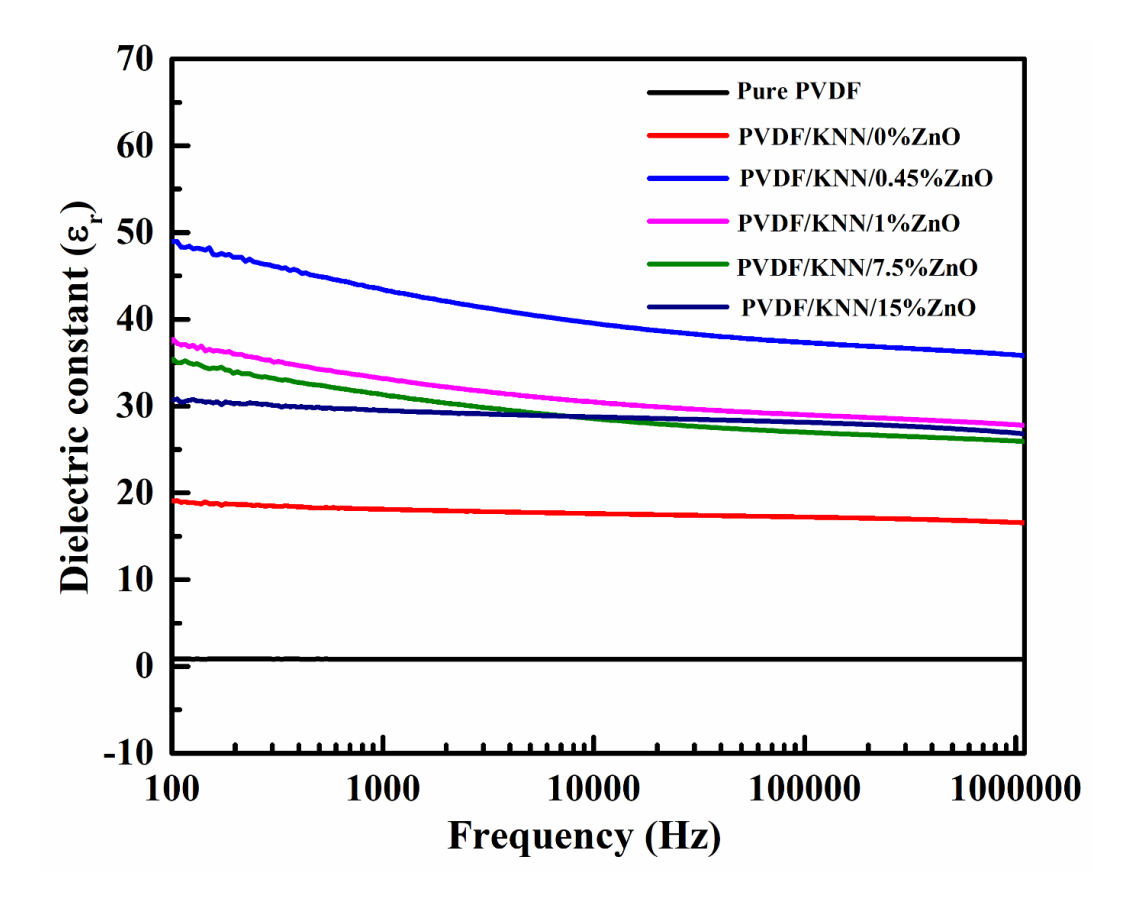


Figure 4.10 Dielectric constant (ε_r) of pure PVDF, PVDF/KNN/0%ZnO, PVDF/KNN/0.45%ZnO, PVDF/KNN/1%ZnO, PVDF/KNN/7.5%ZnO and PVDF/KNN/15%ZnO flexible nanocomposite films.

The dielectric constant in case of nanocomposite films is dependent on the dielectric properties of individual phases and their volume fraction in the composite [30]. The dielectric constant of KNN and ZnO is relatively higher than the pure PVDF resulting in higher values of dielectric constant in all the prepared nanocomposite films in comparison to the pure PVDF film [31, 32, 33]. Besides, in the composite material, the fraction of interfaces is higher in comparison to the single-phase materials which gives rise to higher interfacial polarization. In addition, using semiconducting fillers such as ZnO can significantly change the space charge distribution in the nanocomposite films. However, when the ZnO content is increased beyond 0.45 wt.% in the PVDF matrix, the observed decrease in the dielectric constant values is mainly attributed to the decreasing content of KNN in the PVDF matrix. Therefore, the increase in dielectric constant of the composites – primarily contributed by KNN can lead to an enhanced

Chapter 4: Study of energy harvesting performance of piezoelectric nanogenerator based on three phase PVDF/KNN/ZnO nanocomposite films

piezoelectric constant, ultimately improving the piezoelectric performance of the composite films [2].

4.3.6 Piezoelectric Performance of PVDF/KNN/ZnO PENG Devices

To test the piezoelectric performance of the fabricated PENG devices, dynamic shaker was used to apply mechanical force on the surface of the PENG device. Figure 4.11 (a) – (f) depicts the open-circuit voltage of the fabricated PENG devices with different concentrations of KNN and ZnO in the PVDF matrix on application of repeated force. The peak-to-peak open circuit voltage is found to increase with increase in the ZnO content up to 0.45 wt.% in the PVDF matrix and then decreases. The values of peak-to-peak open circuit output voltage obtained for different PENG is presented in Figure 4.12. It can be noticed from the Figure 4.12 that the open circuit voltage of the device PVDF/KNN/0.45%ZnO is almost 4.5 times in comparison to pure PVDF and 1.5 and 1.33 times in comparison to the device containing only KNN and ZnO in the PVDF matrix, respectively. The obtained better performance of the PVDF/KNN/0.45%ZnO PENG device in comparison to the other fabricated PENGs is mainly attributed to its higher β phase content, better dielectric and ferroelectric properties [34, 19].

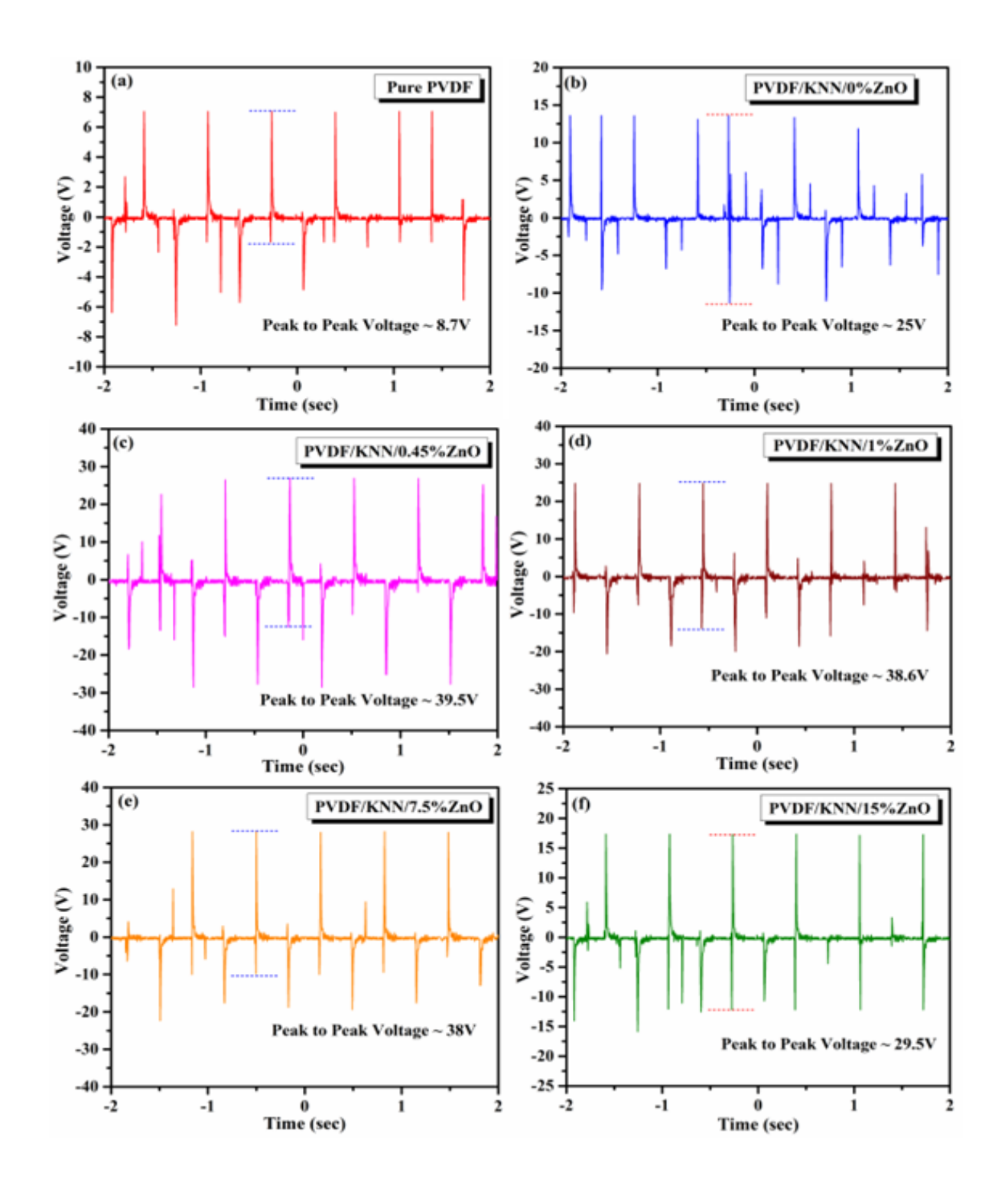


Figure 4.11 The generated open circuit voltage plots of the PENG device (a) pure PVDF, (b) PVDF/KNN/0%ZnO, (c) PVDF/KNN/0.45%ZnO, (d) PVDF/KNN/1%ZnO, (e) PVDF/KNN/7.5%ZnO and (f) PVDF/KNN/15%ZnO.

Chapter 4: Study of energy harvesting performance of piezoelectric nanogenerator based on three phase PVDF/KNN/ZnO nanocomposite films

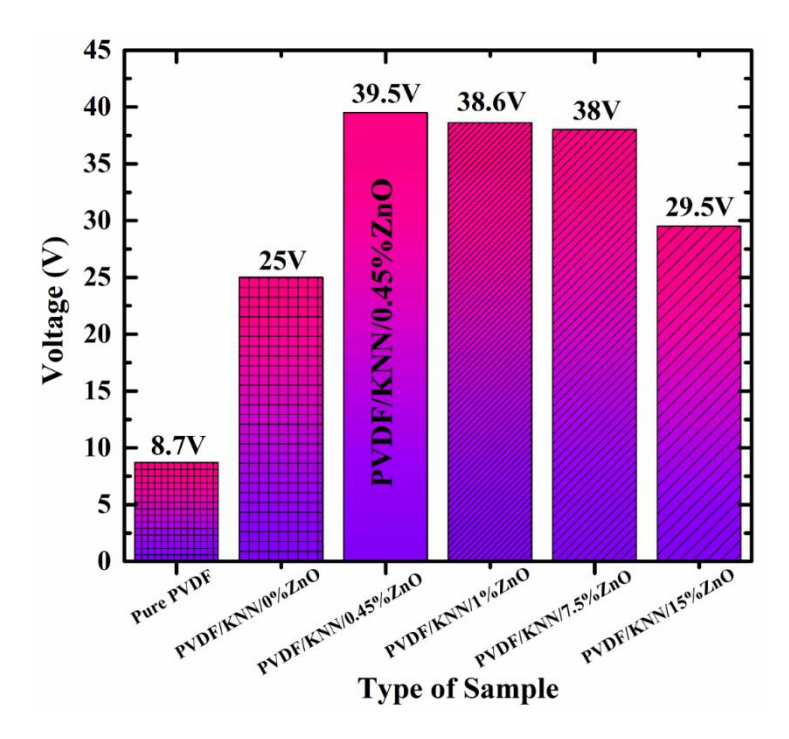


Figure 4.12 Variation of peak-to-peak open circuit voltage of the PENG devices as a function of KNN and ZnO nanoparticles concentration in the PVDF matrix.

Further, the short circuit current generated from different PENG devices has also been measured and the corresponding plots are depicted in Figure 4.13 (a-f). The measured short circuit current follows the same trend as that of output voltage. The peak-to-peak short circuit current for the different PENG devices are presented in Figure 4.14. The maximum short circuit current is obtained for the PVDF/KNN/0.45%ZnO based PENG device which is 8.75 μA. The current densities have also been calculated for different nanogenerators and are presented in Figure 4.15 (a). The power output has also been measured for PVDF/KNN/0.45%ZnO nanocomposite-based PENG device for which maximum output voltage and current has been obtained. The power (*P*) of the PENG can be calculated by using the following relation:

$$P = VI \tag{4.2}$$

where, P, V and I represent the output power, voltage and current, respectively. For power measurement of the PENG device, an external load resistance was varied in the range of 10^5 to 10^9 Ω . Figure 4.15 (b) shows the variation of generated output voltage and current for varying external loads for the PVDF/KNN/0.45%ZnO PENG device. It can be noticed from the plot that the voltage gradually increased, while the current

decreased as a function of increasing load following Ohm's law (V = IR). Further, the variation of measured output power density as a function of load resistance is shown in Figure 4.15 (c). At an external resistance of 8 M Ω (Optimum point), the maximum power density measured was ~ 22.23 μ W/cm².

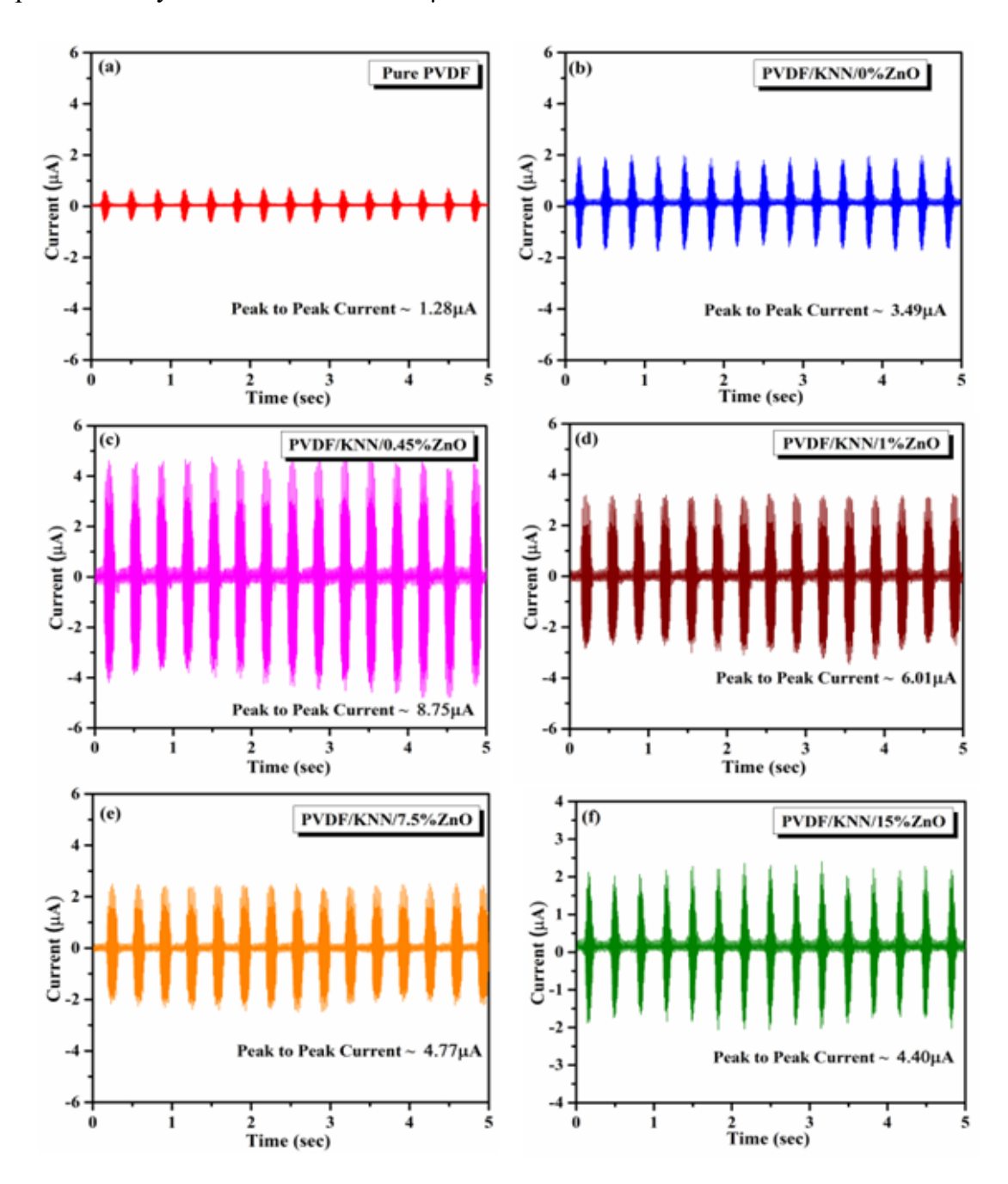


Figure 4.13 The generated short circuit current plots of the PENG device (a) pure PVDF, (b) PVDF/KNN/0%ZnO, (c) PVDF/KNN/0.45%ZnO, (d) PVDF/KNN/1%ZnO, PVDF/KNN/7.5%ZnO and (f) PVDF/KNN/15%ZnO.

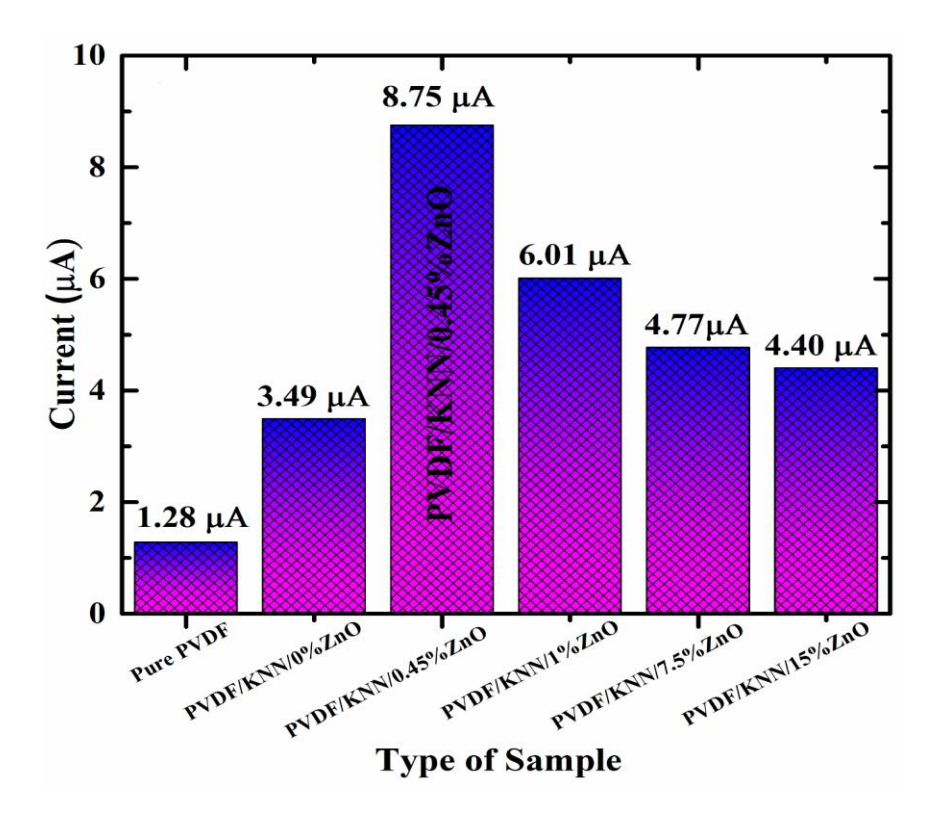


Figure 4.14 Variation of peak-to-peak short circuit current of the PENG device as a function of KNN and ZnO nanoparticles concentration in the PVDF matrix.

Furthermore, in the present study, the room temperature Displacement vs. Voltage (D-V) hysteresis loop was recorded for PVDF/KNN/0.45%ZnO PENG device to determine the inverse piezoelectric coefficient (d_{33}^*) and the related plot is shown in Figure 4.15 (d). Based on the slope of butterfly curve, the maximum and the average values of d_{33}^* are ~ 83.82 pm/V and 32.22 pm/V, respectively. Overall, the results suggest that using KNN and ZnO together as a filler in PVDF matrix offers the higher values of inverse piezoelectric coefficients, which make it a promising candidate for energy harvesting applications.

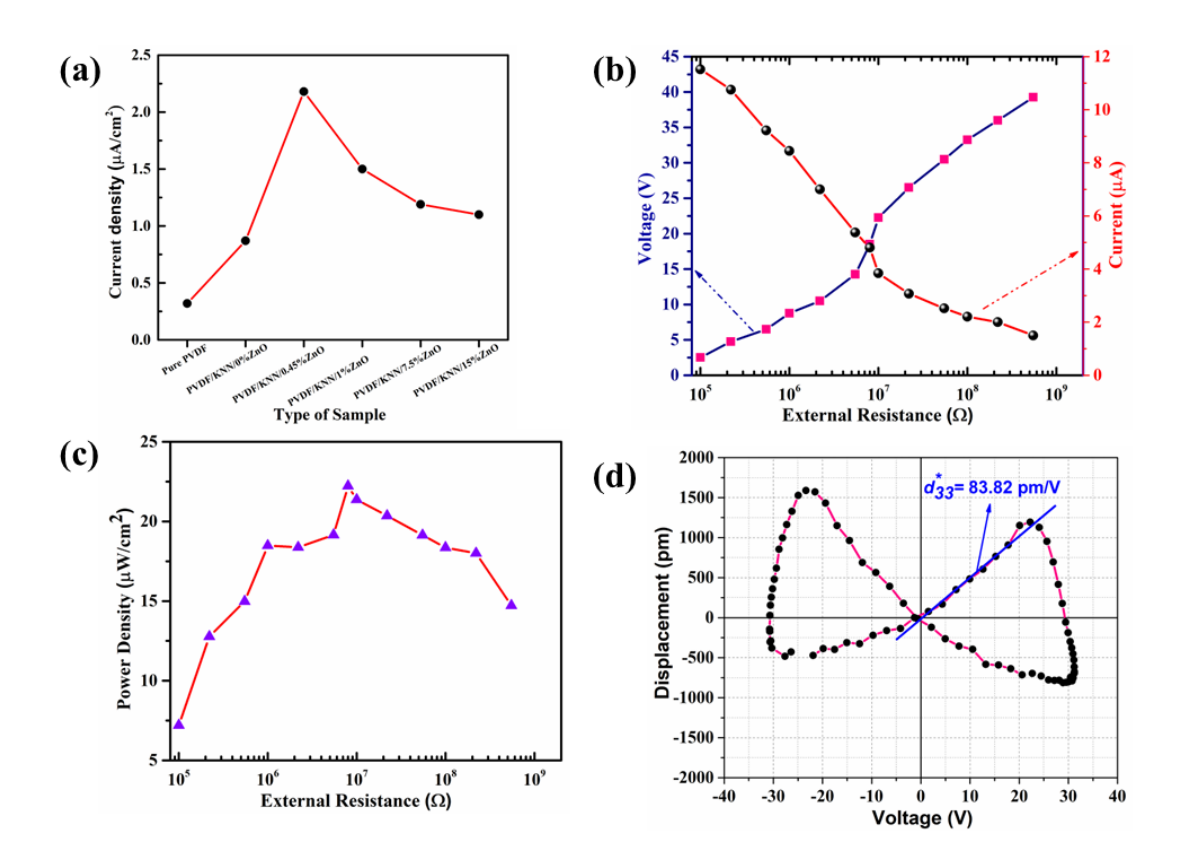


Figure 4.15 (a) Plot of current density with type of sample, (b) Output voltage and current measured with external resistance, (c) Power density measured with external resistance for PVDF/KNN/0.45%ZnO film-based PENG and (d) Displacement vs. Voltage (*D-V*) butterfly curve for PVDF/KNN/0.45%ZnO film-based PENG.

From the obtained data it can be summarized that the PENG fabricated with incorporating KNN and ZnO nanoparticles together in the PVDF matrix has resulted in improved piezoelectric performance in comparison to the PENG fabricated by incorporating only KNN or ZnO in the PVDF matrix. The fabricated device can thus have the potential to be used in applications in which a small amount of energy is needed for self-operation. The comparison of the results obtained in the present work with the reported work in the literature is presented in Table 4.2.

Table 4.2 Comparison of the piezoelectric performance between PVDF/KNN/ZnO PENG fabricated in the present work and various nanogenerators reported in the literature.

S. No.	Filler material in the Polymer Matrix	Polymer used	Film Synthesis Technique	V _{oc} (V)	<i>I_{sc}</i> (μA)	Power Density (μW/cm²)	Ref.
1.	KNN nanorods and ZnO nanorods	PVDF	electrospinning	25	1.81	11.31	[35]
2.	KNN nanorods	PVDF	Twin screw melt mixing	3.7	0.326		[1]
3.	ZnO nanofibers	PVDF	electrospinning	6.4	0.17		[36]
4.	KNN nanorods and CNT	PVDF	electrospinning	23.24	9	52.29	[37]
5.	BTO nanoparticles	PVDF	Solvent casting method	7.2	0.038	0.8	[38]
6.	ZnO nanorods	PVDF	Supersonic spraying	15.2	32	12.5	[39]
7.	BTO nanoparticles	PVDF	Solvent casting	9.3		0.122	[40]
8.	ZnO nanoparticles and MWCNT	PVDF	Drop casting	22		21.41	[41]

Chapter 4: Study of energy harvesting performance of piezoelectric nanogenerator based on three phase PVDF/KNN/ZnO nanocomposite films

9.	KNN nanofibers	PVDF	Twin screw melt mixing	17.5	0.522	0.13	[42]
10.	KNN nanoparticles and ZnO nanorods	PVDF	Drop casting	39.5	8.75	22.26	Present Study

4.3.6.1 Energy Harvesting Performance of PENG Device

To harvest the mechanical energy from different human body motions which otherwise gets wasted, a fabricated PENG device with PVDF/KNN/0.45%ZnO nanocomposite film has been attached on the elbow, finger and wrist of the hand. The generated output voltages for pen tapping, elbow bending, finger moving and wrist stretching were 3.080 V, 1.720 V, 1.460 V and 660 mV, respectively. The corresponding output voltage plots are presented in Figure 4.16 (a) – (d). Furthermore, the constructed device was able to light up four red light emitting diodes (LEDs) and power a digital wrist watch as shown in Figure 4.16 (f) and (g) and the corresponding circuit is shown in Figure 4.16 (e).

4.4 Conclusion

In this chapter, Potassium Sodium Niobate (KNN)/Zinc Oxide (ZnO) incorporated Poly (vinylidene fluoride) (PVDF) polymer-based flexible piezoelectric nanogenerator (PENG) were constructed and the effect of KNN and ZnO concentrations on the various properties and piezoelectric performance of the PENG device investigated. The **FTIR** result showed that was PVDF/14.55%KNN/0.45%ZnO nanocomposite film possesses the highest content of electroactive (β) phase (~59.81%). Furthermore, dielectric and ferroelectric properties of the prepared nanocomposite films were also measured. The maximum values of open circuit voltage, short circuit current and power density were 39.5 V, 8.75 μ A and 22.26 μ W/cm² (with 10 M Ω load resistance), respectively obtained for the PENG fabricated with PVDF/14.55%KNN/0.45%ZnO nanocomposite film. The maximum and average values of inverse piezoelectric charge coefficient were found to be $d_{33}^*_{\rm max} \sim 83.82$ pm/V and $d_{33}^*_{\rm avg} \sim 32.22$ pm/V, respectively for the same

Chapter 4: Study of energy harvesting performance of piezoelectric nanogenerator based on three phase PVDF/KNN/ZnO nanocomposite films

nanocomposite film. The synergistic effect of KNN and ZnO nanoparticles in PVDF polymer matrix considerably improves the resultant piezoelectric performance of the nanogenerator, enabling it to glow four red light-emitting diodes (LEDs) and power a digital wrist watch. Moreover, the developed nanogenerator was also able to generate output voltages of 3.08 V, 1.72 V, 1.46 V and 660 mV for pen tapping, elbow bending, finger moving and wrist stretching, respectively. Finally, it can be concluded that the versatile, durable, and flexible PENG based on PVDF/KNN/ZnO nanocomposite film has the potential for future applications in energy harvesting and portable self-powered electronic devices.

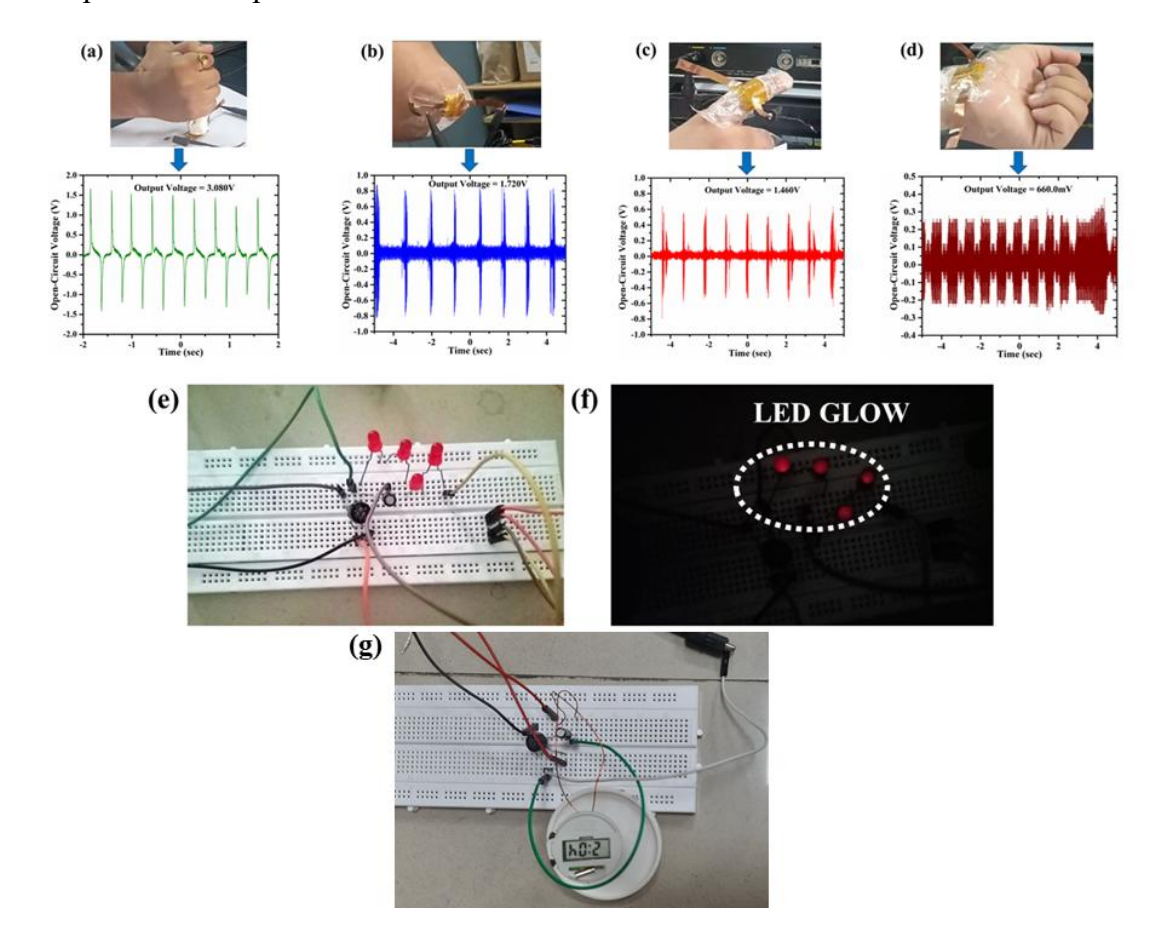


Figure 4.16 The generated voltage with PENG fabricated with PVDF/KNN/0.45%ZnO nanocomposite film by (a) pen tapping, (b) elbow bending, (c) finger moving, (d) wrist stretching, (e) circuit with full wave bridge rectifier for glowing LEDs, (f) showing glowing LED and (g) power a digital wrist watch.

References

- [1] S. Bairagi, S.W. Ali, European Polymer Journal, 116 (2019), 554–561
- [2] V. Jella, S. Ippili, J.-H. Eom, J. Choi, S.-G. Yoon, Nano Energy, 53, (2018), 46–56
- [3] N. Sezer, M. Koç, Nano Energy, 80, (2021), 105567
- [4] J. Yang, Y. Zhang, Y. Li, Z. Wang, W. Wang, Q. An, W. Tong, Materials Today Communication, 26, (2021), 101629
- [5] L. Paralı, M. Koç, E. Akça, Ceramic International, 49, (2023), 18388–18396
- [6] A. Patra, A. Pal, S. Sen, Ceramic International, 44, (2018), 11196-11203
- [7] K. S. Nair, H. Varghese, A. Chandran, U. N. S. Hareesh, A. Chouprik, M. Spiridonov, K. P. Surendran, Materials Today Communication, 31, (2022), 103291
- [8] J. H. Eun, S. M. Sung, M. S. Kim, B. K. Choi, J. S. Lee, Materials & Design, 206, (2021), 109785
- [9] M.M. Alam, A. Sultana, D. Mandal, ACS Applied Energy Materials, 1 (7), (2018), 3103–3112
- [10] C. Jin, N. Hao, Z. Xu, I. Trase, Y. Nie, L. Dong, A. Closson, Z. Chen, J. X.J. Zhang, Sensors and Actuators A: Physica, 305, (2020), 111912
- [11] C. Chen, Z. Bai, Y. Cao, M. Dong, K. Jiang, Y. Zhou, Y. Tao, S. Gu, Jie Xu, X. Yin, W. Xu, Composites Science and Technology, 192, (2020), 108100
- [12] Y. H. Lee, D. H. Kim, Y. Kim, I. Shabbir, M. Li, K. H. Yoo, T. W. Kim, Nano Energy 102, (2022), 107676
- [13] J. Li, S. Chen, W. Liu, R. Fu, S. Tu, Y. Zhao, L. Dong, B. Yan, Y. Gu, Journal of Physical Chemistry C, 123, (2019), 11378-11387
- [14] R. Sahoo, S. Mishra, A. Ramadoss, S. Mohanty, S. Mahapatra, S.K. Nayak, Polymer, 205, (2020), 122869
- [15] P. Thakur, A. Kool, N.A. Hoque, B. Bagchi, F. Khatun, P. Biswas, D. Brahma, S. Roy, S. Banerjee, S. Das, Nano Energy, 44, (2018), 456-467
- [16] J. Ma, Q. Zhang, K. Lin, L. Zhou, Z. Ni, Materials Research Express, 5, (2018), 035057

Chapter 4: Study of energy harvesting performance of piezoelectric nanogenerator based on three phase PVDF/KNN/ZnO nanocomposite films

- [17] J. Yi, Y. Song, Z. Cao, C. Li, C. Xiong, Composites Science Technology, 215, (2021), 109011
- [18] S.A. Riquelme, K. Ramam, A.F. Jaramillo, Results in Physics, 15, (2019), 102800
- [19] X. Lin, F. Fu, X. Zhang, W. Li, Y. Zhao, X. Fei, Q. Li, C. Yang, S. Huang, ACS Applied Nano Materials, 6, (2023), 11955-11965
- [20] R.S. Sabry, A.D. Hussein, Polymer Testing, 79, (2019), 106001
- [21] K. Shi, B. Sun, X. Huang, P. Jiang, Nano Energy, 52, (2018), 153
- [22] A. Samadi, S. M. Hosseini and M. Mohseni, Organic Electronics, 59, (2018), 149–155
- [23] P. K. Sarkar, S, Maji, G. S. Kumar, K. C. Sahoo, D. Mandalb, S. Acharya, RSC Advances, 6, (2016), 910-917
- [24] H. T. T. Nong, A. N. Nguyen, J. Solard, A. Gomez, S. Mercone, Applied Sciences, 12, (2022), 1589
- [25] J. Y. Yin, C. Boaretti, A. Lorenzetti, A. Martucci, M. Roso, M. Modesti, Nanomaterials, 12, (2022), 962
- [26] Y. Hou, Y. Deng, Y. Wang, H. L. Gao, RSC Advances, 5, (2015), 72090–72098
- [27] P. Martins, A.C. Lopes, S. Lanceros-Mendez, Progress in Polymer Science, 39(4), (2014), 683-706
- [28] R. K. Singh, S. W. Lye, J. Miao, Polymers, 214, (2021), 123366
- [29] M. Shoorangiz, Z. Sherafat, E. Bagherzadeh, Ceramics International, 48, (2022) 15180-15188
- [30] M. Chandrasekhar, P. Kumar, Ceramics International, 41, (2015), 5574
- [31] J. Li, Q. Meng, W. Li, Z. Zhang, Applied Polymers Sciences, 122 (3), (2011), 1659–1668
- [32] D. Kaur, A. Bharti, T. Sharma, C. Madhu, International Journal of Optics, 3839, (2021), 1
- [33] J-F. Li, K. Wang, F-Y. Zhu, L-Q. Cheng, F-Z. Yao, Journal of American Ceramic Society, 96 (12), (2013), 3677-3696

Chapter 4: Study of energy harvesting performance of piezoelectric nanogenerator based on three phase PVDF/KNN/ZnO nanocomposite films

- [34] A. Pal, A. Sasmal, B. Manoj, D.P. Rao, A.K. Haldar, S. Sen, Materials Chemistry and Physics, 244, (2020), 122639
- [35] S. Bairagi, S.W. Ali, International Journal of Energy Resources, (2020), 1-19
- [36] M. Kim, Y.S. Wu, E.C. Kan, J. Fan, Polymers, 10, (2018), 10070745
- [37] S. Bairagi, S.W. Ali, Soft Matter, 16, (2020), 4876
- [38] M. Sahu, S. Hajra, K. Lae, P. L. Deepti, K. Mistewicz, H. J. Kim, Crystals, 11, (2021), 85
- [39] D. P. Ojha, B. Joshi, E. Samuel, A. Khadka, A. Aldalbahi, G. Periyasami, D. Choi, S. An, S. S. Yoon, International Journal of Energy Resources, (2023), 3074782
- [40] Y. Yang, H. Pan, G Xie, Y. Jiang, C. Chen, Y. Su, Y. Wang. H. Tai, Sensors and Actuators: A Physical, 301, (2020), 111789
- [41] S. Pratihar, A. Patra, A. Sasmal, S. K. Medda, Soft Matter, 17, (2021), 8483-8495
- [42] S. Bairagi, S. W. Ali, Energy Technology, 7, (2019), 1900538

Chapter 5

Effect of Li, Ta and Sb doping on the output performance of KNN/PVDF based flexible piezoelectric generator

Chapter 5 Effect of Li, Ta and Sb doping on the output performance of KNN/PVDF based flexible piezoelectric generator

This chapter presents the fabrication of a flexible piezoelectric generator (PEG) based on a composite film of (Li, Ta, Sb)-modified (K, Na)NbO₃ (KNNLTS) and poly(vinylidene fluoride) (PVDF). KNNLTS particles were synthesized using the solid-state method and subsequently incorporated into the PVDF polymer to develop PVDF/KNNLTS-based piezoelectric energy harvesters. The integration of KNNLTS into the PVDF matrix significantly enhanced the composite's ferroelectric, piezoelectric, and dielectric properties, leading to improved energy harvesting performance.

5.1 Introduction

Lead-free piezoelectric materials have emerged as promising candidates for sustainable energy harvesting applications due to their environmental friendliness and good piezoelectric properties. There are so many lead-free piezoelectric materials such as barium titanate (BT), bismuth sodium titanate (BNT), potassium niobate (KNN), and potassium tantalate niobate (KTN). Among them, potassium sodium niobate (KNN) has attracted significant attention because of its excellent piezoelectric properties, high curie temperature (T_c) and environmentally friendly nature, making it a promising lead-free material for use in piezoelectric generators (PEGs) [1-3]. For instance, S. Bairagi *et al.* prepared the piezoelectric nanocomposite film based on KNN nanorods embedded into the PVDF matrix. The PENG with 10 wt.% KNN nanorods loading produced an output voltage of 3.4 V and a current of 0.100 μ A. The high piezoelectric performance of the prepared device was attributed to the significant enhancement in the fraction of the β phase of the PVDF and its improved piezoelectricity which was strengthened by the addition of KNN nanorods [4].

A. M. Abdullah *et al.* fabricated the KNN- based piezo-triboelectric hybrid energy films by incorporating the KNN particles in a PVDF polymer matrix and investigated the piezoelectric response of the synthesized energy film under the varying concentrations of KNN in the energy film and varying tapping frequency

Chapter 5: Effect of Li, Ta and Sb doping on the output performance of KNN/PVDF based flexible piezoelectric generator

[5]. The maximum output voltage and current observed are 35.3 V and 15.8 μ A, respectively. In another study, Sharma *et al.* fabricated a flexible piezoelectric nanogenerators (PENGs) based on KNN-PDMS composite films by solution casting method. They found that the output voltage and current generated from the PENG with 40 wt.% KNN was 14.49 V, and 2.10 μ A, respectively [6]. The developed nanogenerator can be further utilized for real life applications.

To further enhance the piezoelectric output performance of the KNN based piezoelectric energy harvester one of the effective approaches is doping the KNN ceramics with suitable dopants to enhance its piezoelectric properties which then lead to superior piezoelectric output performance of the energy harvester device. Guo *et al.* first reported the effect of Li doping on the dielectric and piezoelectric properties of KNN ceramics. They found an improved piezoelectric coefficient of $d_{33} = 200 \sim 235$ pC/N [7]. In another study, Zang *et al.* synthesized the lithium and antimony modified KNN by conventional solid state sintering method, which exhibited a high value of piezoelectric response of 286 pC/N [8]. Furthermore, the incorporation of lithium and tantalum into the KNN lattice has been found to enhance its piezoelectric performance by shifting the orthorhombic-to-tetragonal phase transition nearer to room temperature ($d_{33} \sim 300$ pC/N) [9-11].

Saito et al. in 2004 reported the excellent piezoelectric properties in some KNN based ceramics [12]. The chemical composition $(K_{0.44}Na_{0.52}Li_{0.04})(Nb_{0.86}Ta_{0.10}Sb_{0.04})O_3$ showed a d_{33} of 416 pC/N which was significantly higher than the d_{33} of undoped KNN ceramics. Gao et al. obtained a remarkably strong piezoelectricity in KNN based ceramics doped with Li, Ta and Sb with chemical composition $(K_{0.45}Na_{0.55})_{0.98}L_{i0.02}(Nb_{0.77}Ta_{0.18}Sb_{0.05})$ O₃ $(d_{33} = 413)$ pC/N) which were synthesized by conventional solid – state reaction method [13]. The obtained strong piezoelectric characteristic could be attributed to various factors such as phase coexistence owing to an orthorhombic-tetragonal polymorphic phase transition near room temperature, the higher electronegativity of Sb5+ ions in comparison to Nb⁵⁺ ions and Ta⁵⁺ ions, high density. Besides, there are many reports available in the literature showing the superior piezoelectric properties of KNN

Chapter 5: Effect of Li, Ta and Sb doping on the output performance of KNN/PVDF based flexible piezoelectric generator

ceramics obtained by doping with Li, Ta and Sb elements in comparison to undoped KNN ceramics [14-16].

However, to the best of our knowledge, there are very few reports of studies on the fabrication and characterization of doped KNN ceramic based piezoelectric generators. For instance, Wang et al. developed the composite-type piezoelectric nanogenerator by adding $(K_{0.4425}Na_{0.52}Li_{0.0375})(Nb_{0.86}Ta_{0.06}Sb_{0.08})O_3$ (KNN) particles on which Ag particles are attached and CNT in the PDMS matrix and reported a piezoelectric output voltage of ~282 V and short-circuit current of ~32.2 mA [17]. Wang et al. developed a fully rollable nanogenerator using nominal $0.915(Na_{0.5}K_{0.5})(Nb_{0.94}Sb_{0.06})O_3$ $0.045LiTaO_3$ - $0.04BaZrO_3$ composition of (NKNS-LT-BZ) as a filler material in the PVDF polymer matrix [18]. The fabricated device generated a short-circuit current of 2.6 µA and an open-circuit voltage of 18 V on application of periodical agitation at a compressive force of 50 N. In another study, Kumar et al. developed a piezoelectric energy harvester device using Na_{0.47}K_{0.47}Li_{0.06}NbO₃ mixed with polydimethylsiloxane (PDMS) polymer and obtained a large recordable piezoelectric output voltage of 48 V under vertical compressive force of 2 kgf [19]. Ichangi et al. fabricated a flexible nanogenerator based on electrospun Li and Ta-modified KNN nanofibers yielding a high output voltage of 5.6 V which is about 9 times higher than for the Mn-doped KNN nanofibers. In addition, a high-output power of 9.7 µW was achieved with a nanogenerator composed of 5 wt.% Li and 10 wt.% Ta modified KNN nanofibers [20]. This work highlights the potential of KNN nanofibers as an effective material for capturing ambient vibrations to power self-sustaining sensors and wearable electronic devices.

Based on the above literature report, in the present work, a flexible energy harvestor device has been constructed by employing Lithium (Li), Tantalum (Ta), and Antimony (Sb) modified KNN ((K_{0.45}Na_{0.55})_{0.98}L_{i0.02}(Nb_{0.77}Ta_{0.18}Sb_{0.05}) O₃) as a filler material in the PVDF matrix by drop cast method. Subsequently, the piezoelectric generator device was constructed by placing the PVDF/KNNLTS composite film between two aluminium tapes. The structural and morphology of the PVDF, KNNLTS ceramics and composite film were done by X-ray diffraction (XRD), scanning electron microscopy

(SEM) and Fourier transform infrared spectroscopy (FTIR). Further, the dielectric behaviour, ferroelectric and piezoelectric properties of the PVDF/KNNLTS composite film were investigated. Finally, the piezoelectric output performance of the developed piezoelectric generator was also measured by applying a force on the device surface using a dynamic shaker unit.

5.2 Materials and Experimental Details

5.2.1 Materials

Potassium carbonate (K₂CO₃, 99%), sodium carbonate (Na₂CO₃, 99.8%), lithium carbonate (Li₂CO₃, 99%), niobium oxide (Nb₂O₅, (99%), tantalum oxide (Ta₂O₅, 99.95%), and antimony oxide (Sb₂O₅, 99%) purchased from Alfa Aesar were used as raw materials for the synthesis of (K_{0.45}Na_{0.55})_{0.98}Li_{0.02}(Nb_{0.77}Ta_{0.18}Sb_{0.05})O₃ (KNNLTS) ceramic powder. N, N dimethylformamide (DMF) and the poly (vinylidene fluoride) (PVDF) powder were purchased from Thermo Fischer and Alfa-Aesar, respectively. All of the chemicals were used just as received, with no further treatment.

5.2.2 Synthesis of KNNLTS Ceramic Powder

To synthesize KNNLTS ceramic powder, a traditional solid-state reaction process was used, in which all of the precursors were first mixed in stoichiometric proportions using propanol as a liquid media by ball milling for 10 hours. The obtained homogeneous mixture was dried in a hot air oven at 60 °C for 24 hours. After drying, the powder was calcined in the furnace at 1050 °C for 4 hours to obtain KNNLTS ceramic powder. The obtained calcined KNNLTS ceramic powder was then grounded for further use in preparation of flexible composite film.

5.2.3 Fabrication of PVDF/KNNLTS Flexible Composite Films

The procedure of the fabrication of PVDF and PVDF/KNNLTS based flexible composite films was depicted in Figure 5.1 (a). The concentration of KNNLTS ceramic powder in the PVDF matrix was fixed to 15 wt.%. PVDF powder was dissolved in DMF using a magnetic stirrer for 1 hour at 50 °C to prepare a uniform transparent solution. Simultaneously, KNNLTS powder was added in DMF and ultrasonicated for 30 minutes at room temperature. Finally, the two solutions were mixed together and stirred using a magnetic stirrer at 50 °C for 4 hours followed by ultrasonication for 20

minutes. The prepared homogeneous composite solution was then drop cast onto a clean glass substrate followed by drying in a hot-air oven at 80 °C for 1 hour. Finally, the films were peeled off from the glass substrate to get the PVDF/KNNLTS 15 wt.% flexible composite film.

5.2.4 Fabrication of PVDF/KNNLTS based Piezoelectric Generator (PEG)

To construct the PEG, prepared flexible composite films was cut into small piece of 2 x 2 cm² and aluminium tape was attached on both sides of the film to make top and bottom electrodes. Then, copper wires were attached to the aluminium tape for the measurement of the generated output voltage and current. Figure 5.1 (b) shows the schematic diagram of the fabricated PEG device.

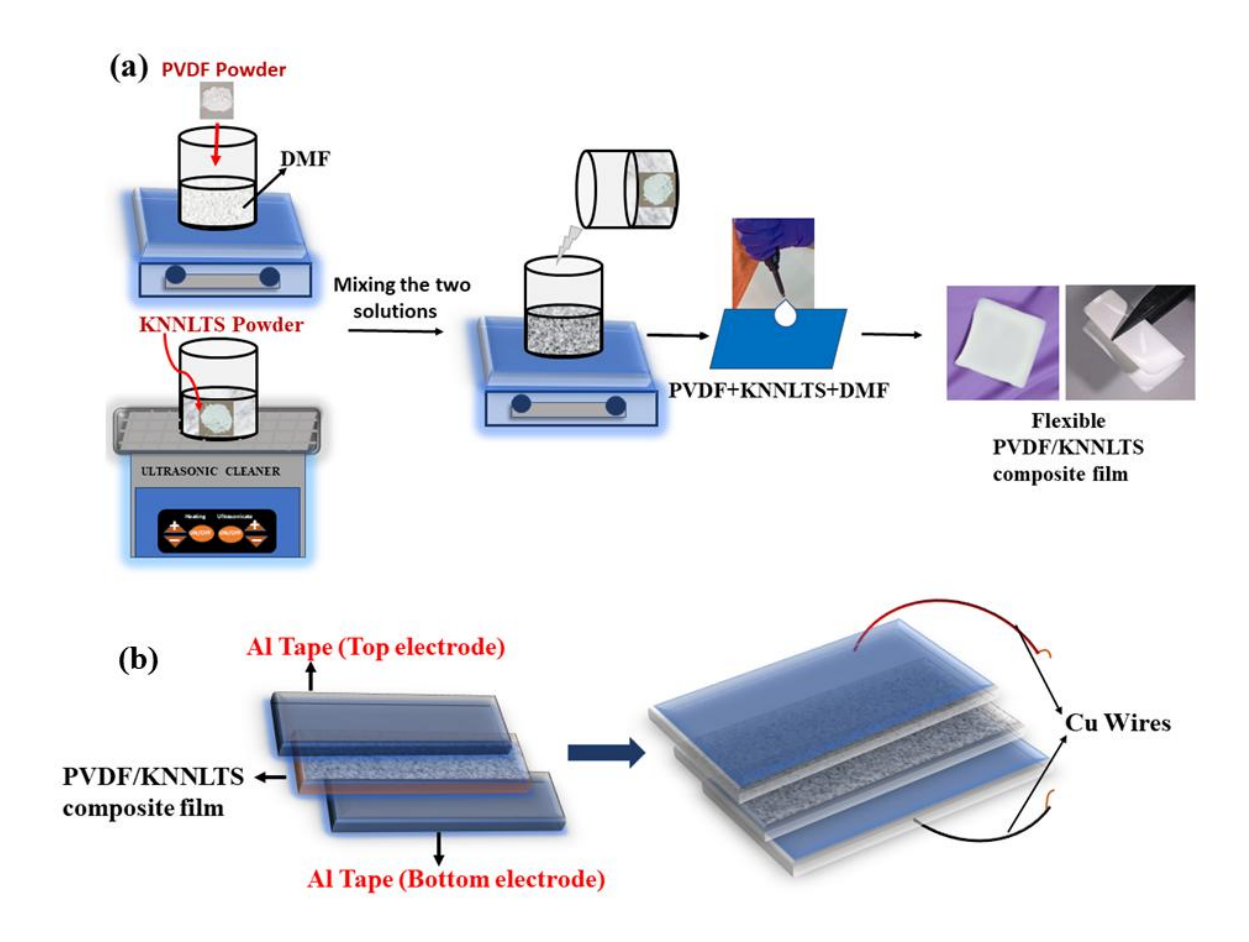


Figure 5.1 (a) Schematic representation of fabrication process of PVDF/KNNLTS flexible composite film and (b) Schematic diagram of the fabricated PEG device.

5.2.5 Characterizations

Firstly, the structural analysis of the KNNLTS ceramic powder, pure PVDF film and the PVDF/KNNLTS flexible composite film were done using an X-ray Diffractometer (Rigaku, Ultima-1V) with a Cu- $K\alpha$ radiation source (1.54 Å). Fourier Transform Infrared Spectroscopy (FTIR) was used to investigate the β -phase formation of PVDF in prepared pure and composite films (Perkin Elmer FTIR spectrum-II). The morphology of synthesized KNNLTS ceramic powder and flexible composite film were studied using Scanning Electron Microscopy (NOVA SEM). The polarisation vs. electric field (P-E) hysteresis loop was also traced on Marine India Instrument. Furthermore, the dielectric measurement as a function of frequency was carried out using a Broadband Dielectric/Impedance Analyzer (Model: C-50 Alpha A; Make: Novocontrol Germany in a frequency range of 20Hz to 2MHz. All the electrical characterizations of the fabricated PEG device were done by applying force on the surface of the device using an electrodynamic shaker (Micron 0020) and generated voltage and current were measured by using a digital storage oscilloscope (DSO; Tektronix, MDO500) and the Electrometer (Keysight B2902B), respectively. Inverse Piezoelectric coefficient (d_{33}^*) value of the composite film was measured using the Strain Measurement System of Radiant Precision LCII Ferroelectric tester (Model No. P-HVi210KSC). Finally, to demonstrate the practical applicability of the fabricated PEG device, various human body movements-such as fist beating, elbow bending, quenching, and fist opening were performed to successfully harvest mechanical energy.

5.3 Results and Discussions

5.3.1 Structural Analysis

5.3.1.1 Structural Analysis of KNNLTS Ceramic Powder

The calcined KNNLTS ceramic powder was examined by XRD and the associated plot is shown in Figure 5.2 (a). From the plot it can be seen that the calcined KNNLTS powder exhibits typical perovskite structure. In addition, no secondary or impurity diffraction peaks are observed in the XRD plot suggesting that the KNNLTS ceramic powder has been successfully synthesized by the solid-state reaction route. The enlarged XRD plot in the 2θ range of $44.5^{\circ} - 47^{\circ}$ is presented in Figure 5.2 (b). From

the plot shown in Figure 5.2 (b), peak splitting can be seen around $\sim 45.5^{\circ}$. By assessing the relative intensities of (002) and (200) diffraction peaks, the phase structure of the ceramic can be determined. As reported in the literature, an orthorhombic (O) phase has a (002)/(200) diffraction peaks intensity ratio of 2:1, while the pure tetragonal (T) phase has a (002)/(200) diffraction peaks intensity ratio of 1:2. A ratio approaching 1:1 indicates a coexisted crystal structure with both O and T phases [21, 22].

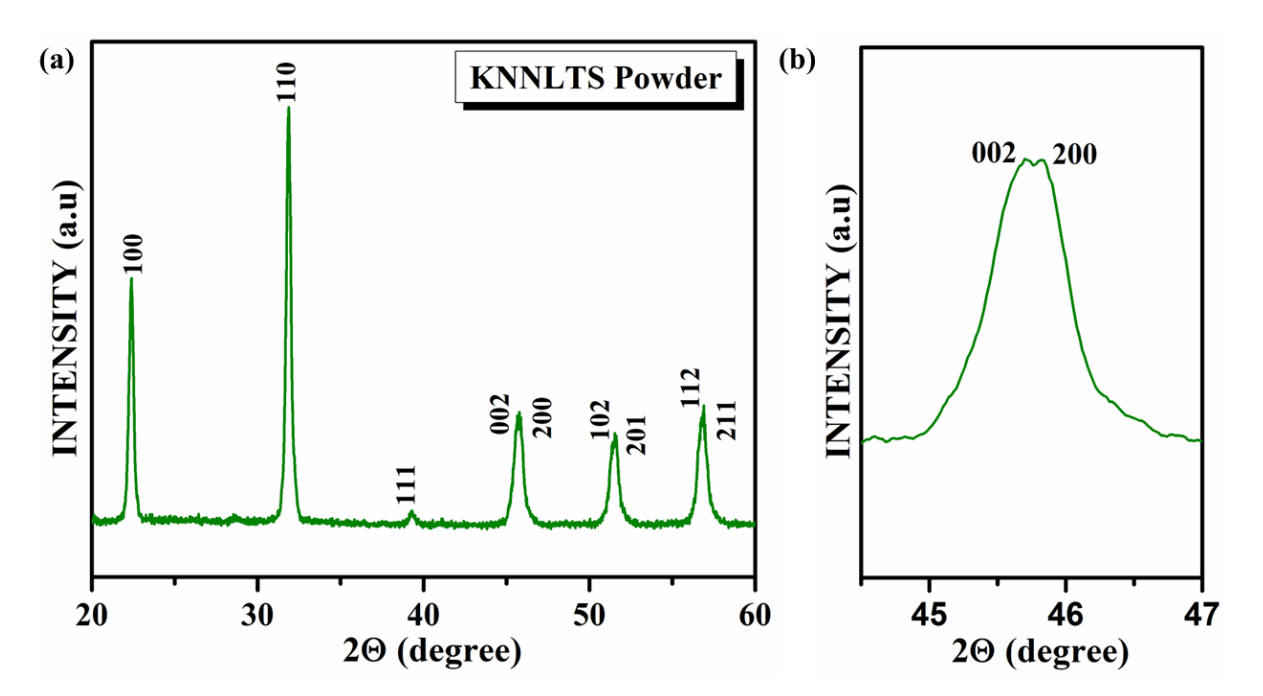


Figure 5.2 (a) XRD pattern of calcined KNNLTS ceramic powder and (b) enlarged XRD pattern in the 2θ range of $44.5^{\circ}-47^{\circ}$.

5.3.1.2 Structural Analysis of Pure PVDF Film and PVDF/KNNLTS Flexible Composite Film

To get the crystallographic information of the prepared pure PVDF film and PVDF/KNNLTS 15 wt.% composite film, XRD analysis was performed and corresponding plots are shown in Figure 5.3. In PVDF, as mentioned earlier, β -phase is the most polar phase and thus responsible for its piezoelectric response whereas α -phase does not show any piezoelectric response. Figure 5.3 (a) represents the XRD plot of pure PVDF film. In the XRD plot of pure PVDF film the diffraction peak at 18.4° can be assigned to the non-polar α -phase of PVDF whereas the peak at 20.2° corresponds to the polar β -phase of the PVDF polymer [23-25]. Additionally, stronger intensity of

the β -phase peak compared to the α -phase suggests that β -phase predominates over α -phase. Furthermore, all the peaks depicted in the XRD plot in Figure 5.3 (b) of the PVDF/KNNLTS 15 wt.% composite film either corresponds to the α and β phases of the PVDF or KNNLTS ceramic powder [13, 26].

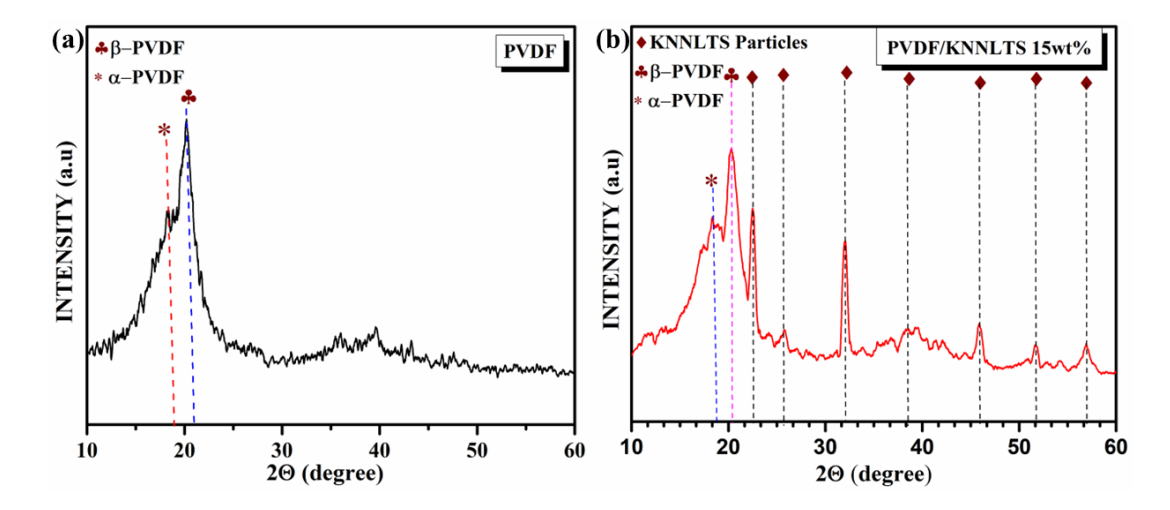


Figure 5.3 X-ray Diffraction pattern of (a) PVDF film and (b) PVDF/KNNLTS 15 wt.% flexible composite film.

5.3.2 Surface Morphology Studies of KNNLTS Ceramic Powder, Pure PVDF Film and PVDF/KNNLTS Composite Film

The morphology of as synthesized calcined KNNLTS ceramic powder was analysed by SEM and corresponding image was shown in Figure 5.4. It was observed from the SEM image that KNNLTS ceramic particles exhibited square or rectangular shaped particles. Further, the surface morphology of the prepared pure PVDF and PVDF/KNNLTS flexible surface film are presented in the Figure 5.5 (a) and (b), respectively. For pure PVDF film, a smooth and dense surface can be seen in the SEM image. From the Figure 5.5 (b), it can be seen that KNNLTS ceramic particles are dispersed uniformly throughout the PVDF, resulting in uniform film. On the surface of the composite film, KNNLTS particles were not seen thereby confirming the insertion of the ceramic particles in the PVDF matrix.

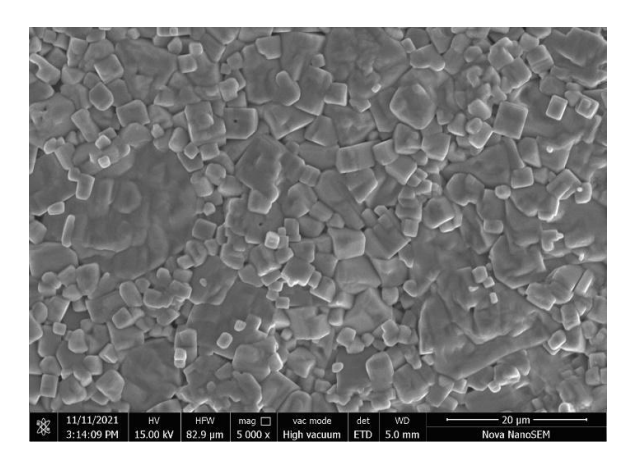


Figure 5.4 SEM image of KNNLTS calcined ceramic powder.

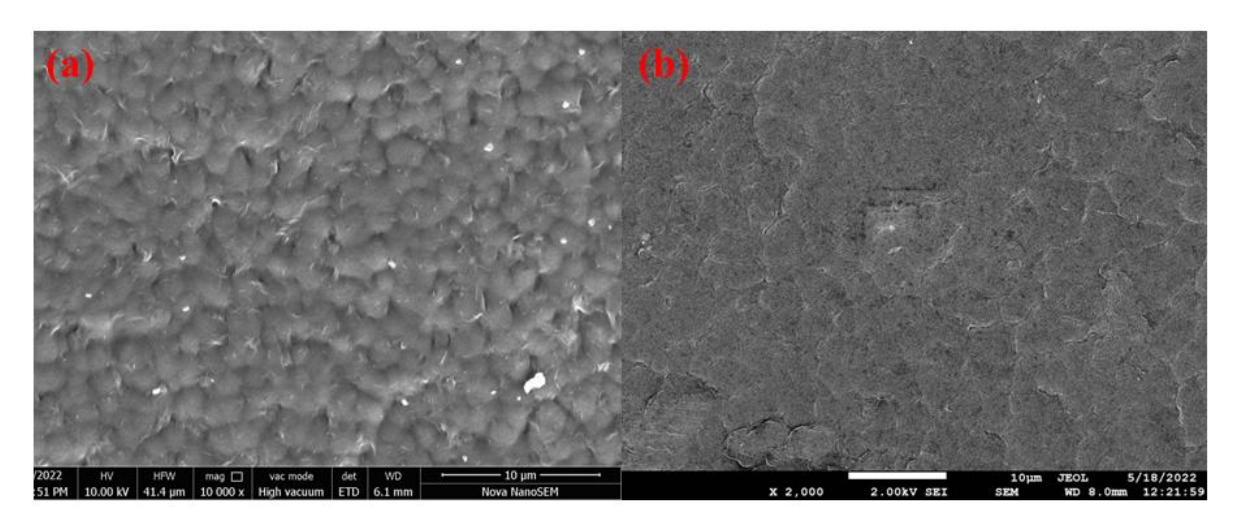


Figure 5.5 SEM surface micrographs of (a) Pure PVDF film and (b) PVDF/ KNNLTS 15 wt.% composite film.

5.3.3 FTIR Analysis of the Pure PVDF Film and PVDF/KNNLTS Composite Film

The FTIR absorption spectra of pure PVDF film and PVDF/KNNLTS 15 wt.% composite film were recorded in the range of 600 - 1500 cm⁻¹ at room temperature and are presented in the Figure 5.6 (a) and (b), respectively. The peaks corresponding to the α phase and β phase of the PVDF are marked in Figure 5.6 [23, 25, 27, 28]. The obtained FTIR data was in agreement with the XRD data depicting the existence of β -phase of the PVDF in pure PVDF film and PVDF/KNNLTS 15 wt.% composite film. The Lambert- Beer law can be used to calculate the quantitative value of the β -phase ($F(\beta)$) by using equation (5.1) [27].

$$F(\beta) = \frac{A_{\beta}}{\binom{K_{\beta}}{K_{\alpha}} A_{\alpha} + A_{\beta}}$$
 (5.1)

where, $K_{\alpha} = 6.1 \text{ x } 10^4 \text{ cm}^2\text{mol}^{-1}$ and $K_{\beta} = 7.7 \text{ x } 10^4 \text{ cm}^2\text{mol}^{-1}$ are the absorption coefficient at 840 cm⁻¹ and 762 cm⁻¹, respectively [29], A_{α} and A_{β} , are the absorbance intensities at 762 cm⁻¹ and 840 cm⁻¹, respectively [23, 30]. The values of $F(\beta)$ of PVDF film and PVDF/KNNLTS 15 wt.% composite film were 43.38 % and 52.5 %, respectively, indicating the enhancement in the β -phase content due to the addition of KNNLTS ceramic powder in the PVDF matrix.

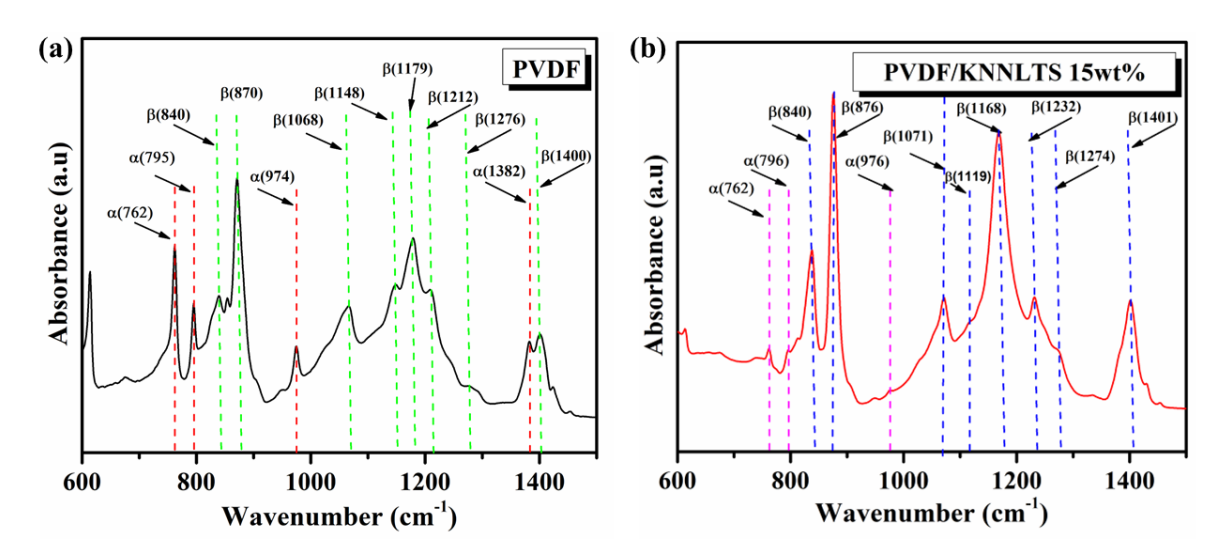


Figure 5.6 FTIR spectra of (a) PVDF film and (b) PVDF/KNNLTS 15 wt.% composite film.

5.3.4 Dielectric Properties of Pure PVDF Film and PVDF/KNNLTS Flexible Composite Film

For studying the electrical properties of the prepared pure PVDF and PVDF/KNNLTS 15 wt.% flexible composite film, dielectric constant (ε_r) was measured as a function of frequency in the range from 50 Hz to 200 KHz at room temperature and corresponding plots are illustrated in Figure 5.7. The dielectric constant of the flexible composite films decreases with increase in the frequency which is attributed to decrease in polarisation with increase in frequency. When frequency is low, different polarisations respond easily, but with increase in frequency, different polarisation mechanisms cease. This results in the decrease of net polarisation of the material, which then leads to decrease of dielectric constant [31]. In addition, the dielectric properties are dependent on the

content of β -phase and the interfacial polarisation taking place due to the addition of KNNLTS ceramic particles in the PVDF matrix. For PVDF/KNNLTS 15 wt.% composite film, ε_r values are 33.56 at 1 KHz, and 29.92 at 10KHz, respectively which is in good accordance with the dielectric constant values reported for KNN-based ceramic composites in the literature [32, 13]. The PVDF/KNNLTS 15 wt.% composite film shows a higher dielectric constant than pure PVDF due to the high dielectric nature of KNNLTS ceramic, interfacial polarisation at the filler–matrix interfaces, and increased β -phase content in PVDF induced by the addition of ceramic particles. These factors enhance the overall polarisation and dielectric response of the composite film [33]. The obtained high value of dielectric constant will lead to enhanced piezoelectric constant and improved piezoelectric performance of the prepared composite film [34].

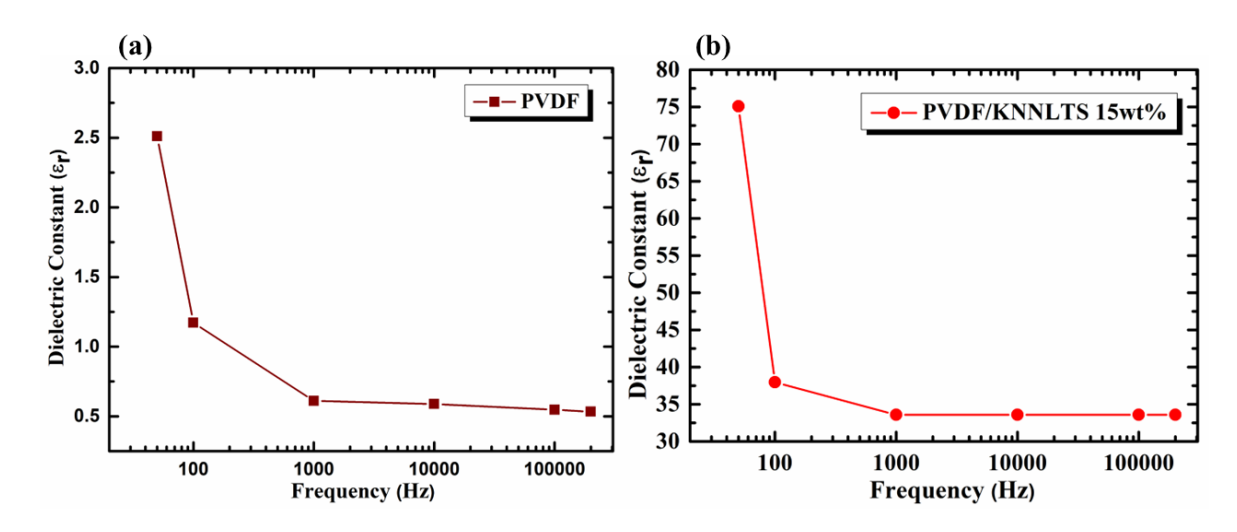


Figure 5.7 Dielectric constant (ε_r) of (a) PVDF, and (b) PVDF/KNNLTS 15 wt.% composite film as a function of frequency.

5.3.5 Polarisation vs. Electric Field (*P-E*) Hysteresis Loops of Pure PVDF Film and PVDF/KNNLTS Flexible Composite Film

The Polarisation vs. Electric Field (*P-E*) hysteresis loop measurement was done for analysing the ferroelectric properties of the prepared pure PVDF film and PVDF/KNNLTS 15 wt.% flexible composite film at room temperature and corresponding plot was shown in Figure 5.8. For tracing the loop, a maximum field of 50 KV/cm was used. PVDF/KNNLTS 15 wt.% flexible composite film demonstrated ferroelectricity; however, even after applying a high electric field of 50 KV/cm to the

composite film, polarisation cannot reach saturation. From the plot it can be seen that the polarisation increases progressively with increase in the applied electric field which is attributed to the better alignment of the electric dipoles at large fields. The measured values of spontaneous polarisation (P_s), remnant polarisation (P_r), and coercive field (E_c) for pure PVDF film were 0.075 μ C/cm², 0.821 μ C/cm², and 0.334 KV/cm, respectively and for PVDF/KNNLTS 15 wt.% were 3.707 μ C/cm², 0.320 μ C/cm² and 2.359 KV/cm, respectively. The higher values obtained for the composite film PVDF/KNNLTS 15 wt.% in comparison to pure PVDF film attributed to the strong piezoelectric nature of KNNLTS, improved β -phase content in PVDF, and better dipole alignment within the composite structure. Furthermore, the obtained values of spontaneous and remnant polarisations in the present work are better than the values reported previously for KNN based composite energy harvester in the literature [35, 32, 17].

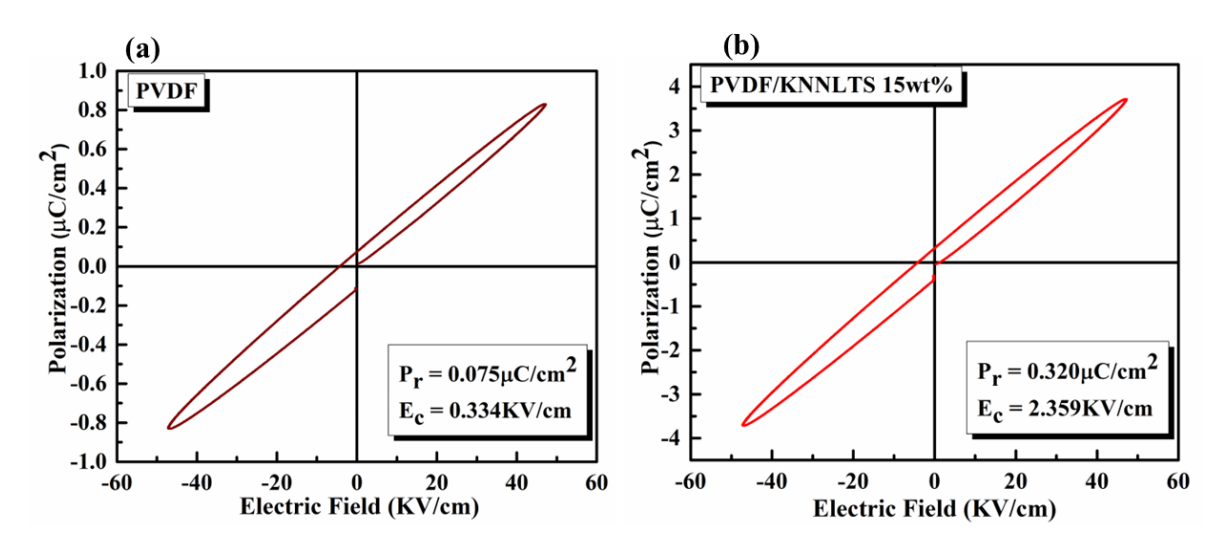


Figure 5.8 Polarisation vs. Electric field (*P-E*) ferroelectric hysteresis loop for (a) PVDF film and (b) PVDF/KNNLTS 15 wt.% composite film at room temperature.

5.3.6 Piezoelectric Performance of PEG Device

The working mechanism of the constructed PEG device is shown in Figure 5.9. Electric dipoles orient themselves in a single direction when a perpendicular force is applied to the device, creating potential differences between the two electrodes. As a result, as shown in Figure 5.9 (a), current flows through an outer circuit from top to bottom electrode. Further, when the applied force on the device is released, the electric dipoles,

Chapter 5: Effect of Li, Ta and Sb doping on the output performance of KNN/PVDF based flexible piezoelectric generator

causing the current to flow from bottom to the top electrode, as presented in Figure 5.9 (b).

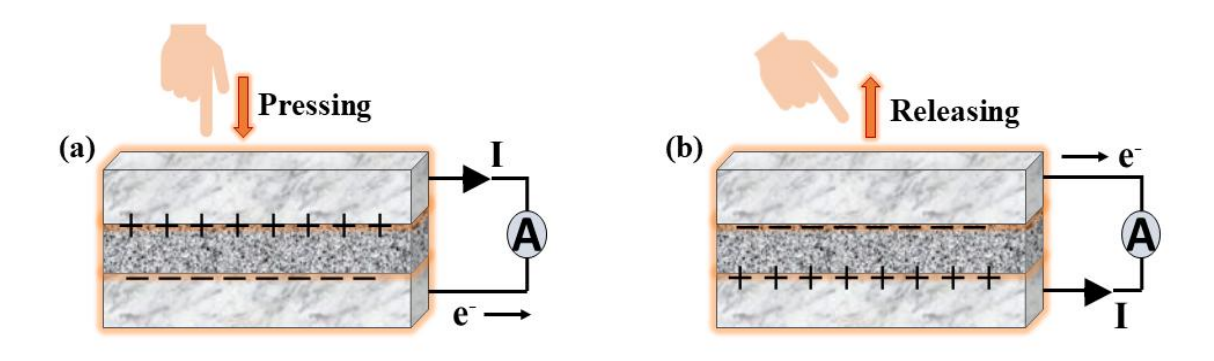


Figure 5.9 Working Mechanism of PEG device.

The open circuit output voltage of the constructed PVDF/KNNLTS PEG device with dimensions of the order of 2 cm x 2 cm was measured by applying a force on the surface of the device using vibrator shaker. When pressure is applied to the device's surface, a potential difference develops across the generator which is then measured by the digital storage oscilloscope. Figure 5.10 and Figure 5.11 illustrate the plot of the open-circuit voltage and short-circuit current generated by the constructed PEG using pure PVDF film and PVDF/KNNLTS 15 wt.% composite film. The maximum peak-to-peak open-circuit voltage (*V*_{P-P}) for the pure PVDF and PVDF/KNNLTS 15 wt.% based PEG were 8.90 V and 36.58 V, respectively showing that addition of KNNLTS in the PVDF matrix, has led to fourfold enhancement in the peak-to-peak open circuit voltage of the PEG device. In addition, the maximum peak-to-peak short-circuit current for the pure PVDF and PVDF/KNNLTS 15 wt.% based PEG were 1.02 μA and 5.04 μA, respectively.

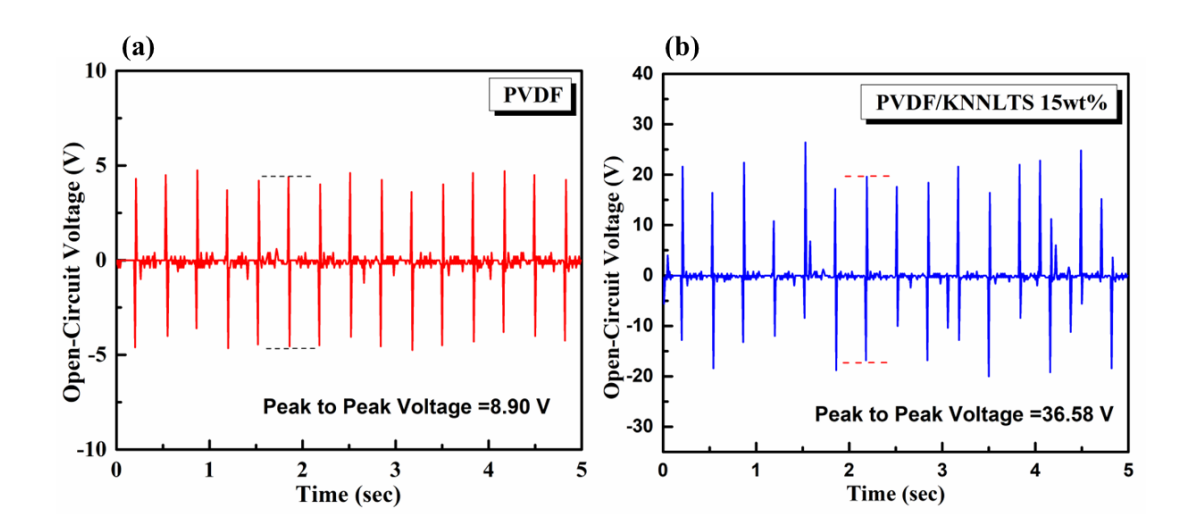


Figure 5.10 Open-circuit voltage generated using (a) PVDF and (b) PVDF/KNNLTS 15 wt.% PEG devices.

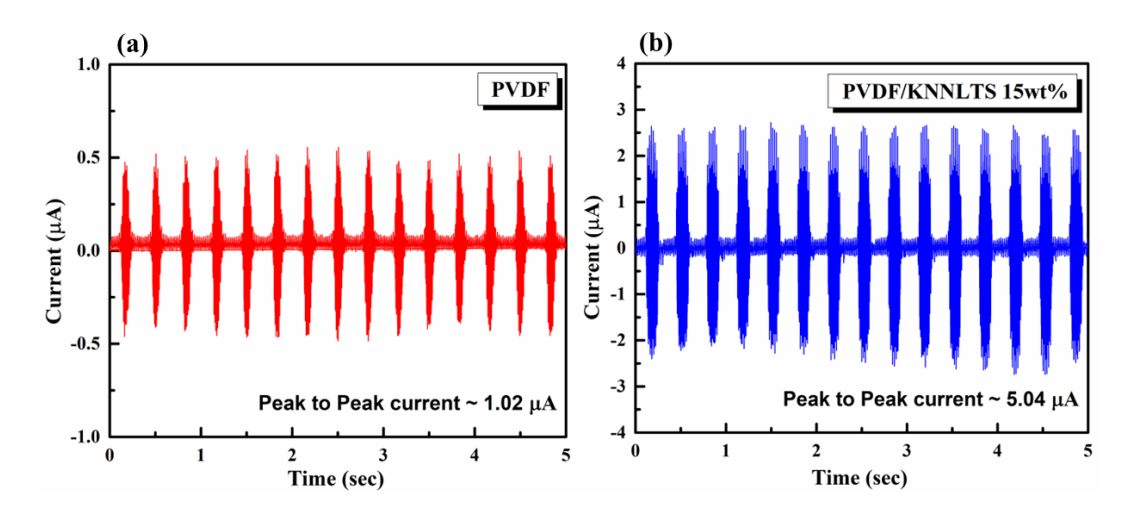


Figure 5.11 Short-circuit current generated using (a) PVDF and (b) PVDF/KNNLTS 15 wt.% PEG devices.

Furthermore, the output power of the fabricated PEG device was also analysed by applying different load resistances in the range $10~M\Omega$ to $100~M\Omega$ and corresponding plots are shown in the Figure 5.12. From the Figure 5.12 (a) and (b) it can be seen that as load resistance increased the voltage drop also increased while the current was decreased with increase in load resistance. The maximum value of output power obtained was around $135.42~\mu W$ for PVDF/KNNLTS 15 wt.% PEG device at a load

resistance of $10 \text{ M}\Omega$. Table 5.1 presents the comparison of the parameters between the PEG device developed in present work with the other reported PEG devices.

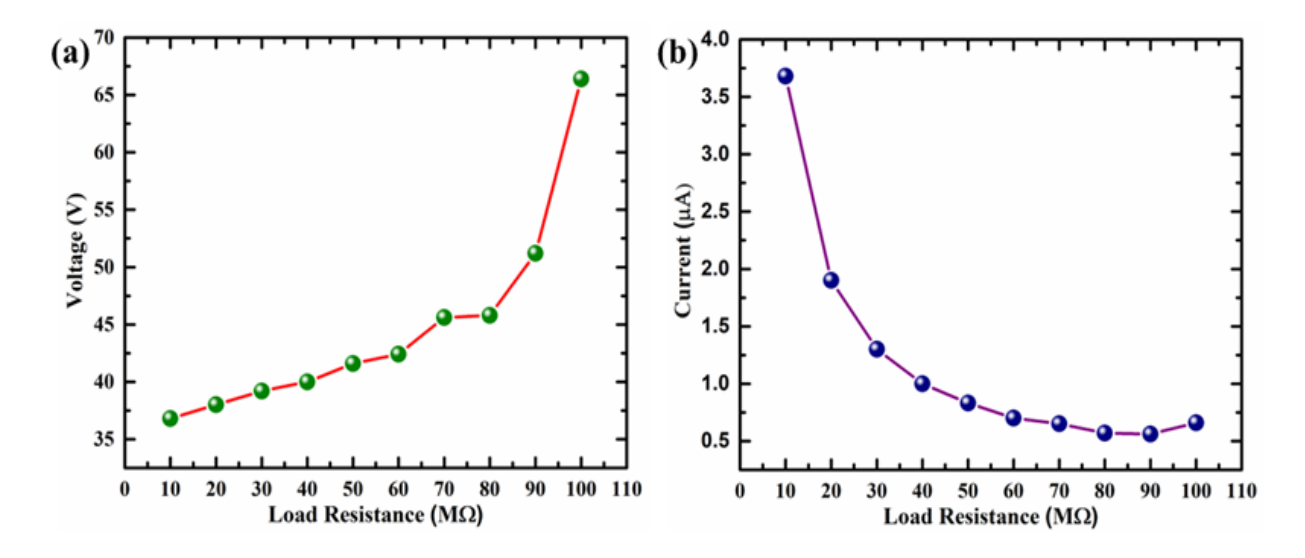


Figure 5.12 Variation in (a) Voltage and (b) Current by varying the load resistance from 10 M Ω to 100 M Ω for PVDF/KNNLTS 15 wt.% PEG device.

Table 5.1 Comparison of the piezoelectric performance of the PEG device developed in present work with other reported PEG devices.

S. No.	Filler material in the Polymer Matrix	Polymer used	Film Synthesis Method	V _{oc} (V)	<i>I_{sc}</i> (μA)	Power / Power Density	Ref.
1.	KNN nano blocks	PVDF	Hot-Injection	2.1	0.042	32.67 mW/cm ²	[13]
2.	KNN nanorods	PVDF	Drop-casting	3.4	0.100		[35]
3.	KNN-BiScO ₃ ceramic particles	Polyimide	Drop-casting	4 V	0.24		[36]
4.	KNN nanofibre	PVDF	Electro- spinning	1.9			[37]

Chapter 5: Effect of Li, Ta and Sb doping on the output performance of KNN/PVDF based flexible piezoelectric generator

5.	KNN nanofibre	PVDF	Melt-spinning	17.5	0.522		[38]
6.	KNN/ZnO nanorods	PVDF	Electro- spinning	25	1.81	11.31 μW/cm ²	[39]
7.	KNN/CNT	PVDF	Electro- spinning	23.24	9	52.29 μW/cm ²	[40]
8.	KNN-ZS nano fibre	PVDF	Electro- spinning	25	2.11		[41]
9.	NKNS-LT- BZ nanoparticles	PVDF	Electro- spinning	18	2.6		[18]
10.	BaTiO ₃ Nanoparticles	PVDF	Spin-coating	6.7	2.4		[42]
11.	NBT-BT Nanoparticles	PVDF	Hot-Pressing	9		81 μW	[43]
12.	KNNLTS ceramic particles	PVDF	Drop-casting	36.58 V	5.04	135.42 μW	Present Work

Furthermore, the presence of piezoelectricity in the prepared PVDF/KNNLTS 15 wt.% composite film was analysed by measuring the inverse piezoelectric coefficient (d_{33}^*) . In the present work, the converse piezoelectric coefficient was measured by recording the Displacement -Voltage (D-V) hysteresis loop at room temperature and corresponding plot is presented in Figure 5.13. The measured loop for the composite

film resembles the shape of a butterfly. The value of d_{33}^* is obtained from the slope of the butterfly curve [44, 45].

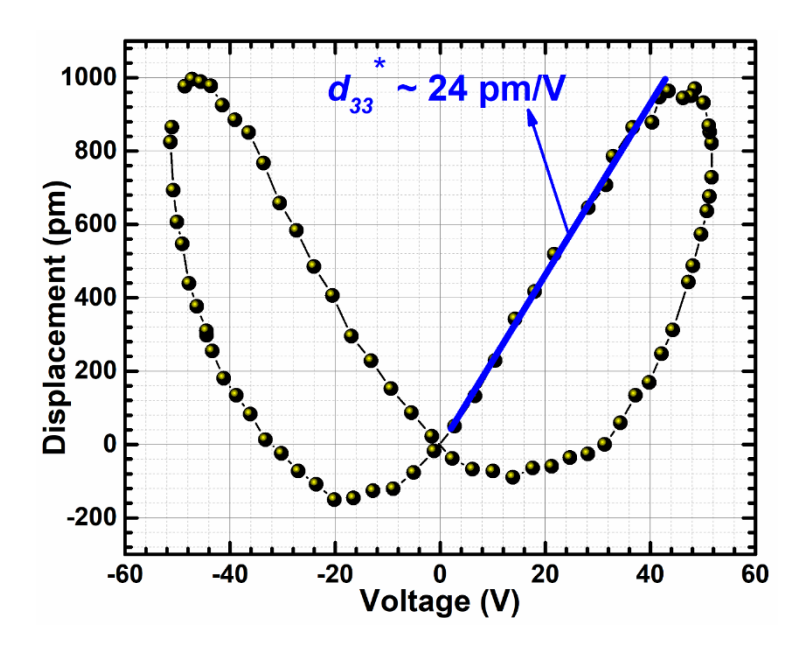


Figure 5.13 Displacement vs. Voltage (*D-V*) butterfly curve for PVDF/KNNLTS 15 wt.% composite film.

5.3.7 Energy Harvesting Performance of PEG Device

To demonstrate the ability of the fabricated PEG device in real time applications, the device was placed at different positions on hand to harvest mechanical energy. Figure 5.14 shows the PVDF/KNNLTS 15 wt.% PEG device employed to harvest mechanical energy from human body motions such as fist beating, elbow bending, (quenching and fist opening). The maximum open circuit voltages obtained by fist beating, elbow bending and (quenching and fist opening) were 5.48 V, 4.12 V and 1.72 V, respectively. In addition, the generated output voltage using PVDF/KNNLTS 15 wt.% PEG device was enough to light up 11 light-emitting diodes (LEDs) as shown in Figure 5.14 (d).

Chapter 5: Effect of Li, Ta and Sb doping on the output performance of KNN/PVDF based flexible piezoelectric generator

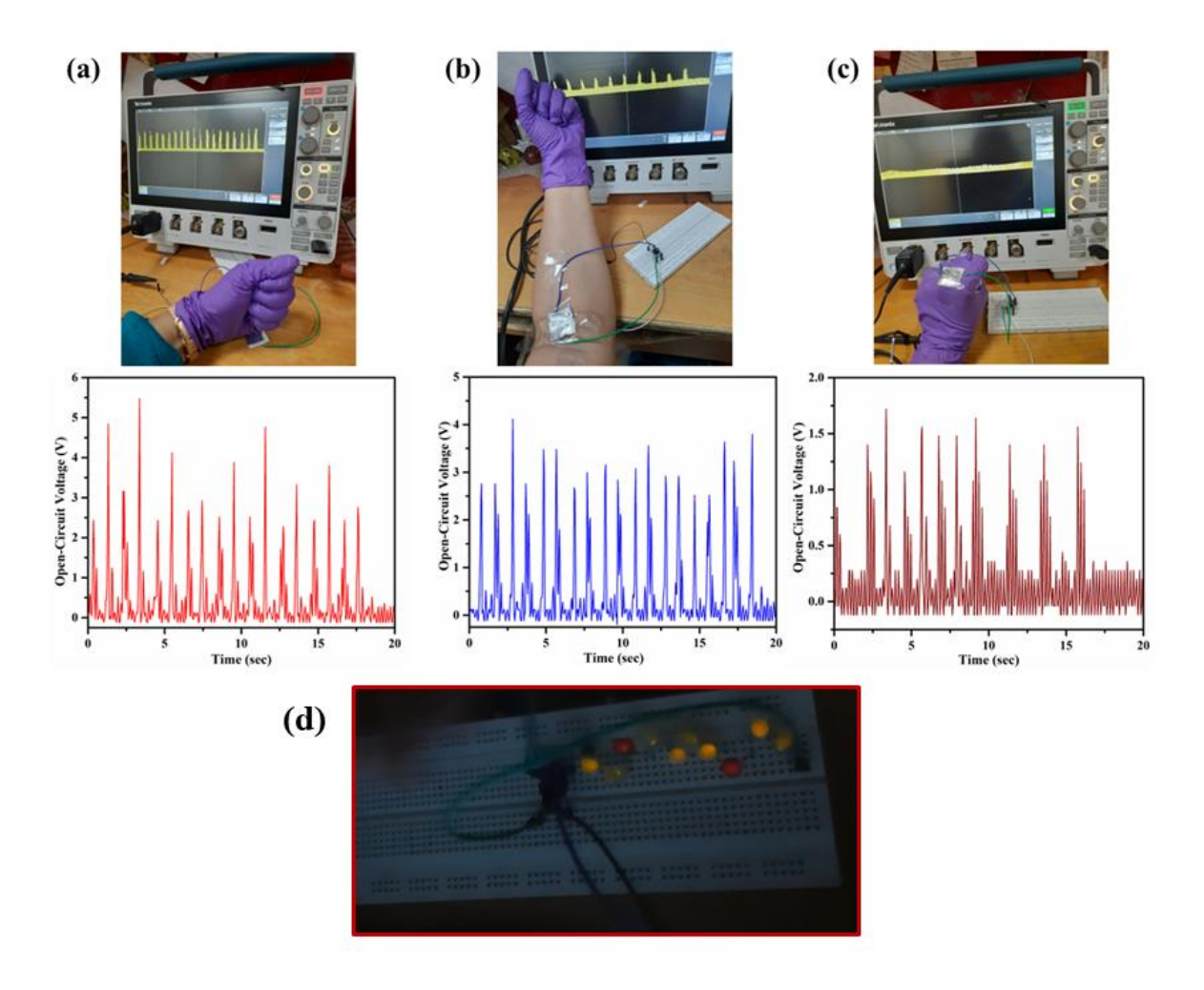


Figure 5.14 The generated open-circuit voltage using PEG device containing 15 wt.% KNNLTS ceramic particles in the PVDF matrix for (a) fist beating, (b) elbow bending, (c) quenching, and fist opening and (d) Glowing LEDs.

5.4 Conclusion

In this chapter, flexible PEGs based on (Li, Ta, Sb) modified (K, Na) NbO₃ (KNNLTS)/poly (vinylidene fluoride) (PVDF) flexible composite film and pure PVDF film were fabricated. The concentration of KNNLTS was fixed to 15 wt.% in the PVDF matrix. For the PVDF/ KNNLTS 15 wt.% composite film, the dielectric constant (ε_r) was measured as 33.56 at 1 KHz and 29.92 at 10 KHz. Additionally, the remnant polarisation (P_r) and maximum polarisation (P_s) were recorded as 0.32 μ C/cm² and 3.70 μ C/cm², respectively for the composite film. These values were significantly higher compared to pure PVDF film. The maximum value of inverse piezoelectric charge coefficient (d_{33}^*) for the same composite film were measured as ~ 24 pm/V.

Furthermore, the maximum generated peak to peak open circuit voltage and short-circuit current for the PVDF/KNNLTS 15 wt.% composite film-based generator were 36.58 V and 5.04 μA, respectively which were higher than the voltage and current obtained using pure PVDF film-based generator. The performance of the PEG was also tested under different human body motions. The output voltages for fist beating, elbow bending, quenching and fist opening were 5.48 V, 4.12 V and 1.72 V, respectively. The fabricated PEG demonstrated practical applicability by successfully lighting 11 LEDs. The present chapter demonstrated that high performance PEG can be developed by modifying KNN ceramics by suitable dopants.

References

- [1] H. Li, M. Li, X. Jiang, C. Zhu, H. Wang, A. Deng, G. Zang, Y. Gu, Materials Lab, 3, (2024), 230019
- [2] L. Wu, J.L. Zhang, C.L. Wang, J.C. Li, Journal of Applied Physics, 103, (2008), 084116
- [3] Y. Zhou, J.L. Yu, M. Guo, M. Zhang, Ferroelectrics, 404, (2010), 69
- [4] T.-Y. Ke, H.-A. Chen, H.-S. Sheu, J.-W. Yeh, H.-N. Lin, C.-Y. Lee, H.-T. Chiu, Journal of Physical Chemistry C, 112, (2008), 8827–8831
- [5] Y. Shiratori, A. Magrez, W. Fischer, C. Pithan, R. Waser, The Journal of Physical Chemistry C, 111, (2007), 18493–18502
- [6] B. Sharma, R. Gupta, A. Sharma, A. Chowdhuri, M. Tomar, Materials Today Communications, 44, (2025), 112140
- [7] Y. Guo, K-I. Kakimoto, H. Ohsato, Applied Physics Letters, 85, (2004), 4121-4123
- [8] G-Z. Zang, J-F. Wang, H-C. Chen, W-B. Su, C-M. Wang, P. Qi, B-Q. Ming, J. Du, L-M. Zheng, Applied Physics Letters, 88, (2006), 212908
- [9] E. Hollenstein, M. Davis, D. Damjanovic, N. Setter, Applied Physics Letters, 87 (18), (2005), 182905
- [10] Y. Chang, Z.-P. Yang, D. Ma, Z. Liu, Z. Wang, Journal of Applied Physics, 104 (2), (2008), 024109
- [11] J. Zhang, X. Zong, L. Wu, Y. Gao, P. Zheng, S. Shao, Applied Physics Letters, 95 (2), (2009), 022909

Chapter 5: Effect of Li, Ta and Sb doping on the output performance of KNN/PVDF based flexible piezoelectric generator

- [12] Y. Satio, H. Takao, T. Tani, T. Nonoyama, K. Takatori, T. Homma, Nature, 423, (2004), 84
- [13] Y. Gao, J. Zhang, Y. Qing, Y. Tan, Z. Zhang, X. Hao, Journal of American Ceramic Society, 94, (2011), 2968
- [14] Y-G. Lv, C-L. Wang, J-L. Zhang, L. Wu, M-L. Zhao, J-P. Xu, Materials Research Bulletin, 44, (2009), 284
- [15] B-Q. Ming, J-F. Wang, P. Qi, G-Z. Zang, Journal of Applied Physics, 101, (2007), 054103
- [16] K. Wang, J-F. L, Journal of American Ceramic Society, 93, (2010), 1101
- [17] Y. Huan, T. Wei, Z. Wang, H. Shen, X. Lin, S. Huang, Journal of Materiomics, 6, (2020), 355
- [18] C. Zhang, Y. Fan, H. Li, Y. Li, L. Zhang, S. Cao, ACS Nano, 12, (2018), 4803
- [19] M-K. Gupta, S-W. Kim, B. Kumar, ACS Applied Materials & Interfaces, 8, (2016), 1766
- [20] A. Ichangi, V-V. Shvartsman, D-C. Lupascu, K. Le, M. Grosch, A.K.S- Verma, C. Bohr, A. Verma, T. Fischer, S. Mathur, Journal of European Ceramic Society, 15 (41), (2021), 7662-7669
- [21] S. Dwivedi, T. Pareek, S. Kumar, RSC Advances 8, (2018), 24286
- [22] M-H. Zhang, K. Wang, J-S. Zhou, J-C. Chu, X. Lv, Acta Materials, 122, (2017),344
- [23] B. Jaleh, A. Jabbari, Applied Surface Science, 20, (2014), 339
- [24] P. Devi, K. Ramachandran, Journal of Experimental Nanoscience, 6, (2011), 281
- [25] H-J. Hwang, J-H. Yang, S-C. Kang, C. Cho, C-G. Kang, Y-G. Lee, Microelectronic. Engineering, 109, (2013), 87
- [26] Y. Li, X. Su, K. Liang, C. Luo, P. Li, J. Hu, Microelectronic Engineering, 244-246, (2021), 111557
- [27] A. Bhatt, V. Singh, P. Bamola, D. Aswal, S. Rawat, S. Rana, Journal of Alloys and Compounds, 960, (2023), 170664.

Chapter 5: Effect of Li, Ta and Sb doping on the output performance of KNN/PVDF based flexible piezoelectric generator

- [28] N. Soin, D. Boyer, K. Prashanth, S. Sharma, A-A. Narasimulu, J. Luo, Chemical Communications, 51 (39), (2015), 8257
- [29] R-S. Sabry, A-D. Hussein, Polymer Testing, 79, (2019), 106001
- [30] J-S. Lee, K-Y. Shin, O-J. Cheong, J-H. Kim, J. Jang, Journal of Scientific Reports, 5, (2015), 7887
- [31] M. Chandrasekhar, P. Kumar, Ceramic International, 41, (2015), 5574
- [32] Z. Mirzazadeh, Z. Sherafat, E. Bagherzadeh, Ceramic International, 47, (2021), 6211
- [33] Y. Huan, X. Wang, L. Li, J. Koruza, Applied Physics Letters, 107, (2015), 202903.
- [34] V. Jella, S. Ippili, J-H. Eom, J. Choi, S-G. Yoon, Nano Energy, 53, (2018), 46
- [35] S. Bairagi and S-W. Ali, Organic Electronics, 78, (2020), 105547
- [36] D-Y. Hyeon, G-J. Lee, S-H. Lee, J-J. Park, S. Kim, M. Lee, Composites Part B: Engineer, 234, (2022), 109671
- [37] A. Teka, S. Bairagi, Md. Shahadat, M. Joshi, S-Z. Ahammad, S-W. Ali, Polymers for Advanced Technology, 29, (2018), 2537-2544
- [38] S, Bairagi, S-W. Ali, Energy Technology, 7, (2019), 1900538
- [39] S. Bairagi, S-W. Ali, International Journal of Energy Resources, 44 (7), (2020)
- [40] S. Bairagi, S-W. Ali, Soft Matter, 16, (2020), 4876
- [41] S. Banerjee, S. Bairagi, S-W. Ali, Energy, 244, (2022), 123102
- [42] P. Hu, L. Yan, C. Zhao, Y. Zhang, J. Niu, Composites Science and Technology, 168, (2018), 327
- [43] M-V. Petrovic, F Cordero, E. Mercadelli, E. Brunengo, N. Ilic, C. Galassi, Journal of Alloys and Compounds, 884, (2021), 161071
- [44] N. Sinha, S. Goel, A-J. Joseph, H. Yadav, K. Batra, M-K. Gupta, B. Kumar, Ceramic International, 44, (2018), 8582
- [45] S. Goel, N. Sinha, H. Yadav, A-J. Joseph, B. Kumar, Physica E: Low-Dimensional Systems and Nanostructures, 91, (2017), 72

Chapter 6

Effect of KNNLTS concentration and conductive filler (MWCNT) in realizing high performance PVDF/KNNLTS/MWCNT flexible piezoelectric nanogenerator for powering electronics devices

Chapter 6 Effect of KNNLTS concentration and conductive filler (MWCNT) in realizing high performance PVDF/KNNLTS/MWCNT flexible piezoelectric nanogenerator for powering electronics devices

This chapter focuses on the development of PVDF/KNNLTS/MWCNT-based piezoelectric energy harvester devices. KNNLTS nanoparticles were synthesized using a high-energy ball milling process, while multi-walled carbon nanotubes (MWCNTs) were procured from Sigma-Aldrich. Both KNNLTS nanoparticles and MWCNTs were incorporated into the PVDF polymer matrix to enhance overall piezoelectric performance of the PENG device. MWCNTs, known for their excellent electrical conductivity, also promote the formation of the electroactive β -phase in PVDF by acting as an effective nucleating agent, thereby enhancing the piezoelectric response of the composite. The combined incorporation of KNNLTS ceramic nanoparticles and MWCNTs into the PVDF matrix significantly improves the overall piezoelectric performance of the piezoelectric nanogenerator (PENG) device, making it a promising candidate for energy harvesting applications.

6.1 Introduction

Advancements in flexible and high-performance piezoelectric nanogenerators (PENGs) have highlighted the importance of optimizing material properties through innovative compositional design. Recent approaches focus on combining ceramic and functional nanofillers in the polymer matrix to achieve superior energy harvesting performance while maintaining flexibility and environmental safety. Based on the data presented in Chapter 5, the constructed KNNLTS/PVDF-PEG device demonstrated superior piezoelectric performance compared to the KNN/PVDF-based PEG device. In this chapter, KNNLTS has been used as filler material in the PVDF matrix. Additionally, MWCNTs have also been introduced as functional nanofiller alongside KNNLTS in the PVDF matrix to improve the overall performance of the constructed PENG device.

Liu *et al.* developed a sensing device based on a PVDF/MWCNT composite nanofiber array using the electrospinning method. They reported that the device generated a peak voltage of 20.2 mV and a current of 39 nA under a 6 Hz vibration. In addition, at an impact testing at 15 Hz, the peak voltage of 24.4 mV with a current of 130 nA can be

obtained [1]. In a notable study, Pal *et al.* fabricated PVDF/PLZT/MWCNT composite films using the tape-casting technique followed by hot press. They found that the incorporation of MWCNTs significantly improved the electrical performance of the PVDF/PLZT system. The resulting film was capable of charging a 40 µF capacitor up to 8 V and the stored energy (~2 mW) was sufficient to power around 50 light emitting diodes (LEDs) [2].

Sun et al. fabricated PVDF/ZnO/MWCNT composite piezoelectric films and developed a flexible sensor for human motion monitoring. The sensor exhibited optimal piezoelectric performance with 0.5 wt.% MWCNT and maintained good stability after 6000 seconds of cyclic vibrations. These results indicated that the prepared flexible piezoelectric sensors had great potential for application in the field of human motion monitoring [3]. Lin et al. developed a piezoelectric film based on MWCNT-BaTiO₃/PVDF composites and demonstrated that the incorporation of MWCNTs into the BaTiO₃/PVDF composite enhanced the performance of the flexible piezoelectric nanogenerator, increasing the open-circuit voltage to 11.4 V, achieving a maximum power output of 8.67 W and a power density of 1.16 W/cm². This output was sufficient to simultaneously light up eight LEDs [4]. Furthermore, Zhu et al. developed a flexible energy harvester by integrating a hybrid triboelectric and piezoelectric nanogenerator based on MWCNTs into a PDMS polymer matrix. They found that the piezoelectric and triboelectric components could generate peak-to-peak voltages of 6.5 V and 30 V, respectively, at a frequency of 5 Hz. The triboelectric nanogenerator achieved a maximum output power of approximately 3.4 µW under a matching resistance of 15 M Ω [5]. Shipu *et al.* constructed a flexible piezoelectric nanogenerator (PENG) using a BaTiO₃/MWCNT/PDMS composite and obtained an output voltage of ~8 V which shows an increase of about 16% in comparison to the PENG constructed without incorporating MWCNT. Additionally, the device was able to effectively charge a 0.1 µF capacitor, achieving a voltage rise of 6.3 V. These findings highlight the device's promising potential as a lead-free PENG for widespread application [6].

Based on the above literature, in the present work lead-free and environmentally friendly flexible PVDF/KNNLTS/MWCNT nanocomposite films have been fabricated for energy harvesting applications. To do this, KNNLTS was synthesised by a solid-

state reaction method followed by a high-energy ball mill process. Different kinds of nanocomposite films (Pure PVDF, PVDF/KNNLTS, PVDF/10%KNNLTS/MWCNT, PVDF/15%KNNLTS/MWCNT, PVDF/20%KNNLTS/MWCNT, and PVDF/25%KNNLTS/MWCNT) have been synthesized and tested. The PENG constructed with PVDF/20% KNNLTS/MWCNT nanocomposite film showed a significantly improved piezoelectric performance in comparison to other PENGs with an open circuit voltage, short circuit current and power density of 87.2 V, 20.3 μ , and 145.48 μ W/cm², respectively. Overall, the fabricated nanocomposite film has shown the potential for developing a PENG device for energy harvesting application due to the combined effect of adding KNNLTS and MWCNT into the PVDF matrix.

6.2 Experimental Section

6.2.1 Materials

Poly (vinylidene fluoride) (PVDF: $M_w = 263000 \text{ g mol}^{-1}$) powder was purchased from Alfa-Aesar. N, N dimethylformamide (DMF, 99% purity) was procured from Thermo Fischer, respectively. Sodium carbonate (Na₂CO₃, 99.8%), potassium carbonate (K₂CO₃, 99%), niobium oxide (Nb₂O₅, 99%), lithium carbonate (Li₂CO₃, 99%), tantalum oxide (Ta₂O₅, 99.95%), and antimony oxide (Sb₂O₅, 99%) raw ingredients acquired Alfa for were from Aesar the synthesis of (K_{0.45}Na_{0.55})_{0.98}Li_{0.02}(Nb_{0.77}Ta_{0.18}Sb_{0.05}) O₃ (KNNLTS) ceramic powder. Multi-walled carbon nanotubes (>98%) were procured from Sigma Aldrich. All the materials listed above were used as received without any further purification.

6.2.2 Synthesis of KNNLTS Nanoparticles

KNNLTS particles were synthesized by using solid-state reaction route. All the raw materials were taken in stoichiometric ratio and mixed together in a ball mill using propanol as a liquid medium for 10 hours. The obtained slurry was then dried for 24 hours at 65 °C in a hot air oven. After drying, the powder was calcined in the furnace at 900 °C for 4 hours in order to get KNNLTS ceramic powder. Now, KNNLTS ceramic powder was further grounded by using a high-energy ball mill (Retsch PM100 planetary high energy ball mill). The weight ratio between the raw materials and milling balls was maintained at 1:5. The KNNLTS calcined powder was milled at a speed of 400

rpm for a fixed duration of 20 hours. Figure 6.1 illustrates the synthesis of KNNLTS nanoparticles via solid-state reaction method followed by a high energy ball mill.

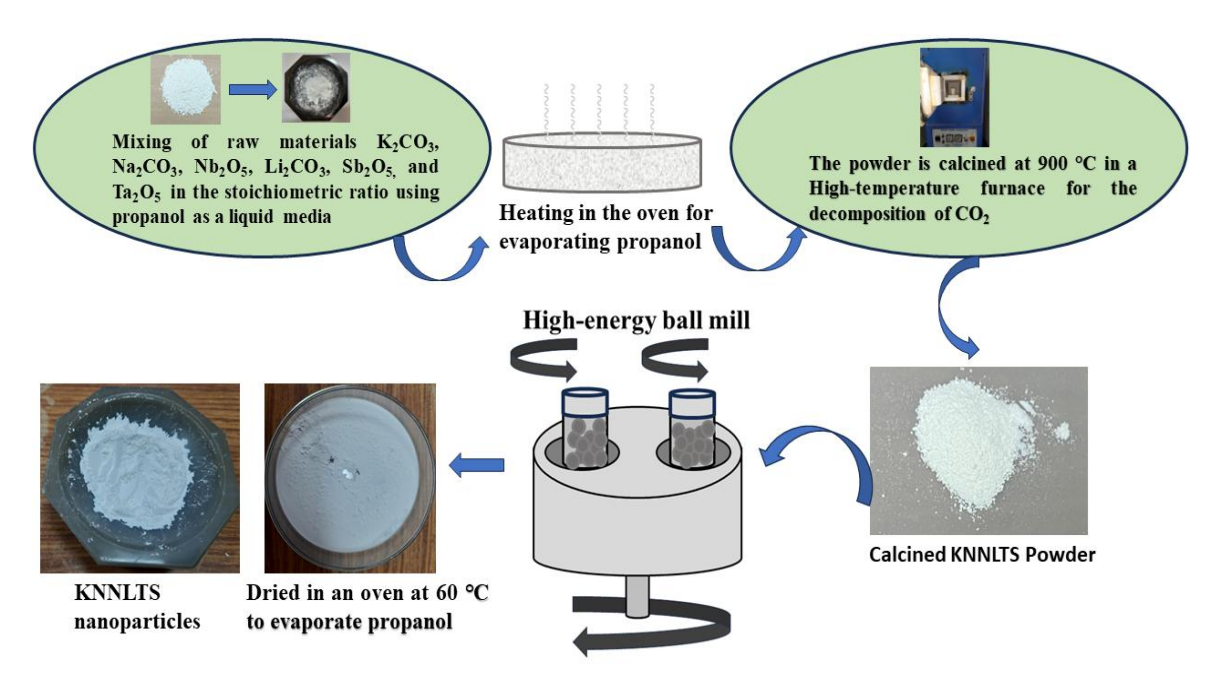


Figure 6.1 Synthesis of KNNLTS nanoparticles via solid-state reaction method followed by high energy ball mill.

6.2.3 Development of Nanocomposite Films based on PVDF/KNNLTS/MWCNTs

To develop the flexible PVDF/KNNLTS/MWCNTs nanocomposite films - 1 gm PVDF powder was first dissolved in a 10 ml DMF solution with continuous stirring at 50 °C until a transparent clear solution was obtained. Then KNNLTS and MWCNT were added into DMF as listed in Table 6.1. It can be seen from Table 6.1, that the content of KNNLTS is varied in the PVDF matrix whereas the amount of MWCNTs was kept fixed. Further, the solution containing KNNLTS and MWCNTs were added into the PVDF solution, with stirring continuously using a magnetic stirrer for 10 hours. After that, the mixture was ultrasonicated for 30 minutes at room temperature to prepare a uniform mixture of PVDF/KNNLTS/MWCNTs. The obtained uniform solutions with varying KNNLTS amounts were poured onto the petri dish and kept in the oven for drying at 80 °C. After this process, flexible PVDF/KNNLTS/MWCNTs nanocomposite films were finally peeled off from the petri dish. For comparison, films of pure PVDF

and PVDF/KNNLTS are also prepared by using a similar method. The detailed synthesis process is shown in Figure 6.2.

Table 6.1 Details of the weight (gm) of PVDF, KNNLTS and MWCNT & volume (ml) of the DMF used in the fabricated flexible nanocomposite films.

S. No.	Sample ID	Amount (gm)			Volume (ml)
		PVDF	KNNLTS	MWCNT	DMF
1.	PVDF	1	0	0	10
2.	PVDF/0%KNNLTS/MWCNT	1	0.00	0.005	10
3.	PVDF/10%KNNLTS/MWCNT	0.9	0.10	0.005	10
4.	PVDF/15%KNNLTS/MWCNT	0.85	0.15	0.005	10
5.	PVDF/20%KNNLTS/MWCNT	0.80	0.20	0.005	10
6.	PVDF/25%KNNLTS/MWCNT	0.75	0.25	0.005	10

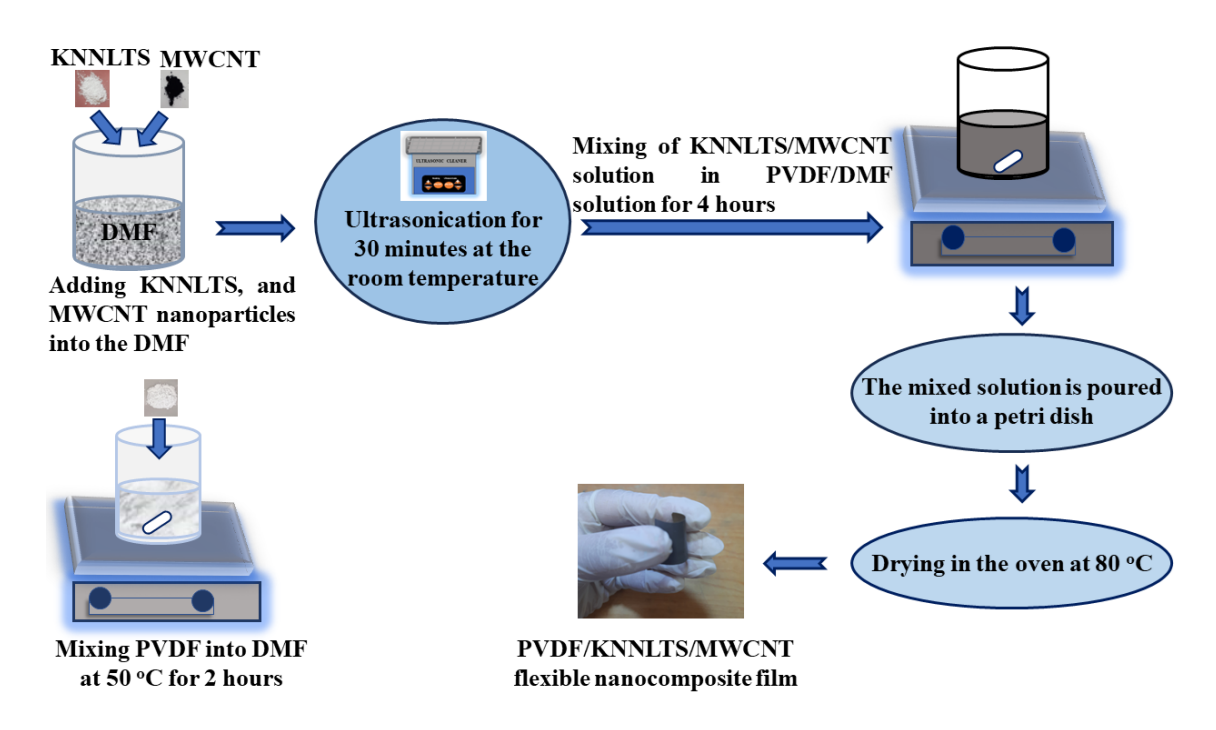


Figure 6.2 Synthesis of PVDF/KNNLTS/MWCNTs flexible nanocomposite films.

6.2.4 Fabrication of Piezoelectric Nanogenerator using the PVDF/KNNLTS/MWCNTs Nanocomposite Films

The developed PVDF/KNNLTS/MWCNTs nanocomposite films were first cut into 1.5 X 1.5 cm². After that, the conductive aluminium tape was attached on both sides of the nanocomposite film, which serves as electrode material. For electrical connections, copper wires were attached to top and bottom electrodes to form the complete device. As seen in Figure 6.3 (b), the entire assembly was then wrapped with Kapton tape to shield it from the environment.

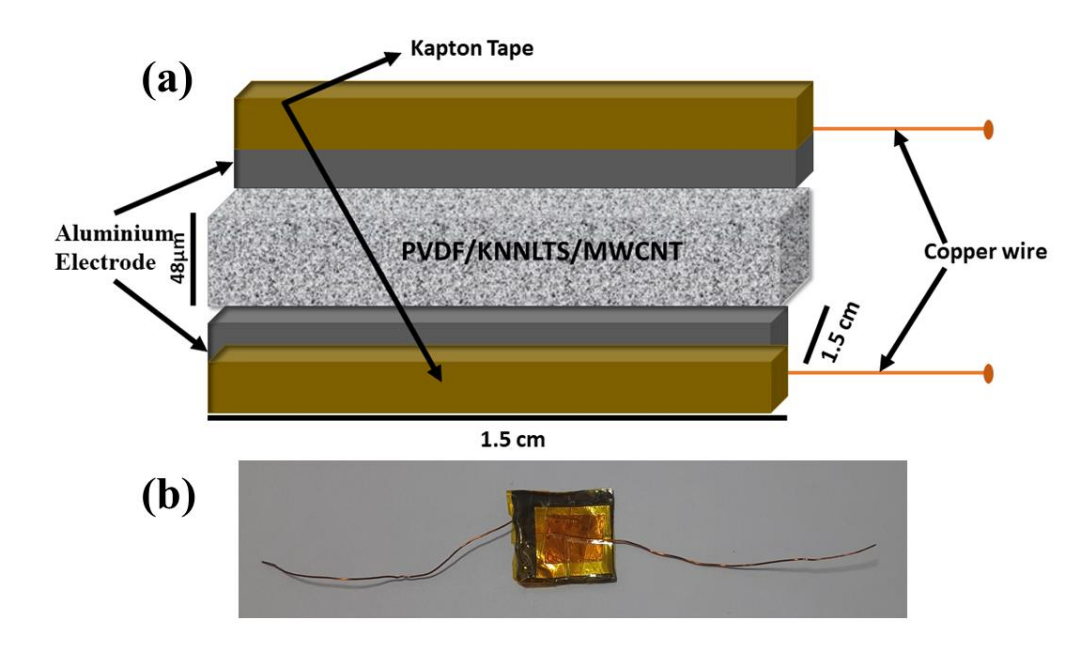


Figure 6.3 (a) Schematic diagram of the fabricated PENG device and (b) Digital photograph of piezoelectric nanogenerator.

6.2.5 Characterizations

To analyse the crystalline structure of the prepared KNNLTS nanoparticles and nanocomposite films, X-ray Diffraction (XRD; Rigaku, Ultima-IV) with Cu- $K\alpha$ radiation source (1.54 Å) was used. The morphology of the developed nanocomposite films was analyzed by scanning electron microscopy (SEM, USIC). Fourier Transform Infrared spectroscopy (FTIR) (Perkin Elmer FTIR spectrum-II) was used to analyse the formation of the β phase in the nanocomposite films. Furthermore, the dielectric measurement as a function of frequency was carried out using a KEYSIGHT Impedance Analyzer E4990A (20Hz- 10MHz) at room temperature. For testing the

piezoelectric output performance of the fabricated PENG devices force was applied on the surface of the device using an electrodynamic shaker (Micron 0020). The generated output voltage and current were measured by using a digital storage oscilloscope (DSO; Tektronix, MDO500) and the Electrometer (Keysight B2902B), respectively. The power output of the nanocomposite-based PENG device was also determined by varying the external load resistance. Inverse Piezoelectric coefficient (d_{33})* value of the nanocomposite film was recorded using the Strain Measurement System of Radiant Precision LCII Ferroelectric tester (Model No. P-HVi210KSC). Finally, to demonstrate the practical applicability of the fabricated PENG device, various human body movements-such as finger tapping, thumb pressing, fist beating, elbow tapping, elbow bending, and wrist stretching were performed after attaching the fabricated PENG device to the body to successfully harvest mechanical energy.

6.3 Results and Discussions

6.3.1 Structural and Microstructural Analysis of KNNLTS Nanoparticles

X-ray Diffraction (XRD) was utilized to analyse the crystal structural of calcined KNNLTS powder and the corresponding plot was displayed in Figure 6.4. The KNNLTS powder clearly exhibits a perovskite structure. The XRD plot shows no extra peak, indicating that the KNNLTS powder has been successfully synthesized without any impurities by solid-state conventional route followed by high-energy ball mill. In the XRD pattern of KNNLTS powder shown in Figure 6.4, peak splitting around ~ 45° can be noticed with peak intensity ratio of (002) and (200) approaches to 1:1 suggesting the presence of coexistence of the orthorhombic and tetragonal phases. The XRD pattern is indexed according to the JCPDS card numbers 71-2171 (orthorhombic) and 77-0037 (tetragonal) [7].

Further, a SEM analysis was performed on the synthesized KNNLTS powder to analyze its morphology and the resulting picture is shown in Figure 6.5. The scan revealed that the KNNLTS particles exhibit square or rectangular shaped particles.

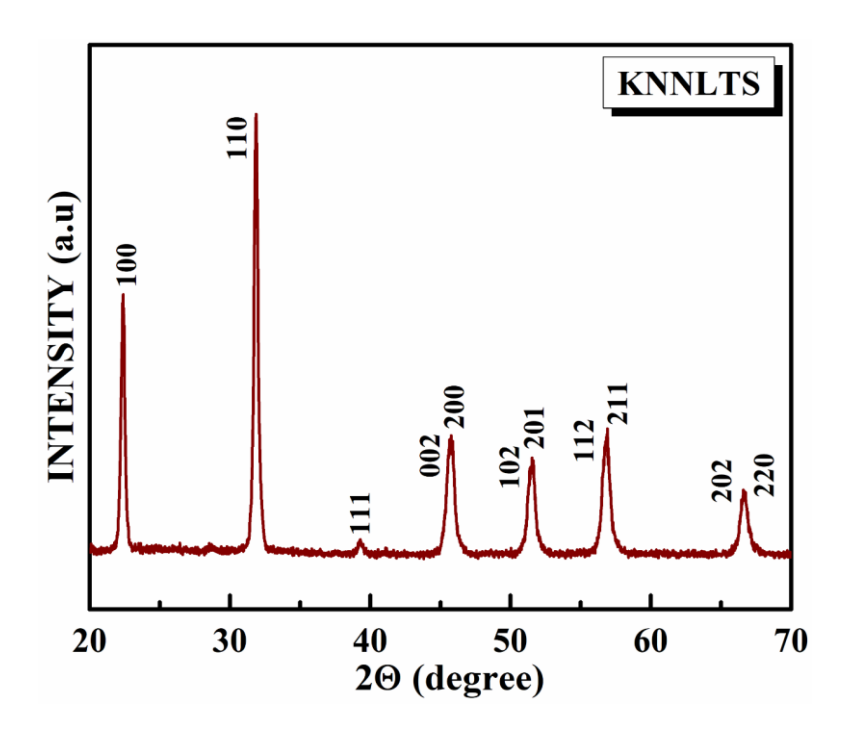


Figure 6.4 XRD pattern of calcined KNNLTS nanoparticles.

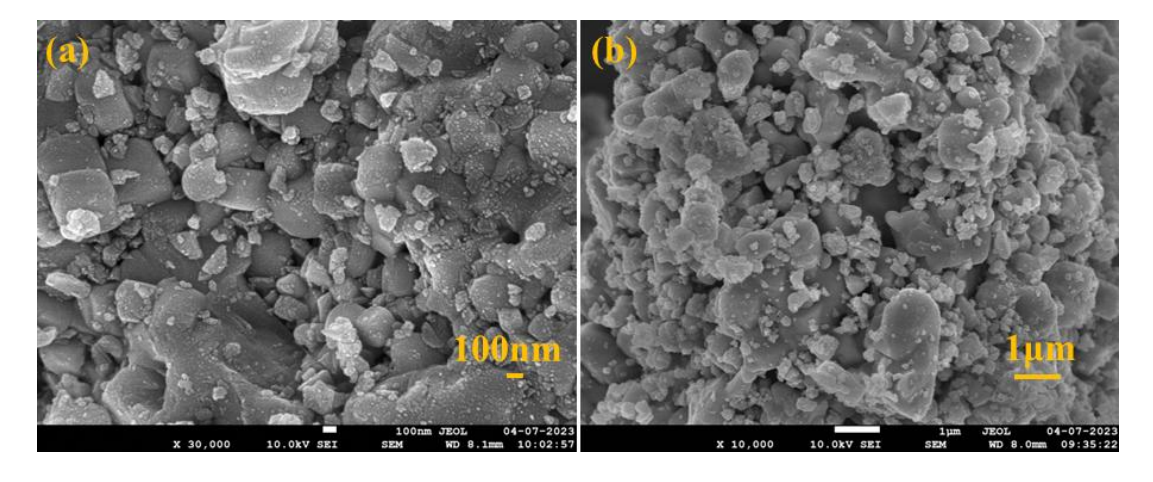


Figure 6.5 SEM image of calcined KNNLTS nanoparticles (a) 100 nm scale & (b) 1μ m scale.

6.3.2 Structural Analysis of the Nanocomposite Films

6.3.2.1 XRD Analysis of the PVDF/KNNLTS/MWCNTs Flexible Nanocomposite Films

X-ray Diffraction (XRD) was used to analyse the structural phases of pure PVDF film and PVDF/KNNLTS/MWCNTs nanocomposite films and related plots are depicted in Figure 6.6. The diffraction peak around 18.6° can be assigned to the α phase of the

PVDF which is non-polar and peak around 20.2° corresponds to the β phase of the PVDF which is polar [8, 9], in all the prepared nanocomposite films. Furthermore, the diffraction peak corresponding to the β phase has a stronger intensity in comparison to the α phase, indicating that the β phase of PVDF predominates over the α phase in all the nanocomposite films. In PVDF, β phase is the polar phase responsible for its piezoelectric response whereas α -phase does not show any piezoelectric response. Additionally, other peaks can be seen in the XRD plots which can be assigned to KNNLTS nanoparticles and is marked by the sign " ϕ ".

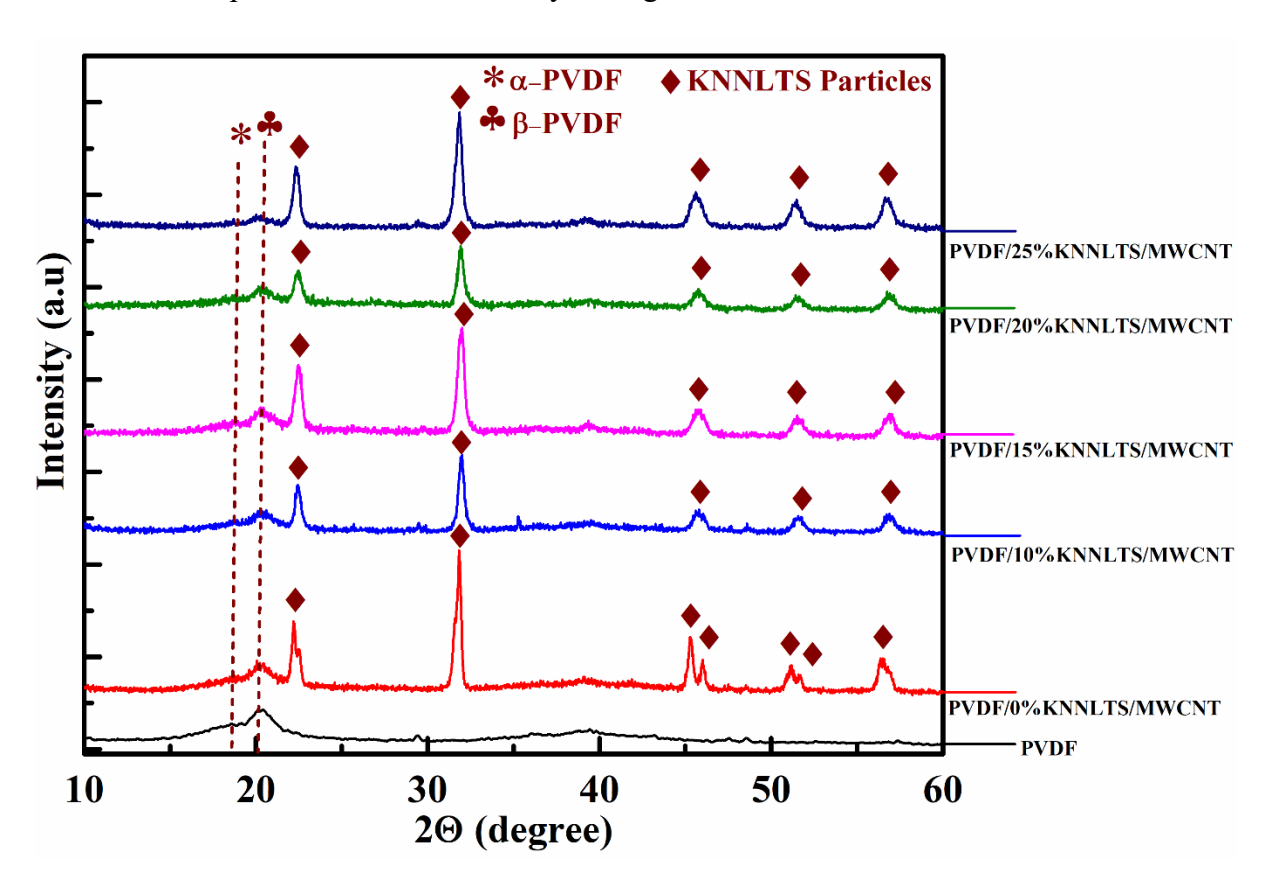


Figure 6.6 X-ray Diffraction patterns of the flexible nanocomposite films produced with pure PVDF and different content of KNNLTS nanoparticles and MWCNT in the PVDF matrix.

6.3.3 FTIR Analysis of PVDF/KNNLTS/MWCNTs Nanocomposites Films

The FTIR analysis of prepared pure PVDF and nanocomposite films was also done to understand the effect of KNNLTS nanoparticles and MWCNTs addition on the crystal structure of PVDF. The FTIR spectra of pure PVDF film and corresponding

PVDF/KNNLTS/MWCNTs nanocomposite films were recorded in the range of 500 – 1500 cm⁻¹ at room temperature and are presented in Figure 6.7. From the FTIR spectra, it can be seen that α and β phases are present in all the prepared nanocomposite films. The absorption bands at 532, 602, 762, 795, 975, 1386, and 1404 cm⁻¹ are assigned as the characteristic peaks of the α phase. On the other hand, the absorption bands at 512, 614, 840, 878, 1075, 1172, 1234, and 1275 cm⁻¹ are assigned as the characteristic peaks of β phase of PVDF [10-16]. The content of β phase F (β) in all the nanocomposite films can be calculated by using Beer-Lambert Law [17].

$$F(\beta) = \frac{A_{\beta}}{\binom{K_{\beta}}{K_{\alpha}} A_{\alpha} + A_{\beta}} \tag{6.1}$$

where, K_{α} and K_{β} denotes the absorption coefficients at 840 cm⁻¹ and 762 cm⁻¹ whose values are $K_{\alpha} = 6.1 \text{ x } 10^4 \text{ cm}^2 \text{ mol}^{-1}$, and $K_{\beta} = 7.7 \text{ x } 10^4 \text{ cm}^2 \text{ mol}^{-1}$, respectively. A_{β} and A_{α} are the absorbance intensities at 762 cm⁻¹ and 840 cm⁻¹, respectively [18]. By introducing KNNLTS and MWCNTs in the PVDF matrix, $F(\beta)$ (β phase fraction) in the PVDF/20%KNNLTS/MWCNT nanocomposite film is found to be more in comparison to the pure PVDF film and other nanocomposite films. The obtained FTIR results are consistent with the XRD result, indicating the presence of β phase of PVDF in all the prepared flexible nanocomposite films. Based on the XRD and FTIR results, it is expected that the PENG device fabricated using PVDF/20%KNNLTS/MWCNTs nanocomposite film may have better energy harvesting performance in comparison to the other nanocomposite films.

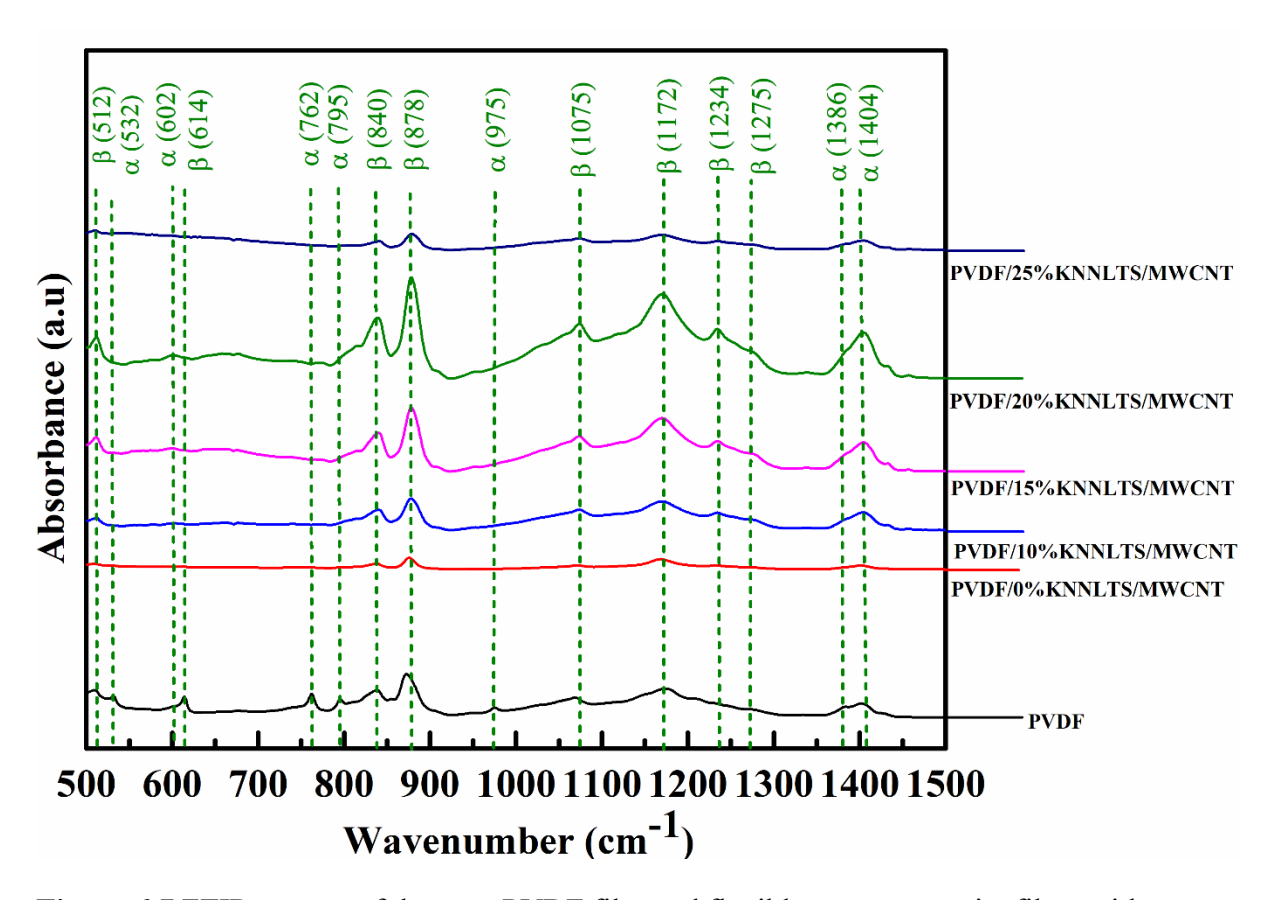


Figure 6.7 FTIR spectra of the pure PVDF film and flexible nanocomposite films with different content of KNNLTS nanoparticles and MWCNT in the PVDF matrix.

6.3.4 Surface Morphology Studies of PVDF/KNNLTS/MWCNTs Nanocomposite Films

The morphology of the surface of the prepared **PVDF** pure PVDF/KNNLTS/MWCNT flexible nanocomposite films were analysed by using Scanning Electron Microscopy (SEM) and corresponding images are depicted in Figure 6.8 (a-f). A smooth and dense surface can be visible for pure PVDF film. In all the nanocomposite films, uniform dispersion and presence of KNNLTS nanoparticles up to 20 wt.% content of KNNLTS in the PVDF matrix can be seen. However, with further increasing the content of KNNLTS to 25 wt.% in the PVDF matrix, some agglomeration is visible in Figure 6.8 (f). The morphology of nanocomposite films plays a critical role in determining the overall performance of the PENG device.

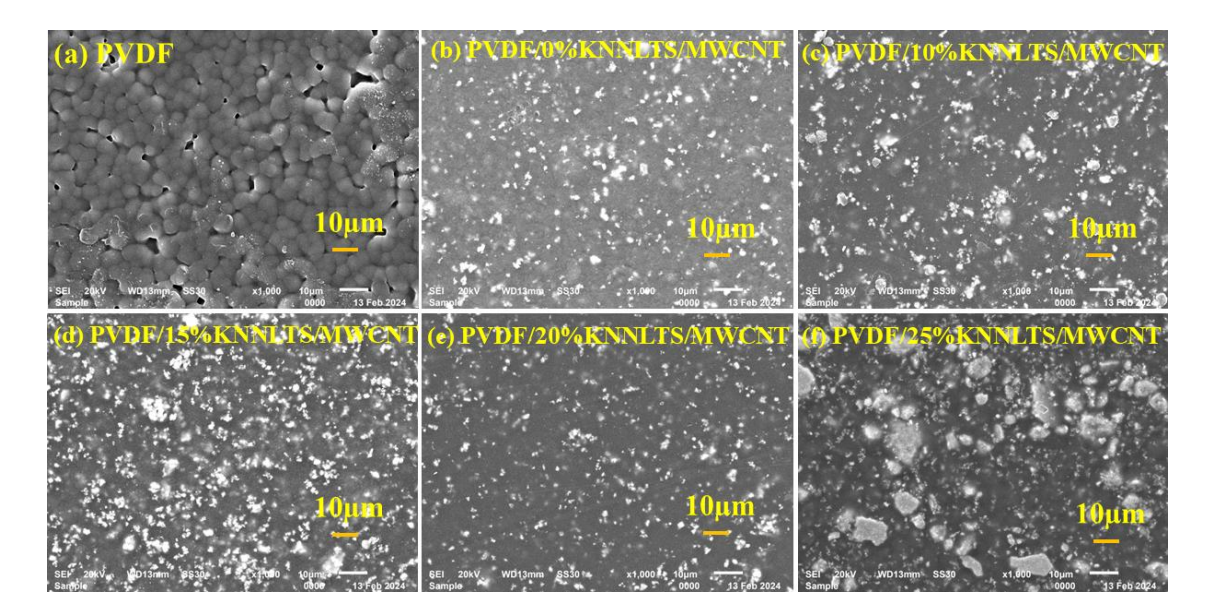


Figure 6.8 SEM surface micrographs related to (a) Pure PVDF, (b) PVDF/0%KNNLTS/MWCNT, (c) PVDF/10%KNNLTS/MWCNT, (d) PVDF/15%KNNLTS/MWCNT, (e) PVDF/20%KNNLTS/MWCNT and (f) PVDF/25%KNNLTS/MWCNT.

6.3.5 Dielectric Properties of PVDF/KNNLTS/MWCNTs Nanocomposite Films

The dielectric constant (ε_r) was measured for the pure and all the nanocomposite films at room temperature by using an Impedance Analyzer in the frequency range 100 Hz to 1 MHz. Figure 6.9 shows the variation of dielectric constant (ε_r) of all the prepared films with varying frequency. The dielectric constant of the flexible composite films decreases with increase in the frequency which is attributed to decrease in polarisation with increase in frequency. When frequency is low, different polarisations respond easily, but with increase in frequency, different polarisation mechanisms cease. This results in the decrease of net polarization of the material, which then leads to decrease of dielectric constant [19].

Table 6.2 presents the dielectric constant values of all the fabricated flexible nanocomposite films at frequencies of 1 KHz and 10 KHz. The dielectric constant was found to increase progressively with the addition of KNNLTS up to 20 wt.%, beyond which a decline in value was observed. Among the samples, the PVDF/20%KNNLTS/MWCNT nanocomposite film exhibited the highest dielectric constant, with values of 44.27 at 1 kHz and 43.44 at 10 kHz. which are significantly

higher in comparison to pure PVDF film. This can be attributed to the synergistic effect of interfacial polarisation from KNNLTS and enhanced charge transport and β -phase induction due to the conductive MWCNTs. Additionally, KNNLTS possesses a high value of dielectric constant as compared to PVDF [20-24]. Therefore, as the concentration of KNNLTS increases into the PVDF matrix from 0 wt.% to 20 wt.%, increase in dielectric constant value has been observed. However, when the content of KNNLTS reaches 25 wt.% in the PVDF matrix, interfacial polarisation effect gets reduced due to comparatively lower interaction between KNNLTS nanoparticles and PVDF polymer caused by particle agglomeration at higher loading levels. This agglomeration is further confirmed by SEM analysis, which shows visible clustering in the PVDF/25%KNNLTS/MWCNT nanocomposite film.

Table 6.2 Dielectric properties of pure PVDF and different nanocomposite films.

S. No.	Sample Name	Dielectric Constant (ε_r)	
		1 KHz	10 KHz
1.	PVDF	9.12	9.07
2.	PVDF/0%KNNLTS/MWCNT	34.01	32.92
3.	PVDF/10%KNNLTS/MWCNT	34.16	33.97
4.	PVDF/15%KNNLTS/MWCNT	39.68	40.04
5.	PVDF/20%KNNLTS/MWCNT	44.27	43.44
6.	PVDF/25%KNNLTS/MWCNT	26.70	26.03

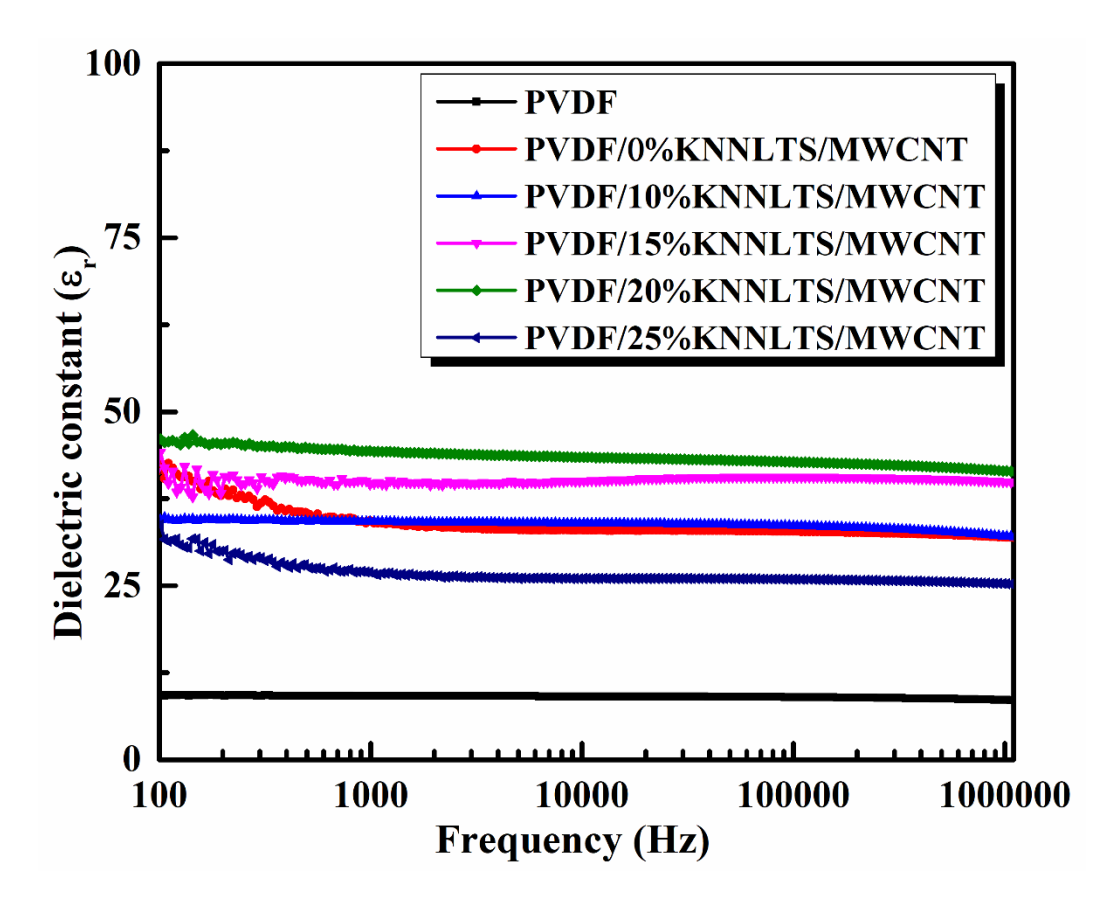


Figure 6.9 Variation of Dielectric constant (ε_r) as a function of frequency of PVDF/KNNLTS/MWCNTs nanocomposite films.

6.3.6 Piezoelectric Performance of PVDF/KNNLTS/MWCNTs PENG Device

To test the piezoelectric performance of the fabricated PENG devices using PVDF/KNNLTS/MWCNTs nanocomposite films, dynamic shaker was used to apply mechanical force on the surface of the PENG device. Figure 6.10 (a-f) displays the open-circuit voltage plots generated by the fabricated PENG devices. The peak-to-peak open circuit voltage is found to increase with increase in the KNNLTS content up to 20 wt.% in the PVDF matrix and then decreases. The values of peak-to-peak open circuit output voltage obtained for different PENG devices is presented in Figure 6.12 (a). It can be noticed that the obtained open circuit voltage for the device PVDF/20%KNNLTS/MWCNT is approximately 14 times of the open circuit voltage obtained for pure PVDF and is approximately 6 times in comparison to the device containing only MWCNT in the PVDF matrix.

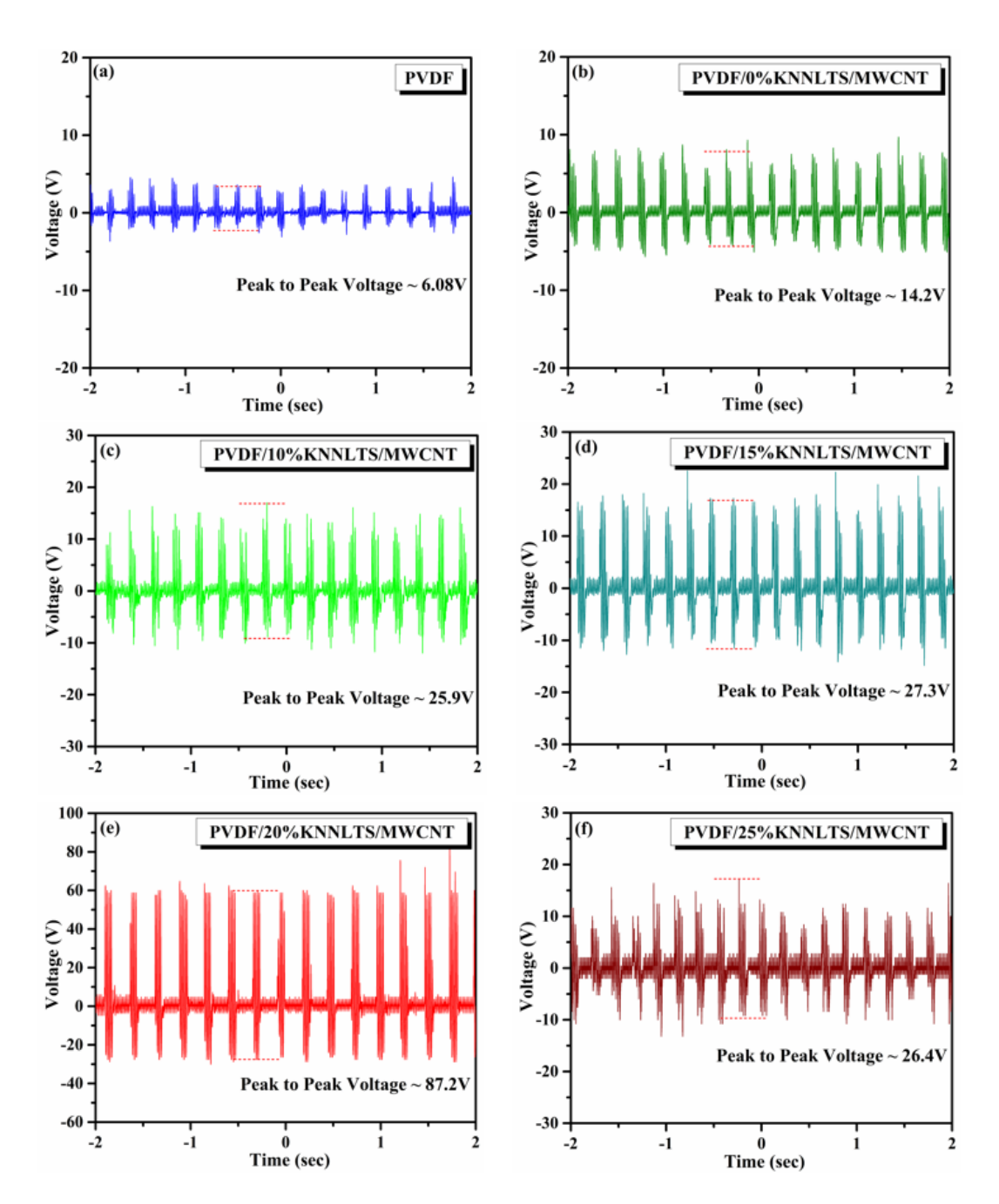


Figure 6.10 The generated open circuit piezoelectric output voltage plots of the PENG (a) Pure PVDF, (b) PVDF/0%KNNLTS/MWCNT, (c) PVDF/10%KNNLTS/MWCNT, (d) PVDF/15%KNNLTS/MWCNT, (e) PVDF/20%KNNLTS/MWCNT and (f) PVDF/25%KNNLTS/MWCNT.

Furthermore, the short circuit current generated from the different PENG devices has also been measured and the corresponding plots are depicted in Figure 6.11 (a-f). The measured short circuit current follows the same trend as that of output voltage. The

peak-to-peak short circuit current obtained for different PENG is presented in Figure 6.12 (b). The current densities have also been calculated for the different nanogenerators and are presented in Figure 6.12 (c). It can be seen from the plots that the highest values of short circuit current and current density were 20.3 μ A and ~ 5.1 μ A/cm², respectively for the PENG device constructed with PVDF/20%KNNLTS/MWCNT nanocomposite film.

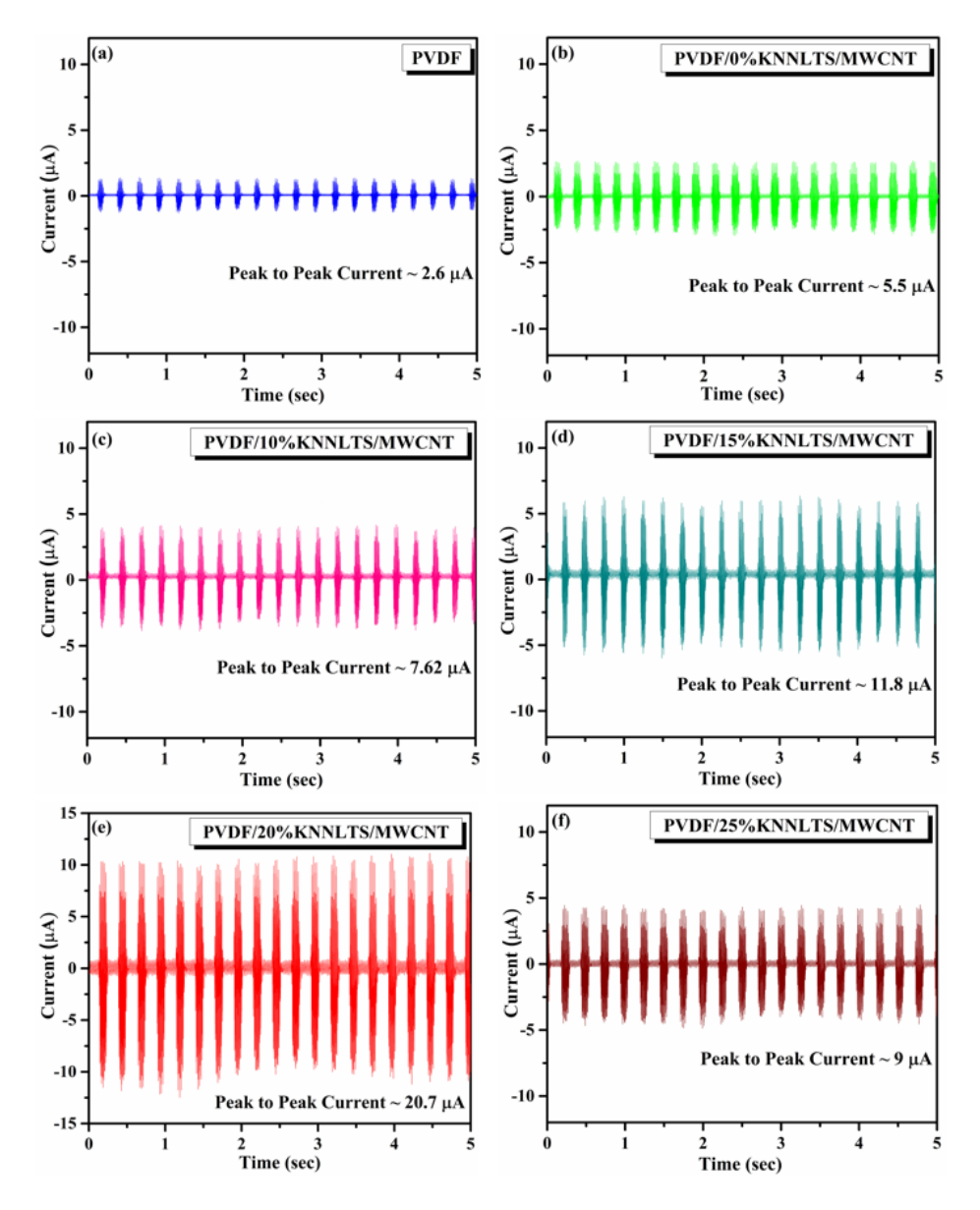


Figure 6.11 The generated short circuit current plots of the PENG (a) Pure PVDF, (b) PVDF/0%KNNLTS/MWCNT, (c) PVDF/10%KNNLTS/MWCNT, (d) PVDF/15%KNNLTS/MWCNT, (e) PVDF/20%KNNLTS/MWCNT and (f) PVDF/25%KNNLTS/MWCNT.

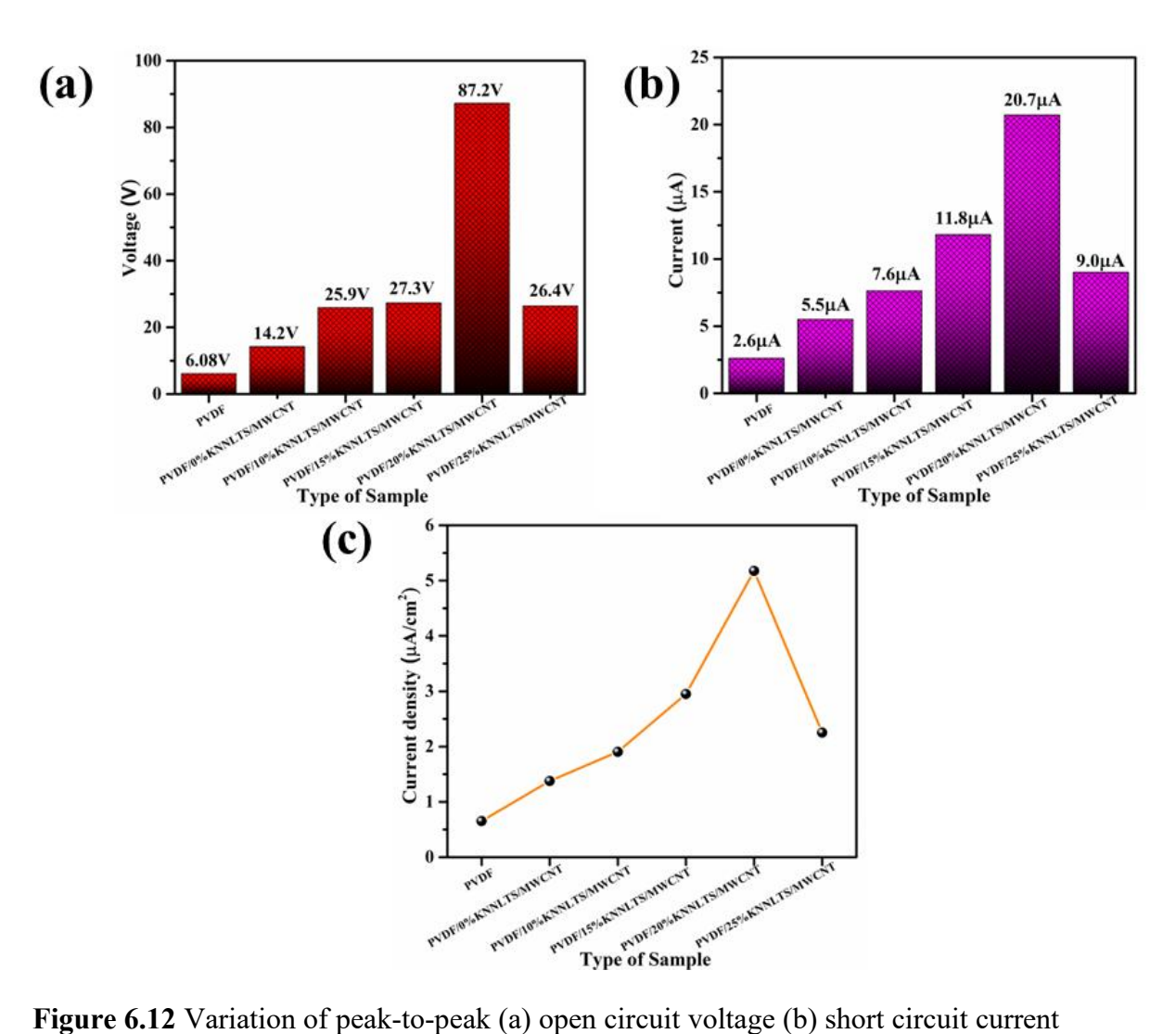


Figure 6.12 Variation of peak-to-peak (a) open circuit voltage (b) short circuit current and (c) current density of the PENG device as a function of KNNLTS and MWCNT nanoparticles concentration in the PVDF matrix.

The power output of the PVDF/20%KNNLTS/MWCNT nanocomposite-based PENG device was also measured by varying an external load resistance in the range of 10^5 to $10^8~\Omega$. Figure 6.13 (a) shows the variation of generated output voltage and current for varying external loads for the PVDF/20%KNNLTS/MWCNT PENG device. It can be noticed from the plots that the voltage gradually increased, while the current decreased as a function of increasing resistance. Using equation $P = \frac{VI}{A}$, the output power density varied with the external resistance, which is shown in Figure 6.13 (b). As can be seen from the plot, the output power density first increases with the external resistance and

then decreases. When the external resistance is 2.2 M Ω , the output power density reaches a maximum value of about ~ 145.48 μ W/cm². Table 6.3 shows the comparison of the piezoelectric performance of PVDF/KNNLTS/MWCNTs PENG device fabricated in the present work with the existing literature.

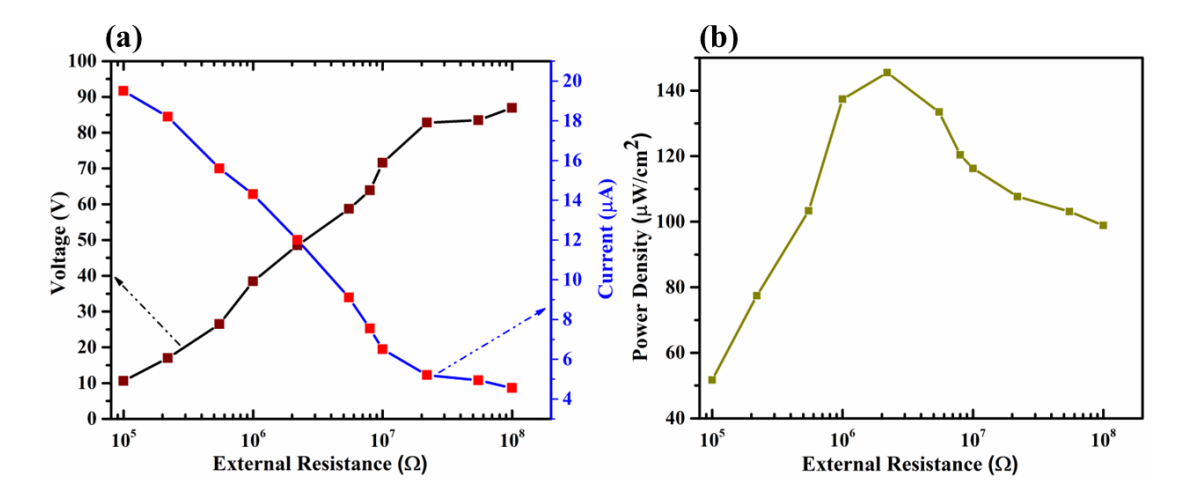


Figure 6.13 (a) Variation of generated output voltage and current with varying external resistance and (b) Variation of power density with external resistance of PVDF/20%KNNLTS/MWCNT film-based PENG device.

Table 6.3 Comparison of the piezoelectric performance between PVDF/KNNLTS/MWCNT PENG nanogenerator fabricated in the present work and various nanogenerators reported in the literature.

S. No.	Filler material in the polymer matrix	Polymer used	Film Synthesis Method	V _{oc} (V)	<i>I_{sc}</i> (μA)	Power Density (µW/cm²)	Ref.
1.	ZnO nanoparticles	PVDF	Drop- casting	1.81	0.57	0.21	[25]
2.	PZT particles	PVDF	Electro- spinning	0.184		30.69	[26]
3.	BaTiO ₃ particles	PVDF	Solvent- casting method	7.2	0.038	0.8	[27]
4.	KNN nanorods &	PVDF	Electro- spinning	23.24	9	52.29	[28]

Chapter 6 Effect of KNNLTS concentration and conductive fillers (MWCNT) in realizing high performance PVDF/KNNLTS/MWCNT flexible piezoelectric nanogenerator for powering electronics devices

	CNT						
5.	KNN particles & MWCNT	PVDF	Drop- casting	35.3	15.8		[29]
6.	BaTiO ₃ nanoparticles & CNT	PVDF	Drop- casting	4.4	0.66		[30]
7.	ZnO nanoparticles & MWCNT	PVDF	Drop- casting	22		21.41	[31]
8.	Pt nanoparticles	PVDF	Electro- spinning	30	6	22	[32]
9.	CNT	PVDF	Electro- spinning	1.89	0.011		[33]
10.	TiO ₂ -Fe ₃ O ₄ - MWCNT	PVDF	Electro- spinning	0.68			[34]
11.	KNNLTS nanoparticles & MWCNT	PVDF	Drop- casting	87.22	20.3	145.48	[Present Work]

Stability is an important parameter for the PENG devices. For testing the stability of the fabricated PVDF/20%KNNLTS/MWCNT PENG device, a continuous tapping was done on the device and the corresponding plot is shown in Figure 6.14. It can be seen from the plot that the measured output voltage was very stable during 2000 tapings indicating that the device exhibits excellent mechanical and electrical stability over repeated use.

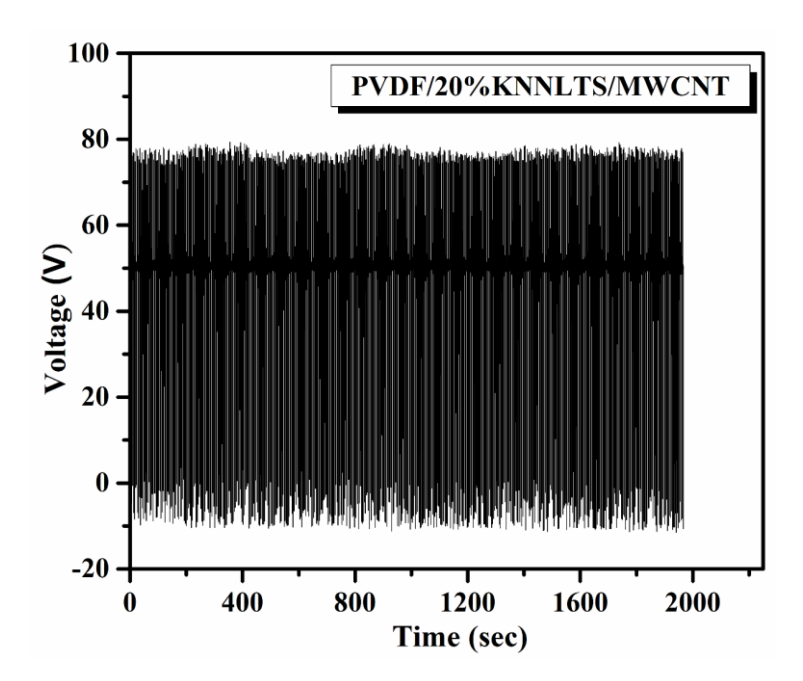


Figure 6.14 Stability test of PVDF/20%KNNLTS/MWCNT film-based PENG under 2000 cycles.

Furthermore, the inverse piezoelectric coefficient (d_{33}^*) of the prepared PVDF/20%KNNLTS/MWCNT PENG device was examined by measuring the room temperature Displacement vs. Voltage (D-V) hysteresis loop and the related plot is displayed in Figure 6.15. Based on the slope of butterfly curve, the maximum and the average values of d_{33}^* were ~ 59.92 pm/V and 28.67 pm/V, respectively.

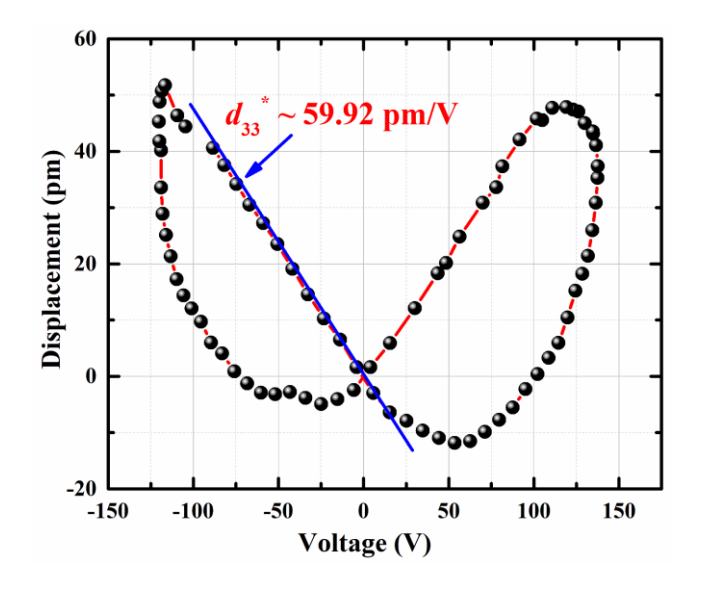


Figure 6.15 Displacement vs. Voltage (*D-V*) butterfly curve for PVDF/20%KNNLTS/MWCNT film-based PENG device.

6.3.7 Energy Harvesting Performance of PENG Device

To demonstrate the practical applicability of the fabricated device, its energy harvesting performance was evaluated under real-world conditions. The generated output voltage using PVDF/20%KNNLTS/MWCNT PENG was enough to light up 18 light-emitting diodes (LEDs) and power a digital thermometer as well as a digital wrist watch as shown in Figure 6.16 (b), (c), and (d). Overall, the results suggest that PVDF/KNNLTS/MWCNTs based PENG device offers higher values of output voltage, current and power density, making it a promising candidate for next-generation flexible energy harvesting devices.

Furthermore, mechanical energy is so abundant available in our surroundings, however it gets wasted in our daily lives. The PVDF/20%KNNLTS/MWCNT PENG device was utilized for harvesting mechanical energy from human body motions such as finger tapping, thumb pressing, fist beating, elbow beating, elbow bending, and wrist stretching and the corresponding generated voltages were ~ 11.4 V, 27.2 V, 24.8 V, 34 V, 37 V, and 55.2 V, respectively as shown in Figure 6.17. This shows that the fabricated PENG device proves the utilization of mechanical energy harvesting in our daily life.

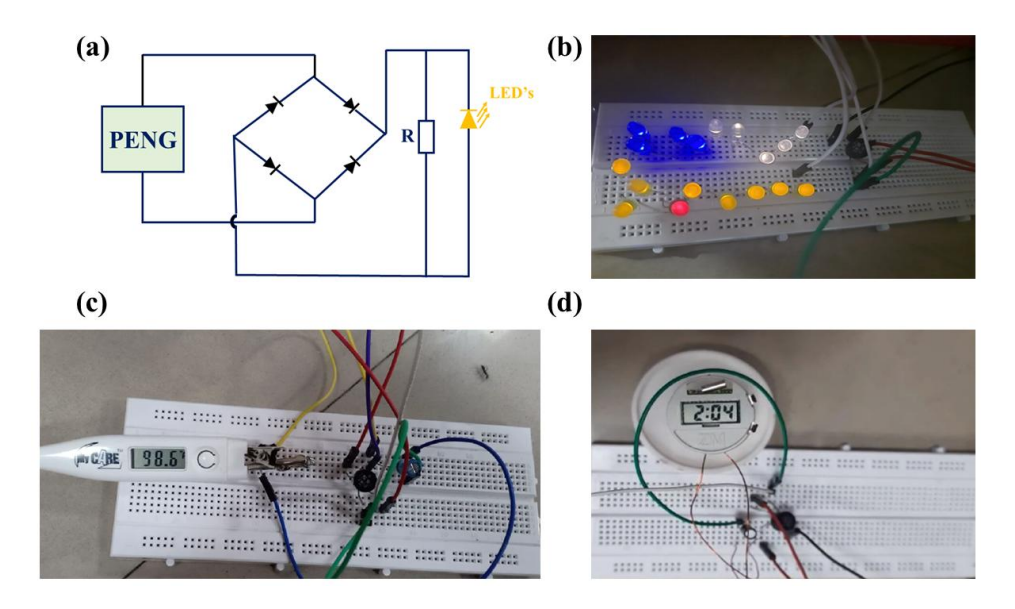


Figure 6.16 (a) Electrical circuit used for powering LEDs (b) Lighting LEDS (c) Pictorial representation of the devices – digital thermometer and (d) digital wrist watch derived by PVDF/20%KNNLTS/MWCNT based PENG device.

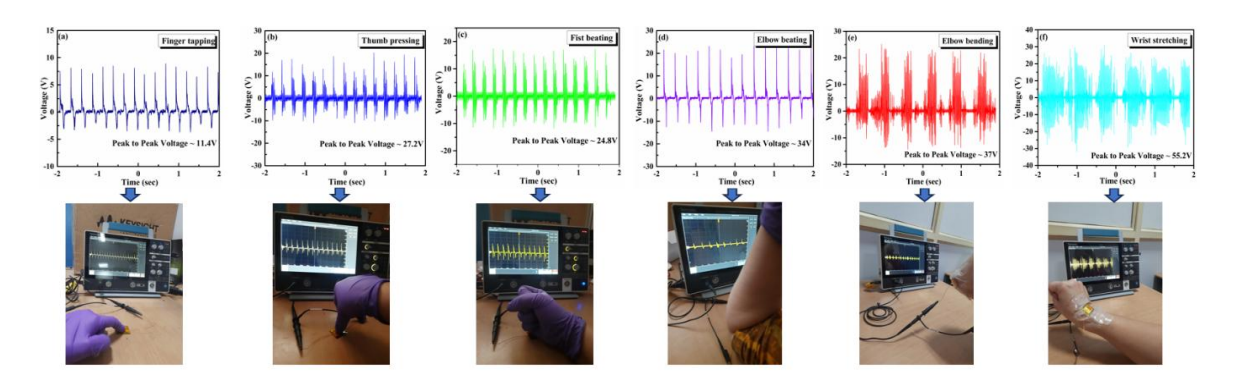


Figure 6.17 The output voltage generated by PVDF/20%KNNLTS/MWCNT film-based PENG by (a) finger tapping, (b) thumb pressing, (c) fist beating, (d) elbow beating, (e) elbow bending, and (f) wrist stretching.

6.4 Conclusion

In this chapter, Polyvinylidene fluoride/ potassium sodium niobate doped with antimony/ multiwall lithium, tantalum, and carbon nanotube (PVDF/KNNLTS/MWCNT) based flexible nanocomposite films have been synthesized and then used for the construction of PENG device. It was observed that KNNLTS incorporated with MWCNT in the PVDF matrix showed improved structural, dielectric and piezoelectric performance. The maximum values of piezoelectric output voltage, output current and power density were measured to be 87.2 V, 20.3 µA and of 145.48 µW/cm², respectively for the PENG device constructed with nanocomposite film containing 20 wt.% KNNLTS and MWCNT in the PVDF matrix. In addition, the PENG device was utilized to test the ability to harness energy from human body motions. The output voltages for finger tapping, thumb pressing, fist beating, elbow beating, elbow bending and wrist stretching were 11.4 V, 27.2 V, 24.8 V, 34 V, 37 V and 55.2 V, respectively. The fabricated PENG demonstrated practical applicability, by powering a digital thermometer, digital wrist watch and successfully lighted 18 LEDs. The present chapter demonstrated that high performance PENG can be developed by employing modified KNN together with conductive filler in the PVDF matrix which has the potential to be used in self-powered wearable and portable electronic gadgets.

References

- [1] Z.H. Liu, C.T. Pan, C.Y. Su, L.W. Lin, Y.J. Chen, J.S. Tsai, Sensors and Actuators A: Physical, 211, (2014), 78-88
- [2] A. Pal, A. Sasmal, B. Manoj, D.P. Rao, A.K. Haldar, S. Sen, Materials Chemistry and Physics, 244, (2020), 122639
- [3] C. Sun, H. Liu, J. Wang, G. Shan, T. Ren, Organic Electronics, 144, (2025), 107290
- [4] X. Lin, F. Fu, X. Zhang, W. Li, Y. Zhao, X. Fei, Q. Li, C. Yang, S. Huang, ACS Applied Nano Materials, 6, (2023),11955-11965
- [5] Y. Zhu, B. Yang, J. Liu, X. Wang, X. Chen, C. Yang, Journal of Microelectromechanical Systems, 24, (2015), 3
- [6] I.U. Shipu, D. Bhowmick, N.L. Dey, International Journal of Scientific and Research Publications, 14, (2024), 6
- [7] P. Kumar, P. Palei, Ceramic International, 36, (2010), 1725-1729
- [8] A. K. Zak, W. C. Gan, W. H. Abd. Majid, M. Darroudi, T. S. Velayutham, Ceramic International, 37, (2011),1653-1660
- [9] S. Bairagi, S. W. Ali, Organic Electronics, 78, (2020), 105547
- [10] X. Cai, T. Lei, D. Sun, L. Lin, RSC Advanced, 7, (2017), 15382–15389
- [11] W.A. Yee, M. Kotaki, Y. Liu, X. Lu, Morphology, Polymer, 48, (2007), 512-521
- [12] L. Ruan, X. Yao, Y. Chang, L. Zhou, G. Qin, X. Zhang, Polymers, 10 (3), (2018), 228
- [13] S. Badatya, D.K. Bharti, A.K. Srivastava, M.K. Gupta, Journal of Alloys and Compounds, 863, (2021), 158406
- [14] T. Prabhakaran, J. Hemalatha, Materials Chemistry and Physics, 137, (2013), 781-787
- [15] D. Guo, K. Cai, P. Deng, G. Si, L. Sun, F. Chen, H. Ning, L. Jin, J. Ma, Journal of Materiomics, 6, (2020), 563-572
- [16] N. Abzan, M. Kharaziha, S. Labbaf, Materials and Design, 167, (2019), 107636

- [17] Y. Li, X. Su, k. Liang, C. Luo, P. Li, J. Hu, G. Li, H. Jiang, K. Wang, Microelectronic Engineering, 111557, (2021), 244-246
- [18] R. K. Singh, S. W. Lye, J. Miao, Polymer, 214, (2021), 123366
- [19] Y. Huan, T. Wei, Z. Wang, H. Shen, X. Lin, S. Huang, X. Wang, Journal of Materiomics, 6, (2020), 355
- [20] A. Rahman, M. Jiang, G. Rao, S. Lee, M-H. Kim, M. Habib, J.U. Rahman, Ceramic International, 48 (14), (2022), 20251-20259
- [21] L. Wu, C. Li, F. Jiang, T. Wei, Ceramic International, 49 (13), (2023), 22015-22021
- [22] Z. Liu, A. Zhang, J. Lu, B. Xie, B. Liang, Y. Mao, H. Fan, Journal of Alloys and Compounds, 817, (2020), 152798
- [23] B. Adak, I. Chinya, S. Sen, RSC Advanced, 6, (2016), 105137-105145
- [24] A. Sasmal, S. Sen, P. Sujatha Devi, Physical Chemistry Chemical Physics, 21, (2019), 5974-5988
- [25] H.H. Singh, S. Singh, N. Khare, Polymer for Advanced Technologies, 29, (2017), 143-150
- [26] N. Chamankar, R. Khajavi, A. A. Yousefi, A. Rashidi, F. Golestanifard, Ceramic International, 46, (2020), 19669-19681
- [27] M. Sahu, S. Hajra, K. Lee, PL. Deepti, K. Mistewicz, H. J. Kim, Crystals, 11 (2), (2021), 85
- [28] S. Bairagi, S. W. Ali, Soft Matter, 16, (2020), 4876
- [29] A. M. Abdullah, M. U. K. Sadaf, F. Tasnim, H. Vasquez, K. Lozano, M. J. Uddin, Nano Energy, 86, (2021), 106133
- [30] A. S. M. I. Uddin, D. Lee, C. Cho, B. Kim, Coatings, 12, (2022), 77
- [31] S. Pratihar, A. Patra, A. Sasmal, S. K. Medda, S. Sen, Soft Matter, 17, (2021), 8483-8495
- [32] S. K. Ghosh, D. Mandal, Nano Energy, 53, (2018), 245-257
- [33] C.-M. Wu, M.-H. Chou, W.-Y. Zeng, 8(6), (2018), 420
- [34] A. Samadi, S.M. Hosseini, Organic Electronics, 75, (2019), 105405

Chapter 7

Conclusion, Future Scope and Social

Impact

Chapter 7 Conclusion, Future Scope and Social Impact

This chapter provides a conclusion of all findings of the present thesis work. The findings of this research lay the groundwork for further advancements in the field of flexible piezoelectric energy harvesters. Additionally, it outlines the future scope, potential social impact and the challenges associated with the research.

7.1 Conclusion

Chapter 1 of the thesis begins by addressing the growing global energy demand and the continued reliance on fossil fuels, highlighting the need for sustainable alternatives. This leads to a discussion on the increasing research interest in renewable and green technologies as viable solutions. The necessity of energy harvesting is then emphasized, followed by an overview of various energy harvesting techniques, including thermal, solar and piezoelectric approaches, etc. Among these, piezoelectric energy harvesting in which mechanical energy is converted into useful electric energy using piezoelectric generators (PEGs) is explored in detail, focusing on its working principle and advantages. To construct PEG, piezoelectric materials are required thus, in the present chapter various organic, inorganic and composite piezoelectric materials along with their different properties and their suitability for energy harvesting applications have been discussed in detail. A comprehensive literature review is also presented, summarizing various research studies related to energy harvesting advancements particularly, the composite-based flexible piezoelectric generator for energy harvesting applications.

Chapter 2 of the thesis elaborates the experimental methods utilized for the synthesis of filler particles in the PVDF matrix and the fabrication of composite films. For the synthesis of the filler materials, solid state method, hydrothermal method and co-precipitation method were used and are discussed in detail in the chapter. Further, for the fabrication of the flexible composite films, drop casting method was employed. In addition, the working principle of various experimental techniques and equipment that were used for the characterization of the prepared samples have also been provided in this chapter to get a comprehensive

understanding. To study the phase formation and morphology of the prepared powders and flexible composite films, X-ray Diffraction (XRD), Scanning Electron Microscopy (SEM), Field Emission Scanning Electron Microscopy (FESEM) and Fourier Transform Infrared Spectroscopy (FTIR) were used. Furthermore, dielectric, ferroelectric and piezoelectric properties of the fabricated composite films were also measured using Impedance analyser, Polarisation vs. Electric field (*P-E*) loop tracer and Strain measurement system (Butterfly loop), respectively. With the aid of a vibrator shaker and finger tapping, force was applied on the surface of the constructed PEG devices and generated open circuit voltage and short circuit current were measured by using digital storage oscilloscope and an electrometer, respectively. Furthermore, load resistances were also attached to the PEG devices to measure the output power of the manufactured PEG device.

Chapter 3 of the thesis was divided in two sections in which comparison of the piezoelectric performance of the PEG devices constructed with KNN synthesized by solid state method and hydrothermal method was done in detail. In Section 1 of Chapter 3, PEG devices based on Potassium Sodium Niobate/Poly (vinylidene fluoride) (KNN/PVDF) flexible composite films with various percentages of KNN ceramic particles (0 wt.%, 5 wt.%, 10 wt.%, 15 wt.% and 20 wt.%) in the PVDF matrix were constructed. Among the different percentages of KNN, 15 wt.% KNN particles @ PVDF composite film demonstrated the highest values of β phase content of PVDF, dielectric constant (ε_r), remnant polarisation (P_r), and spontaneous polarisation (P_s). When force was applied on the surface of the fabricated PEG device, measured values of maximum open-circuit voltage and short-circuit current were 11.2 V and 0.3 μ A, respectively for the device prepared with 15 wt.% KNN in the PVDF matrix.

Further, in **Section 2** of Chapter 3, KNN nanoparticles were synthesized via hydrothermal method and used as filler in the PVDF matrix for fabricating PENG device. Based on the result obtained in the first section, concentration of KNN was fixed to 15 wt.% in the PVDF matrix and different properties of the prepared composite film were investigated. PVDF/KNN 15 wt.% nanocomposite film showed promising results. The nanocomposite film displayed improved β phase

content of PVDF, dielectric, ferroelectric and piezoelectric performance in comparison to the film fabricated with KNN synthesized by solid state reaction method for same filler concentration. The output voltage, output current and power density generated by the nanogenerator were 20.2 V, 2.01 μ A and 8.71 μ W/cm², respectively. Finally, its practical applicability was demonstrated by harvesting energy from human body motions. Overall, the PENG constructed with KNN synthesized by hydrothermal method outperformed PEG constructed with KNN synthesized by solid state method.

In Chapter 4 of the thesis, Potassium Sodium Niobate (KNN) and /Zinc Oxide (ZnO) incorporated Poly (vinylidene fluoride) (PVDF) -based flexible piezoelectric nanogenerator (PENG) were constructed and the effect of KNN and ZnO concentrations on the various properties and piezoelectric performance of the PENG device investigated. The **FTIR** was result showed PVDF/14.55%KNN/0.45%ZnO nanocomposite film possesses the highest content of electroactive (β) phase (~59.81%). Furthermore, dielectric and ferroelectric properties of the prepared nanocomposite films were also measured. The maximum values of open circuit voltage, short circuit current and power density were 39.5 V, 8.75 μ A and 22.26 μ W/cm² (with 10 M Ω load resistance), respectively obtained for the PENG fabricated with PVDF/14.55%KNN/0.45%ZnO nanocomposite film. The maximum and average values of inverse piezoelectric charge coefficient were found to be $d_{33}^*_{\text{max}} \sim 83.82 \text{ pm/V}$ and $d_{33}^*_{\text{avg}} \sim 32.22 \text{ pm/V}$, respectively for the same nanocomposite film. The synergistic effect of KNN and ZnO nanoparticles in PVDF polymer matrix considerably improves the resultant piezoelectric performance of the nanogenerator, enabling it to glow four red light-emitting diodes (LEDs) and power a digital wrist watch. Moreover, the developed nanogenerator was also able to generate output voltages of 3.08 V, 1.72 V, 1.46 V and 660 mV for pen tapping, elbow bending, finger moving and wrist stretching, respectively. Finally, it can be concluded that the versatile, durable, and flexible PENG based on PVDF/KNN/ZnO nanocomposite film has the potential for future applications in energy harvesting and portable self-powered electronic devices.

In Chapter 5 of the thesis, flexible PEGs based on (Li, Ta, Sb) modified (K, Na) NbO₃ (KNNLTS)/poly (vinylidene fluoride) (PVDF) flexible composite film and pure PVDF film were fabricated. The concentration of KNNLTS was fixed to 15 wt.% in the PVDF matrix. For the PVDF/ KNNLTS 15 wt.% composite film, the dielectric constant (ε_r) was measured as 33.56 at 1 KHz and 29.92 at 10 KHz. Additionally, the remnant polarisation (P_r) and maximum polarisation (P_s) were recorded as 0.32 µC/cm² and 3.70 µC/cm², respectively for the composite film. These values were significantly higher compared to pure PVDF film. The maximum value of inverse piezoelectric charge coefficient (d_{33}^*) for the same composite film were measured as ~ 24 pm/V. Furthermore, the maximum generated peak to peak open circuit voltage and short-circuit current for the PVDF/KNNLTS 15 wt.% composite film-based generator were 36.58 V and 5.04 µA, respectively which were higher than the voltage and current obtained using pure PVDF film-based generator. The performance of the PEG was also tested under different human body motions. The output voltages for fist beating, elbow bending, quenching and fist opening were 5.48 V, 4.12 V, and 1.72 V, respectively. The fabricated PEG demonstrated practical applicability by successfully lighting 11 LEDs. The present chapter demonstrated that high performance PEG can be developed by modifying KNN ceramics by suitable dopants.

In Chapter 6 of the thesis, Polyvinylidene fluoride/ potassium sodium niobate doped with lithium, tantalum, and antimony/ multiwall carbon nanotube (PVDF/KNNLTS/MWCNT) based flexible nanocomposite films have been synthesized and then used for the construction of PENG devices. It was observed that KNNLTS incorporated with MWCNT in the PVDF matrix showed improved structural, dielectric and piezoelectric performance. The maximum values of piezoelectric output voltage, output current and power density were measured to be 87.2 V, 20.3 μA and of 145.48 μW/cm², respectively for the PENG device constructed with nanocomposite film containing 20 wt.% KNNLTS and MWCNT in the PVDF matrix. In addition, the PENG device was utilized to test the ability to harness energy from human body motions. The output voltages for finger tapping, thumb pressing, fist beating, elbow beating, elbow bending and wrist stretching were 11.4 V, 27.2 V, 24.8 V, 34 V, 37 V and 55.2 V, respectively. The fabricated

PENG demonstrated practical applicability, by powering a digital thermometer, digital wrist watch and successfully lighted 18 LEDs. The present chapter demonstrated that high performance PENG can be developed by employing modified KNN together with conductive filler in the PVDF matrix which has the potential to be used in self-powered wearable and portable electronic gadgets.

7.2 Future Scope

The findings of the present thesis research pave the way for further exploration and innovation in the field of flexible piezoelectric energy harvesters. Building upon the successful fabrication of modified KNN based PEGs, future work can be focused on the development of advanced nanogenerators, such as Piezoelectric Nanogenerators (PENGs), Triboelectric Nanogenerators (TENGs) and Hybrid Nanogenerators (combining both piezoelectric and triboelectric effects) for energy harvesting applications. Furthermore, the integration of conductive nanomaterials such as reduced graphene oxide (rGO), MXene, and other emerging two-dimensional (2D) materials- including hexagonal boron nitride (hBN) and transition metal dichalcogenides (TMDCs)- with modified KNN into the polymer matrix, is expected to significantly enhance the performance of piezoelectric, triboelectric, and hybrid nanogenerators by improving the overall electrical, mechanical, and piezoelectric properties of the flexible nanocomposite films. However, one of the major challenges associated with using nanofillers into the polymer matrix is their tendency to agglomerate, which can adversely affect the performance of the nanogenerator devices. To address this issue, future work may focus on employing surface modification or functionalization techniques to improve the interfacial compatibility of nanomaterials with the polymer matrix. Such strategies can facilitate uniform dispersion, thereby ensuring enhanced structural integrity and superior piezoelectric performance of nanogenerator devices.

In summary, the development of PENGs, TENGs and hybrid nanogenerators using modified KNN and advanced nanomaterials holds great promise for next-generation nanogenerators for energy harvesting applications.

7.3 Social Impact

The growing global energy crisis underscores the urgent need for sustainable and eco-friendly energy solutions, as conventional energy sources like fossil fuels contribute heavily to carbon emissions and environmental degradation. In this context, piezoelectric energy harvesting technology which converts mechanical energy into electrical energy without releasing pollutants or depleting natural resources has emerged as a promising alternative, for a green and renewable method of energy generation. This sustainable energy harvesting method can be effectively integrated into self-powered electronic devices, wearable technologies and smart infrastructure, reducing dependence on non-renewable energy sources. For instance, piezoelectric energy harvesters can be deployed in everyday infrastructure, such as roads, footwear-based piezoelectric generator (PEG) devices in shoes and pedestrian walkways, where the mechanical stress generated by vehicle movement and human footsteps can be converted into useful electrical energy. The harvested energy can then be stored and utilized to power streetlights, traffic signals and other urban utilities, thereby reducing the reliance on conventional non-renewable energy sources. Such applications not only contribute to energy sustainability but also promote eco-friendly urban development with significant social and environmental benefits.

Their deployment not only promotes the conversion of otherwise wasted mechanical energy into useful electrical energy but also reduces dependence on fossil fuels, aligning with global initiatives toward carbon neutrality and environmental preservation. Thus, the advancement of piezoelectric energy generators represents a significant step towards achieving a sustainable and greener future.



Delhi Technological University Shahbad Daulatpur, Main Bawana Road, Delhi- 110042

PHONE:

+91 7357006763

+91 8901357161

DOB: September 14, 1992 Nationality-Indian Marital Status-Married

EMAIL:

komal phd2k19@dtu.ac.in

ADDRESS:

2708, F-Block, 2nd Floor, OMAXE City, Sector-09, Sonipat, Haryana, Pin: 131001

Komal Verma

Research Fellow (Applied Physics)

Qualifications

- Qualified Graduate Aptitude Entrance Test (GATE), June 2019
- PhD Title: "Fabrication and Characterization of Flexible Generator composed of Sodium Potassium Niobate (KNN) based Ceramics and Polymers for Energy Harvesting Applications"
- M. Sc. (Physics): University of Delhi, Kirorimal College, Delhi, India, First Division (62.8%) 2013 - 2015
- **B. Sc. (H) (Physics)**: University of Delhi, Kirorimal College, Delhi, India, **First Division** (75.2%) 2010 2013
- Senior Secondary (10+2): C. C. A. S. Jain Sr. Sec. School, Ganaur, India (C.B.S.E. Board), First Division (83.8%) 2008 - 2010
- Matriculation: C. C. A. S. Jain Sr. Sec. School, Ganaur, India (C.B.S.E. Board), First Division (75.4%) 2008

Area of Interests

- > Solid State Physics
- > Material Science
- > Ferroelectric and Piezoelectric studies
- > Dielectric studies
- > Piezoelectric energy harvesting materials

Teaching Experience

Four years' experience as an Assistant Professor in Hindu College, Sonipat.

Subjects taught:

- Mechanics (B.Sc. (non-medical, computer science))
- Atomic and Molecular Physics (M.Sc. Physics)
- Electronics (B.Sc. (non-medical, computer science))
- Solid State Physics (B.Sc. (non-medical, computer science))
- Thermodynamics and Statistical Physics (B.Sc. (non-medical, computer science))

Honors/Awards/Distinctions

- 1. Research & Innovation Excellence Awards -2025 (Delhi Technological University)
- 2. Best oral presentation awarded: "A Flexible piezoelectric nanogenerator based on KNN/PVDF nanocomposite film for energy harvesting application" in the International Conference on Advanced Functional Materials and Devices for Sustainable Development (AFMD-2025) from 03-05 March, 2025, Atma Ram Sanathan Dharma College, University of Delhi, New Delhi-110078, India.
- 3. Research & Innovation Excellence Awards -2024 (Delhi Technological University)
- 4. Research & Innovation Excellence Awards -2023 (Delhi Technological University)
- 5. Awarded as the 2nd Prize in Oral Presentation (Researcher Category) in the Environment, Water, Agriculture, Sustainability and Health (EWASH-2022): Strategizing A Greener Future held from 12 to 13 January, 2023.
- 6. Best Oral presentation on: "Graphene oxide and KNN incorporated PVDF matrix to enhance mechanical energy as a flexible piezoelectric energy harvester" at the International Conference on Advanced Materials for Emerging Technologies (ICAMET-2023), held on May 4-6, 2023, at Netaji Subhash University of Technology, New Delhi-110078, India.

List of Publications

- K. Verma, S. Goel, R. Sharma, Influence of calcination and sintering temperature on the microstructure, dielectric, ferroelectric and piezoelectric properties of lead-free KNN ceramics, *J Mater Sci: Mater Electron*, 33 (2022) 26067-26085, https://doi.org/10.1007/s10854-022-09295-2
- **2. K. Verma**, R. Sharma, A flexible generator based on KNN/PVDF composite films: Role of KNN concentration on the piezoelectric performance of generator, Chinese Journal of Physics, 84 (2023) 198-215, https://doi/10.1016/j.cjph.2022.12.007
- **3. K. Verma**, R. Sharma, Development of KNNLTS-PVDF-based flexible piezoelectric generator for energy-harvesting application, *Bulletin of Materials Science*, 47 (2024) 38 https://doi.org/10.1007/s12034-023-03141-9
- **4. K. Verma**, A. Kumar, R. Sharma, Development of flexible piezoelectric nanogenerator based on PVDF/KNN/ZnO nanocomposite film for energy harvesting application, *J Mater Sci: Mater Electron*, 35 (2024) 1732, https://doi.org/10.1007/s10854-024-13402-w

5. K. Verma, A. Kumar, R. Sharma, Fabrication of lead-free PVDF/KNNLTS/MWCNT piezoelectric nanogenerator: Role of MWCNT in the piezoelectric performance of nanogenerator for energy harvesting application, *Journal of Electronic Materials*, 53 (11) (2024) 7574-7592, https://doi.org/10.1007/s11664-024-11463-s

Total Publications: 05

National/International Conferences and Workshops attended

- Oral presentation on: "A Flexible piezoelectric nanogenerator based on KNN/PVDF nanocomposite film for energy harvesting application" in the International Conference on Advanced Functional Materials and Devices for Sustainable Development (AFMD-2025) from 03-05 March, 2025, Atma Ram Sanathan Dharma College, University of Delhi, New Delhi-110078, India.
- Oral presentation on "Comparison of Piezoelectric, Dielectric, and Ferroelectric properties
 of Lead-Free KNN/PVDF- Based Flexible Composite Films" in the International Conference
 on Physics and Chemistry of Materials (ICPCM-2025) during 20th -22nd Feb, 2025 DehradunIndia.
- 3. Attending "A Two-day Workshop on Structural Analysis (X-Ray Diffraction, Rietveld Refinement, HRTEM & SAED)", organized by Centre for Nanoscience and Nanotechnology, International research Centre & Advanced Characterization Facility, Sathyabama Centre for Advanced Studies, SATHYABAMA Institute of Science and Technology, Chennai during February, 24-25, 2025.
- 4. Attended One-week Online Faculty Development Program (FDP) on "Advancements in Emerging Technologies in Electronics & Communication Engineering" scheduled from May 29th to June 3rd, 2024 at Govind Ballabh Pant Institute of Engineering & Technology (Uttrakhand Government).
- 5. Participated in "SAMERPAN-SUSTAINABLE ACTION & MOBILITY FOR EMISSION REDUCTION & PROMOTING AWARENESS NATIONWIDE" organized by the Department of Environmental Engineering, DTU in Association with ALFATECH Services held on 26th day of November, 2024 (World Sustainable Transport Day).
- 6. Participated in 2nd One Day National Seminar on "Recent Trends in Applied Physics and Engineering (RTAPE-2024)" by Shanti Swarup Bhatnagar (SSB) Awardees organized by Department of Applied Physics, Delhi Technological University (DTU) under the initiative of Viksit Bharat on April 12, 2024.
- 7. Attended webinar on "Additive Manufacturing: Emerging Opportunities for Microwave Components" organized by IEEE Student Branch MNNIT Allahabad, held on 22 March, 2024.

- 8. Oral presentation on: "Design of Flexible PVDF/KNaNbO₃ /NrGO nanogenerator and Understanding the Role of Nanofillers in the Output Voltage Signal" in the International Conference on Recent Advanced in Functional Materials (RAFM-2024) held on March 14-16, 2024, at Atma Ram Sanatan Dharma College, University of Delhi, New Delhi-110078, India.
- 9. Participated in One Day National Seminar on "National Science Day (NSD-2023)" organized by Human Resource Development Centre (HRDC) in association with Institution's Innovation Council (IIC) & Department of Applied Physics, Delhi Technological University (DTU) on February 28, 2023.
- 10. Participated "1st Hands-on-Training on Rietveld Refinement of X-Ray Diffraction data (RRD) organized by the Centre for Advanced Computational Research, Delhi from 14th 20th February 2024.
- 11. Participated "A THREE Day ONLINE WORKSHOP ON RECENT TRENDS IN CRYSTAL GROWTH TECHNOLOGY (RTCGT-2024)", organized by the Department of Chemistry & School of Science and Humanities with Centre for Nanoscience and Nanotechnology, Sathyabama Institute of Science and Technology, Chennai during 8-10 February 2024.
- 12. Awarded the 2nd Prize in Oral Presentation (Researcher Category) in the Environment, Water, Agriculture, Sustainability and Health (EWASH-2022): Strategizing A Greener Future held from 12 to 13 January, 2023, HINDU COLLEGE, DELHI UNIVERSITY.
- 13. Presented Poster on: "Fabrication of lead-free PVDF/KNNLTS/MWCNT piezoelectric nanogenerator: Role of MWCNT in the piezoelectric performance of nanogenerator for energy harvesting application" at International Conference on Atomic, Molecular, Material, Nano and Optical Physics with Applications (ICAMNOP-2023), held during December 20-23, 2023 at Delhi Technological University, New Delhi- 110042, India.
- 14. Participated in the "4th Raman Optronics Webinar Series (Rows-2023): Virtual International Conference held on Thursday, 30th November 2023 Organized by Raman International Optronics Society (RIOS) on "Photonic crystal light trapping for next generation solar energy harvesting."
- 15. Participated in the "4th Raman Optronics Webinar Series (Rows-2023): Virtual International Conference held on Wednesday, 29th November 2023 Organized by Raman International Optronics Society (RIOS) on "Photothermal lens and photothermal mirror techniques: Effects and applications."
- 16. Participated in the "4th Raman Optronics Webinar Series (Rows-2023): Virtual International Conference held on Monday, 27th November 2023 Organized by Raman International Optronics Society (RIOS) on "The Raman spectrum of graphene derivatives."

- 17. Participated in the "4th Raman Optronics Webinar Series (Rows-2023): Virtual International Conference held on Friday, 24th November 2023 Organized by Raman International Optronics Society (RIOS) on "Sample characterization by transverse photothermal beam deflection spectrometry"
- 18. Participated in the "4th Raman Optronics Webinar Series (Rows-2023): Virtual International Conference held on Thursday, 23rd November 2023 Organized by Raman International Optronics Society (RIOS) on "UV Resonant Raman: A powerful tool to investigate organic systems, from biophysics to material science"
- 19. Participated in the "4th Raman Optronics Webinar Series (Rows-2023): Virtual International Conference held on Tuesday, 21st November 2023 Organized by Raman International Optronics Society (RIOS) on "Communicating with distortion-free light"
- 20. Participated in the "4th Raman Optronics Webinar Series (Rows-2023): Virtual International Conference held on Monday, 20th November 2023 Organized by Raman International Optronics Society (RIOS) on "Ultra-short laser pulses for material synthesis, lithography and characterization"
- 21. Participated in the "4th Raman Optronics Webinar Series (Rows-2023): Virtual International Conference held on Friday, 17th November 2023 Organized by Raman International Optronics Society (RIOS) on "Effective use of solar spectrum to meet the energy demand of the world"
- 22. Participated in the "4th Raman Optronics Webinar Series (Rows-2023): Virtual International Conference held on Thursday, 16th November 2023 Organized by Raman International Optronics Society (RIOS) on "Photothermal and optical properties of condensed matter in multidisciplinary investigations".
- 23. Attended "One-day Seminar on Noise Fundamentals, Measurement and Analysis" on 26th May 2023, at Mechanical Engineering Department, Delhi Technological University, New Delhi.
- 24. Best Oral presentation on: "Graphene oxide and KNN incorporated PVDF matrix to enhance mechanical energy as a flexible piezoelectric energy harvester" at the International Conference on Advanced Materials for Emerging Technologies (ICAMET-2023), held on May 4-6, 2023, at Netaji Subhash University of Technology, New Delhi-110078, India.
- 25. Oral Presentation on: "Fabrication of Flexible Piezoelectric Generator based on Li modified Potassium Sodium Niobate Ceramic and PVDF for Energy Harvesting Application" in the National Conference on Physics and Chemistry of Materials (NCPCM2023) during 16th 18th March, 2023 at Govt. Holkar (Model Autonomous) Science College, Indore.

- 26. Actively participated in the Second International Faculty Development Program on "Advanced Materials for Technological Application" organized by Department of Physics, Satyabhama Institute of Science and Technology between 24th March to 4th April 2023.
- 27. Organized "One Day National Seminar on "Implementation of NEP-2020 in Special Reference to innovation & Entrepreneurship" held on 24 February 2023 organised by Delhi Technological University, Department of Applied Physics.
- 28. Attending One Day National Seminar on "Recent Advancement in Semiconductor Devices and Materials "RASDM-2023" at Department of Applied Physics, Delhi Technological University, New Delhi.
- 29. Poster presentation on "Fabrication of Flexible Piezoelectric Generator based on (Li, Ta, Sb) modified Potassium Sodium Niobate Ceramic and Poly (vinylidene fluoride) as a polymer" at the IUMRS-ICA 2022 conference held during 19-23 December 2022, at Indian Institute of Technology, Jodhpur.
- 30. Participated in the "Raman Optronics Webinar Series (Rows-2022): Virtual International Conference held on 7th December 2022 Organized by Raman International Optronics Society (RIOS) on "Secure data handling using optical processing".
- 31. Participated in the "Raman Optronics Webinar Series (Rows-2022): Virtual International Conference held on 25th November 2022 Organized by Raman International Optronics Society (RIOS) on "Taming quantum entanglement & such mysterious features of quantum mechanics".
- 32. Participated in the "Raman Optronics Webinar Series (Rows-2022): Virtual International Conference held on 24th November 2022 Organized by Raman International Optronics Society (RIOS) on "Stimulated Raman scattering in gas filled hollow-core photonic crystal fibers".
- 33. Participated in the "Raman Optronics Webinar Series (Rows-2022): Virtual International Conference held on 14th November 2022 Organized by Raman International Optronics Society (RIOS) on "Terahertz spectroscopy of Ga₂O₃ metamaterials and near-filled terahertz maps".
- 34. Participated in the "Raman Optronics Webinar Series (Rows-2022): Virtual International Conference held on 08th November 2022 Organized by Raman International Optronics Society (RIOS) on "Surface Enhanced Raman Spectroscopy for the diagnosis of neurodegenerative disease and cancer progression".
- 35. Attended Five Day Faculty Development Program on "Green Technology for Sustainable Environment (GTSE)" at Department of Mechanical Engineering Sarala Birla University, Jharkhand from September 26-30, 2022.

- 36. Participated One Week Online FDP "Modern Strategies in Physics Research: Ensuring Sustainable Development (MSPR-ESD)", organized by the Department of Physics, Faculty of Science, from 28th June- 2nd July 2022.
- 37. Oral Presentation on "Fabrication of Flexible Piezoelectric Generator based on (Li, Ta, Sb) modified Sodium Potassium Niobate Ceramic and Poly (vinylidene fluoride)" at International Conference on Nanotechnology for Sustainable Living & Environment (ICON-NSLE 2022) (14-16 April 2022) Department of Chemical Engineering, BITS Pilani, Pilani Campus.
- 38. Poster presentation on "Study of Dielectric and Piezoelectric Properties of rare-earth substituted KNN ceramics for Piezoelectric Energy Harvester" in National Webinar on Advances in Physics (June 25-26, 2020), GJU, Hisar, Haryana.
- 39. Participated in the "Raman Optronics Webinar Series 2021: Virtual International Conference held on 29th November 2021 Organized by Department of Optronics on "Artificial Lighting and Human Wellbeing Challenges for the Phosphors Materials Development".
- 40. Participated in International E-Conference on "Sustainable and Futurist Materials" on 29th 30th November,2021organised by International Research Centre and Department of Chemistry, Kalasalingam Academy of Research and Education, Nagpur.
- 41. Participated in the "Raman Optronics Webinar Series 2021: Virtual International Conference held on 18th November 2021 Organized by Department of Optronics on "Smart Materials and Sensors"
- 42. Attended The "Two Weeks International Workshop on Emerging Trends in the field of Science and Technology" organized by the Department of Physics, Sathyabama Institute of Science and Technology, Chennai from 16 to 28 August 2021.
- 43. Participated in "Faculty Development Program on Recent Advance, Trends and Challenges in the field of Nanotechnology" on 16 July 2021 at Amity University, Haryana.
- 44. Attended "International Conference on Atomic, Molecular, Optical and Nano Physics with Application" organized by Department of Applied Physics, Delhi Technological University from 18th to 20th December, 2019 at Delhi Technological University (DTU), Delhi.
- 45. Attended an Annual Five Days Information Literacy Workshop "E-Resource: A Gateway for Research, 5th Edition (2019)" organized by Central Library, Delhi Technological University, from 2nd to 6th September, 2019.

Teaching Assistantship:

Referees:

1. Dr. Richa Sharma

Assistant Professor

Department of Applied Physics, Delhi technological University, Delhi

Email: richa.phy1@gmail.com

Mob. +91 8800235049